University of California
Los Angeles

Quantum Spin Transport and Collective Magnetic Dynamics in Heterostructures

A dissertation submitted in partial satisfaction
of the requirements for the degree
Doctor of Philosophy in Physics

by

Scott Andrew Bender

2014

Abstract of the Dissertation

Quantum Spin Transport and Collective Magnetic Dynamics in Heterostructures

by

Scott Andrew Bender

Doctor of Philosophy in Physics

University of California, Los Angeles, 2014

Professor Yaroslav Tserkovnyak, Chair

This thesis advances the theory of quantum and semiclassical transport in magnetic heterostructures. In the solid state, angular momentum can be carried by individual electrons and collective modes. The flow of angular momentum (a spin current), central to the operation of spintronic devices, is generated by the application of electric and magnetic fields and temperature gradients. In what follows, we explore the physics of such nonequilibrium spin currents in magnetic structures, involving an interplay of charge and magnetic dynamics and thermoelectric effects.

Chapter 1 provides an introduction to the transport of spin in magnets, carried by electrons and collective excitations of the magnetic order. Chapters 2-6 study the role of thermal fluctuations in transport and magnetic dynamics. In Chapter 2, we describe how incoherent thermal fluctuations of the spin density (magnons), which open inelastic scattering channels, contribute to spin and energy transport between a normal metal and a magnet. Such (temperature-dependent) transport may arise from a thermal gradient applied across the metal/magnet interface or a spin accumulation inside the normal metal and may alter or even drive magnetic dynamics.

Chapter 3, is dedicated to the realization of Bose-Einstein condensed magnons (previously observed by microwave pumping [DDD06a]) in a normal metal/insulating ferromagnet heterostructure. As is described in Chapter 2, the combination of a temperature gradient

and normal metal spin accumulation can drive spin into the insulating ferromagnet, accumulating as magnons; upon reaching a critical density, the magnons, which are bosonic, spontaneously form a quasi-equilibrium condensate.

Chapter 4 focuses on thermally driven spin-torques in electrically insulating structures, wherein direct electric control of magnetic dynamics is prohibited. In contrast to the interfacial transport described in Chapter 2, where a spin accumulation is to necessary to observe magnetic dynamics, here we demonstrate how spin-torques can arise from a pure thermal gradient in a heterostructure. These spin-torques can be measured by ferromagnetic resonance and can, under a sufficiently strong bias, actuate magnetic switching.

Chapter 5 concerns charge transport in a single-electron transistor, consisting of a magnetic quantum dot in contact with magnetic and normal metal leads. Microwave-driven precession by the dot induces a pumped electric current, which can be enhanced and made highly nonlinear by electron interactions (Coulomb blockade). The dependence of the resulting electrical response on the power and spectrum of microwave irradiation may be utilized to develop nanoscale microwave detectors analogous to single-electron transistor-based electrostatic sensors and nanoelectromechanical devices.

In Chapter 6 we study bilayers, composed of a nonmagnetic conducting and a magnetic layer. We develop a general phenomenology for the magnetic and charge dynamics, which are coupled by spin-orbit interactions. In contrast to Chapters 2-4, we focus on the long-wavelength magnetic dynamics, which is subject to current-induced torques and produces fictitious electromotive forces that drive charge dynamics.

The dissertation of Scott Andrew Bender is approved.

Louis Bouchard

Robijn Bruinsma

Yaroslav Tserkovnyak, Committee Chair

University of California, Los Angeles

2014

To my mother and father, Judy and Bruce

Thank you for always supporting me, and for thwarting my plans to drop out of preschool on the second day.

Table of Contents

List of Figures

Acknowledgments

Over the course of my education in physics, I have been extremely lucky to have encountered so many dedicated educators and talented academics. First, I would like to thank Brian Granger for introducing me to the field of condensed matter physics and for guiding my first experiences in theoretical research over my summers at Santa Clara University. Betty Young, John Birmingham and Richard Barber all provided indispensable guidance in transitioning from my undergraduate to graduate career. My incredible experience at Santa Clara has shaped my professional course and had a lasting personal impact.

My years here at UCLA have been formative and transformative, to say the least. I feel incredibly fortunate to have had the opportunity to be a part of this vibrant and closely-knit community of students, faculty, research and staff. I could not have asked for a more invigorating or intellectually stimulating environment. First, I'd like to thank all of my classmates with who I weathered the many hours of graduate classes and comprehensive exam preparation. In particular, I would like to thank Brandon Buckley, Brett Friedman, Scott Sullivan and Daniel Aharoni for sharing the experience, as well as my pseudogroupmate Pramey Upadhyaya and perpetual officemate Arash Bellafard. I would also like to thank my groupmates Silas Hoffman, Koji Sato, and Mircea Trif for sharing so many incredible adventures together over the years. A special thank you must be extended to So Takei for many hours of help and advice over the past year.

I would also like to thank Arne Brataas, Rembert Duine and Gerrit Bauer for hosting me at their institutions and providing me with the opportunity to study physics from a different perspective, as well as for their advice on my professional trajectory.

I owe a deep debt of gratitude to my dedicated advisor, Yaroslav Tserkovnyak, who has spent so many years shaping the scientist and person I am today. I have been unbelievably fortunate to have found an advisor who not only is an internationally respected physicist, but who cares greatly for the well-being of all his students.

Vita

2007	B.Sc. Physics Santa Clara University, California
2008-2012	Teaching assistant, UCLA, Los Angeles, California.
2011–present	Graduate Student Researcher, UCLA, Los Angeles, California

Publications

Scott A Bender, Yaroslav Tserkovnyak, and Arne Brataas. Microwave response of a magnetic single-electron transistor. Physical Review B, 82(18):180403, November 2010

Scott A. Bender, Rembert A. Duine, and Yaroslav Tserkovnyak. Electronic Pumping of Quasiequilibrium Bose-Einstein-Condensed Magnons. Phys. Rev. Lett., 108:246601, Jun 2012

Scott A. Bender, Rembert A. Duine, Arne Brataas, and Yaroslav Tserkovnyak. Dynamic phase diagram of dc-pumped magnon condensates. Phys. Rev. B, 90:094409, Sep 2014

Yaroslav Tserkovnyak and Scott A Bender. Spin Hall phenomenology of magnet dynamics. Physical Review B, 90(1):014428, July 2014

Scott A Bender and Yaroslav Tserkovnyak. Interfacial Spin and Heat Transfer between Metals and Magnetic Insulators. arXiv.org, September 2014

CHAPTER 1

Introduction

Spintronics, the quest to reliably manipulate the electron spin degree of freedom, represents a synthesis of disciplines, researchers, and goals. It straddles the divide between pure scientific research, which aspires to disclose hidden truths about the microscopic world, and the development of new technologies, which promise a broader impact for society. The breadth of length and timescales involved is wide, ranging from single and few particle physics (e.g. single-electron transistors and nitrogen-vacancy centers) to the collective excitations of microstructures (e.g. spin waves in a magnetic structures). Some spintronic systems manifest quantum features requiring the full machinery of quantum field theory; others sit comfortably, or uncomfortably, on the mesoscopic divide between the quantum and semiclassical. Brought into the fray are many old ideas, such as magnetoresistance and thermoelectric effects, breathed new life as they mix with new concepts, structures and techniques.

This thesis, which advances the theory of transport in magnetic heterostructures, is, in a sense, an embodiment of this synthesis. Quantum concepts, in the form of magnons, superfluidity, and Bose-Einstein condensation, coalesce with semiclassical magnetic dynamics. We explore the physics of few-electron quantum dots, as well as the collective spin excitations of semiclassical ferromagnets. Transport is engendered by a variety of manners: electronically, via spin-orbit physics, thermally by the Seebeck and Peltier effects, and by magnetic fields.

The purpose of this introduction is to the survey the many subfields and concepts involved in and lay the theoretical context necessary to understand the subsequent chapters. In Sec. 1.1, we introduce the classical and quantum theory of ferromagnets, which play a central role in Chapters 2-4 and 6. In Sec. 1.2, we outline the theory of semiclassical transport of electrons through normal and ferromagnetically ordered metals. The reason for this is

twofold. First, it provides an overview of spin based transport in metals, including the spin Hall effect, which either implicitly (Chapters 2-4) or explicitly (Chapter 6) play an important role in the devices and structures discussed. Second, it provides a convenient basis on which to introduce the concepts of both thermotransport and Onsager reciprocity, which are employed extensively throughout remaining chapters. In Sec.1.3, we consider transport between metals and ferromagnets, obtaining from scattering theory boundary conditions for spin, charge and heat currents. These boundary conditions are building blocks essential to understanding spintronic devices and effects, including the giant magnetoresistance effect, the spin-transfer torque and tunnel magnetoresistance, and provide a framework with which to understand the work presented in all of the remaining chapters.

1.1 Ferromagnetic dynamics

1.1.1 Ferromagnetic ordering in the Landau Model

Because the mass-to-charge ratios of nuclei are significantly larger than that of electrons, it is the latter particle which is essentially responsible for magnetism in the solid state. The electronically generated magnetic field of a solid has two origins. The first is the field induced by the motion of an electron, which is responsible for the diamagnetic response. The second contribution comes from the intrinsic rotation of an electron, i.e. its spin. In most ferromagnetic materials, the magnetic dipole moment of each lattice site of the solid is dominated by the intrinsic spin contribution.

The focus of this thesis will be ferromagnets (as well as ferrimagnets), wherein the coupled magnetic moments of each lattice site spontaneously form collective order over macroscopic distances. Electron spins directly couple with one another via their electromagnetic fields and exchange interactions. In the solid state, electrons move at nonrelativistic speeds, such that their dominant electromagnetic interaction is captured by their magnetostatic dipole field, which is highly nonlocal and generally breaks rotational symmetry in combined spin- and orbital-space. In contrast, the exchange interaction, stemming from quantum mechani-

cal effects, is usually short-ranged and, in the simplest case, invariant under both spin and spatial rotations. Microscopically, the exchange interaction arises from two-body interactions between electrons (e.g. a screened Coulombic potential), which, in second quantized notation, may be written:

$$\hat{V} = \frac{1}{2}\sum_{\sigma\sigma'}\sum_{ijkl}\hat{c}^{\dagger}_{i\sigma}\hat{c}^{\dagger}_{j\sigma'}V_{ijkl}\hat{c}_{k\sigma'}\hat{c}_{l\sigma}\,, \tag{1.1}$$

where

$$V_{ijkl} \equiv \int d^3x d^3y \psi^*_i(\mathbf{x})\,\psi^*_j(\mathbf{y})\,V(\mathbf{x},\mathbf{y})\,\psi_k(\mathbf{y})\,\psi_l(\mathbf{x}) \tag{1.2}$$

is the spin independent two-body interaction potential, and $ij\ldots$ label the orbitals ψ_i, ψ_j etc. Now, consider the $i = k \neq j = l$ term[1]. Using the identities $\frac{1}{2}\sum_j \sigma^{(j)}_{\alpha\beta}\sigma^{(j)}_{\gamma\lambda} = \delta_{\alpha\lambda}\delta_{\beta\gamma} - \frac{1}{2}\delta_{\alpha\beta}\delta_{\gamma\lambda}$ and $\mathbf{s}_i = (\hbar/2)\sum_{\sigma,\sigma'} a^{\dagger}_{i\sigma}\boldsymbol{\sigma}_{\sigma\sigma'}a_{i\sigma'}$ as the spin density of the orbital i, one obtains:

$$\sum_{\sigma,\sigma'}\hat{c}^{\dagger}_{i\sigma}\hat{c}^{\dagger}_{j\sigma'}V_{ijij}\hat{c}_{i\sigma'}\hat{c}_{j\sigma} = -2J_{ij}\left(\frac{\mathbf{s}_i\cdot\mathbf{s}_j}{\hbar^2} + \frac{1}{4}\hat{n}_i\hat{n}_j\right)\,, \tag{1.3}$$

where $J_{ij} = V_{ijij}$. Repulsive ($V_{ijij} > 0$)/attractive ($V_{ijij} < 0$) interactions between orbitals therefore generate ferromagnetic/antiferromagnetic interactions between spins, which minimizes the interaction energy by forming a two-particle wavefunction that is spatially antisymmetric (spin triplet)/symmetric (spin singlet). We will focus on the former scenario (ferromagnetic interactions).

Let us consider spin ordering in a magnetic insulator engendered by the ferromagnetic exchange interaction. For the moment, we will neglect the dipole interactions, which can be subdominant to exchange coupling in small structures and certain materials. Course graining over the lattice spins, we may define a local spin density $\mathbf{s}(\mathbf{x})$ (in units of $\hbar$) with an associated effective free energy density [LL80b]:

$$f = f_0 + \frac{t}{2}M^2 + \frac{u}{4}M^4 + \frac{a}{2}(\nabla M)^2 + f_{\rm sb}\,, \tag{1.4}$$

where $\mathbf{M}(\mathbf{x}) = \gamma\hbar\mathbf{s}(\mathbf{x})$ is the magnetization, γ is the material-dependent gyromagnetic ratio, f_0 is a constant that does not depend on M, and t, u (which is positive), and a are temperature dependent parameters. Omitted from F are contributions which are higher

[1] This is the Fock term. The $i = l \neq k = j$ (Hartree) term does not contribute to the spin-spin interactions.

order in M and spatial derivatives thereof. The terms proportional to t, u, and a are rotationally invariant in spin-space, while the last term, $f_{\rm sb}$, breaks SU(2) symmetry. The quadratic coefficient, t, becomes negative when the magnet temperature T falls below the Curie temperature, T_c; the stiffness parameter a, stemming from the exchange interaction, is always positive for a ferromagnetic interactions.

In the absence of the rotational symmetry breaking ($f_{\rm sb} = 0$) and spatial inhomogeneity, when $T > T_c$, t is positive, the free energy is minimized when $M = 0$ as thermal fluctuations destroy magnetic order, and the magnet is in the paramagnetic phase. When, however, $T < T_c$, t is negative, f is minimized when M is equal to the saturation magnetization $M_s \equiv \sqrt{-t/u}$, and the spins are ferromagnetically ordered, with $\mathbf{s}$ constrained to the manifold $\mathcal{M}$ (defined by $|\mathbf{s}| = s$), where $s = M_s/\hbar\gamma$ is the saturation spin density. The direction of $\mathbf{s}$, however, is degenerate; inhomogeneous excitations of $\mathbf{s}$ around this spontaneously broken symmetry are gapless Goldstone modes. In the presence of a symmetry-breaking term $f_{\rm sb}$, the degeneracy of $\mathbf{s}$ on the manifold $\mathcal{M}$ is lifted. Generally, the symmetry-breaking term $f_{\rm sb}$ (which stems from the anisotropy and applied fields), is small compared to quadratic and quartic contributions to f, so that when T is sufficiently below T_c, the new equilibria defined by $f_{\rm sb}$ lie essentially on $\mathcal{M}$, as do the thermally accessible excitations of $\mathbf{s}$ around these equilibria. These excitations (i.e., spin waves), are gapped by $f_{\rm sb}$.

1.1.2 Classical Dynamics of a Ferromagnet

The equation of motion for the field $\mathbf{s}$ constrained to $\mathcal{M}$ below the Curie temperature may be obtained from the Lagrangian $L = \int d^3x \mathcal{L}$. Writing the spin density on $\mathcal{M}$ as $\mathbf{s} = s\mathbf{n}$, we may parameterize the unit vector $\mathbf{n} = (n_x, n_y, n_z) = (\sin\theta\cos\phi, \sin\theta\cos\phi, \cos\theta)$ by spherical coordinates, allowing for an explicit construction for the Lagrange density:

$$\mathcal{L} = -s\hbar\dot{\phi}\left(1 - \cos\theta\right) - g\left(\mathbf{n}\right) , \tag{1.5}$$

where

$$g\left(\mathbf{n}\right) = \frac{As}{2}\sum_i \left(\nabla_i \mathbf{n}\right)^2 + f_{\rm sb}\left(\mathbf{n}\right) \tag{1.6}$$

is the free energy density of the magnet constrained to $\mathcal{M}$, with $A = a(\gamma\hbar)^2$ as the exchange stiffness and $f_{\rm sb}$ is the symmetry-breaking contribution to the free energy which is anisotropic in spin-space. The equations of motion for $\theta(\mathbf{x},t)$ and $\phi(\mathbf{x},t)$ are obtained from the Euler-Lagrange equations, and have the form:

$$\sin\theta\hbar\dot{\theta} = \partial_\phi g - \partial_{\mathbf{x}}\frac{\partial g}{\partial(\partial_{\mathbf{x}}\phi)}, \quad \hbar\sin\theta\dot{\phi} = -\partial_\theta g + \partial_{\mathbf{x}}\frac{\partial g}{\partial(\partial_{\mathbf{x}}\theta)}\,. \tag{1.7}$$

Alternatively, a classical Hamiltonian formulation of the spin dynamics can be constructed from the Lagrangian as follows. Eq. (1.5) allows for the definition of a canonical momentum density, $\pi(\mathbf{x}) = \partial\mathcal{L}/\partial\dot{\phi} = -s\hbar(1-\cos\theta(\mathbf{x}))$, resulting in a Hamiltonian:

$$\mathcal{H} = \int d^3x(\pi\dot{\phi} - \mathcal{L}) = \int d^3x g(\mathbf{n})\ . \tag{1.8}$$

The canonical momentum density $\pi(\mathbf{x})$ is conjugate to the azimuthal angle $\phi(\mathbf{x})$, satisfying the canonical relation $\{\phi(\mathbf{x}),\pi(\mathbf{y})\}_p = i\delta(\mathbf{x}-\mathbf{y})$, where

$$\{A(\mathbf{x}),B(\mathbf{x})\}_p \equiv i\int d^3z\left(\frac{\delta A(\mathbf{x})}{\delta\phi(\mathbf{z})}\frac{\delta B(\mathbf{y})}{\delta\pi(\mathbf{z})} - \frac{\delta B(\mathbf{x})}{\delta\phi(\mathbf{z})}\frac{\delta A(\mathbf{y})}{\delta\pi(\mathbf{z})}\right) \tag{1.9}$$

is the Poisson bracket and δ denotes a functional derivative. The Hamiltonian $\mathcal{H}$ generates translations in time; consequently, the classical Heisenberg equation for a field $a(\mathbf{x})$ reads: $\dot{a}(\mathbf{x}) = i\{\mathcal{H},\dot{a}(\mathbf{x})\}_p$. Hamilton's equations of motion are derived by substituting $a(\mathbf{x}) = \pi(\mathbf{x})$ and $a(\mathbf{x}) = \phi(\mathbf{x})$, yielding Eqs. (1.7). The equations of motion, Eqs. (1.7), suffer from the disadvantage that they depend on a particular frame of reference which defines θ and ϕ. Alternatively, dynamics can be expressed directly in terms of the spin density $\mathbf{s}$, which, using the canonical relation between $\phi(\mathbf{x})$ and $\pi(\mathbf{y})$, can be shown to satisfy:

$$\{s_i(\mathbf{x}),s_j(\mathbf{y})\}_p = i\epsilon_{ijk}s_k\delta(\mathbf{x}-\mathbf{y})\ . \tag{1.10}$$

Inserting s_i into the classical Heisenberg equation of motion and using Eq. (1.10) yields:

$$\hbar\dot{\mathbf{s}} = \mathbf{H}_{\rm eff}\times\mathbf{s} \tag{1.11}$$

where $\mathbf{H}_{\rm eff} = \hbar\delta_{\mathbf{s}}\mathcal{H}$s is the effective magnetic field. Expressing Eq. (1.11) in spherical coordinates, it is straightforward to obtain Eq. (1.7).

The new equation of motion, Eq. (1.11), is manifestly invariant under time reversal symmetry, which, via Noether's theorem, signifies energy conservation. A phenomenological dissipative term (parameterized by the unitless constant α), which therefore breaks time-reversal symmetry, may be added to the dynamics, capturing angular momentum and energy transfer from magnetic degrees of freedom to a bath, resulting in the Landau-Lifshitz-Gilbert equation [Gil04a]:

$$\hbar\dot{\mathbf{n}} = -\mathbf{n} \times \left(\mathbf{H}_{\rm sb} - A\nabla^2\mathbf{n}\right) - \alpha\hbar\mathbf{n} \times \dot{\mathbf{n}}, \tag{1.12}$$

where $\mathbf{H}_{\rm sb} = \partial_{\mathbf{n}} f_{\rm sb}/s$ is the symmetry breaking effective field. Indeed, using Eq. (4.10), one finds that the rate of change of the local energy density is: $\dot{g} = \dot{\mathbf{n}} \cdot \partial_{\mathbf{n}} g = -\alpha s\hbar\dot{\mathbf{n}}^2 < 0$. The primary physical origin of this so-called Gilbert damping depends on the materials and structure in consideration. For example, distortions in the lattice (phonons) alter the intersite magnetic coupling; magnon-phonon provides one such channel for the conversation of magnetic to bath spin and energy energy [Kit58, BH94, HUW02]. When itinerant electrons are present, electron-magnon scattering provides an additional mechanism for the relaxation of magnetic dynamics [Ber96b, IRL02, TB02a].

The Landau-Lifshitz-Gilbert equation may be written as a continuity equation for the spin density $\mathbf{s} = \hbar s\mathbf{n}$:

$$\dot{\mathbf{s}} = \dot{\mathbf{s}}_{\rm sb} + \dot{\mathbf{s}}_{\alpha} - \sum_i \partial_i \mathbf{j}_i \,. \tag{1.13}$$

Noether's theorem dictates that angular momentum in a given direction is conserved when the system is spin-rotationally invariant around the axis oriented in that direction. Accordingly, angular momentum conservation is violated in the plane normal to the symmetry-breaking field $\mathbf{H}_{\rm sb} = \partial_{\mathbf{n}} f_{\rm sb}/s$, leading to the first term $\dot{\mathbf{s}}_{\rm sb} = -\mathbf{s} \times \mathbf{H}_{\rm sb}/\hbar$ in Eq. (1.13). The second term, $\dot{\mathbf{s}}_{\alpha} = -\alpha\mathbf{s} \times \dot{\mathbf{s}}/s\hbar$, gives the flow of angular momentum into the bath, while the last term describes spin transport between lattice spins, with

$$\mathbf{j}_i^{(s)} = -sA\mathbf{n} \times \partial_i \mathbf{n} \tag{1.14}$$

as the exchange spin current, which is employed in the boundary conditions for $\mathbf{n}$ in the presence of interfaces.

In most simple ferromagnetic materials, the symmetry breaking free energy density $f_{\rm sb}$ of a ferromagnet has three contributions. The first is the Zeeman energy density $f_z = s\mathbf{H}\cdot\mathbf{n}$ due to the external field $\mathbf{H}$. The second contribution, f_c, the magnetic crystalline anisotropy, stems from the spin orbit interaction, breaks spin rotational symmetry with respect to lattice, and has the form:

$$f_c = \frac{s}{2}\mathbf{n}\cdot\hat{\kappa}\cdot\mathbf{n}\,, \tag{1.15}$$

where where $\hat{\kappa}$ is the anisotropy tensor. The last contribution, the dipole interaction energy, similarly breaks the separate rotational symmetries of spin- and coordinate-space, but in contrast to the crystalline anisotropy is highly nonlocal. Whereas the ferromagnetic exchange stiffness and Zeeman terms always favor a uniform spin density, the dipole field engenders more complicated textures (e.g., domain walls). For this reason, the dipole field is often referred to as the "demagnetization field". The exchange length $l_x \equiv \sqrt{A/4\pi M_s^2}$ provides a measure for the competition between the exchange and dipole interactions; over lengthscales smaller than l_x, the exchange interaction dominates, and the magnet is monodomain below the Curie temperature. In such monodomain structures, the dipole free energy density is:

$$f_d = 4\pi s M_s^2 \mathbf{n}\cdot\hat{D}\cdot\mathbf{n} \tag{1.16}$$

where $\check{D}$ is the demagnetization tensor, which is determined by the magnet's shape and has unit trace. For simplicity, let us specialize to magnets with spin-rotational symmetry around one axis, which we shall denote as $\hat{\mathbf{z}}$, so that eigenaxes of $\hat{\kappa}$, and $\hat{D}$ align, with $\kappa_x = \kappa_y = \kappa_\perp$ and $D_x = D_y = D_\perp$, and the applied field is $\mathbf{H} = H\mathbf{z}$. In this case, we may write the anisotropy contributions as:

$$f_a = f_c + f_d = \frac{s}{2}Kn_z^2\,. \tag{1.17}$$

Let us now consider the low energy inhomogeneous excitations (spin waves) of the ferromagnet around the order parameter $\mathbf{n}$, which is pinned along the direction $-\mathbf{z}$ (i.e. $\theta = \pi$). Fluctuations around this equilibrium ($\theta = \pi$) may be described by the quantity

$$\Phi = \sqrt{s\,(1+\cos\theta)}e^{-i\phi}\,, \tag{1.18}$$

which vanishes when $\theta = \pi$. The Landau-Lifshitz-Gilbert equation, Eq. (4.10), for small angles $\pi - \theta \ll 1$ then can be expressed as a dissipative zero-temperature Gross-Pitaevski

equation for an interacting Bose gas of particles with mass $m = \hbar^2/2A$:

$$i\hbar\partial_t\Phi = \alpha\hbar\partial_t\Phi + (H_0 - K)\,\Phi - A\nabla^2\Phi + \frac{K}{s}\,|\Phi|^2\,\Phi \tag{1.19}$$

to order θ^2 (and neglecting terms of order $\theta\nabla\theta$), where K gives rise to a local interaction. When the density $|\Phi|^2$ is sufficiently small, Eq. (1.19) reduces to the noninteracting Schroedinger equation, resulting in a quadratic excitation spectrum:

$$\hbar\omega\,(1 + i\alpha) = \frac{\hbar^2\mathbf{k}^2}{2m} + \hbar\Omega, \tag{1.20}$$

where $\mathbf{k}$ is the excitation wavevector and $\hbar\Omega = H - K$ is the excitation gap. At the coercivity field, $H = K$, the gap closes, and $\mathbf{n} = -\mathbf{z}$ no longer represents a stable equilibrium since $\mathbf{k} = 0$ (i.e. monodomain) dynamics may reorient $\mathbf{n}$ without energy cost; at finite gap, spin-waves are stable against Gilbert damping on timescales shorter than $\sim 1/\alpha\omega$. Physically, a spin wave corresponds to a spin density which is circularly rotating around $-\mathbf{z}$ with frequency ω and wavevector $\mathbf{k}$, so $\Phi_{\mathbf{k}} = \Phi_0 e^{i\mathbf{k}\cdot\mathbf{x} - i\omega t + i\phi_0} e^{-\alpha\omega t} = (\hbar\sqrt{2s})s_-$, where $s_- = s_x - is_y$ and $s_x \approx \hbar s(\pi - \theta_0)\cos\left(\omega t - \mathrm{k}\cdot\mathbf{x} + \phi\right)e^{-\alpha\omega t}$ and $s_y \approx \hbar s(\pi - \theta_0)\sin\left(\omega t - \mathrm{k}\cdot\mathbf{x} + \phi\right)e^{-\alpha\omega t}$ are the x and y components of the spin density near equilibrium ($\theta \lesssim \pi$).

Projecting the spin current $\mathbf{j}_i$ onto the z-axis, one obtains:

$$j_i^{(z)} = \mathbf{z}\cdot\mathbf{j}_i^{(s)} = \hbar\left[\frac{\hbar}{2mi}\left(\Phi^*\partial_i\Phi - \Phi\partial_i\Phi^*\right)\right] \tag{1.21}$$

which is simply $\hbar$ multiplied by the first quantized expression for the particle current density, suggesting that the "wavefunction" Φ carries an angular momentum of $\hbar\mathbf{z}\,|\Phi|^2$. Together with the component of $\mathbf{j}_i$ perpendicular to $\mathbf{z}$,

$$\mathbf{j}_{i\perp} = -As\partial_i\theta\hat{\boldsymbol{\phi}} \tag{1.22}$$

the current $j_i^{(z)}$ provides a boundary condition for the spin density $\mathbf{n}$. For example, consider a ferromagnetic film with surfaces defined at $x' = 0$ and $x' = d$, where the direction x' is arbitrary with respect to the magnetization axis z. If spin transport is prohibited across both interfaces (e.g. when the magnet is interfaced with a vacuum or with poor spin-sink metal), the spin current $\mathbf{j}_i$ vanishes at $x' = 0$ and $x' = d$, which via Eqs. (1.21) and (1.22),

then, is satisfied by standing waves $\Phi_{\mathbf{k}} = \Phi_0 \cos(k'x') e^{i\mathbf{k}_\perp \cdot \mathbf{x} - i\omega t - \alpha t}$, with $k' = 2\pi/d$ as the normal wavevector and $\mathbf{k}_\perp$ as the in-plane wavevector, in complete analogy to the quantum particle-in-a-box.

The circular nature of the spin waves discussed above stems directly from the spin-space rotational symmetry of the free energy around the z axis. Our treatment of the dipole field via the demagnetization tensor (see Eq. (1.16)), however, neglects the nonlocal stray fields associated with an inhomogeneous spin-wave texture. Such stray fields can greatly alter the spin-wave dispersion for low energy excitations in the presence of boundaries, spoiling the rotation symmetry around $\mathbf{z}$ and generating elliptical spin precessions. The exact spin-wave solutions are beyond the scope of this thesis, but we remark for completeness that the exchange boundary conditions discussed above most, in general, be supplemented with magnetostatic bulk fields and boundary conditions, resulting in magnetostatic-exchange waves [KS89b, GM96]. At low energies ($A\mathbf{k}^2 \ll 4\pi s M_s^2$), the exchange contribution to the dispersion and the exchange boundary conditions may be neglected, resulting in pure magnetostatic waves. The dispersions of these magnetostatic modes are no longer quadratic and may include more than one band, depending on the orientation of the magnetization with respect to the magnet's surfaces, namely: forward volume modes (with positive group velocity), backward volume modes (with negative group velocity), and surface waves (localized on the surface of the ferromagnet) [Wal58, DE61]. At high energies $A\mathbf{k}^2 \gg 4\pi s M_s^2$, spin waves are determined by the exchange physics, and the stray-fields may be neglected. We will concern ourselves with room temperature effects, wherein thermal spin-wave excitations generally fall within the exchange regime.

Much of recent work has centered on microstructures, e.g. thin films, which are stable against the formation of magnetic domains, allowing for the quasi-ballistic propagation of spin waves. Small angle dynamics in such structures may be generated experimentally by a number of methods. First, the application of a microwave frequency magnetic field allows for the direct excitation of specific spin wave modes without directly coupling to other degrees of freedom in the ferromagnet. Two such techniques may be distinguished. In perpendicular pumping, an oscillating field is applied normally to the spin density. At

microwave frequency, the corresponding wavelength of light is generally much larger than the dimensions of the structure, the zero-wavelength (i.e. monodomain) dynamical mode is excited in the magnet. As the monodomain rotates at the driving frequency, the dynamics of the spin waves, which are inhomogeneous perturbations around the precessing magnetization, is altered by the fictitious forces in the rotating frame. At a critical frequency and power, a given mode may undergo a Suhl instability, becoming unstable and growing exponentially in time [AEM95, Suh58, Pec88]; in the language of spin wave modes in the lab frame of reference, interactions between the zero and finite wavelength spin waves (stemming from nonlinear contributions to the equation of motion at higher orders in the amplitudes $\Phi_{\mathbf{k}}$ and Φ_0) transfer energy from the former to the latter, overcoming the Gilbert damping of certain modes. As these modes grow interactions transfer angular momentum to other spin waves, curbing the exponential growth [ZLS75]. In contrast to perpendicular pumping, parallel pumping directly couples finite wavelength modes to an oscillating field, which in this case is applied tangentially to the magnetization [Com64, CJ65, SSY80, KKD95]. If the magnet is perfectly rotationally symmetric around the magnetization axis $\hat{\mathbf{z}}$, spin waves are circular and cannot be excited by parallel pumping. However, when spin waves are elliptical in the xy plane, because $\mathbf{n}$ is confined to a unit sphere the component n_z of a spin wave excitation oscillates in time and couples to the applied microwave field. Provided the Hamiltonian is translationally invariant, two modes, $\mathbf{k}$ and $-\mathbf{k}$ are excited [KDD11]. Energy conservation dictates that the frequency of the two spin wave modes is equal to half of that of the oscillating field, so that the entire process can be envisioned as the annihilation of a single microwave photon and the corresponding creation of a pair of spin wave quanta. The main advantage to parallel pumping lies in the fact that it is possible to directly excite specific magnon frequencies, although spin wave interactions generally lead to the subsequent excitation of other modes.

Second, spin waves may be generated electrically, which, from a technological perspective, is preferable to the off-chip parametric pumping techniques described above. In conducting magnets, a spin polarized electric current flows across the magnetic texture under a thermodynamic pressure, such as an applied electric field or a temperature gradient. As the

resulting spin current traverses the texture, the spins of the conducting electrons are reoriented towards the local exchange field; because the exchange interaction conserves angular momentum, electron spins transfer angular momentum to the magnetic texture, resulting in a local bulk spin-transfer torque [BJZ98, ZL04, FSS06, Dol12, WT09, MBC11]. Above a threshold electric current, the delivery of angular momentum to certain modes overcomes losses to Gilbert damping [LHZ05, TBB08]; the exponential growth of these modes is eventually curbed by bleeding energy into the remaining spin wave spectrum and other degrees of freedom. Naturally, such instabilities cannot occur in insulating magnets. There, however, it is still possible to exit spin wave modes electrically via interfacial spin-transfer-torque provided by an adjacent metal, which is discussed below in some detail.

Third, spin waves may be excited thermally. According to the principle of the equipartition of energy, at finite temperature, all spin wave modes are thermally activated in equilibrium. In addition, a nonequilibrium thermal flux may also excite finite wave-length dynamics. In insulators, thermal biasing gives rise to a magnon flux, which carries angular momentum. In analogy to the bulk spin-transfer torque exerted on inhomogeneous magnetic order by a spin polarized electric current, Berry phase effects result in the transfer of angular momentum from an incoherent thermomagnonic flux (which is intrinsically"spin-polarized" along the direction of the order parameter) to the coherent dynamics of ferromagnet, spurring the growth of classical spin waves with well defined phases from thermal fluctuations. Reciprocally, coherent magnetic dynamics of texture $\mathbf{n}(\mathbf{x}, t)$ can thus generate magnonic flow via the spin-motive force [KT12]. We provide a derivation of this effect in the Appendix of this thesis. When interfaced metals, ferromagnetic dynamics may be excited by the application of an interfacial temperature gradient, which will play a central role in this thesis. In Chapter 2, we provide an account of how a temperature gradient, in combination with an electrically driven spin-transfer torque, can both convert electron spins into spin wave excitations and drive coherent magnetic dynamics. In Chapter 3, we explore the condensation of magnons via a thermally assisted spin-transfer torque. In Chapter 4, we propose a mechanism by which coherent magnetic dynamics can be induced by a temperature gradient alone via three magnon scattering.

Decades of research have yielded an array of spin wave detection methods, including neutron scattering [SB60, Tho67, BMB05], FMR linewidth broadening [WLW13], microwave spectroscopy [LYB07] and microantennas [LF11]. Of particular utility is the method of Brillouin Light Scattering (BLS), which employs the inelastic scattering of light off of magnetic texture. In the language of classical spin physics, BLS exploits the fact that a spin wave creates a diffraction grating which, via the magneto-optical interaction, diffracts and doppler shifts light; in the language of quantum mechanics, a photon scatters from a spin wave quanta (a magnon), exchanging energy and momentum [JDM99, Dem01, SSV12]. The scattered light thus contains information about both the frequency and amplitude of a spin wave with a given wavevector, providing BLS a major advantage over other techniques.

In recent years, spin Hall physics (discussed below in detail) has opened up the possibility of the direct conversion of a spin wave flux into an electrical signal. As spin waves scatter off of a normal metal/ferromagnet interface, the magnetization at the interface precesses, pumping spin into the normal metal. The resulting spin current entering the normal metal can in term be detected as an inverse spin Hall voltage [AIS09, SKA10a, SKC11a, AS12]. As is discussed below, spin waves can also be generated by spin-transfer torques, such as those provided by the spin Hall effect [PAR11c]. It follows that if an insulating magnet is placed in contact with two metals with large spin orbit effects, an electrical field in one metal may be converted by the spin Hall effect and spin transfer torque into spin wave excitations, which propagate inside the magnet to the other metal and are converted back into an electrical response via the reciprocal processes, spin-pumping and the inverse spin Hall effect. This type of device has already been demonstrated in [KHT10a] in a Pt/YIG/Pt heterostructure. Such magnetically mediated nonlocal conductance, whose efficiency is set by the spin Hall angles of the normal metal leads, the spin mixing conductances, and Gilbert damping in the magnet, could represent an attractive alternative to the transmission of electrical signals by an electrical conductor, wherein Joule heating is generally a significant disadvantage in microscopic devices.

1.1.3 Quantum Small Angle Dynamics of a Ferromagnet

Thus far, we have treated the spin density $\mathbf{s}$ as a classical object. When the total spin $S_i = 1/2, 1, 3/2 \ldots$ of each lattice site is small, quantum fluctuations become important. In a lattice, the noncommutativity of the positions and momenta of the lattice sites quantizes the elasticity field, the quanta of which are phonons. Similarly, the noncommutativity of the components of the spins of each lattice site result in a quantized spin density field, the quantized excitations of which are called magnons. Following the canonical quantization procedure, the classical spin fields become operator-valued: $\phi \to \hat{\phi}$, $\pi \to \hat{\pi}$ and $\mathbf{s}(\phi, \pi) \to \hat{\mathbf{s}}(\hat{\phi}, \hat{\pi})$, which act on a Hilbert space. The Poisson brackets become commutation relations:

$$\{s_i(\mathbf{x}), s_j(\mathbf{y})\}_p = i\epsilon_{ijk} s_k \delta(\mathbf{x}-\mathbf{y}) \to [\hat{s}_i(\mathbf{x}), \hat{s}_j(\mathbf{y})] = \delta(\mathbf{x}-\mathbf{y}) i\hbar \epsilon_{ijk} \hat{s}_k(\mathbf{y}) . \tag{1.23}$$

There exist several bosonic representations of the quantum spin-algebra, Eq. (1.23), including Schwinger bosons and the Dyson-Maleev and Holstein-Primakoff transformations. The latter two are useful in cases when quantum fluctuations are small and $\langle \hat{\mathbf{s}} \rangle$ is close to a well defined broken symmetry axis. We will employ extensively the Holstein-Primakoff transformation [HP40a], which is given by:

$$\hat{s}_{z'}(\mathbf{x}) = \hbar \left(\hat{\Phi}^\dagger(\mathbf{x}) \hat{\Phi}(\mathbf{x}) - s \right) \tag{1.24}$$

$$\hat{s}_-(\mathbf{x}) = \hbar \sqrt{2s - \hat{\Phi}^\dagger(\mathbf{x}) \hat{\Phi}(\mathbf{x})} \hat{\Phi}(\mathbf{x}) , \tag{1.25}$$

where $\hat{s}_\pm(\mathbf{x}) = \hat{s}_{x'}(\mathbf{x}) \pm i \hat{s}_{y'}(\mathbf{x})$, and the coordinate system $\mathcal{S}'$ (with orthonormal unit vectors $\mathbf{x}'$, $\mathbf{y}'$ and $\mathbf{z}'$) is arbitrary. Provided that $\hat{\Phi}(\mathbf{x})$ is a bosonic field satisfying

$$[\hat{\Phi}(\mathbf{x}), \hat{\Phi}^\dagger(\mathbf{y})] = \delta(\mathbf{x}-\mathbf{y}) , \tag{1.26}$$

it straightforward to show that the Holstein-Primakoff transformation satisfies the spin-algebra, Eq. (1.23). Eqs. (1.24) and (1.25) suggest that the quanta of the field $\hat{\Phi}$, (Holstein-Primakoff) magnons, carry a quantum of angular momentum equal to $\hbar$ in the $+\mathbf{z}'$ direction.

A natural choice for the coordinate system $\mathcal{S}'$ is $\mathbf{z}' = \mathbf{z}$, where $\mathbf{z}$ is the symmetry axis of the magnet. Global rotations of the $x' - y'$ coordinate system around this symmetry axis by an angle ϕ_0 correspond to a U(1) rotation on Holstein-Primakoff field operator: $\hat{\Phi} \to \hat{\Phi} e^{-i\phi_0}$.

The Hamiltonian $\mathcal{H}$, Eq. (1.8), becomes an operator on the Hilbert space, and by rotational symmetry around the z axis, may be expanded in global U(1) invariant combinations of operators, such as $\hat{n} = \hat{\Phi}^\dagger \hat{\Phi}$. To lowest order in field operators, one has the noninteracting Hamiltonian:

$$\hat{\mathcal{H}} = \int d^3x \hat{\Phi}^\dagger (\mathbf{x}) \mathfrak{h} (\mathbf{x}) \hat{\Phi} (\mathbf{x}) \tag{1.27}$$

where $\mathfrak{h} (\mathbf{x}) = \hbar\Omega - A\nabla^2$ is the first quantized noninteracting Hamiltonian. The equation of motion for $\hat{\Phi} (\mathbf{x}, t)$ in the Heisenberg picture is then:

$$i\hbar\partial_t \hat{\Phi} = \mathfrak{h} (\mathbf{x}) \hat{\Phi} , \tag{1.28}$$

yielding a free-particle spectrum $\hbar\omega_{\mathbf{k}} = \hbar\Omega + A\mathbf{k}^2$.

An alternative choice for the $\mathbf{z}'$ axis defining the Holstein-Primakoff transformation is to align $\mathbf{z}' = -\mathbf{n}$, so that magnons carry angular momentum quanta $-\hbar\mathbf{n}$. Denoting the Holstein-Primakoff field operator for this choice of coordinates by $\hat{\varphi} (\mathbf{x})$, we require $\langle \hat{\mathbf{s}}(\mathbf{x}) \rangle \propto \mathbf{n}(\mathbf{x})$ and therefore $0 = \langle \hat{s}_- (\mathbf{x}) \rangle \approx \hbar\sqrt{2s} \langle \hat{\varphi} (\mathbf{x}) \rangle$, so that the excitations $\hat{\varphi} (\mathbf{x})$ are incoherent, i.e. $\langle \hat{\varphi} (\mathbf{x}) \rangle = 0$. One finds, then, that $\langle \hat{\mathbf{s}} \rangle = \tilde{\mathbf{s}} = \tilde{s}\mathbf{n}$, where via Eq. (1.24) $\tilde{s} = s(1 - n/s)$, with $n = \left\langle \hat{\varphi}^\dagger \hat{\varphi} \right\rangle$ is the local magnon density.

The field operators $\hat{\Phi}(\mathbf{x})$ and $\hat{\varphi}(\mathbf{x})$ for the two coordinate systems described above are related by an SU(2) rotation, which may be written as follows. The local magnetic order parameter may be written $\mathbf{n} (\theta, \phi) = R (\pi - \theta, \phi) \cdot (-\mathbf{z})$, where $R (\pi - \theta, \phi)$ is a rotation matrix which rotates a vector by an angle $\pi - \theta$ around $\mathbf{r} = \sin\phi\mathbf{x} - \cos\phi\mathbf{y}$; correspondingly we may write:

$$\hat{\varphi} (\mathbf{x}, t) = \hat{R}^\dagger (t) \hat{\Phi} (\mathbf{x}, t) \hat{R} (t) = \hat{\Phi} (\mathbf{x}, t) - \Phi (\mathbf{x}, t) + \mathcal{O} \left[(\theta - \pi)^2 \right] \tag{1.29}$$

where

$$\begin{aligned} \hat{R}^\dagger (t) = & \exp \left[-i \int d^3y \left[\theta (\mathbf{y}, t) - \pi \right] \mathbf{r} (\mathbf{y}, t) \cdot \hat{\mathbf{s}} (\mathbf{y}, t) / \hbar \right] \\ \approx & \exp \left[\int d^3y \left(\Phi (\mathbf{y}, t) \hat{\Phi}^\dagger (\mathbf{y}, t) - \Phi^* (\mathbf{y}, t) \hat{\Phi} (\mathbf{y}, t) \right) \right] , \end{aligned} \tag{1.30}$$

the second quantized representation of R^{-1}, is a gauge transformation that unwinds the texture $\mathbf{n} (\theta, \phi)$, and $\Phi = \sqrt{s/2} e^{-i\phi} (\pi - \theta)$. Inserting $\hat{\Phi} = \Phi + \hat{\varphi}$ into the equation of

motion, Eq. (1.28), and taking the expectation value, one obtains Eq. (6.1) with ($K = 0$ and $\alpha = 0$); it follows then that the incoherent contribution to the magnetic dynamics obeys a Schroedinger equation of its own, with $i\hbar\partial_t\hat{\varphi} = \mathfrak{h}(\mathbf{x})\,\hat{\varphi}$ and thus exhibits the excitation spectrum $\hbar\omega_{\mathbf{k}} = \hbar\Omega + A\mathbf{k}^2$. To lowest order in the amplitudes Φ and $\hat{\varphi}$, the dynamics for the coherent magnetic texture $\tilde{\mathbf{s}}$ thus reproduces that of the classical theory, while quantum fluctuations, oscillating around this texture, are free particles independent of the coherent dynamics.

Rotational symmetry around the z axis of the magnet implies that the overall phase ϕ_0 of the gauge field $\Phi = \langle\, \hat{\Phi}\, \rangle$ spontaneously breaks U(1) symmetry, in analogy with a superfluid of bosonic particles wherein the boson field operator $\hat{\Psi}$ exhibits correlations in Fock space: $\Psi = \langle\, \hat{\Psi}\, \rangle$. There, the presence of superfluidity corresponds to the gauge transformation [Lan68]:

$$\hat{\Psi}(\mathbf{x},t) \to \hat{\psi}(\mathbf{x},t) = \hat{U}^\dagger(t)\,\hat{\Psi}(\mathbf{x},t)\,\hat{U}(t) = \hat{\Psi}(\mathbf{x},t) - \Psi(\mathbf{x},t) \tag{1.31}$$

with

$$\hat{U}^\dagger(t) = \exp\left[i\int d^3y\left(\Psi(\mathbf{y},t)\,\hat{\Psi}^\dagger(\mathbf{y},t) - \Psi^*(\mathbf{y},t)\,\hat{\Psi}(\mathbf{y},t)\right)\right] = \prod_{\mathbf{k}} e^{\alpha_{\mathbf{k}}\hat{a}^\dagger_{\mathbf{k}} - \alpha^*_{\mathbf{k}}\hat{a}_{\mathbf{k}}}\,, \tag{1.32}$$

where we have expanded $\hat{\Psi}(\mathbf{y}) = \sum_{\mathbf{k}} \hat{a}_{\mathbf{k}}(t)\,\psi_{\mathbf{k}}(\mathbf{y})/\sqrt{V}$ and $\Psi(\mathbf{y},t) = i\sum_{\mathbf{k}} \alpha_{\mathbf{k}}(t)\,\psi_{\mathbf{k}}(\mathbf{y})/\sqrt{V}$ in the orthonormal basis $\{\psi_{\mathbf{k}}\}$. Here $\hat{U}$ is a unitary transformation that rotates the vacuum state of bosons $|0\rangle$ into the product of coherent states $|\alpha_{\mathbf{k}}\rangle = e^{\alpha_{\mathbf{k}}\hat{a}^\dagger_{\mathbf{k}} - \alpha^*_{\mathbf{k}}\hat{a}_{\mathbf{k}}}|0\rangle$. Similarly, the operator $\hat{R}$ rotates the vacuum state of magnons (corresponding to a magnet with order parameter $\mathbf{n} = -\mathbf{z}$ and no fluctuations) into a dynamic, coherent state[2]. The operator $\hat{\psi}(\mathbf{x})$, defined so that $\langle\, \hat{\psi}(\mathbf{x})\, \rangle = 0$, corresponds to an incoherent cloud of bosons, which in equilibrium are described by a thermal distribution function. One of the hallmarks of superfluidity is the notion of phase-rigidity, which is expressed as the flow of particles in response to a phase gradient:

$$j = -\frac{\hbar}{m} n_c \nabla\phi\,, \tag{1.33}$$

[2]Indeed, a global rotation does not change internal state of a magnet; we may think of a monodomain magnet as a coherent state of Holstein-Primakoff magnons, when the Holstein-Primakoff axis no longer coincides with $\mathbf{n}$

where ϕ is the phase of the condensate wavefunction $\Psi = \sqrt{n_c}e^{-i\phi}$ and n_c is the condensate density. Similarly, for the ferromagnet, identifying $n_c = \sqrt{s\left(1+\cos\theta\right)}$ one obtains (for $\theta \lesssim \pi$) a magnon current from Eq. (1.21)

$$j = \frac{\mathbf{z}\cdot\mathbf{j}_i^{(s)}}{\hbar} = -\frac{2A}{\hbar}n_c\nabla\phi \tag{1.34}$$

where ϕ is the U(1) symmetry breaking order parameter phase in the $x-y$ plane. We shall therefore refer to small angle dynamics as "superfluid state" [BV10a, RZ69]. A caveat, however, is necessary. The transformation in Eq. (1.29) is carried out by neglecting the $\hat{\Phi}^\dagger\hat{\Phi}/s$ under the radical in the Holstein-Primakoff transformation, Eq. (1.25), which, as alluded to above, gives rise to interactions. These terms spoil the exact connection between a coherent state of Holstein-Primakoff magnons $e^{\alpha\hat{a}^\dagger-\alpha^*\hat{a}}\left|0\right\rangle$ and rotated state $e^{-i(\pi-\theta)\mathbf{r}\cdot\hat{\mathbf{s}}/\hbar}\left|0\right\rangle$. Fortunately, as shown in the Appendix, it is still possible to draw a direct connection between (interacting) Holstein-Primakoff magnons and an interacting gas of superfluid magnons.

Intimately related to the concept of superfluid is that of condensation, i.e. the macroscopic occupation of a single mode. Following Onsager and Penrose [PO56], we define the single-particle reduced density matrix $\rho\left(\mathbf{x},\mathbf{y}\right) = \left\langle\hat{\Phi}^\dagger\left(\mathbf{x}\right)\hat{\Phi}\left(\mathbf{y}\right)\right\rangle = \sum_{ij}\rho_{ij}\varphi_i^*\left(\mathbf{x}\right)\varphi_j\left(\mathbf{y}\right)$, where $\{\varphi_i\}$ form a complete set. By Hermiticity, ρ_{ij} may be diagonalized by an appropriate choice of eigenbasis, so $\rho\left(\mathbf{x},\mathbf{y}\right) = \sum_i\rho_i\varphi_i^*\left(\mathbf{x}\right)\varphi_i\left(\mathbf{y}\right) = \sum_i\rho_i\left(\mathbf{x},\mathbf{y}\right)$. When several of the values ρ_i are the same (e.g. the degenerate states of a thermal mixture) or similar for a subset s, destructive interference between the contributions of from this subset $\rho_i\left(\mathbf{x},\mathbf{y}\right)$ occurs, and $\sum_{i\in\mathrm{s}}\rho_i\left(\mathbf{x},\mathbf{y}\right)$ vanishes as $\left|\mathbf{x}-\mathbf{y}\right|\to\infty$. However, if $\rho_i \equiv \rho_c$ for a particular mode $\phi_i = \Phi$ is macroscopically occupied, the density matrix is coherent, exhibiting so-called off-diagonal long range order:

$$\rho\left(\mathbf{x},\mathbf{y}\right) = \Phi^*\left(\mathbf{x}\right)\Phi\left(\mathbf{y}\right) + \sum_{i\neq c}\rho_i\varphi_i^*\left(\mathbf{x}\right)\varphi_i\left(\mathbf{y}\right) \to \Phi^*\left(\mathbf{x}\right)\Phi\left(\mathbf{y}\right) \tag{1.35}$$

as $\left|\mathbf{x}-\mathbf{y}\right|\to\infty$, and a (simple) condensate is present. In the case of a ferromagnet, such off-diagonal long range order is a manifestation of ferromagnetic ordering, brought about by the exchange stiffness A which correlates the spin moments of the lattice over macroscopic distances at temperatures below T_c.

Condensation may spontaneously occur in weakly interacting thermal bosonic gases when the cloud of incoherent particles becomes oversaturated. Below the critical density, the distribution of bosonic particles obey a Bose-Einstein profile:

$$f\left(\epsilon_{\mathbf{k}}\right) = \frac{1}{e^{\beta(\epsilon_{\mathbf{k}}-\mu)}-1} \tag{1.36}$$

where $\mu < \min\left[\epsilon_{\mathbf{k}}\right]$. In the presence of a thermal bath which anchors the temperature, the injection of bosons results in an increase in the chemical potential. At a critical value of the density, the chemical potential becomes stuck at the bottom of the boson energy band, and any extra particles added relax via interactions into the ground state, shedding their excess energy to the thermal reservoir and forming a Bose-Einstein condensate. Bose-Einstein condensation, first realized in systems of ultracold atoms [AEM95], have now been observed in photons [KSV10, KSD11], exciton-polaritons[KRK06, KSA08], and, notably, in magnons.

Crucial to the formation of a Bose-Einstein condensate are interactions either with a thermal reservoir or between particles, which, while in the latter case sufficiently weak so as to preserve the notion of a single particle spectrum, must be strong enough to thermalize the gas to a Bose-Einstein profile [ZNG99]. In our treatment of the ferromagnetic Hamiltonian thus far, however, we have neglected higher order contributions to the Hamiltonian obtained by expanding the radical in the Holstein-Primakoff transformation, Eq. (1.25), which give rise to interactions between magnons, interactions between magnons and coherent texture, and nonlinear dynamics within the coherent texture itself (e.g. the interaction term in the Gross-Pitaevski equation, the last term in Eq. (6.1)). Three magnon processes allow for the exchange of angular momentum with the magnetic texture, resulting in a local torque on the magnetic order parameter. In addition, the spatial dependence of the texture $\mathbf{n}\left(\mathbf{x},t\right)$ through which magnons propagate introduces Berry phase effects into the magnon dynamics [KT12], as discussed above. At room temperature, the four-(thermal)magnon scattering rate for thermal magnons due to exchange anisotropy, $\tau_{\text{ex}}^{-1} \sim (T/T_c)^3(T/\hbar)$ near equilibrium [BDB14], is a factor of $\left(T/K\right)^2$ faster than that originating from the anisotropy K, as K is typically much smaller than T in experimental conditions (see Appendix). For a weakly spatially-dependent coherent magnetic texture, however, the dominant coupling between

the thermal cloud and superfluid component arises from anisotropy-induced three-(thermal) magnon scattering with a rate $\tau_{\rm an}^{-1} \sim (K/T)^2 \tau_{\rm ex}^{-1}$. Even in the presence of condensate and magnon-damping (which generally occurs at a rate much slower than thermalization due to exchange), then, to a good approximation the thermal magnon cloud may be treated as a quasi-equilibrium hydrodynamic object described by a generally local Bose-Einstein distribution function, Eq. (1.36), provided driving of the cloud is sufficiently weak that the cloud may come to an internal thermodynamic equilibrium or equilibrate with a bath. It follows that, under appropriate conditions, the gas of quasiequilibrium magnons may undergo Bose-Einstein condensation.

Bose-Einstein condensation of magnetic excitations was first observed in $TlCuCl_3$, where dimers of antiferromagnetically coupled spin 1/2 Cu^+ and Tl^- ions reside in a singlet ground state and a triplet excited state [RCF03]. The dimers are coupled via a relatively weak exchange interaction, so that triplet excitations of one dimer propagate. The resulting (bosonic) collective excitations of the system are called triplons, which, when the density (controlled by the magnetic field) reaches a critical value, Bose condense. More pertinently, Bose-Einstein condensation of magnons in a ferromagnet, such as those considered above, have been claimed to be observed [DDD06a, CMD09]. In [DDD06a] pulsed parallel pumping excites out-of-equilibrium magnons. Before the pumping, the magnon chemical potential $\mu = 0$, with $\min[\epsilon_{\mathbf{k}}] = \hbar\Omega > 0$, so that magnons are in normal phase. After the pulse is turned on and then off, magnon interactions relax the injected angular momentum much more quickly than the losses into the lattice by Gilbert damping, forming a (quasiequilibrium) gas with $0 < \mu \leq \min[\epsilon_{\mathbf{k}}]$ that persists on timescales below that provided by the damping. If the pumping is sufficiently strong, then the magnon density exceeds a critical value, wherein the excess angular momentum is transferred into the ground state, forming a Bose-Einstein condensate. In Chapter 3 we explore in detail the possibility of Bose-Einstein condensation induced by thermally assisted spin-transfer torque, the realization of which holds three key advantages over the pumped condensate. First, it can be created on-chip, without the need for a an external FMR field. Second, in principle the dc-driven condensate may persist on timescales much longer than the quasi-equilibrium condensates created

by ac pumping, providing greater opportunity to investigate condensate properties, such as thermal conductance and nonlocal transport. Last, the combination of spin-transfer torque and a thermal gradient allow for a greater degree of control over magnetic dynamics; in particular, the employment of a temperature gradient to induce coherent magnetic dynamics, which unites the fields of spin caloritronics with magnon condensation, provides a natural setting in which to investigate the thermal properties of a magnon condensate.

1.2 Semiclassical Electron Transport in Metals

We turn now to diffusive transport in metals, a proper understanding of which is essential to characterizing transport in spintronic devices.

1.2.1 Spin-Orbit Interaction

While the exchange and dipole interaction allows for the transfer of angular momentum between individual electrons, the manipulation of spin by an *external* field remains one of the central challenges in spintronics [NKW12, LPL12a, FUK14a]. One key ingredient, the spin-orbit interaction, has been proven to be particularly useful to this end over the past decade, which has seen the discovery of various large spin-orbit effects in a number of materials. Because it allows for the control of the spin degree of freedom by an electric rather than magnetic field, the spin-orbit interaction has become a key component in the development of scalable devices. Utilization of electric fields is preferable to that of magnetic fields (via Zeeman coupling) for two reasons. First, it allows for the possibility of direct integration of spintronic components into existing electronic architectures. Second, magnetic fields originate from electric currents and dipole moments. Both sources are notoriously difficult to scale as they create nonlocal fields. In contrast, electric fields are relatively easier to control locally and may be generated by, e.g., static biasing, rather than relying on magnets or energy-consuming electric currents.

By nature, the spin-orbit interaction is a relativistic effect that, rather surprisingly, may manifest in solid state physics. The fundamental interaction between an external field and

a single electron is governed by the Dirac equation, which in the nonrelativistic limit gives the Hamiltonian:

$$H = \frac{\left(\boldsymbol{p} + e\mathbf{A}\right)^2}{2m_0} - e\Phi + \frac{e\hbar}{2m_0}\boldsymbol{\sigma}\cdot\mathbf{B} + \frac{e\hbar}{4m_0^2c^2}\boldsymbol{\sigma}\cdot\mathbf{E}\times\mathbf{p} \tag{1.37}$$

The electron spin $\mathbf{s} = \hbar\boldsymbol{\sigma}/2$ interacts with the magnetic and electric fields through the third and fourth terms on the left-hand side of Eq. (1.37), respectively. The former is the Zeeman interaction, often written in terms of the electron $\boldsymbol{m} = (-e\hbar/2m_0)\,\boldsymbol{\sigma}$:

$$H_{\mathrm{zm}} = \frac{e\hbar}{2m_0}\boldsymbol{\sigma}\cdot\mathbf{B} = -\boldsymbol{m}\cdot\mathbf{B}\,, \tag{1.38}$$

which couples the electron magnetic moment to the external magnetic field $\mathbf{B}$. The fourth term on the left-hand side of Eq. (1.37),

$$H_{\mathrm{so}} = \frac{e\hbar}{4m_0\left(m_0c^2\right)}\boldsymbol{\sigma}\cdot\mathbf{E}\times\mathbf{p} = -\eta_{\mathrm{so}}^{(0)}\frac{e}{\hbar}\boldsymbol{\sigma}\cdot\mathbf{E}\times\mathbf{p} \tag{1.39}$$

is the spin-orbit interaction, which couples the translational motion of the electron to its spin through the electric field $\mathbf{E}$. Here $\eta_{\mathrm{so}}^{(0)} = -\left(\hbar/2m_0c\right)^2$ is the spin-orbit parameter in vacuum. At nonrelativistic speeds, the value of the effective spin-orbit magnetic field $\mathbf{B}_{\mathrm{so}} = -\mathbf{E}\times\mathbf{p}/2m_0c^2$ is negligible compared to typical applied magnetic fields. In a solid-state environment, where $\eta_{\mathrm{so}}^{(0)}$ is renormalized by the band structure to a material dependent value, the situation may be very different. From $k\cdot p$ perturbation theory, the Dirac gap $2m_0c^2 \sim$ MeV (i.e. the energy required to create a stationary electron/positron pair) is replaced in Eq. (1.39) by the electronic band gap, which may be many orders of magnitude smaller, resulting in an enhanced spin orbit parameter η_{so} [Win03]. Consequently, in many metals, insulators and semiconductors, the spin-orbit interaction is crucial to understanding the coupled dynamics of electrons and their spins.

Spin orbit effects appear in variety of solid-state contexts. The earliest experimental signatures of the spin-orbit interaction date back to the 1880's, when Hall noted that currents normal to applied electric and magnetic fields were enhanced by a factor of ten in ferromagnetic iron compared to nonmagnetic metals. In contrast to the normal Hall effect in nonmagnetic metals, where the transverse (with respect to the electric and magnetic

field) conductance increases linearly from zero in the applied magnetic field, it was noted a decade after Hall that in certain ferromagnetic metals the transverse conductance saturates at high magnetic field to a value proportional to the magnetization [NSO10]. Only later was it realized that this so called extraordinary Hall effect did not originate from interaction of electrons with the magnetic field but with the magnetization (via the spin-orbit interaction) and that the linear relationship (at low magnetic field) between the extraordinary Hall conductance and applied field stems from tendency of magnets to break into domains, destroying the macroscopic magnetic order and hence the transverse current; remarkably, in monodomain ferromagnets, the effect persists at zero magnetic field. Starting in the 1950's, the precise mechanism of the extraordinary Hall effect, now called the anomalous Hall effect (AHE), was a point of debate. Karplus and Looting [KL54] proposed that the origin of the AHE is the anomalous velocity, a momentum space Berry phase [Ber84] effect arising from the spin-orbit coupling of bands. This intrinsic mechanism, however, neglects the role of impurities. Smit [Smi58], meanwhile, argued for asymmetric (skew) scattering off impurities, while later Berger forwarded the side jump mechanism [Ber70].

In the AHE, a current in the direction of an the applied electric field generates a transverse electrical current via spin-orbit interactions, the spin Hall effect refers to the generation of transverse spin currents, which in microstructures manifests as a nonequilibrium spin accumulation along the structures interface. In contrast to the AHE, which requires the presence of an equilibrium magnetic ordering to realize a transverse electric current (and by virtue of the fact that electrons are spin polarized by the exchange field, a spin current), the spin Hall effect (SHE) and inverse spin Hall effect (ISHE) may occur in a normal (i.e. nonmagnetic) metal. As in the AHE, the SHE may have both intrinsic and extrinsic contributions. The intrinsic contribution arises from the Berry curvature of the band structure, which gives rise to an anomalous velocity $\dot{\mathbf{v}}\left(\mathbf{k}_p\right) = -\hbar\dot{\mathbf{k}}_p \times \mathbf{b}\left(\mathbf{k}_p\right)$ for a wavepacket with momentum $\mathbf{k}_p$. Here, $\mathbf{b}\left(\mathbf{k}\right)$ is the Berry curvature of the Bloch state of quasimomentum $\mathbf{k}$ [SN99, Nag06]. In certain metals, such as Pt [KOS07, GMC08], the intrinsic mechanism is the dominant contribution to the spin Hall physics. Following Takahashi and Maekawa [TM08a, MVS12], we shall consider here the extrinsic mechanism, i.e. the spin-dependent

scattering of electrons off of nonmagnetic impurities which results in the translation of charge currents into spin currents and vice versa, yielding the same type of drift-diffusion transport equations as the intrinsic mechanism. We will generalize [MVS12] to include magnetic order (so as to capture the extrinsic AHE) and thermoelectric effects; from a single, semiclassical framework, we will attempt to delineate the many animals of the zoo magnetoelectric and thermomagnetoelectric effects.

1.2.2 Drift-Diffusion Model in the Presence of Extrinsic Spin-Orbit Effects

Consider a monodomain Stoner model with a magnetic order parameter oriented in the direction $\mathbf{n}$, with $\mathbf{n}$ as a unit vector (which here we take to be uniform in space), which defines the quantization axis for electrons. The conduction electrons experience an effective exchange field Δ. The energies of electrons with spin oriented in the $+\mathbf{n}$ ($s =\uparrow$) and $-\mathbf{n}$ ($s =\downarrow$) are shifted by $-\Delta$ and $+\Delta$, respectively. The spectrum of an electron with quasi-momentum $\mathbf{k}$ and spin in the direction s is then equal to $E^{(s)}_{\mathbf{k}} = \epsilon_{\mathbf{k}} - \sigma\Delta$, where we have dropped the band index. For simplicity, we will take the conduction electrons to be free particles, with $\epsilon_{\mathbf{k}} = \hbar\mathbf{k}^2/2m$, where m is the effective electron mass. The spin-resolved electronic distribution function may be written as:

$$\check{f}_{\mathbf{k}} = \sum_{\mathbf{k}s=\pm} \check{u}_s f_{\mathbf{k}s} \tag{1.40}$$

where the $.\check{}.$ denotes 2×2 spin structure, and

$$\check{u}_s = \frac{\check{1} + s\mathbf{n}\cdot\check{\boldsymbol{\sigma}}}{2}, \tag{1.41}$$

is the spin-projection operator, with $\check{\boldsymbol{\sigma}}$ as a unit vector of Pauli matrices. In equilibrium, in the absence of spin-orbit effects, the distribution function is given by:

$$f_{\mathbf{k}s} = f^{(e)}_{\mathbf{k}s} \equiv \frac{1}{e^{\beta_e(\epsilon_{\mathbf{k}} - s\Delta - \epsilon_F)} + 1} = \frac{1}{e^{\beta_e\left(\epsilon_{\mathbf{k}} - \epsilon^s_F\right)} + 1}\,, \tag{1.42}$$

where $\beta_e = 1/T_e$ is the inverse (uniform) equilibrium temperature and ϵ_F is the common Fermi energy, while $\epsilon^{(s)}_F = \epsilon_F + s\Delta = \hbar(k^{(s)}_F)^2/2m$ is the effective spin-dependent Fermi surface, which defines the spin-dependent Fermi momentum $k^{(s)}_F = \sqrt{2m\left(\epsilon_F + s\Delta\right)/\hbar}$. (See Fig. 1.1).

Suppose there are N identical impurities distributed throughout the metal at positions $\{\mathbf{r}_i\}$, with $i = 1 \ldots N$. The associated Hamiltonian is given by:

$$\hat{\mathcal{H}} = \hat{\mathcal{H}}_0 + \hat{V}\,, \tag{1.43}$$

where $\hat{\mathcal{H}}_0 = \hat{p}^2/2m$ and $\hat{V}$ is the impurity potential, which, in the position representation is given by:

$$\check{V}(\mathbf{r}) = \sum_i^N \check{U}(\mathbf{r} - \mathbf{r}_i) \tag{1.44}$$

where

$$\check{U}(\mathbf{r}) = u(\mathbf{r})\,\check{1} + \eta_{\rm so}\check{\boldsymbol{\sigma}} \cdot \frac{\nabla u \times \nabla}{i} \tag{1.45}$$

and $u(\mathbf{r})$ is the effective impurity potential. For simplicity, we take the $u(\mathbf{r})$ to be a delta function in space, with $u(\mathbf{r}) = u_{\rm imp}\delta(\mathbf{r})$.

Electrons interact with impurities through two mechanisms. The first is called side-jump scattering [LH72]. Consider the velocity operator in the vicinity of a single impurity, which in the position representation is given by:

$$\check{\mathbf{v}} = \frac{i}{\hbar}\left[\check{\mathcal{H}}, \mathbf{r}\right] = \frac{\hbar\nabla}{im} + \frac{\eta_{\rm so}}{\hbar}\check{\boldsymbol{\sigma}} \times \nabla u\,. \tag{1.46}$$

The second term in Eq. (1.46) is called the anomalous velocity operator, which, upon tracing over spin indices, depends on the spin orientation of the electron. Thus electrons with opposite spin polarities experience opposite anomalous velocities as they scatter off of an impurity potential, resulting in a spin-dependent displacement (see left panel of Fig. 1.2). Over the course of many such collisions, an electron with a given spin experiences several displacements, translating into spin-dependent velocity. In the born approximation, $|k^+ s\rangle = |ks\rangle + \sum_{k' \neq k} \frac{u_{k'k}}{\epsilon_k - \epsilon_{k'} + i\delta}|k's\rangle$, the impurity-averaged velocity operator $(\check{\mathbf{v}}_{\mathbf{k}})_{ss'} \equiv \langle k^+ s|\,\mathbf{v}\,|k^+ s'\rangle$ can be written:

$$\check{\mathbf{v}}_{\mathbf{k}} = \check{1}\mathbf{v}_{\mathbf{k}} + \sum_s \check{u}_s \mathbf{v}'_{\mathbf{k}s} \tag{1.47}$$

where $\mathbf{v}_{\mathbf{k}} = \mathbf{k}/m$ is the electronic velocity, $\mathbf{v}'_{\mathbf{k}s} = \alpha_{\rm SJ}^{(s)} s\mathbf{n} \times \mathbf{v}_{\mathbf{k}}$ is the anomalous velocity, and $\alpha_{\rm SJ}^{(s)} = \hbar\bar{\eta}_{\rm so}^s/2K_F^s\tau_s$ is the side-jump spin Hall angle, with $\bar{\eta}_{\rm so}^{(s)} = (k_F^{(s)})^2\eta_{\rm so}$ as the unitless spin-orbit parameter, $K_F^{(s)} = (\hbar k_F^{(s)})^2/2m$ as the kinetic Fermi energy for the $s-$band, $\tau_s =$

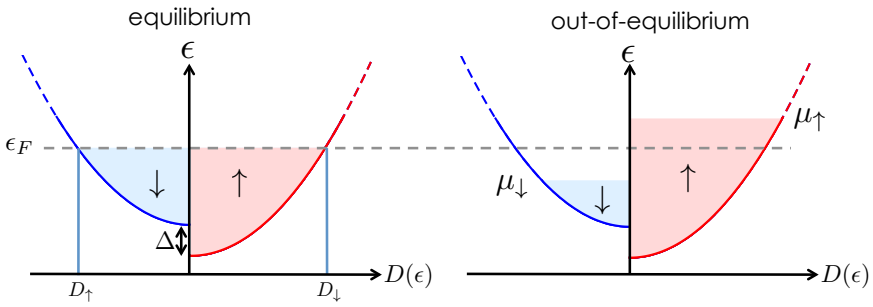

Figure 1.1: Equilibrium and nonequilibrium spin-dependent distributions of electrons in a metallic metal. Spin-injection or spin-orbit effects generally give rise to spin-dependent out-of-equilibrium chemical potentials.

$D_s(2\pi/\hbar)\left|u_{\rm imp}\right|^2 n_{\rm imp}$ as the relaxation time due to disorder scattering, $n_{\rm imp}$ as the impurity density, and D_s as the spin-s Fermi level density of states.

The second mechanism by which spin-orbit effects alter electronic dynamics, called skew scattering, is, roughly speaking, the spin-dependent change in momentum of an electron as it leaves the scattering region of each impurity (represented in the right panel of Fig. 1.2), altering the distribution function. This may be captured by the semi-classical Boltzmann equation:

$$\partial_t \check{f}_{\mathbf{k}} + \mathbf{v}_{\mathbf{k}} \cdot \nabla \check{f}_{\mathbf{k}} - \frac{e\mathbf{E}}{\hbar} \nabla_{\mathbf{k}} \cdot \check{f}_{\mathbf{k}} = \left(\partial_t \check{f}_{\mathbf{k}}\right)_{\rm imp}, \tag{1.48}$$

with $(\partial_t \hat{f}_{\mathbf{k}})_{\rm imp}$ as the collision integral due to impurity scattering. Projecting onto the quantization axis $\mathbf{n}$, we obtain form Fermi's Golden Rule:

$$\partial_t f_{\mathbf{k}s} = \sum_{ks'} \left[P^{ss'}_{kk'} f_{\mathbf{k}s'} - P^{s's}_{k'k} f_{\mathbf{k}s} \right] \tag{1.49}$$

where is the scattering rate from the state $\mathbf{k}'s'$ into the state $\mathbf{k}s$, which to order $u^2_{\rm imp}$ and $u^3_{\rm imp}$, $P^{ss'}_{kk'} = P^{(1)s's}_{k'k} + P^{(2)s's}_{k'k}$, are given by

$$P^{(1)s's}_{k'k} = \frac{2\pi}{\hbar} \frac{\left|u_{\rm imp}\right|^2}{V} n_{\rm imp} \delta_{\sigma\sigma'} \delta\left(\epsilon_k - \epsilon_{k'}\right) + \frac{2\pi}{\hbar} \frac{\left|u_{\rm imp}\right|^2}{V} n_{\rm imp} \left|\boldsymbol{s}_{s's} \cdot \mathbf{k}' \times \mathbf{k} \eta_{\rm so}\right|^2 \delta\left(\epsilon^{(s)}_k - \epsilon^{(s')}_{k'}\right) \tag{1.50}$$

and

$$P^{(2)s's}_{k'k} = -\frac{(2\pi)^2}{\hbar} \boldsymbol{\sigma}_{s's} \cdot \mathbf{k}' \times \mathbf{k} \eta_{so} \frac{\left|u_{imp}\right|^2 u^*_{\rm imp}}{V} n_{\rm imp} D_s \delta_{ss'} \delta\left(\epsilon^{(s)}_k - \epsilon^{(s')}_{k'}\right). \tag{1.51}$$

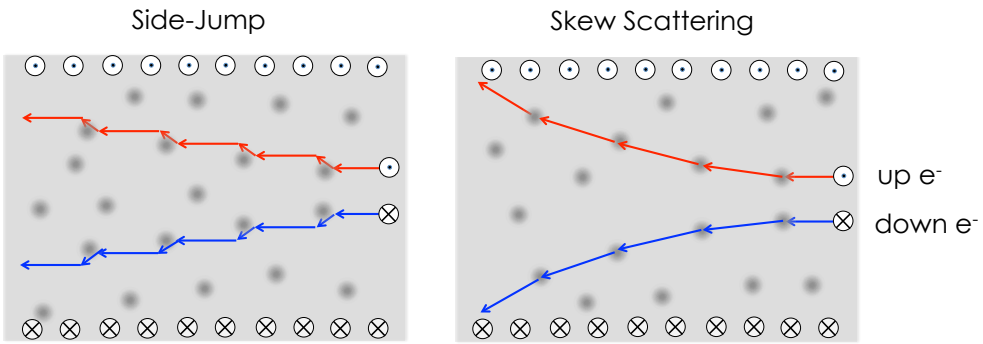

Figure 1.2: Sketch of the side jump and skew scattering mechanisms. In the former, electrons acquire an anomalous velocity in the vicinity of the impurities, which translates to a lateral velocity over many such interactions. In skew scattering, the distribution of momenta is skewed by scattering.

We solve the kinetic equation, Eq. (1.48), by writing

$$f_{\mathbf{k}s} = f^0_{\mathbf{k}s} + g^{(1)}_{\mathbf{k}s} + g^{(2)}_{\mathbf{k}s} \tag{1.52}$$

where $g^{(1)}_{\mathbf{k}s}$ and $g^{(2)}_{\mathbf{k}s}$ are corrections of orders $u^2_{\rm imp}$ and $u^3_{\rm imp}$, respectively, and

$$f^0_{\mathbf{k}s} = \frac{1}{e^{\beta\left(\epsilon_{\mathbf{k}} - \mu_s - \epsilon^s_F\right)} + 1}\,, \tag{1.53}$$

with μ_s as the out-of-equilibrium spin-dependent chemical potential and $\beta^{-1} = T(\mathbf{r}) = T_e + \delta T(\mathbf{r})$[3] as the local temperature. To lowest nontrivial order in $u_{\rm imp}$ (and zeroth order in $\bar{\eta}_{\rm so}$) and in the bias ($\propto \nabla f^{(0)}_{\mathbf{k}s'}$), we find that, in steady state:

$$g^{(1)}_{\mathbf{k}\sigma} = -\tau_\sigma \mathbf{v}_k \cdot \nabla f^{(0)}_{\mathbf{k}\sigma}\,, \tag{1.54}$$

while to the next order in $u_{\rm imp}$

$$\begin{aligned} g^{(2)}_{\mathbf{k}s} = \frac{\sum_{\mathbf{k}'s'} P^{(2)ss'}_{\mathbf{k}\mathbf{k}'} g^{(1)}_{\mathbf{k}'s}}{\sum_{\mathbf{k}'s'} P^{(1)s's}_{\mathbf{k}'\mathbf{k}}} &= \sum_{\mathbf{k}'s'} \left[2\pi \boldsymbol{\sigma}_{ss} \cdot \mathbf{k}' \times \mathbf{k} \eta_{so} u^*_{imp} \delta\left(\epsilon^s_k - \epsilon^{s'}_{k'}\right)\right] \tilde{\tau}_s \mathbf{v}_{k'} \cdot \nabla_x f^0_{k's} \\ &\approx \alpha^{(s)}_{\rm SS} \tau_s s \mathbf{v}_{\mathbf{k}} \cdot [\mathbf{n} \times \nabla f_{k\sigma}] \end{aligned} \tag{1.55}$$

where $\alpha^s_{\rm SS} = (2\pi/3)\bar{\eta}^s_{\rm so} u_{\rm imp} D_s$ is the spin Hall angle due to skew scattering. The corrections $g^{(1)}_{\mathbf{k}s} = -g^{(1)}_{-\mathbf{k}s}$ and $g^{(2)}_{\mathbf{k}s} = -g^{(2)}_{-\mathbf{k}s}$ are asymmetric in $\mathbf{k}$-space (so that the local density is given

[3] The temperatures of the two spin species are generally equal due to strong interspin and electron-phonon scattering [HBZ07]

by the $\mathbf{k}$-space integral of $f^0_{\mathbf{k}s}$) and therefore contribute to neither the particle or spin density, with latter containing contributions from both the equilibrium $(D_\uparrow - D_\downarrow)$ and nonequilibrium $(\mu_\uparrow - \mu_\downarrow)$ contributions.

Let us define the spin-resolved current density:

$$\check{\mathbf{j}}_n \equiv \frac{1}{\mathcal{V}} \sum_{\mathbf{k}} \left(\epsilon_k - \check{\epsilon}_F\right)^n \check{f}_{\mathbf{k}} \check{\mathbf{v}}_{\mathbf{k}} \,. \tag{1.56}$$

with $\check{\epsilon}_F = \sum_s \check{u}_s \epsilon_F^{(s)}$. Denoting the out-of-equilibrium quantities by $\mathbf{X} = (\mu_\uparrow, \mu_\downarrow, \delta T)$, we obtain using Eq. (1.47) and Eqs. (1.48)-(1.56):

$$\check{\mathbf{j}}_n = \sum_s \left(\check{L}^{(n)}_{X_s} \nabla X_s + \check{L}^{(n)}_{X_s \mathrm{so}} \mathbf{n} \times \nabla X_\sigma \right) \tag{1.57}$$

where $\check{L}^{(n)}_{X_s} = \check{u}_s L^{(n)}_{X_s \mathrm{so}}$ and

$$L^{(n)}_{X_s} = -\frac{1}{V} \sum_{\mathbf{k}} \left(\epsilon^s_k - \epsilon_F\right)^n \tau_s v^2_{j\mathbf{k}} \left(\partial_{X_s} f^0_{ks}\right)\big|_e \tag{1.58}$$

is the linear response coefficient characterizing diffusive transport in the absence of spin-orbit effects, while $\check{L}^{(n)}_{X_s} = \check{L}^{(n)}_{X_s} \left(\alpha^s_{\mathrm{SJ}} + \alpha^s_{\mathrm{SS}}\right)$ is the linear response coefficient stemming from spin-orbit effects.

1.2.3 Anomalous and Spin Hall Effects

Consider transport due to an electric field $\mathbf{E}$, with no temperature gradient. Then,

$$X_s = \mu_s = \mu + s\frac{\delta\mu}{2} \,, \tag{1.59}$$

where $\mu = \left(\mu_\uparrow + \mu_\downarrow\right)/2 = -eV$ is the nonequilibrium electrochemical potential and $\delta\mu = \mu_\uparrow - \mu_\downarrow$, the nonequilibrium spin accumulation. An electric field engenders charge transport, which (due to the polarization of the ferromagnet and spin-orbit effects) translates into a spin current and thereby, in the presence of boundaries, a boundary spin accumulation μ'. First, the charge current $\mathbf{j}_q$ is given by:

$$\mathbf{j}_q = (-e)\,\mathrm{Tr}[\check{\mathbf{j}}_0] = \sigma_0 \frac{\nabla\mu}{e} + P\sigma_0 \nabla \frac{\delta\mu}{2e} + P_{\mathrm{so}}\sigma_{\mathrm{so}} \mathbf{n} \times \frac{\nabla\mu}{e} - \sigma_{\mathrm{so}} \nabla \times \frac{\boldsymbol{\mu}}{2e} \tag{1.60}$$

where $\sigma_0 = \sigma_\uparrow + \sigma_\downarrow$ is the total conductivity,

$$\sigma_s = -e^2 L_{\mu_s}^{(0)} = e^2 \frac{1}{V} \sum_{\mathbf{k}} g\tau_s v_{j\mathbf{k}}^2 \frac{e^{\beta\left(\epsilon_{\mathbf{k}}^{(s)} - \epsilon_F\right)}}{\left[e^{\beta\left(\epsilon_{\mathbf{k}}^{(s)} - \epsilon_F\right)} + 1\right]^2} \frac{1}{T} \approx e^2 \frac{\tau_s}{m} \frac{(2/3)}{(2\pi)^2} {k_F^{(s)}}^3 \tag{1.61}$$

is the dc conductivity for the band s, $P = (\sigma_\uparrow - \sigma_\downarrow)/(\sigma_\uparrow + \sigma_\downarrow)$ is the ferromagnetic polarization, $\sigma_s^{(\mathrm{so})} = \alpha_{\mathrm{SH}}^s \sigma_s$ is the spin-orbit conductivity, $P_{\mathrm{so}} = (\sigma_\uparrow^{(\mathrm{so})} - \sigma_\downarrow^{(\mathrm{so})})/(\sigma_\uparrow^{(\mathrm{so})} + \sigma_\downarrow^{(\mathrm{so})})$, is the spin-orbit polarization, and $\boldsymbol{\mu} = \mathbf{n}\delta\mu$, vectorial spin accumulation. The so called spin Hall angle $\alpha_{SH}^s = \alpha_{SJ}^s + \alpha_{SS}^s = \tan\theta$ quantifies the angle θ between the charge and deflected spin current (when the latter is expressed in units of charge current). The first term on the right-hand side in Eq. (1.60) is the standard expression for conductance in the presence of disorder, while the second term corresponds to spin diffusion that, because spin is accompanied by charge in a ferromagnet, yields a charge current $P\sigma_0 \nabla\delta\mu/2e$. The third term is the deflection of electric current $\sigma_0 \mathbf{E}$ in a direction normal to the magnetic order $\mathbf{n}$ due to spin orbit scattering, i.e. the extrinsic anomalous Hall effect. The last term on the right-hand side is the generation of a charge current $\propto \mathbf{n} \times \nabla(\delta\mu)$ normal to the magnetic order from a spin current, i.e. the ISHE. Notice that the side-jump conductivity $\sigma_s^{(\mathrm{SJ})} = \alpha_{SJ}^s \sigma_s = e^2 \hbar \bar{\eta}_{so}^s (2/3) {k_F^{(s)}}^3 / 2mK_F^s (2\pi)^2$ is independent of both the impurity density and strength, whereas the skew scattering conductivity $\sigma_s^{(\mathrm{SS})} = \alpha_{\mathrm{SS}}^s \sigma_s = (2/3)^2 \bar{\eta}_{so}^s e^2 \left(k_F^s\right)^3 D_s^2 \left|u_{\mathrm{imp}}\right|^2 u_{\mathrm{imp}} n_{\mathrm{imp}} / 2\hbar m$ depends on both.

Second, the spin current $\mathbf{j}_i^{(s)}$ (flux of spin oriented in the direction i) is given by:

$$e\frac{\mathbf{j}_i^{(s)}}{\hbar/2} = \mathrm{Tr}\left[\check{\mathbf{j}}_0 \check{\sigma}_i\right] = P\sigma_0 \frac{\nabla\mu}{e} n_i + \sigma_0 \nabla \frac{\mu_i}{2e} + \sigma_{\mathrm{so}} n_i \mathbf{n} \times \frac{\nabla\mu}{e} + P_{\mathrm{so}} \sigma_{\mathrm{so}} \mathbf{n} \times \frac{\nabla\mu_i}{2e} \tag{1.62}$$

While the second term is corresponds to spin diffusion, the first gives the spin flux that accompanies charge current in a polarized magnet. The last term is the spin analog to the AHE, i.e. the deflection of a spin current into a direction normal to the magnetic order. The third term is the SHE [DP71b, DP71a, Hir99], i.e. the generation of a spin current, flowing normal to the applied field, from a charge current. It should be understood that while the AHE is well defined in bulk, the SHE and ISHE are usually understood as the accumulation of spin and charge, respectively, at the edges of a heterostructure; a proper characterization of either phenomena must involve appropriate boundary conditions in conjunction with the bulk transport equations, Eqs. (1.60) and (1.62).

Third, let us consider the heat current density, which is:

$$\dot{\mathbf{Q}} = \mathrm{Tr}[\hat{\mathbf{j}}_1] = \sum_s \left[\sigma_s \Pi_s \left(\frac{\nabla\mu}{e} + s\nabla\frac{\delta\mu}{2e} \right) + s\sigma_s \Pi_s \alpha^s_{\mathrm{SH}} \mathbf{n} \times \left(\frac{\nabla\mu}{e} + s\nabla\frac{\delta\mu}{2e} \right) \right] \tag{1.63}$$

where

$$\sigma_s \Pi_s \equiv e L^{(1)}_{\mu_s} = -e\frac{1}{V}\sum_{\mathbf{k}} \tau_s v^2_{j\mathbf{k}} \frac{e^{\beta\left(\epsilon^s_{\mathbf{k}} - \epsilon_F\right)}}{[e^{\beta\left(\epsilon^s_{\mathbf{k}} - \epsilon_F\right)} + 1]^2} \tag{1.64}$$

is the spin-dependent Peltier coefficient [GSR06, FBS12]. The appearance of a heat current $\propto \mathbf{n} \times \nabla\mu/e = \mathbf{n} \times \mathbf{E}$ (third term in Eq. (1.63)) normal to both the magnetic order and the electric field manifests as a temperature gradient across the sample normal to the applied electric field, known as the anomalous Ettingshausen effect [HK13].

1.2.3.1 Spin Hall Effect in a Normal Metal

While the above equations are derived for a conducting ferromagnet with a well defined magnetization direction $\mathbf{n}$, the extrinsic SHE and ISHE occur in normal metals (nonmagnetic conductors) and semiconductors [Hir99, Zha00, TS06] when doped with heavy nonmagnetic impurities, such as Pt, with large spin-order parameter η_{so}. For the remainder of this subsection, let us focus on the SHE in normal metals. Indeed, in a normal metal where the exchange field Δ and the magnetic polarizations P and P_{SO} vanish, the charge is:

$$\mathbf{j}_q = \sigma_0 \frac{\nabla\mu}{e} - \sigma_{\mathrm{so}} \nabla \times \frac{\boldsymbol{\mu}}{2e} \tag{1.65}$$

while the i-spin current flowing in the direction j is:

$$\frac{j^{(s)}_{ji}}{\hbar/2} = -\frac{\sigma_0}{2e^2}\partial_j \mu_i - \frac{\sigma^{SH}_0}{e^2}\epsilon_{jik}\partial_k \mu \tag{1.66}$$

In a normal metal, all of the linear response coefficients (e.g. Π_σ) no longer depend on the spin polarization, so the heat current becomes:

$$\dot{\mathbf{Q}} = \sigma_0 \Pi \frac{\nabla\mu}{e} - \sigma_0 \alpha_{SH} \Pi \nabla \times \frac{\boldsymbol{\mu}}{2e} \tag{1.67}$$

where $\Pi = 2\Pi_\sigma$.

Note that Eqs. (1.65) and (1.66) do not explicitly depend on a quantization axis $\mathbf{n}$; rather, the spin accumulation $\boldsymbol{\mu}$ is created by the electric field, and must be obtained by solving

Eqs. (1.65) and (1.66) in conjunction. As an example, consider a film of thickness d_N in the z -direction and extending indefinitely in the $x-y$ plane (see Fig. 1.3). While charge is locally conserved ($\nabla \cdot \mathbf{j}_q + \dot{\rho}_q = 0$, where ρ_q is the charge density), spin-flip processes [Asi66] (which are captured by including terms higher order in $\bar{\eta}_{SO}$ in the drift-diffusion model above) result in a decay of the electron spin density $\mathbf{s}$:

$$\sum_j \partial_j j_{ji}^{(s)} + \dot{s}_i = -\frac{s_i}{\tau_{\rm sf}}\,, \tag{1.68}$$

where $\tau_{\rm sf}$ is the spin-flip times. Using $\mathbf{s} = (\hbar/2)\, D_F \delta\mu$ and Eq. (1.65), we therefore find in steady-state that

$$\nabla^2 \boldsymbol{\mu} = \frac{1}{\lambda_{\rm sf}^2}\boldsymbol{\mu}\,, \tag{1.69}$$

where $\lambda_{\rm sf} = \sqrt{\tau_{\rm sf}\sigma_0/D_F e^2}$ is the spin diffusion length. If an electric field $\mathbf{E} = \nabla\mu/e$ is applied in the plane of the film, then the steady-state spin accumulation is found by imposing boundary conditions on the solutions to Eq. (1.69). If spin is prohibited from crossing both the bottom ($z = 0$) and upper ($z = d_N$) surface of the normal metal (which is the case when the spin Hall material is interfaced with either vacuum or a poor spin sink metal such as Cu, with $\lambda_N^{(Cu)} \gg \lambda_N$), the induced spin accumulation is normal to both the plane of the film and the applied electric field, and as a consequence of translational invariance in the film, dependent only on the coordinate z:

$$\boldsymbol{\mu}\,(z) = 2e\lambda_{\rm sf}\alpha_{SH} f_{d_N/\lambda_{\rm sf}} (e^{z/\lambda_{\rm sf}} - e^{-(z-d_N)/\lambda_{\rm sf}}) \mathbf{z} \times \mathbf{E}, \tag{1.70}$$

where $f_{d_N/\lambda_{\rm sf}} = (e^{d_N/\lambda_{\rm sf}} - 1)/(e^{2d_N/\lambda_{\rm sf}} - 1)$. Via Eq. (1.65) the induced spin accumulation results in an induced charge current $\propto \nabla \times \boldsymbol{\mu}$. The thickness-averaged charge current density can be written as $\bar{\mathbf{j}}_q = (\sigma_0 + \delta\sigma)\mathbf{E}$, where $\delta\sigma = -2\sigma_0\alpha_{SH}^2 f_{d_N/\lambda_{\rm sf}} \left(1 - e^{d_N/\lambda_{\rm sf}}\right)(d_N/\lambda_{\rm sf})$ is the spin Hall correction to the structural conductance of the film [VSC13]. Using Eq (1.67), one obtains a (thickness-averaged) Peltier heat current in the direction of the electric field: $\dot{\bar{\mathbf{Q}}} = \sigma_0(\Pi + \delta\Pi)\mathbf{E}$, with $\delta\Pi = \Pi(\delta\sigma/\sigma_0)$.

The spin Hall effect in normal metals plays a central role in this thesis, both implicitly and explicitly. We will in particular be concerned with insulating magnets interfaced with normal metals. First, the spin Hall effect is crucial to the electrical control of magnetic

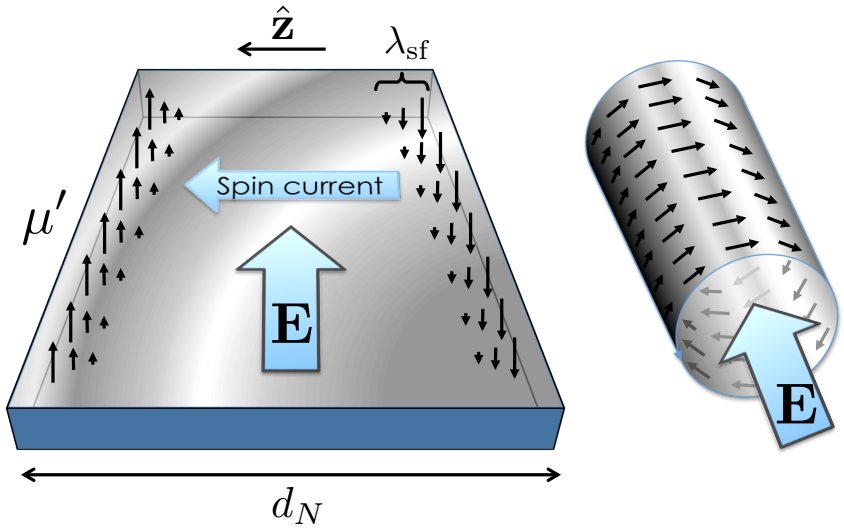

Figure 1.3: Spin Hall effect, Eq. (1.66), in planar and cylindrical geometries. Under the application of an electric field, and charge current flows, resulting in a transient spin flow that accumulates (μ') on the edges of the metals. (Omitted from the schematic of the planar geometry for visual clarity is the spin accumulation on the top and bottom surfaces).

dynamics in the insulator, for which Eqs (1.65)-(1.66) are essential. Second, even in the absence of an applied field $\mathbf{E}$ in the normal metal, the diffusive spin dynamics in the normal metal due to magnetic dynamics requires the full machinery of the drift-diffusion model derived above; indeed, spin injection into the normal metal due to magnetic dynamics in the ferromagnet may be detected by means of an induced ISHE effect voltage [ATI11, OHB14].

1.2.4 Thermoelectric Effects

Returning to the itinerant ferromagnet and setting $X = \delta T(\mathbf{r})$, we obtain from Eq. (1.60) a charge current density:

$$\mathbf{j}_q = \sum_s \left(\sigma_s S_s \nabla T + s\sigma_s S_s \alpha_{SH}^s \mathbf{n} \times \nabla T\right) \tag{1.71}$$

where

$$\sigma_s S_s = L_{T,s}^{(0)} = \frac{e}{V} \sum_{\mathbf{k}} \tau_s v_{j\mathbf{k}}^2 \left(\partial_T f_{ks}^0\right) \tag{1.72}$$

is the spin-dependent Seebeck coefficient[4]; the first term in Eq. (1.71) is the spin-dependent Seebeck effect [Gui06, ECS12, MVS12]. In essence, hot electrons at one end of the metal move at a higher velocity than those at of the cold end; as a consequence, the hot electrons diffusive more quickly into opposite end, resulting in electron transport or, in steady-state open circuit conditions, an induced voltage. Spin-orbit effects yield an electric current normal to both the applied temperature gradient and the magnetic order parameter; correspondingly, in the presence of boundaries, the voltage resulting from the second term in Eq. (1.71) is known as the anomalous Nernst effect [HK13]. Notice that in the absence of magnet order ($S_\uparrow \alpha_{SH}^\uparrow = S_\downarrow \alpha_{SH}^\downarrow$), the anomalous Nernst effect vanishes.

The spin current is given by:

$$(-e)\,\frac{\mathbf{j}_i^{(s)}}{\hbar/2} = \sum_s n_i \left(s\sigma_s S_s \nabla T + \sigma_s S_s \alpha_{SH}^s \mathbf{n} \times \nabla T\right) \tag{1.73}$$

The first term is a spin-dependent spin Seebeck effect [AUS13], i.e. the transport of spin from high to low temperature regions. In a ferromagnet, the spin Seebeck is a corollary of the Seebeck effect, since a charge current is always accompanied by a spin current. Indeed, in a normal metal, the spin Seebeck effect vanishes. However, consider an insulating ferromagnet. In contrast to metallic electrons, magnons (as well as phonons) transport spin without charge; here, a spin Seebeck effect is possible without an accompanying charge current. An interfacial spin seebeck transport across normal metal/insulating ferromagnet interface is also possible and will play a crucial role in this thesis. The last term in Eq. (1.73) is an anomalous spin Nernst effect. For completeness, the heat current is:

$$\dot{\mathbf{Q}} = \sum_s \left(\kappa_s \nabla T + \kappa_s \alpha_{SH}^s s\mathbf{n} \times \nabla T\right) \tag{1.74}$$

where $\kappa_s = L_{T,s}^{(1)}$ is the spin-dependent thermal conductance.

[4]The spin-dependent Seebeck should be distinguished from the spin Seebeck; whereas the former is a single-particle two parallel channel effect, with spin-up and spin-down electrons carrying charge and spin separately, the latter is a collective spin effect, referring to a pure spin current carried by magnons.

1.2.5 Onsager Reciprocity

We may summarize the preceding sections by writing the linear response matrix:

$$\begin{pmatrix} \mathbf{j}_q \\ \left(\frac{-e}{\hbar/2}\right)\mathbf{j}_s^{(i)} \\ \dot{\mathbf{Q}} \end{pmatrix} = \begin{pmatrix} \hat{\sigma}^{(qq)} & \hat{\sigma}_i^{(qs)} & \sigma_0\hat{S} \\ \hat{\sigma}_i^{(sq)} & \hat{\sigma}_i^{(ss)} & \sigma_0\hat{S}_i \\ \sigma_0\hat{\Pi} & \sigma_0\hat{\Pi}^{(s)} & \hat{\kappa} \end{pmatrix} \begin{pmatrix} \nabla(\mu/e) \\ \nabla(\delta\mu_i/2e) \\ \nabla T \end{pmatrix}. \tag{1.75}$$

Here $.\hat{.}.$ denotes 3×3 tensorial structure, and the response coefficients

$$\begin{aligned} (\hat{\sigma}^{(qq)})_{lk} =& \sigma_0\delta_{lk} + P_{so}\sigma_{so}n_j\epsilon_{ljk} \\ (\hat{\sigma}_i^{(ss)})_{lk} =& P\sigma_0\delta_{lk} + \sigma_{so}n_j\epsilon_{ljk} \\ &\vdots \end{aligned} \tag{1.76}$$

are obtained from Eqs. (1.60), (1.62), (1.63), (1.71), (1.73) and (1.74). Many of the off diagonal elements are related. For example, using

$$(\sigma_0\hat{S})_{lk} = \sum_s \sigma_s S_s \left(\delta_{lk} + sn_j\epsilon_{ljk}\right) \tag{1.77}$$

and

$$\left(\sigma_0\hat{\Pi}\right)_{lk} = \sum_s \sigma_s \Pi_s \left(\delta_{lk} + \sigma n_j\epsilon_{ljk}\right) \tag{1.78}$$

with $\Pi_s = TS_s$ from Eqs. (1.64) and (1.72) we have $\hat{\Pi} = T\hat{S} = T\hat{S}^T(-\mathbf{n})$, which is known as the (generalized) second Thompson relation. In other words, the charge current flow induced by a temperature gradient is reciprocal to the heat current driven by a electric field. Similarly, $(\hat{\sigma}_i^{(qs)})^T = -\hat{\sigma}_i^{(sq)}(-\mathbf{n})$, i.e. the ISHE is reciprocal to the SHE. Moreover, one finds that each of the on-diagonal linear response subtensors obey reciprocity relations: $\hat{\sigma}^{(qq)} = (\hat{\sigma}^{(qq)})^T(-\mathbf{n})$, $\hat{\sigma}^{(ss)} = (\hat{\sigma}^{(ss)})^T(-\mathbf{n})$ and $\hat{\kappa} = \hat{\kappa}^T(-\mathbf{n})$.

The above reciprocal relations are a statement of a general theorem known as Onsager reciprocity [LL80b]. Onsager's theorem is based on microscopic time-reversibility of a thermodynamic system with a well-defined equilibrium state. Let $U(\mathbf{X})$ be the free energy corresponding to the physically relevant statistical ensemble, which is dependent on the set of state variables $\mathbf{X}$. Changes in the thermodynamic potential may be written: $\delta U = -\mathbf{F}\cdot\delta\mathbf{X}$,

where $\mathbf{F} = -\partial_{\mathbf{X}} U$, is the thermodynamic force, the components of which form a conjugate pair with the corresponding state variables, $\{X_i, F_i\}$. Linearizing around the equilibrium state (which exists by assumption), the response matrix has the form:

$$\dot{X}_i = \sum_j L_{ij} F_j \,. \tag{1.79}$$

Onsager's theorem states that the off-diagonal elements of L_{ij} are related:

$$L_{ij}\left(\mathbf{X}\right) = (-1)^{\eta_i+\eta_j} L_{ji}\left(T[\mathbf{X}]\right), \tag{1.80}$$

where $T[\mathbf{X}]$ stands for the time-reversal of $\mathbf{X}$, and $\eta_i = \pm 1$ when $T[X_i] = \pm X_i$. Onsager principle is a powerful tool which is useful in both checking the self-consistency of a linear response calculation, and of obtaining unknown linear response coefficients.

1.3 Transport Across Normal Metal/Ferromagnet Interfaces

Having thus discussed magnetic dynamics and spin-based transport in normal metals, let us turn to the boundary conditions for charge, spin and heat at a normal metal/ferromagnet interface, which are central to this thesis.

1.3.1 Scattering Theory at Magnetic Interfaces

In this section, we derive the charge, spin and heat currents passing through an interface between a normal metal and a dynamic ferromagnet using Floquet scattering theory [But92, BPT93, Bro98a, MB04, MB02]. This classical theory provides a powerful framework with which to understand a variety of phenomena involving a parametric pumping and interfacial spin-dependent conductance.

Consider N channels, each connected to a common scattering region R. An electron in channel l either scatters into a different channel l', or is reflect back into channel l. We focus on a time-dependent scattering potential $V\left(t\right) = V\left(t + 2\pi/\omega\right)$ in R which is periodic in time with period $2\pi/\omega$. Pumping by this periodic potential scatters electrons with energy E into sidebands with energy $E_n = E + n\hbar\omega$, where n is an integer.

The operator for an electron in the lead l with spin α and energy E impinging on R is denoted by $\hat{c}_{l\alpha}$. The corresponding distribution function is defined by:

$$\left\langle \hat{c}_{l\sigma}^{\dagger}\left(E\right)\hat{c}_{l'\sigma'}\left(E\right)\right\rangle =f_{l,\sigma\sigma'}^{(\mathrm{in})}\delta_{ll'} \tag{1.81}$$

Operators for electrons scattered into channel l' with spin σ' from region R are denoted by $\hat{b}$, with a distribution function $f_{l',\sigma\sigma'}^{(\mathrm{out})}$ defined analogously. The Floquet scattering matrix $s_{ll'\sigma\sigma'}=\left(\hat{s}_{ll'}\right)_{\sigma\sigma'}$ relates incident and scattered amplitudes between the side-bands:

$$\hat{d}_{l\sigma}\left(E\right)=\sum_{l'\sigma'}s_{ll'\sigma\sigma'}\left(E,E_{n}\right)\hat{c}_{l'\sigma'}\left(E_{n}\right)\ . \tag{1.82}$$

If the total incident flux is equal to the total scattered flux (i.e. neither charge nor spin accumulate in the scattering region R), the scattering matrix is subject to the identity:

$$\sum_{l}\sum_{E_{n}>0}\check{s}_{il}^{\dagger}\left(E_{n},E\right)\check{s}_{jl}\left(E_{n},E\right)=\delta_{ij}\check{1} \tag{1.83}$$

In each scattering channel l, the distribution function $\check{f}_{l}^{(\mathrm{in})}\left(E\right)$ may be decomposed into spin majority ($\uparrow$) and minority ($\downarrow$) components, respectively oriented parallel and antiparallel to the direction $\mathbf{n}$ by means of projection operators $\hat{u}_{\alpha}$:

$$\check{f}_{l}^{(\mathrm{in})}\left(E_{n}\right)=\sum_{\sigma}\check{u}_{l\sigma}f_{l\sigma}\left(E_{n}\right)\approx\sum_{\sigma}\check{u}_{\sigma}\left[f_{l\sigma}\left(E\right)+\frac{\partial f_{l\sigma}}{\partial E}n\hbar\omega\right] \tag{1.84}$$

where $f_{l,\sigma}\left(E\right)=\left[e^{\beta\left(\epsilon-\mu_{l\sigma}\right)}+1\right]^{-1}$ is the Fermi-Dirac distribution function for an electron with spin-dependent electrochemical potential μ_{α}. Using Eqs. (1.81)-(1.83), the spin-resolved current flowing from channel l

$$\check{I}_{l,p}\equiv\frac{1}{h}\int_{0}^{\infty}dE(E-E_{F})^{p}\left[\check{f}_{l}^{(\mathrm{out})}\left(E\right)-\check{f}_{l}^{(\mathrm{in})}\left(E\right)\right], \tag{1.85}$$

(where h is Planck's constant) can be shown to have two contributions (to linear order in the dynamics $\dot{X}$ and biases): $\check{I}_{l}=\check{I}_{l}^{(\mathrm{bias})}+\check{I}_{l}^{(\mathrm{pumped})}$. The first current,

$$\check{I}_{l,p}^{(\mathrm{bias})}=\mathrm{Re}\left[\frac{1}{h}\int_{0}^{\infty}dE(E-E_{F})^{p}\sum_{E_{n}>0}\sum_{l'}\left(\check{s}_{ll'}\left(E,E_{n}\right)\check{f}_{l'}^{(in)}\left(E\right)-\hat{f}_{l}^{(in)}\left(E\right)\check{s}_{ll'}\left(E,E_{n}\right)\right)\right] \times\check{s}_{ll'}^{(F)\dagger}\left(E,E_{n}\right) \tag{1.86}$$

is a generalized Landauer-Buttiker equation, which describes particle flow stemming from voltage or spin bias between channels. The second current,

$$\check{I}_{l,p}^{(\text{pumped})} = \text{Im}\left[\frac{\hbar\omega}{h}\int_0^\infty dE(E-E_F)^p \sum_{l'}\frac{\partial f_{l'}^\sigma}{\partial E}\check{u}_{l'\sigma}\sum_{E_n>0} n\hat{s}_{ll'}\left(E,E_n\right)\check{s}_{ll'}^\dagger\left(E,E_n\right)\right] \tag{1.87}$$

originates from the dynamics of the scattering potential in R, whose time-dependence may be described the periodic variation of a quantity $X = X\left(t\right)$ with period $2\pi/\omega$. In the adiabatic approximation ($\hbar\Omega \ll E_N$), the Floquet scattering matrix $s_{ll'\alpha\beta}\left(E,E_n\right)$ may be identified with the $n\omega$-frequency Fourier component of the instantaneous scattering matrix $\check{s}_{ll'}\left(E,X\left(t\right)\right)$, allowing one to identify the instantaneous current,

$$\check{I}_{l,p}^{(\text{pumped})}\left(t\right) = \text{Im}\left[\frac{1}{2\pi}\int_0^\infty dE(E-E_F)^n \sum_{l'}\frac{\partial f_{l'}^\sigma}{\partial E}\hat{u}_{l'\sigma}\left(\frac{\partial}{\partial t}\hat{s}_{ll'}^{(F)}\left(E,X\left(t\right)\right)\right)\hat{s}_{ll'}^{(F)\dagger}\left(E,X\left(t\right)\right)\right] \tag{1.88}$$

where $\check{I}_{l,n}^{(\text{pumped})}$ is the time-average of $\check{I}_{l,n}^{(\text{pumped})}\left(t\right)$ over one period. Here we have made use of the identity $\check{s}_{ll'}^{(F)}\left(E_n,E\right) = \check{s}_{ll'}^{(F)}\left(E,E_{-n}\right)$ which asserts that the amplitude for scattering from a channel with energy E to a channel with energy $n\hbar\omega$ higher is the same that for scattering from a channel with energy $E-n\hbar\omega$ to E.

The bias and pumped currents in Eqs. (1.86) and (1.87) describe an array of phenomena. Here we shall be concerned with the transfer of spin and charge across normal metal(N)/ferromagnet(F) interfaces.

1.3.2 Spin-Transfer Torque

First, let us study the bias current, Eq. (1.86). A normal metal/ferromagnet interface may be biased in a number of ways. For example, if charge or spin accumulation on either side of the interface is different, or if the orientation of the spin accumulation in the normal metal is different that the spin accumulation inside the ferromagnet, an interfacial spin and/or charge current may result. Such biases may be created by the application of a voltage bias across the interface, or the injection of spin into system. Let us suppose that transverse spin coherence length inside the ferromagnet (which defines the length over which electron spin perpendicular to the magnetic order parameter is absorbed) is short compared to the thickness of the

ferromagnet, which we take to be monodomain here for simplicity; the nonequilibrium spin accumulation $\boldsymbol{\mu}_F$ in the ferromagnet is therefore parallel to the ferromagnetic order parameter, whose direction is denoted by the unit vector $\mathbf{n}$. The spin accumulation $\boldsymbol{\mu}_N$ in the normal metal is oriented in the $\mathbf{n}'$ direction. Assuming strong electron-electron scattering, electrons on the normal and ferromagnetic sides of the interface are locally equilibrated to the respective Fermi-Dirac distribution functions $\check{f}_n(\epsilon) = \sum_s \check{u}_{Ns} f_{ns}(\epsilon)$ and $\check{f}_f(\epsilon) = \sum_s \check{u}_{Fs} f_{fs}(\epsilon)$, where $\check{u}_{Ns} = (\hat{1} + s\mathbf{n}' \cdot \check{\boldsymbol{\sigma}})/2$, $\check{u}_{Fs} = (\check{1} + s\mathbf{n} \cdot \check{\boldsymbol{\sigma}})/2$, $f_{Ns}(\epsilon) = [e^{\beta(\epsilon - \mu_{Ns} - \epsilon_F)} + 1]^{-1}$, and $f_{Fs}(\epsilon) = [e^{\beta(\epsilon - \mu_{Fs} - \epsilon_F)} + 1]^{-1}$, and n and f label the Fermi surface states in the normal metal and ferromagnet, respectively. We may decompose the scattering matrix into reflection and transmission coefficients:

$$\check{s}_{nn'} \equiv \check{r}_{nn'} = \sum_s \check{u}_{Fs} r^{(s)}_{nn'} \tag{1.89}$$

and

$$\check{s}_{nf} \equiv \check{t}_{nf} = \sum_s \check{u}_{Fs} t^{(s)}_{nf} \tag{1.90}$$

where the scattering matrix $\check{s}$ above is taken to be constant and evaluated in the vicinity of the normal metal Fermi surface ϵ_F and the ferromagnet Fermi surfaces ϵ_{Fs}. Here the spin quantization axis for the scattering coefficients $t^{(\uparrow)}_{nf}$, $r^{(\downarrow)}_{nn'}$, etc. are defined by the ferromagnet.

One obtains an interfacial charge current [BNB01, NB00, BTB06] into the normal metal by setting $l = n$ in Eq. (1.86) and tracing over spin indices:

$$I_q^{(\mathrm{bias})} = (-e)\mathrm{Tr}\left[\check{I}^{(\mathrm{bias})}_{N,0}\right] = I_\uparrow + I_\downarrow \tag{1.91}$$

where

$$I_\sigma = -G_\sigma \frac{(\mu_F - \mu_N)}{e} - \sigma G_\sigma \mathbf{n} \cdot \frac{(\delta\mu_F \mathbf{n} - \delta\mu_N \mathbf{n}')}{2e} \tag{1.92}$$

with $\mu_F = (\mu_{F\uparrow} + \mu_{F\downarrow})/2$, $\delta\mu_F = \mu_{F\uparrow} - \mu_{F\downarrow}$, $\mu_N = (\mu_{N\uparrow} + \mu_{N\downarrow})/2$, $\delta\mu_F = \mu_{F\uparrow} - \mu_{F\downarrow}$ and $G_\sigma = (e^2/h)\sum_{nf} \left|t^\sigma_{nf}\right|^2$ is the Landuaer-Buttiker conductance. The first term in Eq. (1.92) gives the charge current flowing into the normal metal as a consequence of charge accumulation or electrostatic biasing, while the second term gives the electronic current stemming spin accumulation which, by virtue of the fact that the interfacial conductance may be in general different for difference spins ($G_\uparrow \neq G_\downarrow$), results in net a flow of electrons.

The spin current into the normal metal is [TB02b]:

$$\mathbf{I}_s^{(\text{bias})} = \frac{\hbar}{2}\text{Tr}\left[\check{I}_{N,0}^{(\text{bias})}\check{\boldsymbol{\sigma}}\right]$$
$$= \frac{\hbar}{2(-e)}\left(I_\uparrow - I_\downarrow\right)\mathbf{n} - \left(\frac{\hbar}{2e^2}\right)\text{Im}\left[G_{\uparrow\downarrow}\right]\delta\mu_N\left(\mathbf{n}\times\mathbf{n}'\right) - \left(\frac{\hbar}{2e^2}\right)\text{Re}\left[G_{\uparrow\downarrow}\right]\delta\mu_N\mathbf{n}\times\left(\mathbf{n}\times\mathbf{n}'\right) \tag{1.93}$$

where

$$G_{\uparrow\downarrow} = \frac{e^2}{h}\sum_{nn'}(\delta_{nn'} - r_{nn'}^{\uparrow}[r_{nn'}^{\downarrow}]^*) \tag{1.94}$$

is the spin mixing conductance. Only electrons with spin collinear with the ferromagnet magnetization are transmitted (since the ferromagnet is much larger than the transverse coherence length for spin transport), which is captured by the first term. Reflected electrons, however, can change their spin orientation, imparting spin angular momentum (but not charge) to the ferromagnet. Whereas electrons transmitted into the ferromagnet from the normal metal carry longitudinal (i.e. collinear with $\mathbf{n}$) angular momentum, resulting in a spin accumulation or depletion of itinerant ferromagnet electron spin, the spin current stemming from reflected electrons (second term in Eq. (1.93)) is normal to the spin density of $\mathbf{n}$, and the excess spin current injected into the ferromagnet results in a spin-transfer torque on $\mathbf{n}$. Such spin-transfer torque is central to the field of spintronics, which seeks to control magnetic orientation by electrical means.

The heat current carried by electrons crossing the interface is found from:

$$\dot{Q}^{(\text{bias})} = \text{Tr}\left[\hat{I}_{N,1}^{(\text{bias})}\right] = \left(G_\uparrow + G_\downarrow\right)\Pi_I\frac{\left(\mu_F - \mu_N\right)}{e} + \left(G_\uparrow - G_\downarrow\right)\Pi_I\mathbf{n}\cdot\frac{\left(\delta\mu_F\mathbf{n} - \delta\mu_N\mathbf{n}'\right)}{2e} \tag{1.95}$$

where

$$\Pi_I = \frac{1}{e}\int dE\frac{\left(E-\epsilon_F\right)/T}{\left[e^{\beta\left(E-\epsilon_F\right)}+1\right]^2} \tag{1.96}$$

is the interfacial Peltier coefficient.

We may also inquire as to transport in presence of an interfacial temperature gradient, $T_F - T_N$, which may be interpreted as the effective difference in electron temperatures a thermal coherence length away from the interface on either side. Then, the resulting charge, spin and heat currents are:

$$I_q^{(\Delta T)} = I_\uparrow^{(\Delta T)} + I_\downarrow^{(\Delta T)} = S_I\left(G_\uparrow + G_\downarrow\right)\left(T_F - T_N\right) \tag{1.97}$$

where

$$S_I = \frac{1}{e}\int dE \frac{(E-\epsilon_F)/T^2}{\left[e^{\beta(E-\epsilon_F)}+1\right]^2} = \frac{\Pi_I}{T}, \tag{1.98}$$

(as required by Onsager reciprocity), while

$$\mathbf{I}_s^{(\Delta T)} = \frac{\hbar}{2(-e)}\left(I_\uparrow^{(\Delta T)} - I_\downarrow^{(\Delta T)}\right)\mathbf{n} \tag{1.99}$$

and

$$\dot{Q}^{(\Delta \mathrm{T})} = \left(\kappa_{I\uparrow} + \kappa_{I\downarrow}\right)\left(T_F - T_N\right) \tag{1.100}$$

with

$$\kappa_{I\sigma} = \frac{G_\sigma}{e^2}\int dE \frac{(E-\epsilon_F)^2/T^2}{\left[e^{\beta(E-\epsilon_F)}+1\right]^2} \tag{1.101}$$

as the interfacial thermal conductance. Eqs. (1.98) and (1.99) are the spin-dependent interfacial Seebeck effect and interfacial spin Seebeck effect, respectively, which have recently been demonstrated in [ZHL09, YGY10].

When the ferromagnet is insulating ($t_s = 0$), charge and heat transport by *electrons* is prohibited. Spin transfer normal to the ferromagnetic order parameter is, however, possible [DS12, KHT10a], and is crucial to subsequent chapters in this thesis. Furthermore, heat and longitudinal spin transport into the insulating ferromagnet is still possible by other mechanisms. In Chapter 2 we develop a theory for magnon transport analogous that of electrons outlined above; while the transverse components of electron spin accumulation in the normal metal exert a torque on the ferromagnetic order parameter, the longitudinal transfer of angular momentum is mediated by magnons.

1.3.3 Spin Pumping

Next, let us consider a dynamic (uniform) magnetization, $\mathbf{n}(t)$, which we take to be periodically precessing around an axis of broken symmetry. Taking $X(t)$ as the instantaneous angle of $\mathbf{n}$ in the plane of precession, we may employ the expression for the pumped current, Eq (1.88). One obtains a spin current into the normal metal:

$$\mathbf{I}_s^{(\mathrm{pumped})} = \frac{\hbar}{2}\mathrm{Tr}\left[\check{I}_{N,0}^{(\mathrm{pumped})}\check{\boldsymbol{\sigma}}\right] = -\left(\frac{\hbar}{2e^2}\right)\left(A_R\mathbf{n}\times\dot{\mathbf{n}} - A_I\dot{\mathbf{n}}\right) \tag{1.102}$$

where A_R and A_I are the real and imaginary part of $A = G_{\uparrow\downarrow} - \left(t_\uparrow t_\downarrow^*\right) e^2/h$ [TB02b, BT12, MVS12], while the pumped charge current $I_q^{(\text{pumped})}$ vanishes.

Spin pumping is Onsager reciprocal to and may therefore be derived from spin-transfer torque [MVS12, BT12, TB14b]. To see this, let us specialize to a thin magnetic insulator (with thickness smaller than the magnetic exchange length so that the magnet may be taken to be monodomain) in contact with a normal metal with spin accumulation $\boldsymbol{\mu}$. Then, adding the spin current $\mathbf{I}_{\text{N}\to\text{F}}$ absorbed by the ferromagnet from the normal metal to the equation of motion for the magnet, Eq. (4.10), yields a modified Landau-Lifshitz-Gilbert equation:

$$\hbar\left(1 + \alpha\mathbf{n}\times\right)\dot{\mathbf{n}} + \mathbf{n}\times\mathbf{H} = \frac{\mathbf{I}_{\text{N}\to\text{F}}}{\mathcal{V}_F s}\,, \tag{1.103}$$

where $\mathcal{V}_F$ is the volume of the ferromagnet. In the absence of spin flip processes at the interface, the spin current entering the ferromagnet is equal to that leaving the normal metal. If the normal metal layer is thinner than the metal's spin-diffusion length and spin current is only allowed to pass through the metal/ferromagnet interface, the rate of change of the metal spin density $\boldsymbol{\rho}$ (in units of $\hbar$) is given by:

$$\hbar\mathcal{V}_N\dot{\boldsymbol{\rho}} = -\mathbf{I}_{\text{N}\to\text{F}}\,. \tag{1.104}$$

To linear order in the spin accumulation and magnetic precession frequency, the current $\mathbf{I}_{N\to F}$ has two contributions (spin-transfer torque and spin pumping), which may be generally written:

$$\mathbf{I}_{\text{N}\to\text{F}} = \hat{R}\boldsymbol{\mu}' + \hat{P}\dot{\mathbf{n}}\,. \tag{1.105}$$

where $.\hat{.}.$ denotes tensorial structure. Let us suppose that the spin-transfer torque is known, so that $\hat{R} = (\hbar/2e^2)(\hat{n} + \hat{n}^2)$ with $\hat{n}_{ij} = \epsilon_{ijk}n_k$ is obtained from Eq. (1.93), $G_\sigma = 0$ for an insulating ferromagnet, and $\hat{P}$ is by assumption to be determined. Then, writing the energy of the entire system $U = U(\mathbf{n}, \boldsymbol{\rho})$, we may identify the thermodynamic forces $\mathbf{H} = \partial_{\mathbf{n}}U/\mathcal{V}_F s$ and $\boldsymbol{\mu}' = \partial_{\boldsymbol{\rho}}U/\mathcal{V}_N$ (with $\mathcal{V}_N$ as the normal metal volume), forming the respective conjugate pairs: $(\mathbf{n}, \mathbf{H})$ and $(\boldsymbol{\rho}, \boldsymbol{\mu}')$. The linear response system has the form:

$$\begin{pmatrix} \mathcal{V}_F s\hbar\dot{\mathbf{n}} \\ \mathcal{V}_N\hbar\dot{\boldsymbol{\rho}} \end{pmatrix} = \begin{pmatrix} \hat{L}_{FF} & \hat{L}_{FN} \\ \hat{L}_{NF} & \hat{L}_{NN} \end{pmatrix} \begin{pmatrix} \mathbf{H} \\ \boldsymbol{\mu}' \end{pmatrix}, \tag{1.106}$$

where the response coefficients $\hat{L}_{FF}$, $\hat{L}_{FN}$ etc. are determined by rearranging the equations of motion, Eq. (1.103) and (1.105). For example, the spin-transfer torque response coefficient is $\hat{L}_{FN} = \hat{A}^{-1}\hat{R}$, with $\hat{A} = 1 + \alpha\hat{n} - \hat{P}/\mathcal{V}_F s\hbar$, while the normal metal spin response to **H**-induced dynamics is given by the coefficient $\hat{L}_{FN} = \hat{P}\hat{A}^{-1}\check{n}/\hbar$. Onsager's theorem dictates that these coefficients are related by: $\hat{L}_{FN} = \hat{L}_{NF}^{T}(-\mathbf{n})$, from which it is a straightforward exercise to obtain $\hat{P} = -\hbar\hat{R}\hat{n}$, which then yields the spin-pumped current Eq. (1.102) (with $t_s = 0$).

1.3.4 Dynamics of a Monodomain Insulating Ferromagnet

The full, modified dynamics for a thin insulating monodomain (zero temperature) magnet adjacent to a normal metal N (see Fig. 1.4), Eq. (1.103), may therefore be written:

$$\hbar\left(1 + \alpha\mathbf{n}\times\right)\dot{\mathbf{n}} + \mathbf{n}\times\mathbf{H} = -\alpha_i'\hbar\dot{\mathbf{n}} + \alpha_i'\boldsymbol{\mu}'\times\mathbf{n} - \alpha_r'\hbar\mathbf{n}\times\dot{\mathbf{n}} + \alpha_r'\mathbf{n}\times\boldsymbol{\mu}'\times\mathbf{n} \tag{1.107}$$

where α_r' and α_i' are the real and imaginary parts of $\alpha' = \hbar G_{\uparrow\downarrow}/2e^2S$. The first two terms on the right-hand side of Eq. (1.107) are nondissipative; the first term renormalizes the the remaining parameters, while the second contributes an effective magnetic field $\alpha_i'\boldsymbol{\mu}'$. In most materials, α_i' is small in comparison to α and α_r', and the first two terms are usually neglected. Henceforth, we shall abbreviate $\alpha' = \alpha_r'$. In general, Eq. (1.107) must be solved in tandem with the appropriate diffusion equation for $\boldsymbol{\mu}$ in the normal metal; if however, $\boldsymbol{\mu}$ is driven by, for example, the SHE, we may take the spin accumulation to be fixed, focusing instead on the magnetic dynamics of the ferromagnet.

The third term in Eq. (1.107) is the spin pumping, which complements the intrinsic Gilbert damping. Spin pumping was first measured as an enhancement to FMR linewidth [MAM02, TBB01, CMM06, RRS13]. More recently, direct electrical detection of the spin pumped by a precessing magnetization into a normal metal has been made possible. In [CSW06], a metallic magnet (Pemalloy), is excited by an FMR field; the resulting spin accumulation in an adjacent normal metal is then converted into a charge current in the magnet via Eq. (1.91). When spin-orbit effects in the normal metal are significant, the ISHE has proven useful in demonstrating electrically the spin pumping effect, including cases in

which the magnet is insulating.

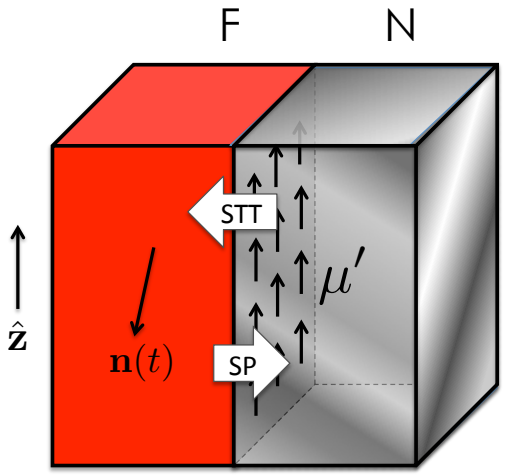

Figure 1.4: Insulating ferromagnet F interfaced with normal metal N.

The fourth, damping-like term in Eq. (1.107) describes the transfer of angular momentum into the ferromagnet via spin-transfer torque, which can excite coherent magnetic dynamics [LMR11a, LPL12a, YUF14]. When the spin accumulation is parallel with the rotational symmetry axis of the magnet ($\boldsymbol{\mu} = \mu'\mathbf{z}$), it is convenient to write Eq. (1.107) in terms of spherical coordinates θ and ϕ (see Eq. (1.7)):

$$\hbar\dot{\theta} = (\alpha + \alpha')\,\hbar\sin\theta\dot{\phi} - \alpha'\mu'\sin\theta \tag{1.108}$$

$$\sin\theta\hbar\dot{\phi} = \sin\theta H + K\sin\theta\cos\theta - (\alpha + \alpha')\,\hbar\dot{\theta} \tag{1.109}$$

Substituting Eq. (1.108) into Eq. (1.109) and neglecting terms of order α^2, $(\alpha')^2$ and $\alpha\alpha_r$ (since generally $\alpha, \alpha' \ll 1$), one obtains:

$$\hbar\dot{\theta} = (\alpha + \alpha')\,(H + K\cos\theta)\sin\theta - \alpha'\mu'\sin\theta\,. \tag{1.110}$$

To characterize the phase behavior of the system in the presence of a spin-transfer torque provided by the spin accumulation $\boldsymbol{\mu}$ (which for simplicity we take to be fixed by, for example, by spin Hall physics in the normal metal, and therefore independent of feedback from the magnetic dynamics), it is sufficient to expand the dynamics around the poles $\pm\mathbf{z}$, yielding the linearized equations of motion: $\hbar\dot{\theta} = -\epsilon_-(\theta - \pi)$ near $\mathbf{n} = -\mathbf{z}$ and $\hbar\dot{\theta} = -\epsilon_+\theta$. The constants $\epsilon_\pm = (\alpha + \alpha')\,(\mp H - K) \pm \alpha'\mu'$ give the effective damping near their respective poles. When $\epsilon_\pm$ is positive (negative), $\mathbf{n} = \pm\mathbf{z}$ is a stable (unstable); when both poles are destabilized, the system enters into a dynamical phase in which $\mathbf{n}$ precesses around the z axis at nonzero μ'. The phases are summarized in Fig. 1.5.

The incitement of magnetic dynamics by a spin transfer-torque is, in its essence, the coherent emission of $\mathbf{k} = 0$ magnons resulting from an out-of-equilibrium population inversion

of electron spins in the normal metal. Berger first termed this process swasing [Ber96b], (where swaser stands for "spin wave amplification by stimulated emission of radiation"). If one allows for a finite exchange stiffness, swasing of finite $\mathbf{k}$ spin wave modes also becomes possible, representing an additional method of exciting spin waves [PAR11c]. In this case, the excitation threshold for a given mode is determined by the spin-wave gap $\epsilon_{\mathbf{k}} = A\mathbf{k}^2 + \hbar\Omega$. When the angular momentum injection via spin-transfer torque due to normal metal spin-accumulation $\boldsymbol{\mu}$ (which itself generated by means of the spin Hall effect or nonlocal spin injection) overcomes spin-pumping and Gilbert damping of a particular mode, that mode begins to grow. In contrast to parallel pumping and bulk spin-transfer torque, wherein excited spin wave modes may be directly excited, in interfacial spin-transfer torque the lowest energy modes (including monodomain precession) are necessarily excited first.

Although we have focused above on the magnetic dynamics in an insulating ferromagnet, it should be emphasized that spin-transfer torque is traditionally realized in conducting structures. In magnetic structures which are thicker[5] than the transverse spin coherence length of the ferromagnetic components, Eqs. (1.91)-(1.93) must be solved in tandem with spin diffusion equations in the normal and ferromagnetic metals [BFG05]. It is, however, straightforward to understand the essential physics. For example, a metallic spin-valve consists of two ferromagnetic layers, one fixed (reference layer) and one free, separated by a normal metal spacer. When weakly electrically biased, no magnetic dynamics are induced as Gilbert damping dissipates the torque provided to the free layer; however, different relative orientations of the two magnet layers result in different structural resistances, stemming from the spin-dependence of the interfacial (Eq. (1.92)) and bulk (see directly below Eq. (1.60)) conductances. This is the giant magnetoresistive effect [BBF88, BGS89], the important of which to modern memory devices is difficult to overstate. Under a sufficiently large electrical bias, the resulting spin polarized may exert such a torque on the free layer [GCH01, MRK06, KPR04] so as to reverse the magnetization; in combination with the giant magnetoresistance, this type of spin-transfer torque holds promise for new read-write memory schemes.

[5]When the thickness of the ferromagnet is shorter than the transverse coherent length, the Landau-Lifshitz phenomenology must be complemented with Bloch type dynamics for the conduction electrons traversing the magnet.

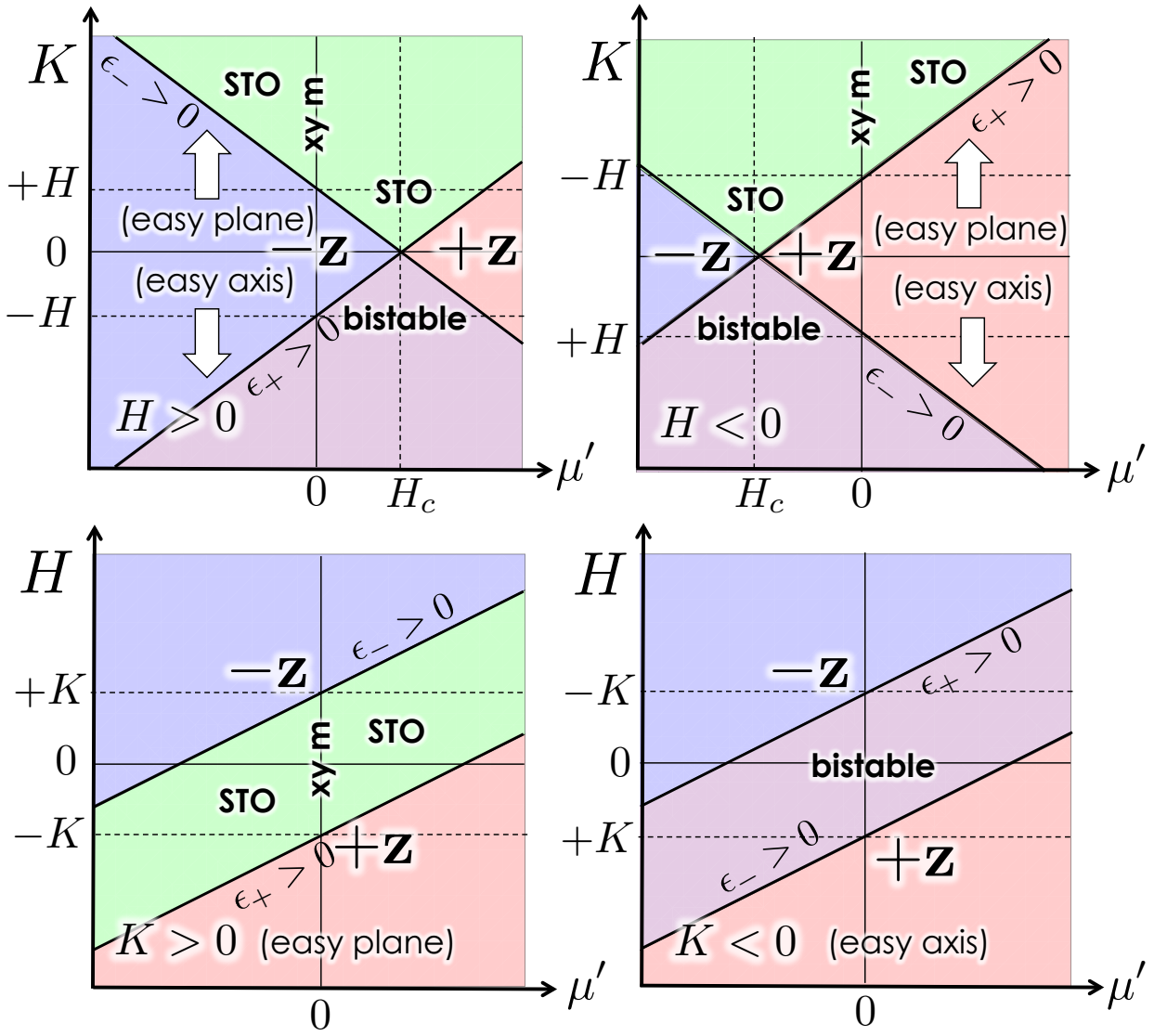

Figure 1.5: Phase diagram for a spin-torque driven monodomain ferromagnet for fixed magnetic field based on Eqs. (1.110), exhibiting bistability and a spin-torque oscillator (STO) phase. (At μ', in the STO rotates at zero frequency, and is therefore an xy magnet tilted out of plane by the finite magnetic field). The top two subfigures are obtained for fixed magnetic field H, with $\mu_c = H_c = (\alpha + \alpha')/\alpha'$ exhibiting a quadruple point; the lower two subfigures correspond to fixed anisotropy.

1.4 Transport Across Tunnel Junctions

1.4.1 Julliere Model of Tunnel Magnetoresistance

In a metallic spin valve, the normal metal spacer breaks direct exchange between the two magnets, ensuring that the free layer is coupled to the fixed only in the presence of a bias applied across the structure. When the normal metal is replaced by a tunnel barrier, the heterostructure is known as a magnetic tunnel junction (MTJ). While the structural conductance is naturally generally lower than metallic spin valves, the differential spin transport properties of MTJs make them attractive candidates from a device applications perspective; metal-oxide based MTJs have already found a foothold in hard-disk drive and magnetic random access memory devices.

Transport across a tunnel barrier between electrodes may be described by the tunneling Hamiltonian:

$$\hat{\mathcal{H}}_T = \sum_{\nu_1\nu_2} \left(T_{\nu_1,\nu_2} \hat{c}^\dagger_{\nu_2 s_2} \hat{c}_{\nu_1 s_1} + T^*_{\nu_1,\nu_2} \hat{c}^\dagger_{\nu_1 s_1} \hat{c}_{\nu_2 s_2} \right) \tag{1.111}$$

where $\hat{c}_{\nu_i}$ is the annihilation operator for an spin s_i electron in orbital state ν_i in electrode $i = 1, 2$. When the hopping matrix element $T_{\nu_1 s_1 \nu_2 s_2}$ is sufficiently small (corresponding to a thick and/or high tunnel barrier), it is suffices to treat electron transport perturbatively; Fermi's Golden Rule yields a current entering electrode 2:

$$I = G_T \left(V_1 - V_2 \right) \tag{1.112}$$

where

$$G_T = e^2 2\pi \left| T \right|^2 \sum_{s_1 s_2} D_{1 s_1} D_{2 s_2} \left| \langle s_2 | \, s_1 \rangle \right|^2 \tag{1.113}$$

is the tunnel junction conductance, with $D_{1 s_1}$ and $D_{2 s_2}$ are the spin-dependent (Fermi surface) densities of states. Here, we have assumed a weak dependence of on the hopping element $T_{\nu_1 s_1, \nu_2 s_2} \approx T$. Crucially, the conductance G_T depends on the relative orientation of the magnetic leads through the spin overlap products $\langle s_2 | \, s_1 \rangle$. When the magnets are parallel, $\langle \uparrow_2 | \downarrow_1 \rangle = \langle \uparrow_1 | \downarrow_2 \rangle = 0$, and (due to the absence of interfacial spin-flip processes), majority electrons in electrode 1 may only transfer to majority states in 2, resulting in a

conductance: $G_{\rm p} = e^2 2\pi \left|T\right|^2 \left(D_{1\uparrow}D_{2\uparrow} + D_{1\downarrow}D_{2\downarrow}\right)$, consisting of two parallel spin channels ($\uparrow\rightarrow\uparrow$ and $\downarrow\rightarrow\downarrow$). When the magnets are antiparallel, $\langle\uparrow_2|\uparrow_1\rangle = \langle\downarrow_1|\downarrow_2\rangle = 0$, and the conductance is: $G_{\rm ap} = e^2 2\pi \left|T\right|^2 \left(D_{1\uparrow}D_{2\downarrow} + D_{1\downarrow}D_{2\uparrow}\right)$. If, as in a metallic spin valve, one magnetic layer is fixed and one is free (with the equilibrium orientations of the latter collinear with the former), the differences in conductances provide information about the state of the free layer. The unitless tunnel magnetoresistance ratio TMR$\equiv (G_{\rm ap} - G_{\rm p})/G_{\rm p}$ provides a measure of the effectiveness of the differential spin transport. Using the above expressions for $G_{\rm p}$ and $G_{\rm ap}$, one obtains [Jul75]:

$$\mathrm{TMR} = \frac{2P_1P_2}{1 - P_1P_2}, \tag{1.114}$$

where P_i is the spin polarization of the i^{th} lead, defined in Section 1.2.3. MGo vs Ti0.

1.4.2 Coulomb Blockade

We have, however, neglected electron-electron interactions, which become crucial to understanding transport in three-dimensionally confined structures such as quantum dots. When connected via tunnel junctions to metallic leads, quantum dots exhibit a highly nonlinear response to biasing as a result of Coulomb Blockade [FD87, BF04], which may be captured by the following simple capacitive model. The energy E_N as associated with an occupancy of N electrons on the dot is:

$$E_N = \frac{E_c}{2} N\left(N-1\right) - eV_g N \tag{1.115}$$

where $E_c > 0$ is the geometry-dependent capacitive energy of the dot and V_g is the applied gate voltage. Consider a dot connected to a source ($i = 1$ lead) and drain ($i = 2$ lead); in the sequential transport regime, one electron may tunnel first onto the dot from the source and then into the the drain. For a fixed gate voltage, when eV_g is not equal to an integer multiple of eV_g, E_N is minimized for one integer value N (so that N electrons inhabit the dot), and transitions $N \rightarrow N \pm 1$ are blocked, blockading sequential transport of electrons; when, however, eV_g is an integer multiple of E_c, $\min\left[E_N\right]$ becomes degenerate for an adjacent value $N' = N \pm 1$ of electrons, and single electron transport is permitted via the channel $N \leftrightarrow N \pm 1$. (See Fig 1.6).

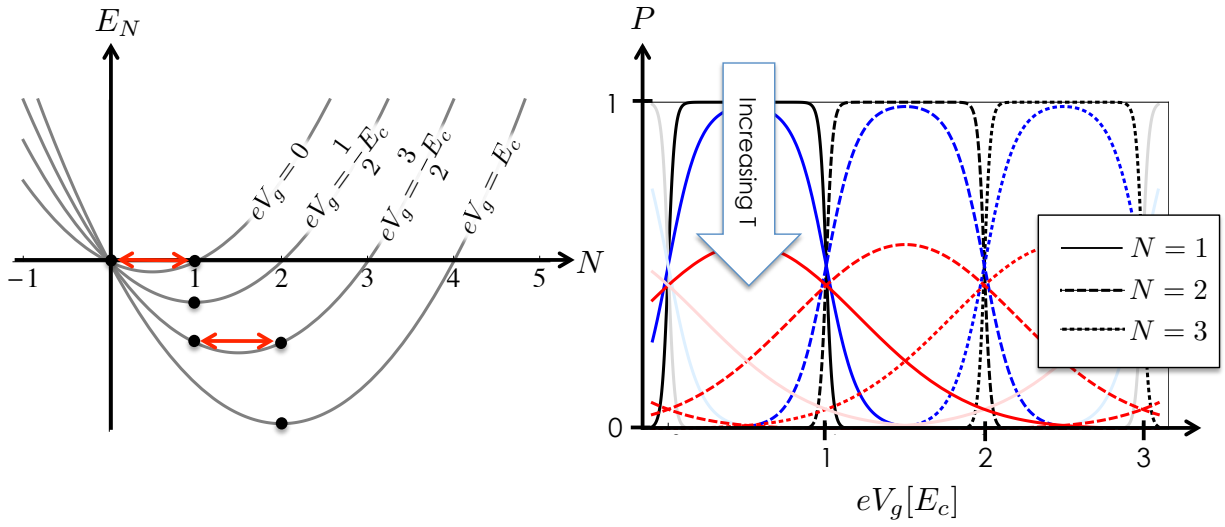

Figure 1.6: Coulomb blockade of a quantum dot. When eV_g is not an integer value of E_c, the Coulomb energy E_N is minimized for one value of N, making it possible to control the electronic dot occupancy precisely at low temperatures. The occupancy probability of a dot (for which electrons are supplied by metallic leads) at temperatures $T = E_c/50$ (black), $T = E_c/10$ (blue), and $T = E_c/2$ (red); at temperatures higher than E_c, thermal fluctuations blur the occupancy probabilities.

Transport through the dot in the sequential tunneling regime must be approached via the master equation approach, wherein N -electron occupancy of the dot is assigned a probability P_N. The master equation gives the rate of change P_N

$$\dot{P}_N = \left(P_{N-1}\Gamma_{N-1\to N} + P_{N+1}\Gamma_{N+1\to N}\right) - P_N\left(\Gamma_{N\to N-1} + \Gamma_{N\to N+1}\right), \tag{1.116}$$

where $\Gamma_{N\to N\pm1} = \sum_{i=s,d}\Gamma^{(i)}_{N\to N\pm1}$ is the total tunneling rate from N to $N\pm1$ occupancy, with

$$\Gamma^{(i)}_{N\to N\pm1} = \frac{G_i}{e^2} f\left(E_{N\pm1} - E_N + \mu_d - \mu_i\right) \tag{1.117}$$

as the tunneling rate in the dot (with single particle chemical potential μ_d) from the source and drain, $f(T,E) = E/[e^{E/T}-1]$ and G_i as the conductance through the dot-i junction. The steady state ($\dot{P}_N = 0$) solution the master equation is given by: $\Gamma_{N\to N-1}P_N = \Gamma_{N-1\to N}P_{N-1}$, with a current passing through the dot:

$$I = (-e)\sum_N P_N\left(\Gamma^{(i)}_{N\to N+1} - \Gamma^{(i)}_{N\to N-1}\right). \tag{1.118}$$

When the structural temperature T is much lower than the Coulomb blockade energy E_c, the flow of current resulting from the application of an electrical bias $\mu_1 = -eV$, (with a grounded drain, $\mu_2 = 0$) is nonlinear in V: below a threshold bias V_T (determined by the capacitance energy E_c and the gating V_g), no current flows through the structure. For this reason, the source-dot-drain may used as a single electron transistor (SET). (See Fig. (1.7)). SET's have been realized for several types of , including metal island/metal oxide barrier [SMM97, NKT96, RBT97], semiconductor-based structures [HI99, KRL97]. Lateral quantum dot-lead structures, created by electrically gating regions of a two dimensional electron gas, provide a additional degree of control, as the tunnel barriers may be arbitrarily tuned.

Spin-based transport through quantum dots has been an active area of research in recent years, including Kondo physics and spin transport [RSL00]. In Chapter 6, we introduce magnetic dynamics and investigate charge pumping by precessing magnetic dot.

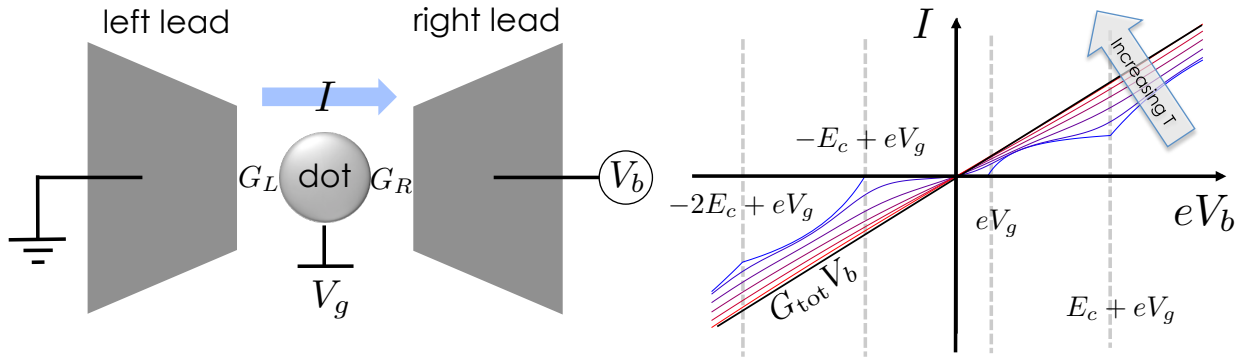

Figure 1.7: Current-voltage characteristics of a single-electron transistor, consisting of a quantum dot attached to left and right leads. The charge current I (shown for temperatures $T = 0$ (blue) in increasing steps of $E_c/10$ to $T = \infty$) flowing through the structure as a response to a bias voltage V_b can be controlled by gating of the dot. When $T \ll E_c$, the structure acts as a single transistor, demonstrating a nonlinear response asymmetric in bias voltage; when $T \gg E_c$, Coulomb blockade effects are washed out by thermal fluctuations, and the total conductance $G_{\rm tot} = 1/(G_L^{-1} + G_R^{-1})$ is constant in voltage.

CHAPTER 2

Interfacial Magnon-Mediated Spin and Heat Transfer

The excitation of magnetic dynamics by spin-transfer torque [Ber96a, Slo96, RS08], and the reciprocal process of spin pumping [TBB02a, TBB05], introduced in the last chapter, are essential components in the field of metal-based spintronics. Interfacial spin-transfer torque was first realized in conducting magnetic heterostructures, such as spin valves, wherein angular momentum is exchanged with the magnetic order as spin-polarized electrons traverse the structure [TJB98, MRK99]. Subsequent was the demonstration of the electrical coupling of magnetic insulators interfaced with normal conductors, wherein itinerant-electron spins interact with the magnetic order over atomistically short length scales near the interface. This broadens the ferromagnetic-resonance linewidth [HBM11, BHK12a], allows for spin Hall generation and detection of magnetic dynamics by electrical means [SKA10b, SKC11b, HdH], and engenders spin Seebeck and Peltier effects that couple magnetic dynamics with heat currents [UXA10, BSv12a, FDW14]. Despite this tremendous experimental progress, the basic theoretical problem of the *finite-temperature* transfer of angular momentum across thermodynamically biased normal-metal (N)/ferromagnetic-insulator (F) interfaces remains open.

The out-of-equilibrium magnonic spin transport in an N/F bilayer is well understood in the case when the spin accumulation in N is *collinear* with the magnetic order parameter in F [BDT12, BDB14]. In this Letter, we develop a complete description of spin and heat transfer from both the large-angle coherent (i.e., magnetic order) and small-angle incoherent (i.e., magnons) dynamics in F, including the interplay of the two (wherein magnon transport exerts a torque on the magnetic order parameter and vice versa), for arbitrary relative orientations of the N spin accumulation and F magnetization. While the longitudinal spin density

injected into F from N is absorbed by the thermal cloud of magnons, the net transverse spin current has to be accommodated by the dynamical reorientation of the ferromagnetic order parameter, i.e., a (temperature-dependent) torque. The strength for both processes can be parametrized by the spin-mixing conductance [BNB00], which we relate to the quantum-mechanical matrix elements describing elastic and inelastic electron scattering off of the N/F interface.

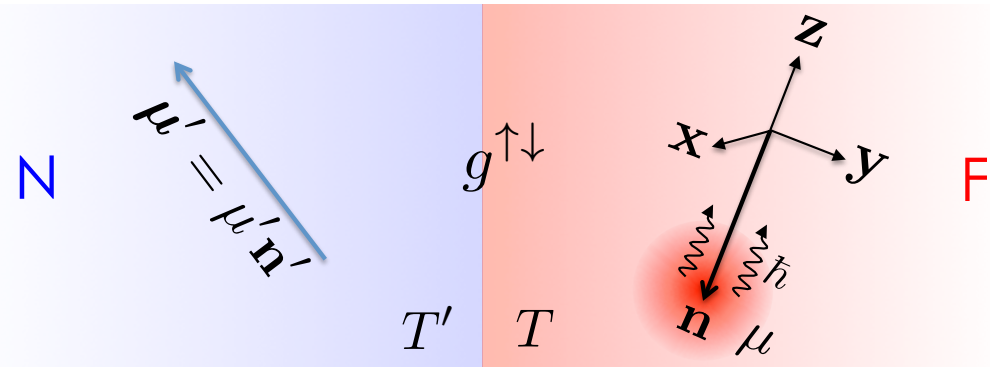

Figure 2.1: Schematic of the N/F junction. $\mathbf{n}$ is the orientation of the ordered spin density in F and $\mathbf{n}'$ is the spin-accumulation direction in N, both near the interface. Itinerant electrons carrying spin $\pm\hbar/2$ along $\mathbf{n}'$ transfer angular momentum via exchange coupling with both the (macroscopic) order parameter $\mathbf{n}$ and magnons in F, the latter each carrying angular momentum $\hbar$ in the $-\mathbf{n}$ ($= \mathbf{z}$) direction and obeying a Bose-Einstein distribution with chemical potential μ. Spin and heat currents across the interface are driven by the out-of-equilibrium spin accumulation $\mu' = \mu_+ - \mu_-$ in N, chemical potential μ in F, and/or an effective interfacial temperature drop $\delta T = T - T'$. The interfacial exchange coupling is quantified by the spin-mixing conductance $g^{\uparrow\downarrow}$ (see text).

2.1 Main results

We start by summarizing our main results for spin and energy transport across an N/F interface (see Fig. 2.1 for a schematic), where the spins of itinerant electrons in N are exchange coupled to the magnetic moments of F. In N, the out-of-equilibrium spin density (in units of $\hbar$) $\boldsymbol{\rho}$ corresponds to spin accumulation $\boldsymbol{\mu}' \equiv \mu' \mathbf{n}' = 2\boldsymbol{\rho}/D$, where $\mathbf{n}'$ is a unit vector, D

is the density of states (per spin and unit volume), and $\mu' \equiv \mu_+ - \mu_-$ is the difference in electrochemical potentials for the electrons up and down along $\mathbf{n}'$ [BNB00]. In the absence of coupling with the ferromagnet, the electronic distribution function, $\langle c^\dagger_{k'\sigma'} c_{k\sigma} \rangle = f_{k\sigma\sigma'}\delta_{kk'}$, can be written as $\check{f}_k = \sum_{a=\pm} \check{u}_a f_{ka}$, where $\{\check{f}_k\}_{\sigma\sigma'} = f_{k\sigma\sigma'}$, $\check{u}_\pm = \left(\check{1} \pm \mathbf{n}' \cdot \check{\boldsymbol{\sigma}}\right)/2$ are spin-projection matrices, and $f_{ka} = [e^{\beta'(\epsilon_k - \mu_a)} + 1]^{-1}$ is the Fermi-Dirac distribution function with a common temperature $T' \equiv 1/\beta'$ (setting $k_B = 1$). ϵ_k is the single-electron energy and T' is assumed to be much smaller than the Fermi energy ϵ_F so that D can be treated as a constant.

If the equilibrium spin density (the macroscopic order parameter) in F lies in the direction of the unit vector $\mathbf{n}$, its excitations (magnons) carry $\hbar$ of angular momentum in the $-\mathbf{n}$ direction (neglecting dipolar and spin-orbit interactions, which is possible when the ambient temperature is much larger than the associated energy scales). Built in our treatment is the assumption that magnons maintain an internal thermal equilibrium, which can be achieved, for example, by strong magnon-magnon scattering (which is enhanced at high temperatures) or by coupling to an external heat sink (e.g., an adjacent copper layer). Thermal magnons in F then follow the Bose-Einstein distribution function: $\langle \hat{a}^\dagger_{q'} \hat{a}_q \rangle = n[\beta(\epsilon_q - \mu)]\delta_{qq'}$, where $n(x) = (e^x - 1)^{-1}$, ϵ_q is the single-magnon energy, μ and $T \equiv \beta^{-1}$ are the effective magnon chemical potential and temperature, respectively. This temperature, T, understood as the average magnon temperature a correlation length away from the interface, may be different from that of the electrons at the interface, T'; the corresponding interfacial thermal bias $\delta T \equiv T - T'$ will affect the flow of spin and heat across the interface.

The relevant variables whose dynamics we wish to study are the vectorial spin density $\boldsymbol{\rho}$ and (scalar-valued) entropy on the electric side and, likewise, vectorial spin density (whose magnitude is determined by the magnonic distribution function and direction by the ordering axis $\mathbf{n}$) and entropy on the magnetic side. The respective thermodynamic forces are $\boldsymbol{\mu}'$ and T' on the N side and μ, $\mathbf{H} \perp \mathbf{n}$, and T on the F side, as will be detailed later. As the central results of this Letter, we calculate, as functions of the temperatures T and T', chemical potentials μ and μ', and spin-density orientations $\mathbf{n}$ and $\mathbf{n}'$, the spin and energy currents across the interface.

First, when the magnetic order $\mathbf{n}$ is *static,* we obtain the interfacial spin-current density $\mathbf{j} = -\hbar\dot{\boldsymbol{\rho}} d_N$ out of the normal-metal film of thickness d_N, up to first order in n/s (with n as the thermal magnon density and s as the saturation spin density of F in units of $\hbar$):

$$\mathbf{j}|_{\dot{\mathbf{n}}=0} = \frac{1}{4\pi}\left(\tilde{g}_i^{\uparrow\downarrow} + \tilde{g}_r^{\uparrow\downarrow}\mathbf{n}\times\right)\boldsymbol{\mu}' \times \mathbf{n} + \tilde{\mathbf{j}}\,, \tag{2.1}$$

where $\tilde{g}_i^{\uparrow\downarrow} = (1 - n/s)g_i^{\uparrow\downarrow}$ and $\tilde{g}_r^{\uparrow\downarrow} = (1 - 2n/s)g_r^{\uparrow\downarrow}$ [**?**]. $g_r^{\uparrow\downarrow}$ and $g_i^{\uparrow\downarrow}$ here are, respectively, the real and imaginary parts of the $T = 0$ spin-mixing conductance per unit area, $hG^{\uparrow\downarrow}/\mathcal{A}e^2 = g^{\uparrow\downarrow} = g_r^{\uparrow\downarrow} + ig_i^{\uparrow\downarrow}$ [BNB00]. The first term in Eq. (5.1) stems from elastic scattering of electrons off of the F macroscopic order, while the last term $\tilde{\mathbf{i}}$ is rooted in thermally-activated electron-magnon scattering at the interface:

$$\tilde{\mathbf{j}} = \sum_{a,b=\pm} M_{ab}[(1 - a\mathbf{n}\cdot\mathbf{n}')(1 + b\mathbf{n}\cdot\mathbf{n}')\mathbf{n} + (a/2 - b/2 + ab\mathbf{n}\cdot\mathbf{n}')\mathbf{n}\times\mathbf{n}'\times\mathbf{n}]\,, \tag{2.2}$$

with

$$M_{ab} = \frac{g_r^{\uparrow\downarrow}}{4\pi s}\int_0^\infty d\epsilon g(\epsilon)\,(\epsilon + \hbar\Omega - \mu_{ab})\,\{n\,[\beta(\epsilon - \mu^*)] - n\,[\beta'(\epsilon + \hbar\Omega - \mu_{ab})]\} \tag{2.3}$$

Here, $\mu_{ab} \equiv \mu_a - \mu_b$, $g\,(\epsilon)$ is the magnon density of states (per unit volume), $\hbar\Omega$ is the magnon gap (so that each magnon carries energy $E = \epsilon + \hbar\Omega$), and $\mu^* \equiv \mu - \hbar\Omega$. We are supposing that the structure of the thermal magnons is dominated by exchange interactions, such that they are circularly polarized and carry a well-defined spin. Regarding the energy-current density $\dot{q} = -(d/dt)\sum_k \epsilon_k\langle\hat{a}_k^\dagger\hat{a}_k\rangle/A$ out of N through the interfacial area A, elastic scattering does not contribute, while inelastic scattering yields:

$$\dot{q} = -\sum_{a,b=\pm} N_{ab}\,(1 - a\mathbf{n}\cdot\mathbf{n}')\,(1 + b\mathbf{n}\cdot\mathbf{n}')\,, \tag{2.4}$$

where

$$N_{ab} = \frac{g_r^{\uparrow\downarrow}}{4\pi\hbar s}\int_0^\infty d\epsilon g\,(\epsilon)\,(\epsilon + \hbar\Omega)\,(\epsilon + \hbar\Omega - \mu_{ab}) \times \{n\,[\beta(\epsilon - \mu^*)] - n\,[\beta'(\epsilon + \hbar\Omega - \mu_{ab})]\}\,.$$

Second, in order to furthermore include order-parameter *dynamics* $\mathbf{n}(t)$, we specialize the above results to linear response, thus allowing us to utilize the Onsager reciprocity [**?**] (see

discussion below). Our final expressions (assuming weak thermodynamic biases and slow order-parameter dynamics) for the total spin and heat currents (into F) at the interface are:

$$\mathbf{j} = \frac{1}{4\pi}\left(\tilde{g}_i^{\uparrow\downarrow} + \tilde{\mathfrak{g}}_r^{\uparrow\downarrow}\mathbf{n}\times\right)(\boldsymbol{\mu}'\times\mathbf{n} - \hbar\dot{\mathbf{n}}) + \left[g\left(\mu + \mathbf{n}\cdot\boldsymbol{\mu}'\right) + \mathcal{S}\delta T\right]\mathbf{n}\,,$$
$$\dot{q} = -\kappa\delta T - \Pi\left(\mu + \mathbf{n}\cdot\boldsymbol{\mu}'\right)\,. \tag{2.5}$$

Here,

$$\tilde{\mathfrak{g}}_r^{\uparrow\downarrow} = \tilde{g}_r^{\uparrow\downarrow} + 4\pi\sum_{a,b=\pm}\partial_{\mu'}M_{ab}\left(a/2 - b/2 + ab\mathbf{n}\cdot\mathbf{n}'\right)$$

is the total effective (real part of the) spin-mixing conductance, $g = 4\partial_\mu M_{++}$ and $\mathcal{S} = 4\partial_T M_{++}$ are respectively the spin conductance and spin Seebeck coefficient, $\kappa = 4\partial_T N_{++}$ and $\Pi = 4\partial_\mu N_{++} = T\mathcal{S}/\hbar$ are the (magnonic) thermal conductance and spin Peltier coefficient. All these transport coefficients are evaluated in equilibrium and pertain to the interface. g, κ, $\mathcal{S}$, and Π are all thermally activated, while $\tilde{\mathfrak{g}}_r^{\uparrow\downarrow}$ and $\tilde{g}_i^{\uparrow\downarrow}$ reduce to the real and imaginary components of the familiar [BNB00, TBB02a] zero-temperature spin-mixing conductance $g^{\uparrow\downarrow}$ at $T = 0$ and acquire thermal corrections that scale as $\sim (T/T_c)^{3/2}$ when $T \gg \hbar\Omega$ (assuming quadratic magnon dispersion), where T_c is the Curie temperature.

The transverse (i.e., $\perp$ $\mathbf{n}$) component of the spin current (2.5) exerts a torque on the magnetic order parameter, which enters on the right-hand side of the generalized Landau-Lifshitz equation:

$$(1 + \alpha\mathbf{n}\times)\hbar\dot{\mathbf{n}} + \mathbf{n}\times\mathbf{H} = (\alpha_i' + \alpha_r'\mathbf{n}\times)(\boldsymbol{\mu}'\times\mathbf{n} - \hbar\dot{\mathbf{n}})\,,$$

where α is the bulk Gilbert damping, $\mathbf{H}$ is the effective magnetic field (in appropriate units), $\alpha_i' = \tilde{g}_i^{\uparrow\downarrow}/4\pi\tilde{s}d_F$, $\alpha_r' = \tilde{\mathfrak{g}}_r^{\uparrow\downarrow}/4\pi\tilde{s}d_F$, $\tilde{s} = s - n$, and d_F is the ferromagnet's thickness. (Note that the torque depends on $\boldsymbol{\mu}'$ and Onsager-reciprocal spin pumping $\propto \dot{\mathbf{n}}$ but not on μ or δT.) The longitudinal (i.e, $\parallel$ $\mathbf{n}$) spin current, on the other hand, is accommodated by the magnon flux into the ferromagnet, $i_m = \dot{n}d_F = -\mathbf{n}\cdot\mathbf{i}/\hbar$, driven by the thermodynamic forces μ, $\boldsymbol{\mu}'$, and δT:

$$\hbar i_m = -g\left(\mu + \mathbf{n}\cdot\boldsymbol{\mu}'\right) - \mathcal{S}\delta T\,,$$

which does not depend on the precession of $\mathbf{n}$.

2.2 Interfacial Coupling

As an effective model for the coupling between the spin degrees of freedom of N interfaced with F, we take the exchange Hamiltonian:

$$\hat{\mathcal{H}} = -J \int d^2\mathbf{r}\, \hat{\boldsymbol{\rho}}\left(\mathbf{r}\right) \cdot \hat{\mathbf{s}}\left(\mathbf{r}\right) \,, \tag{2.6}$$

where integration is performed over the interfacial area. Here, $\hat{\boldsymbol{\rho}}(\mathbf{x}) = \sum_{\sigma\sigma'} \hat{\psi}^\dagger_\sigma(\mathbf{x})\boldsymbol{\sigma}_{\sigma\sigma'}\hat{\psi}_{\sigma'}(\mathbf{x})/2$ is the N spin density (with $\hat{\psi}_\sigma$ being spin-σ itinerant electron field operators and $\boldsymbol{\sigma}$ a vector of Pauli matrices) and $\hat{\mathbf{s}}$ is the F spin density associated with localized electron orbitals, both expressed in units of $\hbar$. We will take $-\mathbf{n}$ to be the spin-quantization axis for the electrons in N, such that an itinerant electron with $\sigma = \uparrow\,(\downarrow)$ carries an angular momentum of $\hbar/2$ in the $\mp\mathbf{n}$ direction. Expanding $\hat{\psi}_\sigma(\mathbf{x}) = \sum_k \psi_k(\mathbf{x})\hat{c}_{k\sigma}$ in terms of the electron annihilation operators $\hat{c}_{k\sigma}$ within an orthonormal basis $\psi_k(\mathbf{x})$ labeled by orbital quantum numbers k (corresponding to spin-degenerate energy eigenstates in the absence of magnetic coupling, $J = 0$), we write

$$\hat{\boldsymbol{\rho}}(\mathbf{x}) = \frac{1}{2}\sum_{\sigma\sigma' kk'} \psi^*_k(\mathbf{x})\psi_{k'}(\mathbf{x})\hat{c}^\dagger_{k\sigma}\boldsymbol{\sigma}_{\sigma\sigma'}\hat{c}_{k'\sigma'} \,.$$

Orienting a spin-space Cartesian coordinate system for the z axis to point in the $-\mathbf{n}$ direction, we write the F spin density $\hat{\mathbf{s}}$ in terms of the incoherent operator via the Holstein-Primakoff transformation [HP40b] Eqs. (1.24) and (1.25) for the incoherent operator $\hat{\varphi}$. Expressing $\hat{\phi}\left(\mathbf{x}\right) = \sum_q \phi_q\left(\mathbf{x}\right)\hat{a}_q$ in the orthonormal spin-wave basis $\phi_q\left(\mathbf{x}\right)$ ($\hat{a}_q$ being the magnon annihilation operators) and inserting the above spin densities into Eq. (2.6), we obtain to second order in $\hat{a}_q$:

$$\hat{\mathcal{H}} \approx \sum_{kk'\sigma} U_{kk'\sigma}\hat{c}^\dagger_{k\sigma}\hat{c}_{k'\sigma}(1 - \hat{n}/s) + \Big(\sum_{kk'q} V_{kk'q}\hat{c}^\dagger_{k\uparrow}\hat{c}_{k'\downarrow}\hat{a}_q + \text{H.c.}\Big) \,, \tag{2.7}$$

The first term in Eq. (2.7) has matrix elements

$$U_{kk'\uparrow} \equiv J\frac{s}{2}\int d^2\mathbf{r}\, \psi^*_k\left(\mathbf{r}\right)\psi_{k'}\left(\mathbf{r}\right) = -U_{kk'\downarrow}$$

and describes the elastic scattering of electrons off the static magnetization of F. When the spin of an incoming electron in N is collinear with $\mathbf{n}$, scattering by $U_{kk'\sigma}$ mixes orbital states

while preserving the spin, such that no torque is exerted on F. In general, we can supply electrons that are polarized along a different axis $\mathbf{n}'$, as sketched in Fig. 2.1. Rewriting the first term in Eq. (2.7) in the corresponding $\pm$ basis, we would obtain the spin-flip terms $\propto \hat{c}^{\dagger}_{k_+}\hat{c}_{k'_-}$, which result in a spin angular-momentum transfer to F. The second term in Eq. (2.7) has matrix elements

$$V_{kk'q} \equiv -J\sqrt{\frac{s}{2}}\int d^2\mathbf{r}\,\psi^*_{\mathbf{k}}(\mathbf{r})\,\psi_{\mathbf{k}'}(\mathbf{r})\,\phi_{\mathbf{q}}(\mathbf{r})\ ,$$

and, along with its conjugate, describe inelastic spin-flip scattering processes wherein an up-electron/down-hole pair is created (annihilated) in N, along the z axis, destroying (creating) a magnon in F. As we show below, in contrast to elastic scattering processes, such inelastic spin flips generate a temperature-dependent spin current with a component along $\mathbf{n}$.

The first term in Eq. (2.1) arises from elastic scattering $U_{kk'\sigma}$, which governs coefficients $g_i^{\uparrow\downarrow} = DU$ and $g_r^{\uparrow\downarrow} = D^2\left|U'\right|^2$, where

$$U \equiv \frac{2\pi}{\mathcal{A}D}\sum_k \delta(\epsilon_F-\epsilon_k)(U_{kk\uparrow}-U_{kk\downarrow})\,, \tag{2.8}$$

$$\left|U'\right|^2 \equiv \frac{\pi^2}{2\mathcal{A}D^2}\sum_{kk'}\delta(\epsilon_F-\epsilon_k)\delta(\epsilon_F-\epsilon_{k'})\left[\left|U_{kk'\uparrow}\right|^2+\left|U_{kk'\downarrow}\right|^2-2\mathrm{Re}\left(U_{kk'\uparrow}U^*_{kk'\downarrow}\right)\right]\ . \tag{2.9}$$

Thus the reactive ($g_i^{\uparrow\downarrow}$) and dissipative ($g_r^{\uparrow\downarrow}$) spin currents arising from elastic scattering depend on the orientations of the N and F spin densities but not on thermal bias. From the form of this spin current [i.e., the first term in Eq. (2.1)], which survives a nonperturbative scattering-matrix treatment [BNB00], we identify $g_r^{\uparrow\downarrow}$ and $g_i^{\uparrow\downarrow}$ as the real and imaginary parts of the spin-mixing conductance.

In contrast, the magnonic contribution $\tilde{\mathbf{i}}$ to spin current, which arises from inelastic processes $V_{kk'q}$, is additionally dependent on the magnon distribution function in F and temperature in N.

2.3 Calculation of Spin Currents

Having established the equilibrium states of magnons in F and electrons in N (held at different temperatures, T and T', and spin chemical potentials, μ and μ') when $J = 0$, we

treat the transport perturbatively for a finite J. To this end, we utilize the Kubo formula to calculate the spin current $\mathbf{i}$, up to second order in exchange J, yielding an expression in the form of Eq. (5.1).

2.3.1 Current in Parallel Configuration

Let us start by obtaining the interfacial spin current when spin accumulation is oriented in the $+\mathbf{z}$ direction, so that the $\pm$ electron basis (along the $\mp\mathbf{n}'$ direction) coincides with the basis $\uparrow\downarrow$ basis. In this case, the elastic term $U_{kk'\sigma}$, which in this case is diagonal in the $\pm$ basis, does not contribute to the spin current, since spin flip processes $\hat{c}_{\pm}^{\dagger}\hat{c}_{\mp}$ are absent: when the spin accumulation is collinear with the order parameter $\mathbf{n}$, by rotational symmetry, no coherent torque is exerted on $\mathbf{n}$. The inelastic term, however, does yield a spin current, corresponding to the absorption of incoherent magnons (with angular momentum $-\hbar\mathbf{n}$) by the F spin density. There, a down-spin hole/up-spin electron pair (with up/down referring to the z quantization axis) of total spin $\hbar\mathbf{z}$ annihilates to create a circularly polarized magnon in F (similar to Andreev reflection at a normal metal/superconductor interface), injecting a spin current $+\hbar\mathbf{z}$ into F, while the reverse process results in the transfer of $+\hbar\mathbf{z}$ into N.

Assuming that dephasing, arising from coupling to the environment (e.g. magnon-phonon interactions, magnon-electron interactions, etc.) is large enough to destroy coherence between N electrons and F magnons, spin transport across the N/F interface may be captured by Fermi's Golden Rule, which yields a spin current into F

$$\mathbf{I}_F = (-\mathbf{n})\hbar\left(\Gamma_+ - \Gamma_-\right) \tag{2.10}$$

where

$$\Gamma_{\pm} = 2\pi \sum_{if_{\pm}} \left|\langle f_{\pm}| \hat{V} |i\rangle\right|^2 W_i \delta\left(E_{f_{\pm}} - E_i\right) \tag{2.11}$$

is the magnon hopping rate into (+) or out of F (-), bringing the system from a state $|i\rangle = |F_i\rangle \otimes |N_i\rangle$ with magnons to a final state $|f_{\pm}\rangle$ with ± 1 magnons, with $\hat{V}$ as the inelastic Hamiltonian and W_i as the statistical weight for the state i. Using $\langle f_+| = \langle i|\, \hat{c}_{k\uparrow}^{\dagger}\hat{c}_{k\downarrow}\hat{a}_q/\sqrt{n_{qi}+1}$ and $\langle f_-| = \langle i|\, \hat{c}_{k\uparrow}^{\dagger}\hat{c}_{k\downarrow}\hat{a}_q/\sqrt{n_{qi}}$, assuming a thermal ensemble $W_i = W_{Fi}W_{\uparrow i}W_{\downarrow i}$, with $\sum_i W_{Fi}\left\langle \hat{a}_q^{\dagger}\hat{a}_{\tilde{q}}\right\rangle_i =$

$\delta_{q\tilde{q}} \left\langle \hat{a}_q^\dagger \hat{a}_q \right\rangle$ and $\sum_i W_{si} \left\langle i \right| \hat{c}_{ks}^\dagger \hat{c}_{\tilde{k}\tilde{s}} \left| i \right\rangle = \left\langle \hat{c}_{ks}^\dagger \hat{c}_{\tilde{k}\tilde{s}} \right\rangle$, one has

$$(\Gamma_+ - \Gamma_-) = 2\pi \sum_{kk'q} |V_{kk'q}|^2 \left[f_{k\uparrow} \left(1 - f_{k'\downarrow}\right) \left(1 + N_q\right) - \left(1 - f_{k\uparrow}\right) \left(f_{k'\downarrow}\right) N_q \right] \delta \left(\epsilon_q + \epsilon_{k'} - \epsilon_k\right) \tag{2.12}$$

where $N_q = \left\langle \hat{a}_q^\dagger \hat{a}_q \right\rangle$ is the number of magnons in the state q.

Let us first suppose consider the spin current $\mathbf{I}_F$ for a zero-temperature condensate, where one mode q is macroscopically occupied (i.e. a condensate), and all others vanish. In the thermodynamic limit (wherein the volume of F is taken to infinity at fixed magnon density), $N_q \gg 1$. Inserting a factor of

$$1 = \int d\epsilon \int d\epsilon' \delta \left(\epsilon - \epsilon_{k'}\right) \delta \left(\epsilon - \epsilon_{k'}\right) \tag{2.13}$$

into Eq. (2.12), assuming a weak energy-dependence of the electronic density of states:

$$D\left(\epsilon\right) = \sum_k \delta \left(\epsilon - \epsilon_k\right) \approx D\left(\epsilon_F\right) = D \tag{2.14}$$

and using the identities

$$n_F\left(x\right) \left[1 - n_F\left(y\right)\right] = n_B\left(x - y\right) \left[n_F\left(y\right) - n_F\left(x\right)\right] \tag{2.15}$$

and

$$\int_{-\infty}^{\infty} \left[n_F\left(x\right) - n_F\left(x + z\right)\right] dx = z \tag{2.16}$$

one obtains a current density

$$\mathbf{j}_q = \frac{\mathbf{I}}{\mathcal{A}} = (-\mathbf{n}) n_q 2D^2 \left|V_0\right|^2 \left(\mu' - \hbar\Omega\right), \tag{2.17}$$

where $\mathcal{A}$ is the interfacial area and

$$\left|V_q\right|^2 \equiv \frac{\pi d_F}{D^2} \sum_{kk'} \left|V_{kk'q}\right|^2 \delta \left(\epsilon_F - \epsilon_k\right) \delta \left(\epsilon_F - \epsilon_{k'}\right) . \tag{2.18}$$

For a thermal ensemble, $N_q = n_B\left[\beta\left(\epsilon_q - \mu\right)\right]$; using $n_B\left(-x\right) n_B\left(y\right) - n_B\left(x\right) n_B^L\left(-y\right) = n_B\left(x\right) - n_B\left(y\right)$ together with Eqs. (2.15) and (2.16), the current density can be written in terms of the magnon density of states $g\left(\epsilon\right)$ (per ferromagnetic volume $\mathcal{V}_F$):

$$\mathbf{j}_x = \frac{\mathbf{I}}{\mathcal{A}} = (-\mathbf{n}) 2D^2 \int d\epsilon \left|V_x\right|^2 \left(\epsilon\right) g\left(\epsilon\right) \left(\Delta\mu - \hbar\Omega\right) \left[n_B\left[\beta_F\left(\epsilon - \mu\right)\right] - n_B\left[\beta_N\left(\epsilon - \mu'\right)\right]\right] \tag{2.19}$$

where the weakly energy-dependent quantity

$$|V_x|^2(\epsilon) = \frac{\pi d_F}{D^2 \mathcal{V}_F g(\epsilon)\hbar} \sum_{kk'q} |V_{kk'q}|^2 \delta(\epsilon_k - \epsilon_F)\delta(\epsilon_{k'} - \epsilon_F)\delta(\epsilon_q - \epsilon), \tag{2.20}$$

2.3.1.1 Thermodynamics of Inelastic Magnon Scattering

Eq. (2.19) suggests that spin flow to and from excited magnon states vanishes when there is no thermal or spin gradient, i.e., when $\beta = \beta'$ and $\mu' = \mu$. However, when either of these conditions is not met, $\mathbf{j}_\mathrm{x} \neq 0$ and spin (as well as energy) is transported across the insulator/conductor interface. In a steady state (i.e., zero spin current), in normal phase with thermal bias, $\beta - \beta' \neq 0$, a spin chemical potential difference $\Delta\mu = \mu' - \mu$ develops to oppose it:

$$\Delta\mu \approx (\beta' - \beta) \frac{\int_{\hbar\Omega}^{\infty} d\epsilon\,(\epsilon - \bar{\mu})(\epsilon - \mu')\, n'_\mathrm{B}\left(\bar{\beta}(\epsilon - \bar{\mu})\right)}{\bar{\beta}\int_{\hbar\Omega}^{\infty} d\epsilon\,(\epsilon - \mu')\, n'_\mathrm{B}\left(\bar{\beta}(\epsilon - \bar{\mu})\right)},$$

where $\bar{\beta} \equiv (\beta + \beta')/2$, $\bar{\mu} \equiv (\mu_L + \mu')/2$, $n'_B = \partial_\epsilon n_B(\epsilon)$, and the thermodynamic biases are assumed to be small (i.e. $\beta' - \beta \ll \bar{\beta}, \mu' \ll \bar{\mu}$).

On the other hand, the condensed spin current j_0 is independent of both T and T, and, provided $\hbar\Omega > \mu'$, always carries spin away from the conductor, irrespective of the temperature gradient between the two systems. The explanation for this behavior can be understood as follows. Consider a single tunneling event involving the creation (destruction) of a ground-state magnon ($\Delta N_0 = \pm 1$) and the corresponding creation of a down-(up-)spin electron-hole excitation in the conductor ($\Delta N_R = -\Delta N_0$), which we call process A (B) in Fig. 2.3. The entropy change in the insulator associated with either process vanishes when the magnons form a BEC, so that the entropy change of the whole system is just dS_R, which can be found by enforcing energy conservation:

$$\Delta S_\mathrm{tot} = \Delta S_R = \frac{1}{T_R}(\hbar\Omega - \mu')\Delta N_R\,.$$

Thus, process B (A) is favored ($\Delta N_R \gtrless 0$) for tunneling events involving ground-state magnons when $\hbar\Omega \gtrless \mu'$, in agreement with Eq. (2.17). Put differently, if $\mu' = 0$ the phase space of the conductor is unaffected with either the introduction of an up-spin excitation

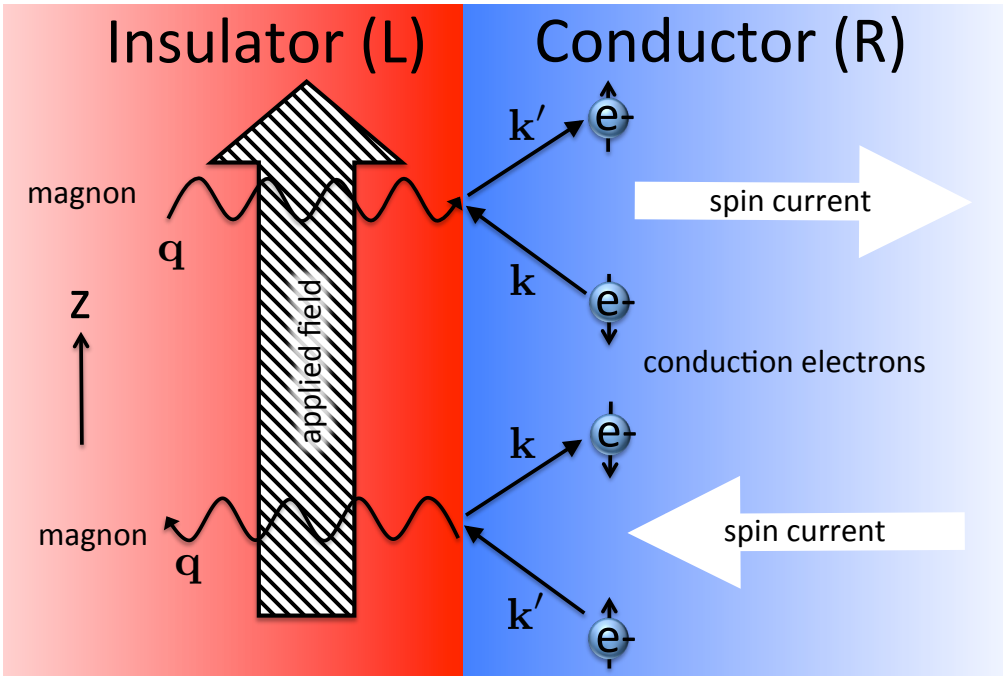

Figure 2.2: The magnetic moments of insulator (left) atoms are coupled to the itinerant electrons of an adjacent conductor (right); an electron scatters inelastically off the interface, flipping its spin and creating or annihilating a magnon in the insulator. While coupling across the interface requires some degree of overlap between electrons in the conductor and localized electron orbitals in the insulator, a net electron tunneling between the two subsystems is prohibited, so that only spin density is transferred. The magnetic field in the insulator, and hence static magnetization, point in the positive z direction; for a negative gyromagnetic ratio the static spin density is therefore oriented in the $-z$ direction, so that magnons carry spin $+\hbar$.

or the introduction of a down-spin excitation. However, process A requires the conductor to surrender an energy quantum $\hbar\Omega$ to the insulator, whereas process B means a net gain in energy for the conductor; the overall entropy gain in the conductor (and therefore the entire system) is thus greater for process B than A. The zero-temperature version of this explanation is presented graphically in Fig. 2.3.

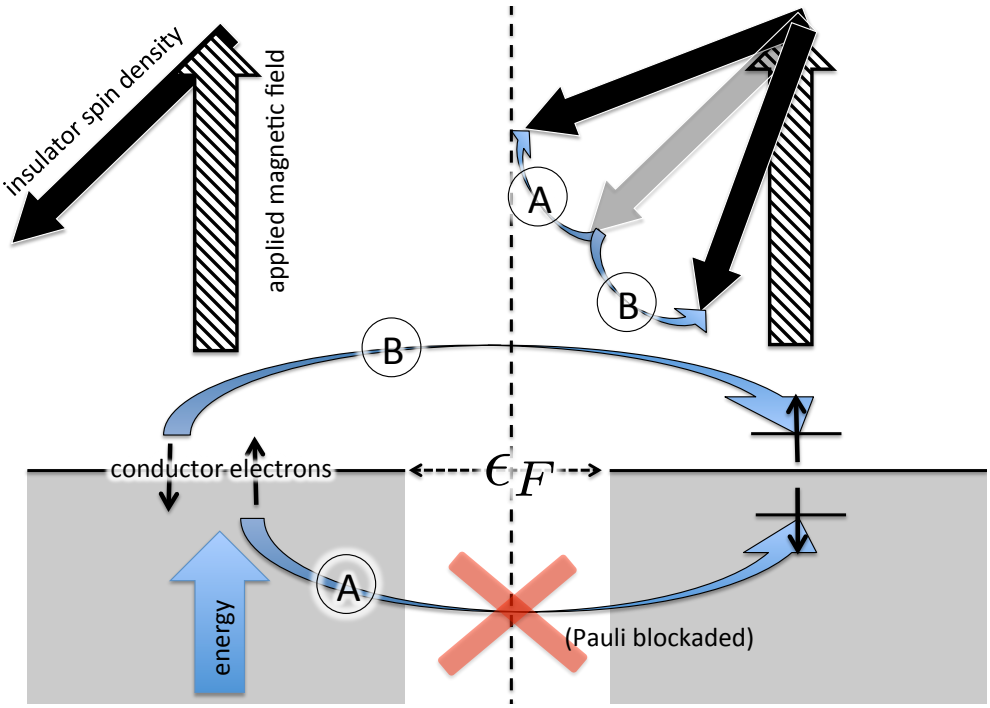

Figure 2.3: A down electron may relax the ferromagnetic insulator, carrying away the excess energy away in a scattering state above the Fermi surface ϵ_F (process B). An incident up electron on the Fermi surface, however, cannot transfer up spin to the insulator magnetization (process A), since such an energy-preserving process would raise the energy of the magnet, lowering that of the electron and therefore landing it below the Fermi surface, which is Pauli blockaded. Process B therefore dominates, and the insulator magnetization relaxes towards the easy axis.

2.3.2 Current in General Configuration

Let us now generalize to cases wherein the orientation between the interfacial N spin accumulation $\boldsymbol{\mu}$ and the F spin density order parameter $\mathbf{n}$ is arbitrary. The simple picture of

spin transfer as well defined tunneling processes, transferring one unit of angular momentum between up-electron/down-hole pairs and magnons, no longer holds, necessitating a different perturbative approach.

First, consider the current engendered by perturbation $\hat{U}$, which for convenience we write:

$$\hat{U} = (1 - \hat{n}/s) \sum_{kk'} \sum_{\nu\nu'} U^{(kk')}_{\nu\nu'} \hat{c}^\dagger_{k\nu} \hat{c}_{k'\nu'} \,, \tag{2.21}$$

where $U^{(kk')}_{\uparrow\uparrow} = U_{kk'\uparrow}$, $U^{(kk')}_{\downarrow\downarrow} = U_{kk'\downarrow}$, and $U^{(kk')}_{\uparrow\downarrow} = U^{(kk')}_{\downarrow\uparrow} = 0$. We define the elastic spin resolved current operator entering on the normal metal side:

$$\begin{aligned} \hat{I}^{(e)}_{kss'} &= \frac{d}{dt}\left(\hat{c}^\dagger_{ks}\hat{c}_{ks'}\right) = i\left[\hat{U}, \hat{c}^\dagger_{ks}\hat{c}_{ks'}\right] \\ &= -i\,(1-\hat{n}/s)\sum_{\nu}\sum_{q\neq k} U^{(qk)}_{\sigma'\nu}\hat{c}^\dagger_{q\sigma}\hat{c}_{k\nu} + i\,(1-\hat{n}/s)\sum_{\nu}\sum_{q\neq k} U^{(kq)}_{\nu s}\hat{c}^\dagger_{k\nu}\hat{c}_{q\sigma'}. \end{aligned} \tag{2.22}$$

The lowest order (in $\hat{U}$) contribution to the current is found by taking thermal average $I^{(e,1)}_{k\sigma\sigma'} = \left\langle \hat{I}^{(e)}_{k\sigma\sigma'} \right\rangle \equiv [\check{I}^{(e,1)}_k]_{\sigma\sigma'}$; making use of Eqs. (2.15) and (2.16) the spin current into N are then given by:

$$\mathbf{j}^{(e,1)}_s = \frac{1}{\mathcal{A}}\left(\frac{\hbar}{2}\right)\sum_k \mathrm{Tr}\left[\check{I}^{(e,1)}_k \check{\boldsymbol{\sigma}}\right] = \left(1 - \frac{n}{s}\right)\frac{DU}{4\pi}\mathbf{n}\times\boldsymbol{\mu}' \,, \tag{2.23}$$

with U is defined in Eq. (2.8), while the energy current $\dot{Q}^{(e,1)} = \sum_k \mathrm{Tr}[\check{I}^{(e,1)}_k \epsilon_k]$ vanishes (where ϵ_k is the magnon excitation energy, vanishing for zero wavevector).

To obtain the second order current, we make use of the Kubo formula:

$$\left\langle I^{(e)}_{k,\sigma\sigma'}(t)\right\rangle_2 = -i\int_{t_0}^{t} dt' \left\langle \left[\hat{I}_{k,\sigma\sigma'}(t), \hat{U}(t')\right]\right\rangle \tag{2.24}$$

where the time-dependence of the electron operators $\hat{\mathcal{O}}(t)$ denotes evolution in the interaction picture. By application of Wick's theorem and defining $[\check{I}^{(e,2)}_k]_{\sigma\sigma'} \equiv \left\langle \hat{I}^{(e)}_{k\sigma\sigma'}\right\rangle_2$, one obtains

$$\begin{aligned} \check{I}^{(e,2)}_k(t) = \eta\sum_{p\neq k}\int_{t_0}^{t} dt' \left[\check{G}^{>}_p(t-t')\,\check{U}^{(pk)}\check{G}^{<}_k(t'-t), \check{U}^{(kp)}\right] \\ -\eta\sum_{p\neq k}\int_{t_0}^{t} dt' \left[\check{G}^{<}_p(t-t')\,\check{U}^{(pk)}\check{G}^{>}_k(t'-t), \check{U}^{(kp)}\right] \end{aligned} \tag{2.25}$$

where $\eta = (1 - 2n/s)$ (neglecting terms to order n^2/s^2), and

$$[\check{G}_p^{>}(t-t')]_{\sigma\sigma'} = -i\left\langle \hat{c}_{p\sigma}(t)\,\hat{c}_{p\sigma'}^{\dagger}(t')\right\rangle, \quad [\check{G}_p^{<}(t-t')]_{\sigma\sigma'} = i\left\langle \hat{c}_{p\sigma'}^{\dagger}(t')\,\hat{c}_{p\sigma}(t)\right\rangle. \tag{2.26}$$

are the greater than and lesser than Green's functions. Here, we have taken advantage of the fact that in thermal equilibrium, ensemble averages are diagonal in the eigenbasis of the unperturbed Hamiltonian: $\left\langle \hat{c}_p^{\dagger}\hat{c}_{p'}\right\rangle \propto \delta_{pp'}$. Using the spin projection operators $\hat{u}_\alpha(\mathbf{n})$ to express the Green's functions $\hat{G}_k^{(\gtrless)}(t-t') = \sum_\alpha \hat{u}_\alpha G_{k\alpha}^{(\gtrless)}(t-t')$ in the spin quantization basis provided by $\mathbf{n}$, the resulting second order currents are then obtained by performing the integrations over time (and neglecting electron-electron interactions, so that, for example, $G_{k\alpha}^{(<)}(t) = -i(1 - n_{F\alpha}(\epsilon_k))e^{-\epsilon_k t}$) and tracing over the spin indices:

$$\mathbf{j}_s^{(e,2)} = \frac{1}{\mathcal{A}}\left(\frac{\hbar}{2}\right)\mathrm{Tr}\left[\check{I}_k^{(e,2)}\check{\boldsymbol{\sigma}}\right] = \eta\frac{D^2\left|U'\right|^2}{4\pi}\mathbf{n}\times\boldsymbol{\mu}'\times\mathbf{n}\,, \tag{2.27}$$

where $|U'|^2$ defined in Eq. (2.9). Adding Eqs. (2.23) and (2.27), one obtains the first term in Eq. (5.1).

Now, consider contributions from the inelastic Hamiltonian, $\hat{V}$. Because the magnons, precessing around the order parameter $\mathbf{n}$ are incoherent, the first order in $\hat{V}$ currents ($\sim \langle\hat{a}\rangle$) vanish, as do currents which are of order $\hat{U}\hat{V}$. The remaining terms contribute to order $\hat{V}^2$, and are, again, obtained via the Kubo formula:

$$\left\langle I_{k,\sigma\sigma'}^{(i)}(t)\right\rangle = -i\int_{t_0}^{t} dt'\left\langle\left[\hat{I}_{k,\sigma\sigma'}(t),\hat{V}(t')\right]\right\rangle = W_{\sigma\sigma'}^{(k)} - \left(W_{\sigma'\sigma}^{(k)}\right)^{*} \tag{2.28}$$

where

$$\begin{aligned}\check{W}^{(k)} = &\sum_{qk'}\int_{t_0}^{t} dt' D_q^{<}(t'-t)\left[\check{G}_{k'}^{>}(t-t')\,\hat{V}_{qkk'}\hat{G}_p^{<}(t'-t),\hat{V}_{qk'k}^{\dagger}\right]\\ &-\sum_{qk'}\int_{t_0}^{t} dt' D_q^{>}(t'-t)\left[\hat{G}_{k'}^{<}(t-t')\,\hat{V}_{qkk'}\hat{G}_p^{>}(t-t'),\hat{V}_{qk'k}^{\dagger}\right]\end{aligned} \tag{2.29}$$

First, consider the spin current associated with a single mode q at energy $\epsilon_q \ll \epsilon_F$ that is macroscopically occupied with $n_q A d_F \gg 1$ magnons. In this case, we obtain from Eq. (2.29), after performing the integration in from Eq. (2.28) and tracing over spin indices:

$$\tilde{\mathbf{j}}_q = \frac{1}{\mathcal{A}}\sum_k\left(\frac{\hbar}{2}\right)\mathrm{Tr}\left[\check{I}_k^{(i)}\check{\boldsymbol{\sigma}}\right] = n_q\left|V_q\right|^2 D^2\left[\mathbf{n}\times\boldsymbol{\mu}'\times\mathbf{n} + 2\mathbf{n}(\mathbf{n}\cdot\boldsymbol{\mu}' + \hbar\Omega)\right], \tag{2.30}$$

where $|V_q|^2$ is given by Eq. (2.18).

The macroscopic occupation of the $q = 0$ mode is, in essence, a precessing macrospin, which may be excited at zero temperature while all of the thermal modes are frozen out. The spin current (2.30) (with $q = 0$) into F may then be compared with the standard expression [TBB02a] for spin current $\mathbf{i}_0(t)$ produced by a single classical macrospin pointing in the direction $\mathbf{n}_0(t)$:

$$\mathbf{j}_0\left(t\right) = \frac{1}{4\pi}\left(g_i^{\uparrow\downarrow} + g_r^{\uparrow\downarrow}\mathbf{n}_0\times\right)\left(\boldsymbol{\mu}'\times\mathbf{n}_0 - \hbar\dot{\mathbf{n}}_0\right) .$$

Suppose $\mathbf{n}_0(t)$ precesses at a small angle θ circularly around $\mathbf{n}$ at a frequency Ω. Identifying $n_0 = s(1-\cos\theta) \approx s\theta^2/2$, we get for the cycle-averaged spin current (for a constant $\boldsymbol{\mu}'$):

$$\langle\mathbf{j}_0\rangle = \frac{1}{4\pi}\left(g_i^{\uparrow\downarrow} + g_r^{\uparrow\downarrow}\mathbf{n}\times\right)\boldsymbol{\mu}'\times\mathbf{n} - \frac{n_0}{4\pi s}\left\{g_i^{\uparrow\downarrow}\boldsymbol{\mu}'\times\mathbf{n} + g_r^{\uparrow\downarrow}\left[\mathbf{n}\times\boldsymbol{\mu}'\times\mathbf{n} - 2\mathbf{n}(\mathbf{n}\cdot\boldsymbol{\mu}' + \hbar\Omega)\right]\right\},$$

to first order in n_0/s. This classical result is matched with our quantum-mechanical calculation, Eqs. (2.1) and (2.30), provided we identify:

$$4\pi s|V_0|^2D^2 = g_r^{\uparrow\downarrow} . \tag{2.31}$$

Crucially, this remarkable identification is only possible once the matrix elements $U_{kk'\sigma}$ are properly related to the spin-mixing conductance and the n/s corrections are included in $\tilde{g}^{\uparrow\downarrow}$, as described above.

For thermal magnons with finite wave numbers (that are still much smaller than the Fermi momentum of electrons) normal to the interface [HST13, KB13], $|V_q|^2 = 2|V_0|^2$, because of the Neumann (exchange) boundary conditions at the F film boundaries. Having thus related $|V_q|^2$ to the real part of the spin-mixing conductance, according to Eq. (2.31), we finally calculate the magnonic spin current using Eqs. (2.29) and (2.28), with the Bose-Einstein distribution for magnons instead of the macroscopic occupation. The resultant expression for the thermal spin and heat currents are given by Eqs. (2.2) and (2.4), respectively. We conclude that the spin-mixing conductance $g^{\uparrow\downarrow}$ captures all the relevant, both elastic and inelastic, matrix elements that govern interfacial spin transport.

It is instructive to specialize the spin current (2.2) to two limits. First, suppose that $\mathbf{n}' = -\mathbf{n}$: The term $\propto \mathbf{n}\times\mathbf{n}'\times\mathbf{n}$ is zero, and only the term with $a = +$ and $b = -$

contributes to the sum on the first line, reproducing the previously derived result Eq. (2.19) for the spin current for collinear magnetization and spin accumulation [BDT12]. Simplifying things further, consider the case when the spin accumulation vanishes, so that $\mu_{ab} = 0$: Here, M_{ab} is independent of a and b, the sums over terms involving a and b vanish, and we have $\tilde{\mathbf{i}} \propto \mathbf{n}$. In particular, the spin current does not depend on the direction $\mathbf{n}'$ that has no physical meaning in this regime.

The energy current density, $\dot{q} = \frac{1}{\mathcal{A}} \sum_k (\epsilon_k) \operatorname{Tr} \left[\check{I}_k^{(i)} \check{\boldsymbol{\sigma}} \right]$, (2.4) is calculated in a similar fashion. Once again, setting $\mathbf{n}' = -\mathbf{n}$ reproduces the known expression for energy transfer [BT]. For an arbitrary direction $\mathbf{n}'$ of spin accumulation, energy transport may be understood in terms of magnons, each of which carries angular momentum $-\hbar\mathbf{n}$: Comparison of the product $-\mathbf{n} \cdot \tilde{\mathbf{i}}/\hbar$ using Eq. (2.2) with $\dot{q}$ in Eq. (2.4), and, correspondingly, M_{ab} with N_{ab}, suggests that the transfer of each magnon out of F is accompanied by a transfer of energy $\epsilon + \hbar\Omega$. Similarly, the energy current associated with the macrospin dynamics is $\dot{q}_0 = -\Omega \mathbf{n} \cdot \tilde{\mathbf{i}}_0$ [BT].

2.4 Nonequilibrium Thermodynamics

Supposing that the internal relaxation of thermal magnons is sufficiently fast in comparison with the resonant precessional dynamics Ω of the macroscopic order parameter $\mathbf{n}$ [BDB14], an instantaneous state of the magnet can be described by three variables: the spin order $\mathbf{n}$, magnon density n, and entropy S_F. The normal layer is characterized by its spin density $\boldsymbol{\rho}$ and entropy S_N. The most natural thermodynamic potential for our purposes is the total internal energy $U(\mathbf{n}, n, \boldsymbol{\rho}; S_F, S_N)$ of the N/F bilayer as a function of these variables. These parameters (when conveniently normalized) form the following conjugate pairs with their respective thermodynamic forces: $(Ad_F s\mathbf{n}, \mathbf{H})$, $(Ad_F n, \mu)$, $(Ad_N \boldsymbol{\rho},\ \boldsymbol{\mu}')$, (S_F, T), and (S_N, T'). We now consider the structure of the Onsager-reciprocal relaxation of our system when perturbed away from the equilibrium. Since for a closed system, the total entropy $S = S_F + S_N = \text{const}$, at linear response, only the entropic flow $\delta S = (S_F - S_N)/2$ is relevant, whose thermodynamic conjugate is δT.

We start by deriving the spin current (5.1) in the absence of the order-parameter dynamics, i.e., $\dot{\mathbf{n}} = 0$, which is then entered in the equations of motion for spin densities:

$$\hbar\dot{\boldsymbol{\rho}} d_N = -\mathbf{j} + \text{Bloch relaxation}\,, \tag{2.32}$$

$$\hbar\left[(s-n)\dot{\mathbf{n}} - \dot{n}\mathbf{n}\right] d_F = \mathbf{j} + \text{LLGB dynamics}\,, \tag{2.33}$$

where "Bloch relaxation" stands for the possible spin relaxation inside N and, similarly, "LLGB dynamics" for the subsequent Landau-Lifshitz-Gilbert precession of the order parameter along with a Bloch relaxation of magnons. Equations (2.32), (2.33) could, furthermore, serve as boundary conditions for subsequent spin diffusion carried by electrons and/or magnons away from the N/F interface. According to the Onsager principle, $\boldsymbol{\mu}'$ thus affecting magnetic dynamics $\dot{\mathbf{n}}$ [through the spin current (2.1) on the right-hand side of Eq. (2.33)] implies that $\mathbf{H}$ must similarly enter in the equation for $\dot{\boldsymbol{\rho}}$. As can be shown [HBT10] by straightforward manipulations of Eqs. (2.32), (2.33), this is accomplished by the substitution $\boldsymbol{\mu}' \to \boldsymbol{\mu}' - \hbar\mathbf{n}\times\dot{\mathbf{n}}$ in Eq. (2.1), leading finally to Eq. (2.5).

Regarding the longitudinal spin current that is carried by magnons [second line in Eq. (2.5)], its Onsager reciprocity with the heat flux (2.5) is guaranteed by the equivalence between the spin Peltier and Seebeck coefficients, $\Pi = T\mathcal{S}/\hbar$, which arises naturally within our Kubo calculation and is analogous to the so-called second Thompson relation in thermoelectrics. (We remark here that $A\dot{q} = \delta\dot{S}T$, within the linear response.) Note there is no linear response in $\dot{\mathbf{n}}$ to μ or δT, nor (reciprocally) is there a linear response in the magnon and heat currents to the precessional order-parameter dynamics, within our exchange approximation.

2.5 Conclusion

Magnon-induced torques and spin currents may manifest in a variety of F/N heterostructures. In general, our expressions for spin and energy currents serve as boundary conditions which must be complemented by the appropriate bulk transport theory for both electrons and magnons. For example, in heterostructures utilizing spin Hall effect in order to convert between spin and charge currents on the normal-metal side, the temperature-dependent spin

currents flowing through the structure in response to a thermoelectric bias (as is, for example, the case in the conventional spin Seebeck effect), as well as the temperature-dependent spin Hall resistance, could be obtained by self-consistently solving the spin Hall diffusion equations in conjunction with Eqs. (2.32) and (2.33) employed at the boundaries. Thermal spin torques may also play an important role in magnetic-resonance measurements in the presence of thermal gradients [PAR11a, LSJ12a, JAA13]. For thin ferromagnetic insulators, the interfaces could form a bottleneck for longitudinal spin transport with spin conductance $\sim (T/T_c)^{3/2}$. Our theory provides an essential building block for understanding the instabilities and dynamics of ferromagnets in the presence of thermal gradients in magnetic heterostructures or spin-transfer torque at finite temperature [Slo10a].

CHAPTER 3

Bose-Einstein Condensation of Magnons

In Sec. 1.1.3, we discussed condensation of magnons by microwave pumping; in this chapter, we propose the realization of magnon condensation through dc electronic pumping. The pumping of the ferromagnet is provided by an adjacent normal metal, which supplies angular momentum by a combination of interfacial magnon-mediated spin Seebeck effect and spin-transfer torque, described in Chapter 2. In normal insulator phase, spin transport is governed solely by the presence of thermal and spin-diffusive gradients; the presence of Bose-Einstein condensation (BEC), meanwhile, gives rise to a temperature-independent condensate spin current, Eq. (2.17). Depending on the thermodynamic bias of the system, spin may flow may in either direction across the interface, engendering the possibility of a dynamical phase transition of magnons. We discuss experimental feasibility of observing a BEC steady state (fomented by a spin Seebeck effect), which is contrasted to the more familiar spin-transfer induced classical instabilities.

As discussed in Sec. 1.1.3, excitations of uniform ferromagnets (magnons) are bosonic in nature, thus exhibiting properties similar in character to those of cold atoms, photons, and excitons. Each of these systems can undergo a bosonic condensation wherein the lowest-energy mode displays a macroscopic occupation. The condensate, thereafter, manifests a macroscopic phase, spontaneously breaking U(1) gauge symmetry. Magnons have been expected [KS89a, KS91] and observed [DDD06b] to undergo condensation under microwave pumping. Their condensate phase has a transparent physical interpretation as the precessional angle of collective magnetic dynamics.

In our proposal, a ferromagnetic insulator, e.g., yttrium iron garnet (YIG), is directly attached to a conducting normal metal. Spin-pumping by the precessing magnet (or spin

waves), governed by a sizable spin-mixing conductance across the interface, results in a loss of magnons and the corresponding creation of particle-hole excitations in the normal metal. This magnetic bleeding may be overcome either by increasing the current in the normal metal, which transports angular momentum into the ferromagnet by the spin Hall effect, [ATH08, LMR11b] or by utilizing a temperature gradient across the interface, thus actuating the spin Seebeck effect [UTH08, UXA10]. Under a critical spin Hall and/or Seebeck biases, an excess of incoherently pumped magnons can precipitate a spontaneous condensation.

The chapter is organized as follows. In Sec. 3.1, we start by constructing the nonlinear dynamics of the condensate (A) and incoherent dynamics of the cloud (B), including its interaction with the condensate. In Sec. 3.2, we derive rate equations for spin and energy transfer into the normal metal N and the phonon bath. In Sec. 3.3, we consider the combined dynamics of the system in the absence of damping and nonlinearity, obtaining the partial phase diagram below the swasing threshold. In Sec. 3.4, we study the effects of nonlinear dynamics and damping by phonons on a system of interacting electronically pumped magnons in a ferromagnet. The nonlinear effects are crucial for constructing the dynamic phase diagram, which describes how "swasing" and Bose-Einstein condensation emerge out of the quasiequilibrated thermal cloud of magnons. We analyze the system in the presence of magnon damping and interactions, demonstrating the continuous onset of stable condensates as well as hysteretic transitions. The dynamic phase diagram of the pumped magnetic system is constructed, focusing on two special limits: (A) the fixed magnon temperature regime, which is controlled by spin flows between different subsystems (of magnons, electrons, and phonons), (B) the floating magnon temperature regime, in which the steady state is determined by self-consistent flows of both spin and energy. In both cases, we find regions of stable condensate with second-order as well as first-order hysteretic transitions out of the normal phase. Finally, Sec. 3.7 summarizes our findings and offers an outlook.

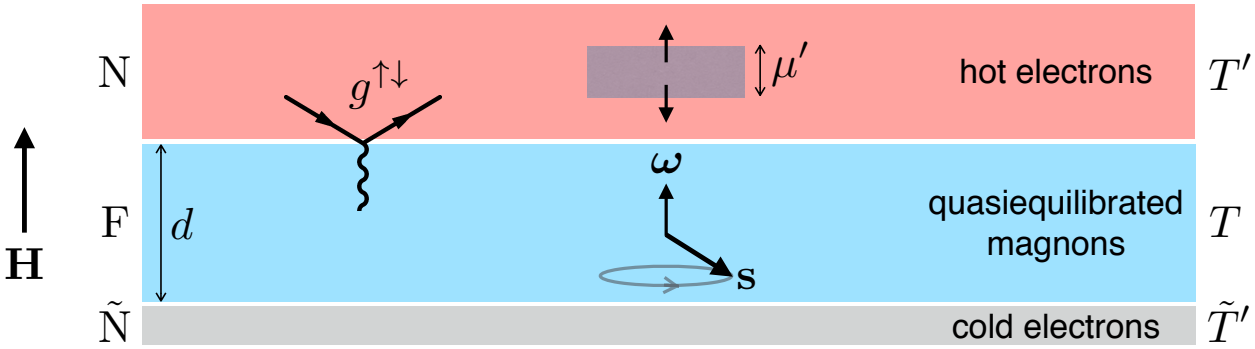

Figure 3.1: Schematic of the proposed heterostructure. On the top, the normal metal N, with electron temperature T', provides spin torque through spin accumulation $\boldsymbol{\mu}' = \mu'\mathbf{z}$ at the interface with the ferromagnet (F). The F is assumed to be sufficiently thin such that its magnon temperature T is uniform throughout. Collective spin density $\mathbf{s}$ in the F precesses with frequency $\boldsymbol{\omega}$, which is controlled by the applied field $\mathbf{H}$, both pointing in the z direction. Electron-magnon interaction at the N|F interface is parametrized by the spin-mixing conductance $g^{\uparrow\downarrow}$. The normal metal $\tilde{\text{N}}$ is a poor spin sink, which can, nevertheless, drain energy from magnons and phonons in the ferromagnet.

3.1 Magnetic dynamics

3.1.1 Condensate dynamics

We start by considering dynamics at absolute zero temperature, assuming only the lowest mode is excited. For simplicity, we neglect magnetostatic effects, such that the lowest-frequency excitation is given by homogeneous (monodomain) magnetic precession. Supposing, furthermore, cylindrical symmetry about the z axis, the effective monodomain Hamiltonian can be phenomenologically expanded as

$$\mathcal{H} = HS_z + \frac{KS_z^2}{2S}\,, \tag{3.1}$$

where S is the total (macro)spin of the ferromagnet (in units of $\hbar$), S_z is its z-axis projection, H is the applied field in the z direction (upon absorbing the gyromagnetic ratio), and K is the axial anisotropy (with $K > 0$ corresponding to an easy xy plane). We suppose that $H > K$, such that spin is oriented in the $-z$ direction in the ground state.

The spin algebra, $[S_i, S_j] = i\epsilon_{ijk}S_k$, can be conveniently recast in terms of the Holstein-Primakoff bosons:[HP40b]

$$S_+ = a^\dagger\sqrt{2S - a^\dagger a}\,, \;\; S_z = a^\dagger a - S\,, \tag{3.2}$$

where $S_+ \equiv S_x + iS_y$, S is the total spin, and a is a time-dependent ground-state magnon operator satisfying commutation relation $[a, a^\dagger] = 1$. The Hamiltonian in Eq. (3.1) is thus rewritten in terms of free-boson and interacting contributions (dropping a constant offset):

$$\mathcal{H} = (H - K)a^\dagger a + \frac{K(a^\dagger a)^2}{2S}\,. \tag{3.3}$$

A classical precession for large spin S corresponds to a coherent state for boson a: $|\alpha\rangle = e^{\alpha a^\dagger - \alpha^* a}|0\rangle$, such that $a|\alpha\rangle = \alpha|\alpha\rangle$, where $|0\rangle$ is the ground state with $S_z = -S$. The quantum-to-classical correspondence is provided by $\alpha^*\sqrt{2S - |\alpha|^2} \leftrightarrow S_+$, where the phase of $\alpha = |\alpha|e^{-i\phi}$ corresponds to the azimuthal angle of spin $\mathbf{S}$ in the xy plane: $\phi = \tan^{-1}(S_x/S_y)$. For small-angle precession, $|\alpha|^2 \ll S$:

$$S_+ \approx \alpha^*\sqrt{2S} = \sqrt{2SN}e^{i\phi}\,, \tag{3.4}$$

where $N = |\alpha|^2 = S_z + S$.

In the Heisenberg picture,

$$\begin{aligned} i\hbar\partial_t a &= -[\mathcal{H}, a] = \partial_{a^\dagger}\mathcal{H} \\ &= (H - K)a + \frac{K\{a^\dagger a, a\}}{2S} \to \hbar\omega a\,, \end{aligned} \tag{3.5}$$

where $\hbar\omega = H - K + K(N - 1/2)/S$, when acting on the magnon-number, $N \equiv a^\dagger a$, eigenstate $|N\rangle$, and $\{,\}$ stands for the anticommutator. (This $\hbar\omega$ corresponds to the energy for adding a magnon to the state $|N - 1\rangle$.) In the classical limit, $S \gg 1$, this gives the familiar Larmor precession frequency:

$$\hbar\omega \equiv \hbar\dot{\phi} = \partial_N\mathcal{H} = H + \frac{KS_z}{S}\,. \tag{3.6}$$

Indeed, the variables $\hbar S_z$ and ϕ are canonically conjugate: $\hbar\dot{\phi} = \partial_{S_z}\mathcal{H}$, $\hbar\dot{S}_z = -\partial_\phi\mathcal{H}$. Viewing this as a special (cylindrically-symmetric) instance of the Landau-Lifshitz equation, [LP80] we can easily extend the Hamiltonian (3.1) to include more general magnetic

interactions. A common phenomenology for dissipation, furthermore, is provided by the Gilbert damping [Gil04b], which endows frequency (3.6) with an imaginary component, $\omega \to \omega(1 - i\alpha)$, where α is a material-dependent constant. The corresponding magnon-number relaxation rate, $\tau^{-1} = 2\alpha\omega$, is proportional to the precession frequency.

3.1.2 Thermal cloud

At a finite temperature T, the thermally-excited magnons also contribute to the total spin angular momentum. For large bulk samples of volume V, it is now natural to switch from the total spin $\mathbf{S}$ to the spin density $\mathbf{s} = \delta\mathbf{S}/\delta V$. Extending Eq. (3.4) to this case, while assuming that $T \ll T_c$, the Curie temperature (such that we limit our attention to small-angle magnetic dynamics), this spin density can be written [relative to the saturated value $-s\mathbf{z}$ at $T = 0$, where $s = S/V$]:

$$\mathbf{s} \approx \left(\sqrt{2s}\Re\psi, \sqrt{2s}\Im\psi, n\right) . \tag{3.7}$$

Here, $n = n_c + n_x$, in terms of the condensate magnon density n_c (i.e., density of magnons occupying the lowest mode) and the thermal cloud density n_x (which is composed of the magnon states excited above the lowest-energy mode); $\psi \equiv \sqrt{n_c}e^{i\phi}$ plays the role of the condensate order parameter, with ϕ being the xy-plane azimuthal angle of the coherent spin precession. Note that only the magnon condensate component contributes to the xy spin-density projections.

The intrinsic dynamics of magnons with wavenumber q, by extension of Eq. (3.6), is given by

$$\hbar\omega_q = H - K\left(1 - \frac{n_c}{s}\right) + Aq^2 = \hbar\Omega + K\frac{n_c}{s} + Aq^2 , \tag{3.8}$$

where A is the ferromagnetic exchange stiffness (in appropriate units) and $\Omega \equiv (H - K)/\hbar > 0$ is the (monodomain) ferromagnetic-resonance frequency. Here, for simplicity, we are retaining only the nonlinear term stemming from the anisotropy term $KS_z^2/2S$ in the Hamiltonian, which would arise from, e.g., the global shape anisotropy [Suh57]. This is justified so long as the key nonlinearity stems from the feedback of the condensate n_c on the frequency of the magnon modes. Gilbert damping still gives $\tau_q^{-1} = 2\alpha\omega_q$ for the q-dependent relaxation rate.

3.2 Transport Rate Equations

The rate equation for the magnon-number density, $\dot{n} = \dot{n}_c + \dot{n}_x$, is governed by the Landau-Lifshitz-Gilbert (LLG) dynamics of the condensed and thermal magnons, including their interactions, damping of spin and energy to the lattice, and spin and energy transport between the ferromagnet and the normal-metal reservoirs that are governed by the electron-magnon scattering. The zero-temperature condensate dynamics are described by the classical LLG equation of motion (extended to include spin-transfer torques) for the unit-vector collective spin direction $\mathbf{n}$:

$$(1 + \alpha\mathbf{n}\times)\hbar\dot{\mathbf{n}} + \mathbf{n} \times \mathbf{H}_{\text{eff}} = (\Im\alpha' + \Re\alpha'\mathbf{n}\times)\left(\boldsymbol{\mu}' \times \mathbf{n} - \hbar\dot{\mathbf{n}}\right) , \tag{3.9}$$

where $\mathbf{H}_{\text{eff}} \equiv \partial_{\mathbf{S}} H = (H + K\mathbf{n}\cdot\mathbf{z})\mathbf{z}$ is the effective field, $\boldsymbol{\mu}' = \mu'\mathbf{z}$ is the vectorial spin accumulation in N,

$$\alpha' = \Re\alpha' + i\Im\alpha' \equiv \frac{g^{\uparrow\downarrow}}{4\pi s d} , \tag{3.10}$$

in terms of the complex-valued spin-mixing conductance $g^{\uparrow\downarrow}$ (in units of e^2/h, and per unit area) of the F|N interface and the F layer thickness d. The left-hand side of Eq. (3.9) is the standard LLG equation [LP80, Gil04b], while the right-hand side consists of the static spin-transfer torques [Slo96, Ber96a] $\propto \boldsymbol{\mu}'$ and spin-pumping torques [TBB02a, TBB05] $\propto \dot{\mathbf{n}}$ (which are Onsager reciprocal [TM08b]). We are assuming the spin transport is blocked across the F|$\tilde{\text{N}}$ interface.

Rewriting Eq. (3.9) in spherical coordinates, in terms of the condensate density n_c,

$$\mathbf{n} = (n_\perp \cos\phi, n_\perp \sin\phi, n_c/s - 1) , \tag{3.11}$$

where $n_\perp = \sqrt{2n_c/s - (n_c/s)^2}$, we have

$$\begin{aligned} (1 + \Im\alpha')\,\hbar\dot{n}_c &= -\left[(\alpha + \Re\alpha')\,\hbar\dot{\phi} - \Re\alpha'\mu'\right](2n_c - n_c^2/s) , \\ (1 + \Im\alpha')\,\hbar\dot{\phi} &= \hbar\omega + \Im\alpha'\mu' + (\alpha + \Re\alpha')\,\frac{\hbar\dot{n}_c}{2n_c - n_c^2/s} . \end{aligned} \tag{3.12}$$

Here, $\omega \equiv \omega_0$ is given by Eq. (3.8), with $q = 0$. These equations generalize the Hamilton's equations of motion for the canonically-conjugate pair of variables (n_c, ϕ) to include dissipation (magnon-lattice coupling) and spin-transfer torques/spin-pumping (magnon-electron

coupling). Assuming that $\alpha, |\alpha'| \ll 1$, which is nearly always the case in practice, Eqs. (3.12) give for the condensate rate equation

$$\hbar \dot{n}_c = i_c + i'_c \,, \tag{3.13}$$

where

$$i_c + i'_c = -2\left[(\alpha + \Re\alpha')\hbar\omega - \Re\alpha'\mu'\right] n_c(1 - n_c/2s) \tag{3.14}$$

captures the effects of Gilbert damping and spin-transfer torque. [Here, we combined the expressions for $\dot{n}_c$ and $\dot{\phi}$ in Eq. (3.12) and dropped the terms that are quadratic in α and α'.] Since $\Im\alpha'$ is eliminated by this substitution, hereafter α' stands for $\Re\alpha'$ only.

According to Eq. (3.14), the condensate rate of change (3.13) is scaled by the geometrical factor $1 - n_c/2s$, which can be divided out and, if $n_c \ll s$, disregarded. When in the following we complement the magnon rate equation with thermal contributions, this factor could be absorbed by an appropriate rescaling of the thermal terms, which would lead to small cross terms between the quantities associated with the condensate and the thermal cloud. The Gilbert-damping and spin-transfer contributions to the zero-temperature condensate rate equation are then respectively given by

$$i_c = -2\alpha\hbar\omega n_c \,, \tag{3.15}$$

$$i'_c = -2\Re\alpha'(\hbar\omega - \mu')n_c \,. \tag{3.16}$$

Equation (3.16) was derived in Ref. [BDT12] in a perturbative treatment of the electron-magnon scattering, which is consistent with neglecting terms that are quadratic in α's.

At finite temperatures,

$$\hbar \dot{n}_c = (i_c + i'_c) + i_{xc} \,, \tag{3.17}$$

where i_{xc} is the rate of spin transfer from the thermal cloud to condensate. The thermally-excited magnons also obey generalized LLG/spin-torque relations, which we derive below. In order to simplify the following discussion, we will limit our attention to the situations when spin-preserving magnon-magnon exchange interactions are fast enough that magnons form a Bose-Einstein distribution with an effective temperature $T = (k_B\beta)^{-1}$ and chemical

potential μ.[?] The total thermal-cloud density is then given by

$$n_x = \int_0^\infty d\epsilon D(\epsilon) n_{\rm BE}\left[\beta\left(\epsilon - \mu^*\right)\right] , \tag{3.18}$$

where $\mu^* \equiv \mu - \hbar\omega \leq 0$ is the magnon chemical potential relative to the band edge (set at $\epsilon = 0$), which, on the absolute scale, is shifted by the condensate frequency $\hbar\omega$; $D(\epsilon) = \sqrt{\epsilon}/4\pi^2 A^{3/2}$ is the magnon density of states; and $n_{\rm BE}(x) \equiv (e^x - 1)^{-1}$. Writing the thermal-cloud rate equation, $\hbar\dot{n}_x = i_x + i'_x$, in terms of the Gilbert-damping, i_x, and spin-torque, i'_x, contributions, we assert for the former:

$$i_x = \hbar \int_0^\infty d\epsilon D(\epsilon) \frac{n_{\rm BE}\left[\beta''\left(\epsilon + \hbar\omega\right)\right] - n_{\rm BE}\left[\beta\left(\epsilon - \mu^*\right)\right]}{\tau(\epsilon)} , \tag{3.19}$$

where $\beta'' \equiv (k_B T'')^{-1}$ is the inverse (effective) temperature of phonons (which are assumed to be responsible for the Gilbert damping) and $\hbar/\tau(\epsilon) = 2\alpha(\hbar\omega + \epsilon)$. The spin-torque rate is given by [BDT12]

$$\begin{aligned} i'_x =& 4\alpha' \int_0^\infty d\epsilon D(\epsilon)(\epsilon + \hbar\omega - \mu') \\ & \times \left\{ n_{\rm BE}\left[\beta'\left(\epsilon + \hbar\omega - \mu'\right)\right] - n_{\rm BE}\left[\beta\left(\epsilon - \mu^*\right)\right] \right\} , \end{aligned} \tag{3.20}$$

where β' is the inverse normal-metal N electron temperature.[?] The rate equation for the thermal-cloud is given by

$$\hbar\dot{n}_x = \left(i_x + i'_x\right) + i_{cx} , \tag{3.21}$$

where i_{cx} is the rate of spin transfer from the condensate to cloud.

The total spin current i passing through the normal-metal interface is found by adding Eqs. (3.17) and (3.21):

$$i = \hbar\dot{n}_c + \hbar\dot{n}_x = \left(i_c + i'_c\right) + \left(i_x + i'_x\right) , \tag{3.22}$$

where we set $i_{xc} + i_{cx} = 0$, assuming magnon-number preserving magnon-magnon interactions (which is rooted in spin conservation for a cylindrically-symmetric magnetic system). The expression for the net spin current i, using rate equations for the condensate, Eqs. (3.15) and (3.16), and thermal cloud, Eqs. (3.19) and (3.20), forms one of our key results. In order to find steady states, we will have to solve for $i = 0$. Subject to external conditions

of pumping, two unknowns thus need to be established: the effective temperature, T, and chemical potential, μ, of magnons.

In order to evaluate a common temperature and chemical potential for the magnons, we also need to consider the energy flow into the system. The total magnon energy density in our model is given by $e = e_c + e_x$, where

$$e_c = \hbar\Omega n_c + \frac{K n_c^2}{2s} \tag{3.23}$$

is the condensate energy and

$$e_x = \int_0^\infty d\epsilon(\epsilon + \hbar\omega) D(\epsilon) n_{\rm BE}\left[\beta(\epsilon - \mu^*)\right] \tag{3.24}$$

is the thermal-cloud energy. We recall, in particular, that $\omega \equiv \omega_0 = \Omega + K n_c/\hbar s$ in the above equations is affected by the presence of the condensate n_c. The total energy-transfer rate from N and the lattice into magnons is thus given by:

$$j = \dot{e}_c + \dot{e}_x = \left(\omega + \frac{K}{\hbar s} n_x\right)(i_c + i_c') + (j_x + j_x')\,, \tag{3.25}$$

where j_x and j_x' are given by the expressions similar to Eqs. (3.19) and (3.20) but with an additional factor of $(\omega + \epsilon/\hbar)$ in the integrands.

3.3 Condensate dynamics in the absence of damping and nonlinearity

In this section, we neglect the anisotropy ($\Omega = \omega$) and damping ($\alpha = 0$), and focus on the regime ($\mu' < \hbar\Omega$) in which angular momentum is supplied to the ferromagnet through magnon cloud, which condenses once the magnon density is sufficiently high. We focus on the regime where the temperatures of both the N and F subsystems are fixed so that any energy gain or loss, independent of spin gain or loss, is completely absorbed or resupplied by thermal reservoirs. At fixed T the density of excited magnons $n_{\rm x}$ becomes a monotonic function of $\mu' \leq \hbar\Omega$ alone. Let us further suppose that spin accumulation μ' in the right reservoir is independent of spin diffusion from the insulator and fixed. If the total density

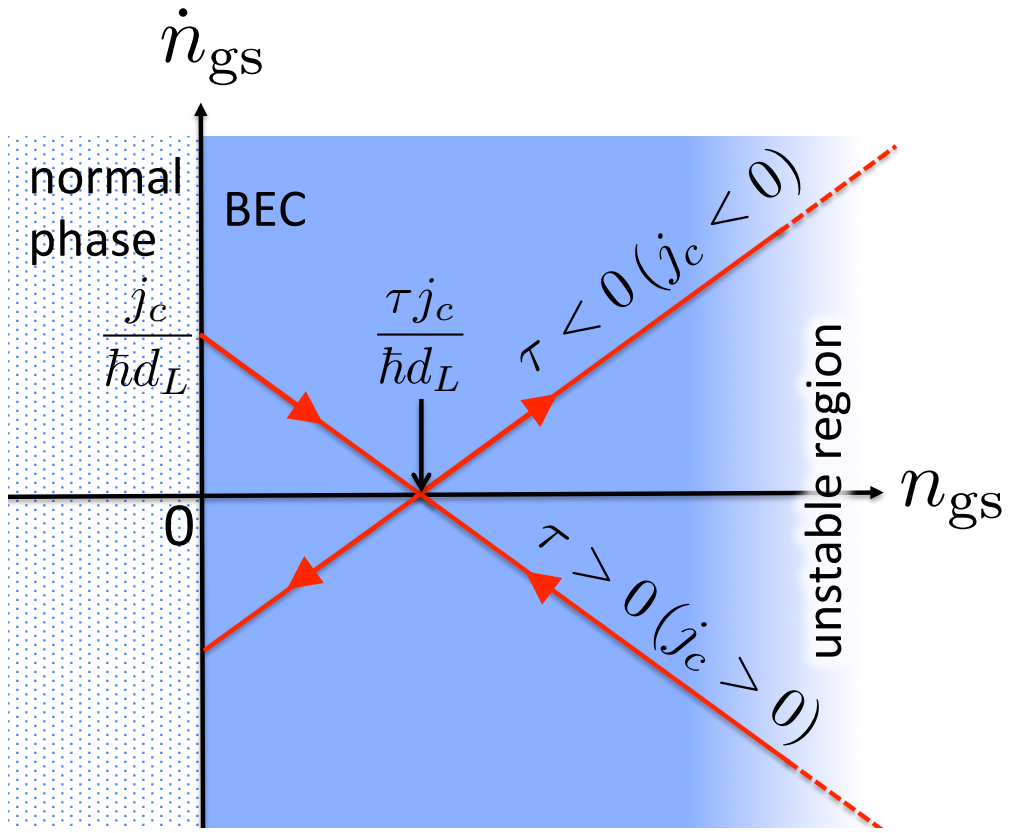

Figure 3.2: Behavior of $n_{\rm gs}$ as predicted by the rate equation, $\dot{n}_{\rm gs} = j_{\rm tot}/\hbar d_L = j_c/\hbar d_L - n_{\rm gs}/\tau$. If j_c had the sign opposite to that shown in the figure, the crossing point $\tau j_c/\hbar d_L$ would fall in the normal phase ($n_{\rm gs} = 0$), thus precluding a BEC formation.

of magnons exceeds the critical BEC density n_c (corresponding to $\mu = \hbar\Omega$), $n_{\rm x}$ reaches and remains pinned at this value, $n_{\rm crit}$, and only n_c is free to vary. In BEC phase, then, the time dependence of n_c is given by

$$n_c(t) = \frac{\tau i_{\rm crit}}{\hbar} + \left[n_c(0) - \frac{\tau i_{\rm crit}}{\hbar} \right] e^{-t/\tau} \,, \tag{3.26}$$

where the excited magnon flux $i_{\rm crit} = i_{\rm x}(\mu \to \hbar\Omega)$ is time independent, as long as μ is anchored by the condensate at $\hbar\Omega$, $\hbar/\tau \equiv \alpha'(\hbar\Omega - \mu')$. The behavior of the Bose-Einstein condensed system thus falls into one of four regimes, as depicted in Fig. 3.2. In the first, $\mu' > \hbar\Omega$ (so that $\tau^{-1} < 0$) and $n_c(0) > \tau i_{\rm crit}/\hbar$, n_c grows exponentially until saturating at a value $\sim M_s/\mu_B$ (where M_s is the magnetization of the ferromagnet and μ_B is the Bohr magneton). In this case, magnon-magnon interactions become important ultimately and the system must be treated more carefully here. This is a realization of the "swaser" (i.e., a spin-wave analog of a laser) put forward in [Ber96a] and observed in the context most similar to ours (in a magnetic insulator YIG) in [KHT10b]. We consider the swasing regime in detail in the following section. In the second regime, $\mu' > \hbar\Omega$ but $n_c(0) < \tau i_{\rm crit}/\hbar$ (requiring $i_{\rm crit} < 0$), n_c decreases towards zero, and the system enters normal phase; the system is therefore hysteric, depending on the initial conditions. The last two regimes (corresponding to $i_{\rm crit} > 0$ and $i_{\rm crit} < 0$), which are of more interest to us, occur when spin splitting in the conductor is sufficiently small that $\mu' < \hbar\Omega$ and thus $\tau^{-1} > 0$, as depicted in Fig. 3.3. Here, the steady-state phase no longer depends on the initial condition: When $i_{\rm crit} > 0$, the magnons will Bose-Einstein condense (lower half of the main panel in Fig. 3.3), and if $i_{\rm crit} < 0$, normal phase with $n_c = 0$ must eventually be reached (upper half of the main panel in Fig. 3.3).

In the normal phase ($n_{\rm x} < n_{\rm crit}$), μ acquires time dependence, and the rate of change of the total number of magnons is $\dot{n}_{\rm tot} = \dot{n}_{\rm x} = i_{\rm x}(t)/\hbar$. To illustrate these dynamics in a specific example, we consider a simple model where the density of magnon states per unit insulator volume $\mathcal{V}_F$ has the form $g_F(\epsilon) = \mathcal{G}_F(\epsilon/\epsilon_{\rm gs} - 1)^w$ (with $w > 0$ and $\mathcal{G}_F$ a positive real number). In terms of the polylogarithm function

$$\mathrm{Li}_{w+1}(z) \equiv \frac{1}{\Gamma_{w+1}} \int_0^\infty dx \frac{x^w}{e^{x - \ln z} - 1} \,, \tag{3.27}$$

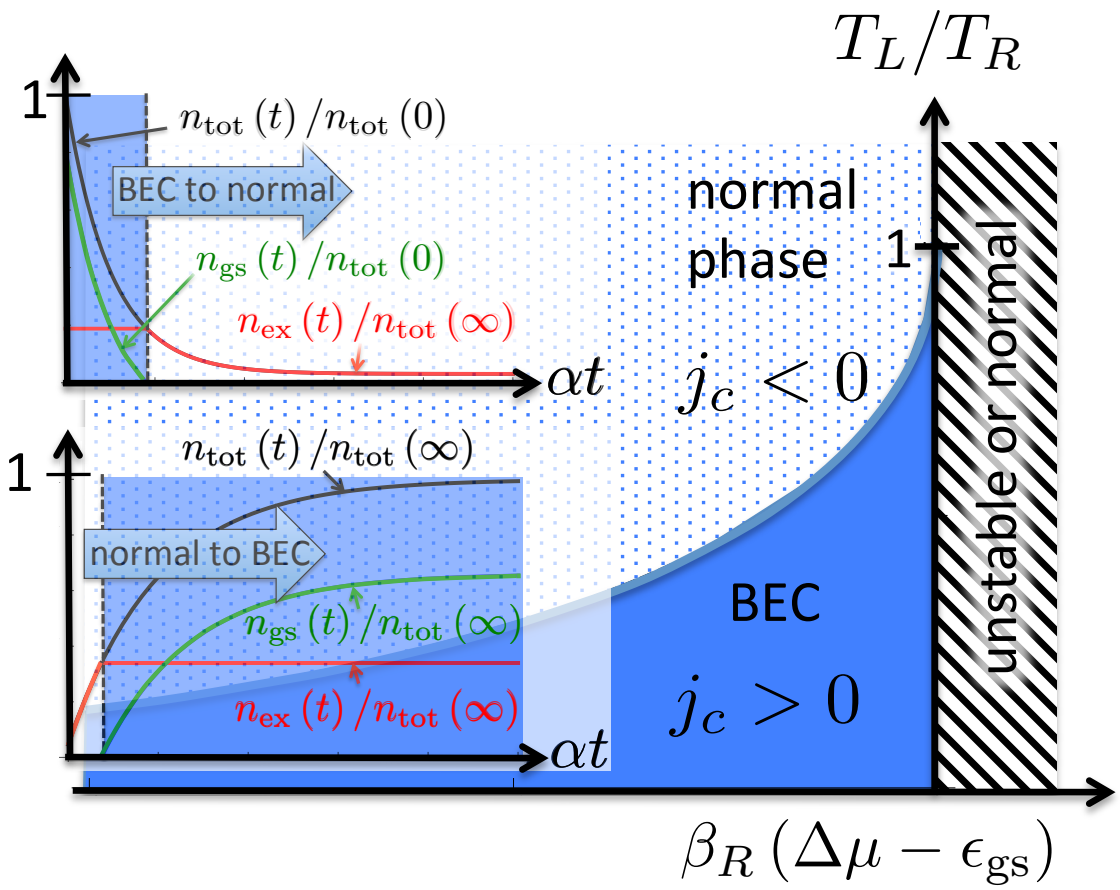

Figure 3.3: When $\Delta\mu < \epsilon_{\rm gs}$, the steady-state phase is insensitive to the initial condition for $n_{\rm gs}$, but depends on the temperature bias $T_L - T_R$ and the difference $\Delta\mu - \epsilon_{\rm gs}$. As the splitting $\Delta\mu$ increases, the critical temperature for T_L increases until it equals T_R. Examples of time dependence in the normal and BEC phase regions are shown in the upper and lower left panels, respectively. When $\Delta\mu > \epsilon_{\rm gs}$, depending on the initial condition, the driven magnon system is either unstable or relaxes towards the normal phase.

the density of excited magnons becomes

$$n_{\rm x} = \eta^{(w)}(\beta,\mu) \equiv \mathcal{G}_L \frac{\Gamma_{w+1}{\rm Li}_{w+1}(z_F)}{\beta^{w+1}\epsilon_{\rm gs}^w}\,, \tag{3.28}$$

where $z_F(\beta,\mu) \equiv e^{\beta(\mu-\hbar\Omega)}$ is the effective magnon fugacity (with $z_F = 1$ corresponding to a BEC). Assuming for simplicity that $V_{\rm ex}(\epsilon)$ is energy independent and equal to $V_{\rm gs}$, one obtains an excited spin current

$$i_{\rm x} = \frac{\hbar}{\tau}\left(\frac{\eta_R^{(w+1)} - \eta_L^{(w+1)}}{1-\mu'/\hbar\Omega} + \eta_R^{(w)} - \eta_L^{(w)}\right), \tag{3.29}$$

where $\eta_F^{(w)} \equiv \eta^{(w)}(\beta,\mu)$ and $\eta_N^{(w)} \equiv \eta^{(w)}(\beta',\mu')$. In general, to find the spin accumulation in the normal phase as a function of time, one must solve the rate equation for the magnon fugacity z_F. At low temperatures, $(T,T') \ll |\hbar\Omega - \mu'|$, the first term in Eq. (3.29) can be neglected, allowing for a simple solution to the excited magnon density:

$$n_{\rm ex}(t) = \eta_R^{(w)} + \left[n_{\rm ex}(0) - \eta_R^{(w)}\right] e^{-t/\tau}\,, \tag{3.30}$$

provided $n_{\rm x} < n_{\rm crit}$. If $\mu' < \hbar\Omega$, $\tau^{-1} > 0$, and $n_{\rm ex}$ decays towards $\eta_R^{(w)}$, irrespective of its initial condition. If $\eta_R^{(w)} < n_{\rm c}$, the insulator always remains in normal phase; when $\eta_R^{(w)} > n_{\rm c}$, on the other hand, the magnons eventually Bose-Einstein condense, and the system is henceforth described by Eq. (3.26). Notice that the conditions $\eta_R^{(w)} \gtrless n_{\rm c}$ are (in the spirit of the aforementioned low-temperature approximation) equivalent to $i_{\rm crit} \gtrless 0$, which are consistent with the conditions considered above for the system to settle in the BEC or normal phase, respectively, as $t \to \infty$. The time dependence in the opposite high-temperature regime, $T, T' \gg |\hbar\Omega - \mu'|$, is more complicated than but in principle similar in behavior to the low-temperature solution given by Eq. (3.30).

If the insulator temperature T is left floating, the energy flow between the two subsystems would give rise to the dynamics of T (supposing for simplicity T' is still fixed). In the most extreme case, the insulator is allowed to exchange energy only with the conductor (and only by the electron-magnon scattering discussed above, neglecting phonon heat transfer), so changes in T are dictated by the rate at which energy is transferred across the barrier along with spin. The coupled rate equations for energy and spin transfer can then be solved

to give time-dependent solutions to the temperature T and the ground and excited magnon densities, n_x and n_c.

All of the relevant quantities may be readily inferred from existing measurements. In particular, the squared matrix element $|V_{\rm gs}|^2$ is directly related to the real spin-mixing conductance (per unit area) $g^{\uparrow\downarrow}$ by equating the ground-state current density $j_{\rm gs}$ for $\Delta\mu = 0$ with the expression for current pumped by a precessing magnetic monodomain given in Ref. [TBB02a]: One obtains $|V_{\rm gs}|^2 = g^{\uparrow\downarrow}/4\pi^2 s g_R^2$, where s is the ferromagnetic spin density in units of $\hbar$. From this relation, the "magnon dwell time" $\tau_d \equiv \tau|_{\Delta\mu=0} = 2\pi s d_L/g^{\uparrow\downarrow}\omega_r$ and the effective Gilbert damping constant $\alpha' \equiv 1/2\omega_r\tau_d = g^{\uparrow\downarrow}/4\pi s d_L$ (corresponding to the interfacial, i.e., spin-pumping [TBB02a], magnon decay) are expressed in terms of the spin-mixing conductance. ($\omega_r \equiv \epsilon_{\rm gs}/\hbar$ here is the ferromagnetic-resonance frequency.) We use the term "Gilbert damping" here to refer to dynamical magnetization damping generally, including damping of inhomogeneous fluctuations, in lieu of the alternative "Landau-Lifshitz" damping; while the two are mathematically equivalent, historically the former has become generally favored over the latter, and so we follow this convention. In YIG films ($4\pi M_s \approx 2$ kG, $g^{\uparrow\downarrow} \sim 10^{14}$ cm^{-2} [KHT10b, HBM11]), the spin-pumping Gilbert damping α' dominates over the intrinsic Gilbert damping ($\alpha \sim 10^{-4}$) below thicknesses $d_L \sim 100$ nm. Theoretically predicted [JXB11] and recently measured [BHK12b] mixing conductance that is a factor of five larger ($g^{\uparrow\downarrow} \approx 5 \times 10^{14}$ cm^{-2}) proportionately increases the maximum film thickness. Having fixed α' for a given d_L, the applied magnetic field can be chosen to be sufficiently small that the timescale $\tau_{\rm th}$ for magnon thermalization is significantly less than the characteristic dwell time $\tau_d = 1/2\alpha'\omega_r$. For example, taking $\tau_{\rm th} \sim 100$ ns for room-temperature YIG [DDD06b, DDD08], the dwell time $\tau \sim 1$ μs for damping $\alpha' \sim 10^{-4}$ corresponds to a frequency of ~ 100 MHz or (effective) field of ~ 10 G. At this field, the condition for the formation of BEC ($j_c > 0$) requires a temperature bias $\Delta T = T_R - T_L \sim \epsilon_{\rm gs}/k_B$ of a few mK for $w = 1/2$ (i.e., quadratic dispersion), in the absence of any spin bias (i.e., $\Delta\mu = 0$). In practice, for a good thermal contact at the interface, this corresponds to a temperature difference maintained across the magnon correlation length, which we estimate by the magnetic exchange length (~ 10 nm in YIG); such thermal gradients have already

been realized in experiment [UAO10].

Considering that the classically unstable region ($\mu' > \hbar\Omega$) has already been realized in practice [KHT10b] in a Pt/YIG bilayer spin-biased by the inverse spin Hall effect, and the spin-caloritronic properties [Bau] are presently under intense experimental scrutiny in such composites [SKC11b, UXA10], the experimental observation of current-induced BEC phase in Pt/YIG hybrids appears very feasible. YIG film thickness larger than the characteristic de Broglie wavelength of magnons (~ 1 nm at room temperature using standard YIG parameters [BLV73]) would justify a three-dimensional treatment of BEC. A $d_F \lesssim 1$ μm-thick YIG film with Gilbert damping $\alpha \lesssim 10^{-4}$ like that employed in Ref. [KHT10b] appears adequate to our ends, in order for the spin-pumping efficiency α' to be comparable to the intrinsic Gilbert damping α.

We conclude that BEC phase can be established under a steady-state transport condition when the ferromagnet is colder than the normal metal (thus facilitated by a spin Seebeck effect [Bau]) and the spin accumulation μ' is slightly below the spin-transfer torque instability ($\mu' \sim \hbar\Omega$), in our model. Implicit in our discussion is the assumption that the magnon gas is dilute and can therefore be treated as noninteracting, aside from thermalization effects. In reality, these interactions must be accounted for, in order to fully understand the ensuing dynamics of the magnon condensate. In such treatment, spectral properties would be self-consistently modified deep in the BEC phase, but the essential behavior of the system close to the transition point could still be addressed by the present theory. The emergent magnon superfluid properties [BV10b] due to their interactions are left for a future work.

3.4 Dynamic phase diagrams for finite anisotropy and damping

In this section, we reintroduce the nonlinearity (K) and damping (α). Nonlinear effects can play an important role in stabilizing coherent dynamics under large spin Hall/Seebeck biases, as well as accounting for the interaction of the condensate with the thermal magnon cloud. Gilbert damping due to magnon-lattice coupling and allow for an additional energy-sink channel by attaching a poor spin-sink normal metal on the other side of the ferromagnet.

See Fig. 3.1 for a schematic of our setup. The role of this second normal metal in our model is to (i) anchor the adjacent lattice temperature and (ii) provide a reservoir that dissipates excess energy injected along with magnons from the first normal metal, which helps in fomenting condensation.

3.4.1 Fixed magnon temperature

The magnon temperature in a magnetic film sandwiched by two metals, as sketched in Fig. 3.1, can be fixed by the electron temperatures T' and $\tilde{T}'$ [for example, $T \to (T' + \tilde{T}')/2$ in a mirror-symmetric structure], either through direct magnon-electron scattering at the interfaces or via magnon-phonon interaction. Having thus anchored the magnon temperature, we may disregard the energy current j. In this limit, the spin current i fully determines the state of the system. Under the reigning assumption that the magnonic cloud and condensate maintain internal thermodynamic equilibrium at all times, the magnet is always either in normal phase (NP) or condensate phase (CP). Then, only one variable is left free to vary: μ^* in NP or n_c in CP, which is controlled by the spin current i flowing into the magnetic subsystem.

In a normal phase, the condensate is absent ($n_c = 0$), and the magnon current goes entirely into the thermal cloud:

$$\hbar \dot{n}_x = i \,, \tag{3.31}$$

where $i = i_x + i'_x$ consists only of the normal component, Eqs. (3.19), (3.20), which depend on μ^*. We will be treating the dependence $i(\mu^*)$ inside NP numerically.

If the magnons are condensed (i.e., $\mu^* = 0$) while their temperature T is fixed, the spin current, Eq. (3.22), must, via magnon-magnon interactions, be entirely transformed into the condensate density:

$$\hbar \dot{n}_c = i \,. \tag{3.32}$$

Even in this simple limit, however, we cannot obtain an exact analytic solution for $n_c(t)$, since the flux i has an implicit nonlinear dependence on n_c [through the dependence of $(i_x + i'_x)$ on $\omega(n_c)$]. When $n_c/s \ll 1$, which is the limit we are focusing on throughout, we

can expand i in its powers:

$$i = \imath_x - \sigma\frac{n_c}{s} - \zeta\left(\frac{n_c}{s}\right)^2 + \mathcal{O}\left(\frac{n_c}{s}\right)^3 . \tag{3.33}$$

Here, $\imath_x \equiv i_x + i'_x$, after setting $\mu^* = 0$ and $n_c = 0$ in Eqs. (3.19) and (3.20). According to Eqs. (3.15) and (3.16),

$$\sigma = 2s(\alpha + \alpha')\hbar\Omega - 2s\alpha'\mu' + \delta\sigma \tag{3.34}$$

and

$$\zeta = 2s(\alpha + \alpha')K + \delta\zeta\,, \tag{3.35}$$

where $\delta\sigma$ and $\delta\zeta$ are thermal-magnon corrections. Using Eqs. (3.19) and (3.20), the latter are evaluated at $k_BT \gg \hbar\Omega$ to be:

$$\frac{\delta\sigma}{sK} \sim (\alpha + 2\alpha')\left(\frac{T}{T_c}\right)^{3/2} \tag{3.36}$$

and

$$\frac{\delta\zeta}{sK} \sim -(\alpha + 2\alpha')\sqrt{\frac{T}{T_c}}\frac{K}{k_BT_c}\,, \tag{3.37}$$

up to numerical factors of order unity. Here, $k_BT_c \sim s^{2/3}A$ is the Curie temperature. These corrections are clearly unimportant, so long as $K \ll k_BT_c$ (recalling that $T \ll T_c$ throughout), and will be omitted in the following. We thus conclude, in particular, that $\zeta > 0$.

3.4.2 Swasing

We start by considering the low-temperature limit of a stiff ferromagnet, where the thermal-current contribution $\imath_x$ in Eq. (3.33) can be disregarded. The condensate dynamics, $\hbar\dot{n}_c = i$, is then governed by two transport coefficients: σ and ζ.

The coefficient σ in Eq. (3.33) represents an effective damping of the condensate and describes a competition between, on the one hand, damping by phonons and electrons (captured by the first term in σ, proportional to $\Omega > 0$, where α parametrizes Gilbert damping and α' spin pumping [TBB02a]) and, on the other, spin-transfer torque from the normal-metal N (captured by second term in σ, proportional to spin accumulation μ'). When the former contribution is larger, σ is positive, and the torque provided by the second term

Eq. (3.33) relaxes the condensate spin density (with the total spin decaying towards the $-z$ axis). Conversely, upon the application of a sufficiently large and positive spin accumulation μ', σ is negative, and the net torque from the linear in n_c term in Eq. (3.33) drives the condensate spin towards the $+z$ axis. The quadratic term proportional to ζ in Eq. (3.33) describes a nonlinear enhancement of damping, which ultimately curbs the exponential growth of the condensate when $\sigma < 0$, leading to the fixed point

$$\frac{n_c}{s} \to \frac{|\sigma|}{\zeta} = \frac{|(1+\alpha/\alpha')\hbar\Omega - \mu'|}{(1+\alpha/\alpha')K}\,. \tag{3.38}$$

In the absence of intrinsic Gilbert damping, i.e., $\alpha = 0$, the effective damping σ is proportional to $\hbar\Omega - \mu'$. This was first pointed out by Berger,[Ber96a] who coined the term *swaser* (spin-wave amplification by stimulated emission of radiation) to describe the coherent emission of spin waves, signified by negative damping, when the pumping μ' overcomes the intrinsic threshold associated with the gap $\hbar\Omega$. This *swasing* instability may be understood thermodynamically: Because the condensate carries no entropy, the free-energy change due the creation of δN magnons and the corresponding annihilation of the up-electron/down-hole pairs is

$$\delta F = (\hbar\Omega - \mu')\delta N\,. \tag{3.39}$$

When $\mu' < \hbar\Omega$, the condensate is damped by the transfer of angular momentum and energy out of the magnet into N; when $\mu' > \hbar\Omega$, however, the absorption of energy by the condensate becomes entropically beneficial, signaling an instability.

A finite α in Eq. (3.34) raises the swasing instability threshold to

$$\mu' = \left(1 + \frac{\alpha}{\alpha'}\right)\hbar\Omega\,, \tag{3.40}$$

in analogy to the lasing threshold in a lossy optical cavity. In particular, when Gilbert damping dominates over spin pumping (which is the case in sufficiently thick magnetic films), i.e., $\alpha \gg \alpha'$, we obtain $\mu' \approx (\alpha/\alpha')\hbar\Omega$, which reproduces the classical Slonczewski's spin-transfer torque instability.[Slo96]

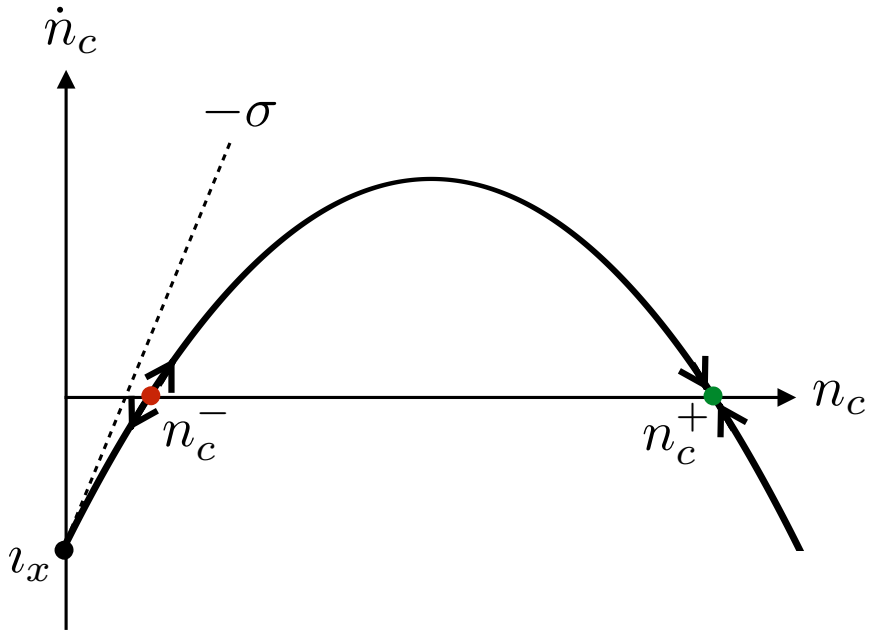

Figure 3.4: A graphical representation for obtaining solutions (3.41) to the equation $\hbar\dot{n}_c = i$ with i given by Eq. (3.33). Here, $\sigma < 0$ and $\imath_x < 0$ (corresponding to region IV_1, as described in the text), resulting in two fixed points: unstable at n_c^- and stable at n_x^+.

3.4.3 Bose-Einstein condensation

We now focus on the finite-temperature steady-state behavior (fixed points), determined by the condition $i = 0$. Namely, for a given set of parameters (T, T', μ', ...), we look for possible solutions for both NP (defined by the existence of a real value of $\mu^* < 0$ for which $i_x + i'_x = 0$) and CP (defined by the existence of a real, positive value of n_c for which $i = 0$). While the NP solutions $i_x + i'_x = 0$ are found numerically, the analytic expansion in Eq. (3.33) allows for a general CP solution to $i = 0$:

$$\frac{n_c^\pm}{s} = \frac{\pm\sqrt{\sigma^2 + 4\zeta\imath_x} - \sigma}{2\zeta}\,, \tag{3.41}$$

which is depicted in Fig. 3.4.

The resultant phase diagram may be divided into four regions, I-IV, according to the signs of the coefficients σ and $\imath_x$: $\sigma > 0$ and $\imath_x < 0$ (region I), $\sigma > 0$ and $\imath_x > 0$ (region II), $\sigma < 0$ and $\imath_x > 0$ (region III), and $\sigma < 0$ and $\imath_x < 0$ (region IV). In parameter space, regions I and III each share phase boundaries with regions II and IV. All four regions meet

when $\sigma = 0$ and $\imath_x = 0$, which appears as a single critical point P in the phase diagram. We now discuss in some detail the physical behavior in each of the four regions, with the help of Fig. 3.5 as visual guidance.

In region I, neither solution $n_c^{\pm}$ is real and positive, dictating that the magnons must settle in NP at some $\mu^* < 0$ for which $i_x = 0$, as we find numerically. In region II, n_c^+ represents a real-valued, stable solution to the condensate equation of motion. While the condensate is damped through the second and third terms in Eq. (3.33), it is replenished by the thermal cloud, $\imath_x > 0$, which can be driven by thermal gradient $T' - T$. The magnet reaches a steady state, wherein angular momentum is pumped into the thermal cloud and transferred to the condensate by magnon-magnon interactions, which in turn decays by the combination of Gilbert damping and spin pumping. Numerically, we find no NP solution coexisting with CP in region II. Note that here $\lim_{\zeta \to 0} n_c^+/s = \imath_x/\sigma$ is finite even in the absence of the nonlinearity ζ.

The boundary between regions I and II is defined by the condition $\imath_x = 0$, corresponding to $n_c = 0$. It thus follows that n_c is continuous at the associated NP/CP phase transition, given by $n_c \equiv 0$ in region I and $n_c \propto \imath_x$ in the incipient region II. Conversely, $\mu^* \equiv 0$ in region II and decreases continuously, $\mu^* < 0$, in region I. We identify this dynamic second-order phase transition as a *Bose-Einstein condensation,* whose order parameter is given by $\psi = \sqrt{n_c} e^{i\phi}$, where $\dot{\phi} \approx \omega$. In contrast to swasing, where $\sigma < 0$, the condensate decay is compensated here by the thermal magnon injection, $\imath_x > 0$, that replenishes it.

3.4.4 Full phase diagram

Similarly to region II, region III produces a positive, stable solution n_c^+ to the condensate equation of motion. In contrast to region II, however, $n_c^+/s \to |\sigma|/\zeta$ diverges as $\zeta \to 0$, demonstrating the importance of the nonlinearity ζ in stemming the condensate growth. In this region, swasing is supplemented with thermal spin transfer $\imath_x$, which increases n_c^+. Because no solution to $i_x = 0$ exists for $\mu^* < 0$ (in our numerical calculation), we conclude that only CP is present in region III.

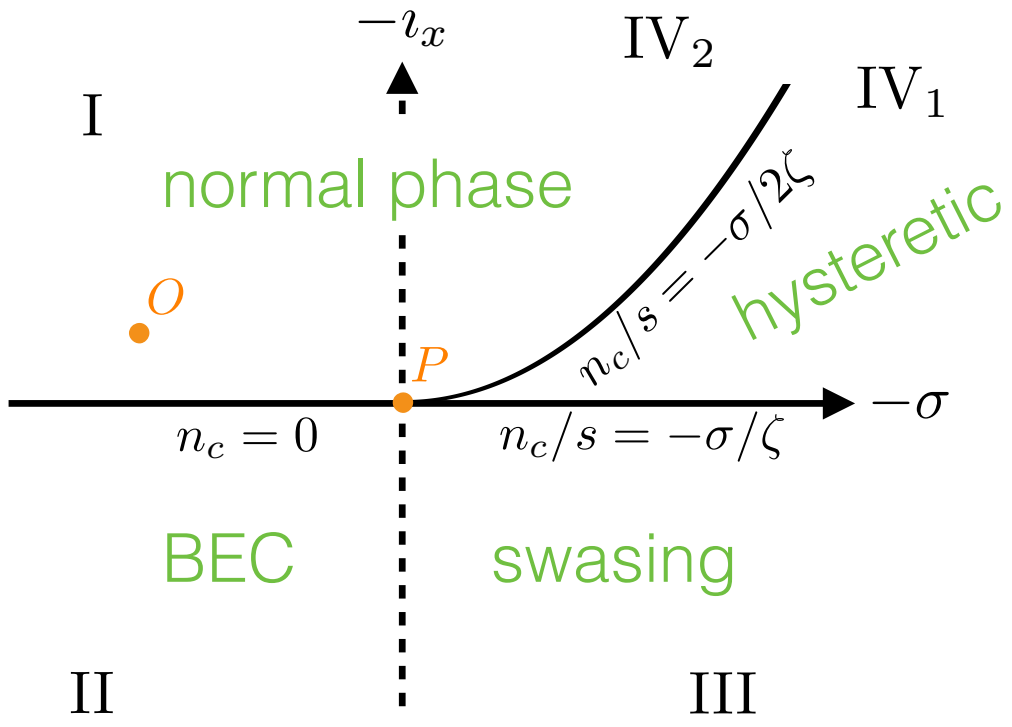

Figure 3.5: Phase diagram for the solutions of Eqs. (3.32) and (3.33) for n_c in the abstract $(\sigma, \imath_x)$ space. O stands for the unperturbed (i.e., thermal-equilibrium) point, while P is the critical point for a driven system. The solid lines, $\imath_x = 0$ and $\imath_x = -\sigma^2/4\zeta$, trace out phase transitions between distinct dynamic states: second-order transition between the NP and BEC (I/II boundary) and hysteretic first-order transitions at the IV$_2$/IV$_1$ and IV$_1$/III boundaries, where the normalized condensate density, n_c/s, jumps by $-\sigma/2\zeta$ and $-\sigma/\zeta$ relative to 0, respectively. The condensate associated with these first-order transitions is interpreted to be "swasing."[Ber96a]

Region IV may itself be divided further into two subregions: IV_1 and IV_2 defined respectively by $\sigma^2 \gtrless -4\zeta\imath_x$. In subregion IV_1, both n_c^+ and n_c^- are real, but only the former solution is stable (see Fig. 3.4). Depending on whether $n_c \gtrless n_c^-$ at $t = 0$, the magnetic system flows towards CP fixed point at n_c^+ or NP, respectively, at $t \to \infty$, indicating CP/NP hysteresis. In contrast, both n_c^+ and n_c^- are complex in subregion IV_2, precluding CP. In all of region IV, therefore, an NP solution $\mu^* < 0$ to $i_x = 0$ exists, which evolves continuously within this region. The CP solution existing in subregion IV_1, on the other hand, evolves continuously into a CP swasing phase in region III. Region IV is opposite to II both in the reversal of the sign of σ (such that the condensate tends to swase) and $\imath_x$ (such that the thermal magnons are pumped out of the magnet, thus suppressing the condensate). The balancing act between negative σ and $\imath_x$, as depicted in Fig. 3.4, allows for a stable condensate in subregion IV_2.

We summarize the above discussion in Fig. 4.12: The boundary between regions I and II describes a continuous phase transition between an NP and the Bose-Einstein condensate (BEC). The boundary between I and IV_2 is a crossover within the NP, while the boundary between II and III is a crossover between swasing and BEC (both instances of a CP). Boundaries delineating the hysteretic region IV_1 define history-dependent first-order transitions: An NP in IV_1 jumps to a finite condensate density $n_c/s = -\sigma/\zeta > 0$ when entering III, and a CP phase in IV_1 jumps from a finite condensate density $n_c/s = -\sigma/2\zeta$ to a normal state with a finite $\mu^* < 0$ when entering IV_2. All the phase-transition lines and crossovers emanate from the critical point P.

When drawing the physical phase diagram in terms of the experimentally-controlled parameters (μ', T') (which, in turn, determine σ and $\imath_x$), the essential structure of Fig. 4.12 is preserved, albeit somewhat distorted, as shown in Fig. 3.6. While μ' corresponds linearly to $-\sigma$, according to Eq. (3.34), $\imath_x$ is generally a nonlinear function of T' and μ'. Since, for a fixed μ', $\imath_x$ increases with increasing temperature T', however, we can think of $-\imath_x$ as parametrizing $1/T'$ (keeping T fixed). This explains why the structure of the physical phase diagram in Fig. 3.6 is anticipated by Fig. 4.12.

Let us now parametrize in detail the phase-transition lines depicted in Fig. 3.6. We

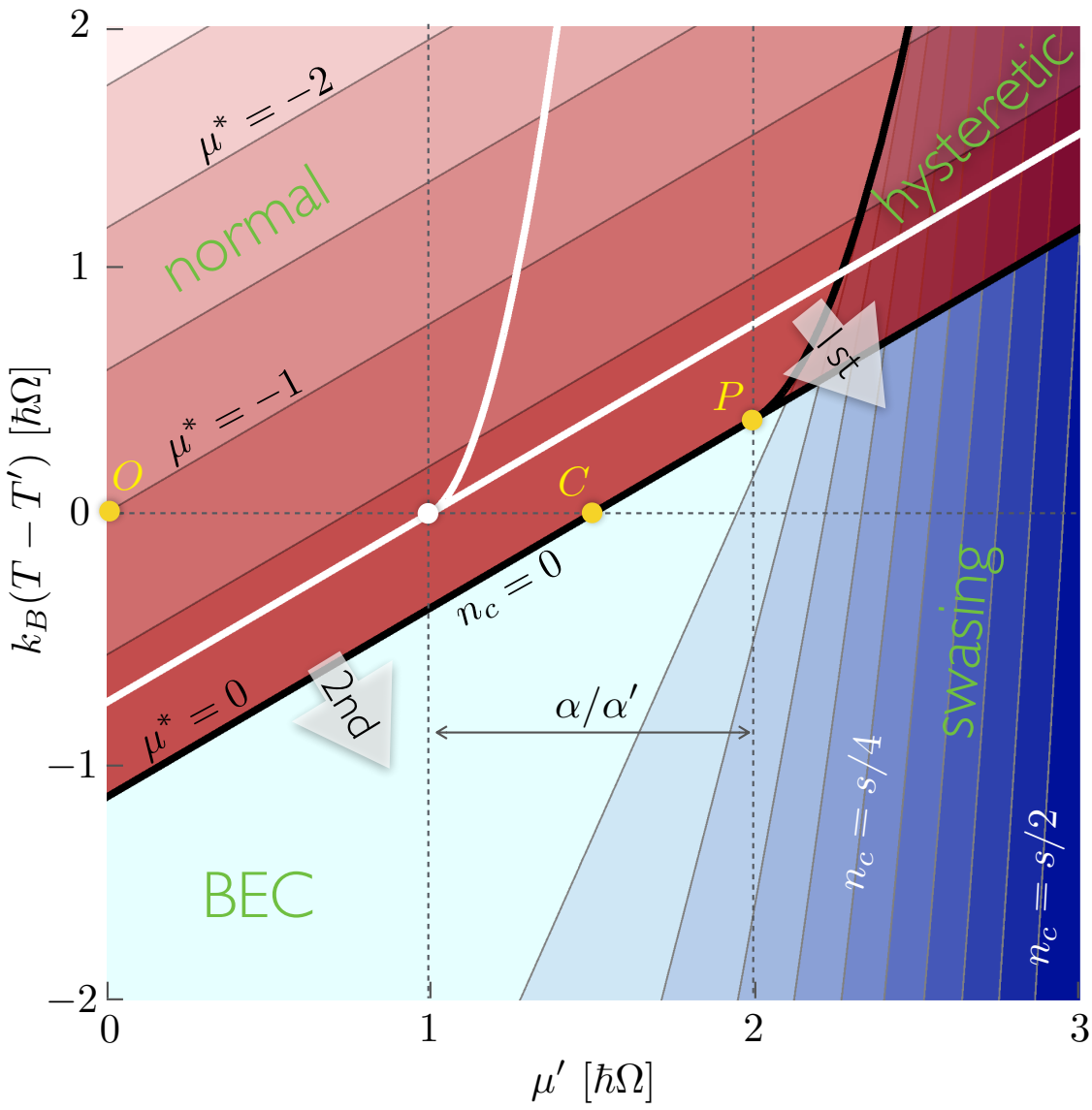

Figure 3.6: Physical phase diagram in the presence of anisotropy $K = \hbar\Omega$ at $k_BT = k_BT'' = 10^2\hbar\Omega$, $s\,(A/\hbar\Omega)^{3/2} = 10^4$, and $\alpha/\alpha' = 1$ (black curves), calculated using the linearized current $\imath_x$ in Eq. (3.33) [see discussion preceding Eq. (3.42)]. The white curves show the idealized $\alpha/\alpha' = 0$ case. The analytically evaluated diagram shown here is essentially indistinguishable from the numerical diagram (not shown) produced by the exact expression for i in Eq. (3.33). The phase-transition lines and crossovers that delineate different dynamic regimes can be inferred from Fig. 3.5.

denote by T_1' the phase boundary corresponding to the $\imath_x = 0$ abscissa in Fig. 3.5 (i.e., the curve delineating phases II and III) and by T_2' the boundary between regions IV_1 and IV_2 [strictly above the swasing instability (3.40), i.e., $\mu'/\hbar\Omega > 1 + \alpha/\alpha'$], which emanates out of the critical point P. When $k_B\left(T - T'\right), \mu', \hbar\Omega \ll k_B T$ (i.e., the ambient temperature sets the largest relevant energy scale), the current $\imath_x$ may be linearized in $k_B\left(T - T'\right)$, μ', and $\hbar\Omega$, allowing us to analytically derive the expressions for $T_1'\left(\mu'\right)$ and $T_2'\left(\mu'\right)$. In this regime, the former is linear in μ' and given by:

$$k_B\left(T - T_1'\right) = \frac{2\zeta_{3/2}}{5\zeta_{5/2}}\left[\mu' - \left(1 + \frac{\alpha}{2\alpha'}\right)\hbar\Omega\right], \tag{3.42}$$

where ζ is the Riemann zeta function. Below the swasing threshold, condensate forms when T' exceeds T_1'. In the absence of a temperature bias, $T' = T$, Eq. (3.42) indicates the formation of a condensate when μ' exceeds $\left(1 + \alpha/2\alpha'\right)\hbar\Omega$ (denoted in Fig. 3.6 by C).

The curve T_2', in turn, is defined by:

$$k_B\left(T_1' - T_2'\right) = \frac{\left[\mu' - (1 + \alpha/\alpha')\hbar\Omega\right]^2}{5\Gamma_{5/2}\zeta_{5/2}(1 + \alpha/\alpha')}\frac{\pi^2 s A^{3/2}}{K(k_B T)^{3/2}}, \tag{3.43}$$

where Γ is the gamma function. The curves T_1' and T_2', according to Eqs. (3.42) and (3.43) are shown in Fig. 3.6 as solid black lines for $\alpha/\alpha' = 1$ and solid white lines $\alpha/\alpha' = 0$. The dependence of the transition lines on a gradual change in the strength of damping α and nonlinearity K is shown in Fig. 3.7.

3.4.5 Floating magnon temperature

In addition to angular momentum, energy transfer from the ferromagnet into the adjacent normal metals and its crystal lattice, in general, also needs to be balanced. In the previous section, we made a simplifying assumption that the magnon temperature was pinned by phonons and/or electrons, which provided a very efficient energy sink. Here we relax that assumption, which necessitates keeping track of the total magnon energy on par with the magnon number. We still, however, suppose that magnon-magnon interactions are sufficiently strong that the magnons remain internally thermalized to a Bose-Einstein distribution with a well-defined effective temperature T and chemical potential μ^* (relative

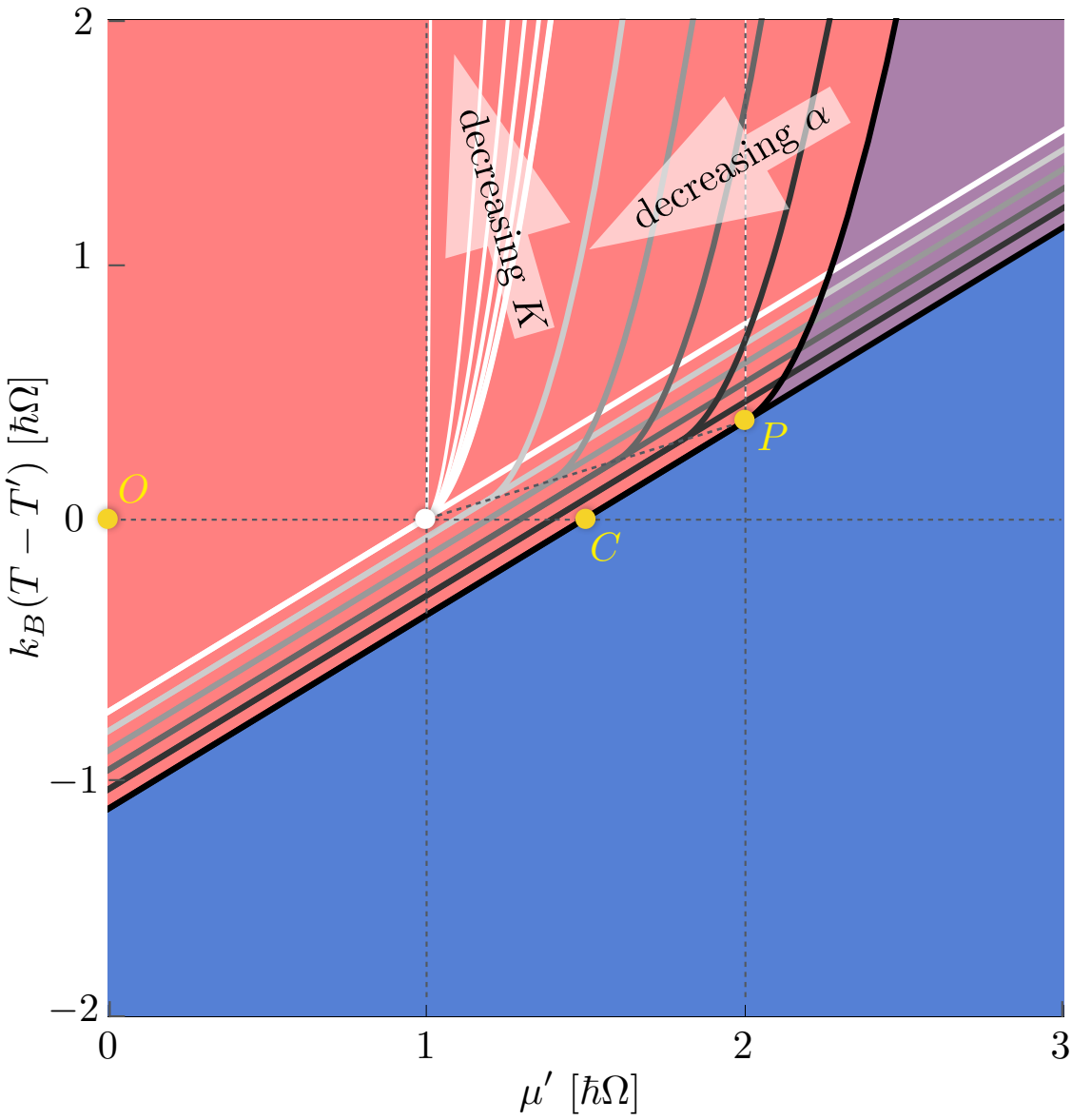

Figure 3.7: Effects of intrinsic damping α/α' (starting at 1 and decreasing to 0 in increments of 0.2) and nonlinearity $K/\hbar\Omega$ (going from 1 to 0 in increments of 0.2), while keeping $\hbar\Omega$ fixed, on the phase-diagram structure, using Eqs. (3.42) and (3.43). Decreasing Gilbert damping α [which lowers the swasing threshold (3.40)] increases the size of the condensate regions, while decreasing anisotropy K increases the size of the hysteretic region [as is evident from Eq. (3.43)].

to the magnon-band bottom) at all times. We also retain the assumption that cloud and condensate always remain in mutual equilibrium, namely, that n_c vanishes for $\mu^* < 0$ (NP) and $n_c > 0$ requires that $\mu^* = 0$ (CP). In analogy with the condensate and normal-phase spin currents discussed above, we define the condensate and normal-phase energy currents $\jmath_c \equiv \omega(i_c + i'_c)$ and $\jmath_x \equiv (j_x + j'_x)|_{\mu^*=0,n_c=0}$, respectively, according to Eq. (3.25), which simplifies the stability analysis of the CP. We will suppose the phonon temperature T'' is fixed (and controlled by T' and $\tilde{T}$), while the F|$\tilde{\text{N}}$ interface blocks both spin and energy transport for magnons.

At any time, there now exist two dynamical variables. In NP, these are μ^* and T, governed by the implicit, coupled rate equations $\hbar\dot{n}_x = i_x + i'_x$ and $\dot{e}_x = j_x + j'_x$; in CP, n_c and T, governed by Eqs. (3.22) and (3.25). In contrast to the expansion of the magnon current i in n_c, Eq. (3.33), a simple general analytic expansion of the currents in T in either phase is not possible, and we must resort to a numerical treatment.

In general, the steady-state temperature T and the chemical potential μ^* (or condensate spin density n_c) in each phase are determined from the stable fixed points of the respective pair of coupled rate equations. The resultant numerical phase diagram is shown in Fig. 3.8. The energy accompanying angular-momentum transfer into the ferromagnet creates additional heating (cooling) when $T' \gtrless T''$ (phonon temperature), which hinders (facilitates) condensation relative to the fixed-temperature regime. In particular, condensation via temperature gradient alone (i.e., $\mu' = 0$) no longer occurs. Below the swasing instability (i.e., $\sigma > 0$), each steady-state solution $\mu^* = 0$ in NP coincides with a solution $n_c = 0$ in CP, indicating the second-order phase transition. Above the threshold for swasing, on the other hand, hysteretic regions appear, where, depending on the initial conditions, the solutions flow toward stable fixed points in NP or CP. These features are qualitatively similar to those discussed in the case of a fixed magnon temperature, Sec. 3.4.1.

In the case of a low temperature gradient ($T' \approx T''$), the incipient condensation may be understood by expanding $\imath_x$ and $\jmath_x$ in $k_B\,(T'' - T')$, $k_B\,(T'' - T)$, and μ' (all of which are assumed to be much smaller than the ambient temperature) and solving the steady-state equations to obtain analytic solutions for T and n_c. When $\mu' \leq (1 + \alpha/2\alpha')\hbar\Omega$ (denoted

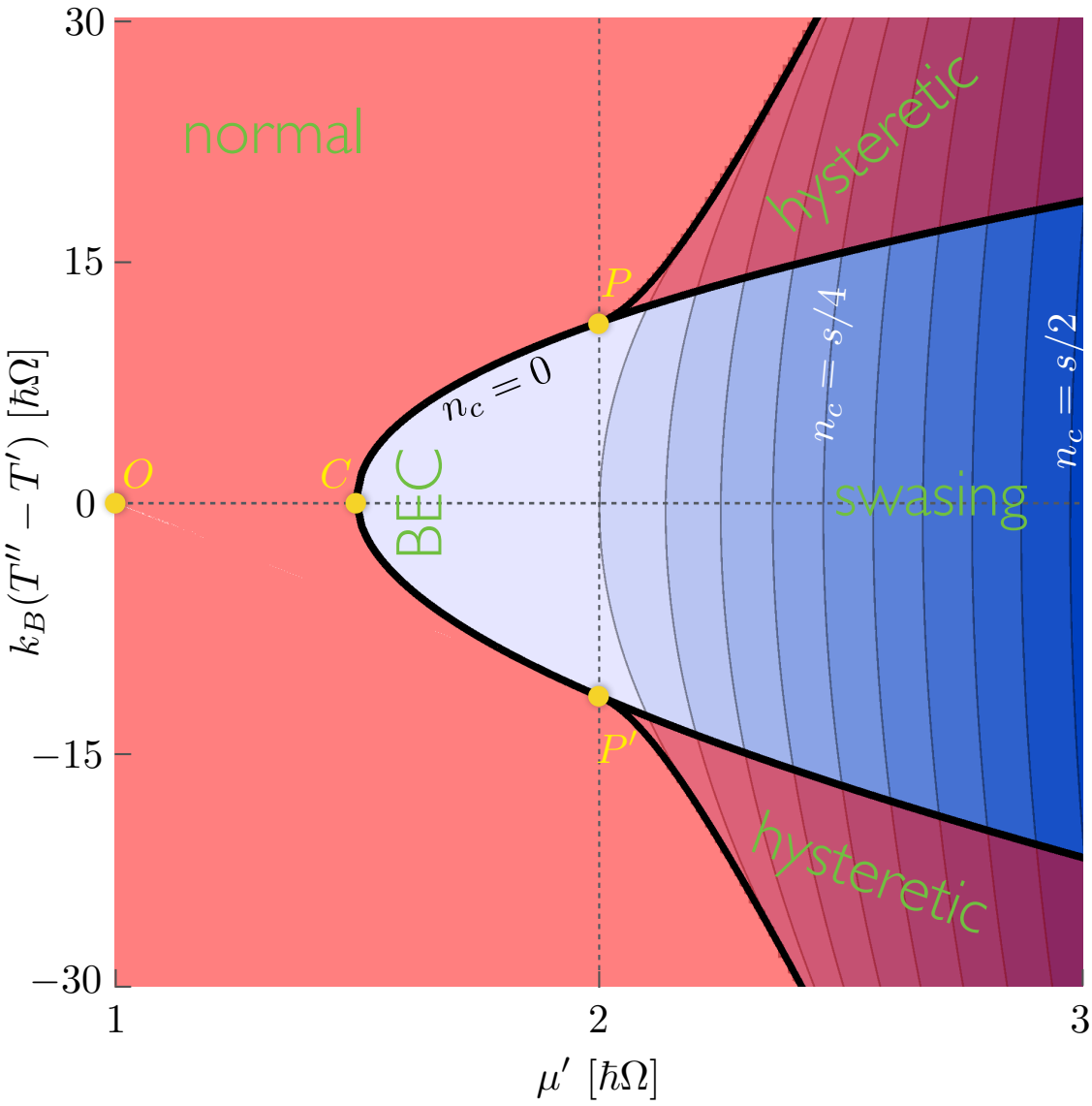

Figure 3.8: Phase diagram with a floating magnon temperature T and density determined by the conditions $i = 0$ and $j = 0$. Here, $\alpha/\alpha' = 1$, $K = \hbar\Omega$, $s\,(A/\hbar\Omega)^{3/2} = 10^4$, and $k_B T'' = 10^2\hbar\Omega$, similarly to the other plots.

by C in Fig. 3.8), no condensate solution exists; increasing μ' beyond this critical point, the condensate density continuously increases from zero. (Note that the same bias μ' at C describes the onset of condensation under zero temperature bias both in the fixed- and floating-temperature regimes.) As in the fixed-temperature case, furthermore, when $\mu' \geq (1+\alpha/\alpha')\hbar\Omega$, unstable analytic solutions for n_c appear, suggesting the presence of hysteresis when the temperature gradient is restored; correspondingly, (two) critical points P and P' manifest under a sufficient temperature bias at the swasing instability (3.40).

The above linearized treatment for the currents $\imath_x$ and $\jmath_x$, however, fails to capture the detailed phase behavior when $T' \neq T''$. There, the spin and energy fluxes that are quadratic in thermal bias are essential for generating the full structure of the phase boundaries depicted in Fig. 3.8. In particular, we see that the condensate is suppressed under large temperature biases of both signs: When $T' \ll T''$, the magnons injected by the normal metal are relatively cold but there are ultimately too few of them to precipitate a condensate; when $T' \gg T''$, on the other hand, the magnon injection rate is high but they are too hot to condense. Only at intermediate thermal biases do we reach a compromise between the magnon injection rate and the energy they carry, which allows for a stable condensate to form.

3.5 Finite Condensate-Cloud Interactions

In the simple model of Bose-Einstein condensation presented above, the timescale characterizing transport i_{cx} between the condensate and the cloud was assumed to be much shorter than those of Gilbert damping and interfacial spin transfer; in this regime, F is either in normal phase, with no condensate and $\mu^* < 0$, or in condensate phase with $\mu^* = 0$. Let us now allow for finite cloud-condensate interactions, writing a phenomenological expression (which is given a microscopic basis in the next chapter) for the interaction:

$$i_{cx} = 2\alpha_{\rm sc}\mu^* n_c \,, \tag{3.44}$$

where $\alpha_{\rm sc}$ is a parameter describing scattering between the cloud magnons and the condensate. When $\mu^* < 0$, condensate magnons evaporate into the thermal cloud. The infrared

divergence of the Bose-Einstein distribution $n_B[\beta(\epsilon - \mu^*)]$ when $\mu^* \to 0$ suggests that μ^* is prohibited from becoming negative. If, however, one allows for finite interactions, under out-of-equilibrium conditions (i.e. driving by N), the distribution function for thermal magnons is skewed from the equilibrium Bose-Einstein profile and must be obtained from kinetic theory. At biases much weaker than the temperature ($\mu', T - T' \ll T$), however, the non equilibrium corrections appear only at the lowest energy modes; high energy modes (which dominate transport) may still be parameterized by a chemical potential, including the case in which the cloud becomes oversaturated and $\mu^* > 0$, wherein Eq. (3.44) predicts that the cloud sheds the excess angular momentum into the condensate.

Returning to the fixed temperature case, the evolution of F in the $\mu^* - n_c$ phase plane is now obtained by solving Eqs. (3.17) and (3.21) in conjunction for $\mathbf{p}(t) = (\mu^*(t)/\hbar\Omega, n_c(t)/s)$ using Eq. (3.44). Expanding to linear order in the biases and in the response $\delta\mu = \mu^* + \hbar\Omega$, one has the coupled rate equations:

$$\hbar\dot{n}_c = 2\alpha'\mu' n_c - 2(\alpha + \alpha')\left(\hbar\Omega + K(n_c/s)^2\right) n_c + 2\alpha_{\rm sc}\mu^* n_c \,, \tag{3.45}$$

$$\hbar\dot{n}_x = \imath_x - 2\alpha_{\rm sc}\mu^* n_c \,. \tag{3.46}$$

where

$$\imath_x \approx -\frac{g_\alpha}{d_F}(\mu^* + \hbar\Omega) + \frac{g}{d_F}(\mu' - \mu^* - \hbar\Omega) + \frac{S}{d_F}(T' - T) \tag{3.47}$$

has been expanded around the point $\mu^* = 0$. Here, g_α is the Gilbert damping spin conductance, obtained from Eq. (3.19), while g and $\mathcal{S}$ are the interfacial spin conductance and Seebeck coefficients, obtained from Eq. (3.20), all with $\mu^* = 0$ [1]. In steady-state, one obtains three fixed points, given by $\mathbf{p}_0 = (\mu^*(0)/\hbar\Omega, 0)$ (normal phase) and $\mathbf{p}_\pm = (\mu^*(\tilde{n}_s^\pm)/\hbar\Omega, \tilde{n}_s^\pm/s)$ (condensate phase), where

$$\mu^*(n_c) = \frac{g\mu' + \mathcal{S}(T' - T) + 2\alpha_{\rm sc} n_c d_F}{g_\alpha + g + 2\alpha_{\rm sc} n_c d_F}\hbar\Omega - \hbar\Omega \tag{3.48}$$

and

$$\frac{\tilde{n}_c^\pm}{s} = \frac{\pm\sqrt{\tilde{\sigma}^2 + 4\zeta\tilde{\imath}_x} - \tilde{\sigma}}{2\zeta} \,, \tag{3.49}$$

[1] Because $T \gg \hbar\Omega$, the expansion coefficients g and g_α around $\mu^* = 0$ are approximately the same as those obtained around equilibrium $\mu^* = -\hbar\Omega$

with ζ given by Eq. (3.35),

$$\tilde{\sigma} = \sigma + \frac{(\alpha + \alpha')}{\alpha_{\rm sc}} K(g_\alpha + g)/d_F \tag{3.50}$$

and

$$\tilde{\imath}_x = \imath_x - \sigma/\alpha_{\rm sc}\,. \tag{3.51}$$

Consider now the strongly interacting limit $\alpha_{\rm sc} \to \infty$. When $n_c = 0$, Eq. (3.48) is just the linearized response of the cloud to a temperature bias $T' - T$ and spin-transfer torque μ'; when, however, n_c is finite, $\mu^* \to 0$ (corresponding to an ideal Bose-Einstein condensate), and $\tilde{n}_c^\pm = n_c^\pm$, reproducing the expressions in Section 3.4.3.

The stability of the fixed points may be obtained by expanding the rate equations around the fixed points: $\dot{\mathbf{p}}|_0 \approx \hat{q}_0(\mathbf{p} - \mathbf{p}_0)$ and $\dot{\mathbf{p}}|_\pm \approx \hat{q}_\pm(\mathbf{p} - \mathbf{p}_\pm)$, where the matrices $\hat{q}_0$ and $\hat{q}_\pm$ are obtained by differentiating Eqs. (3.45) and (3.46). The two eigenvalues of $\hat{q}_0$ are proportional to $-(g + g_\alpha) < 0$ and $-\tilde{\imath}_x$; when $\tilde{\imath}_x < 0$, the point $\mathbf{p}_0$ is destabilized, and the ferromagnet enters a condensate phase, spontaneously breaking the U(1) symmetry of $\mathbf{p}_0$. Conveniently, all of the structure of Section 3.4.3 still holds (with σ and $\imath_x$ replaced by $\tilde{\sigma}$ and $\tilde{\imath}_x$, respectively), though the instability of $\mathbf{p}_-$ and stability of $\mathbf{p}_+$ now must be shown numerically in the regions of interest by diagonalizing $\hat{q}_\pm$. The resulting phase diagram is shown in Fig. 3.9.

3.6 Detection of phase transition

The BEC-normal phase transition presents some of the most interesting physics of the system, yet as can be seen from Fig. 3.3 of the main text, it is difficult to discern from the total magnetization of the insulator alone: Whereas for fixed T the density of excited magnons $n_{\rm x}$ plateaus as $z_F \to 1$, the rate of change of the total number of magnons $\dot{n} = \dot{n}_{\rm x} + \dot{n}_c$ remains always continuous function of time. The transition can, however, be observed by Brillioun light scattering, wherein the scattered light intensity scales quadratically with the lateral junction size if the ground-state condensate is indeed coherent.

Alternatively, electron spin resonance (or, for that matter, any spectroscopic probe of a

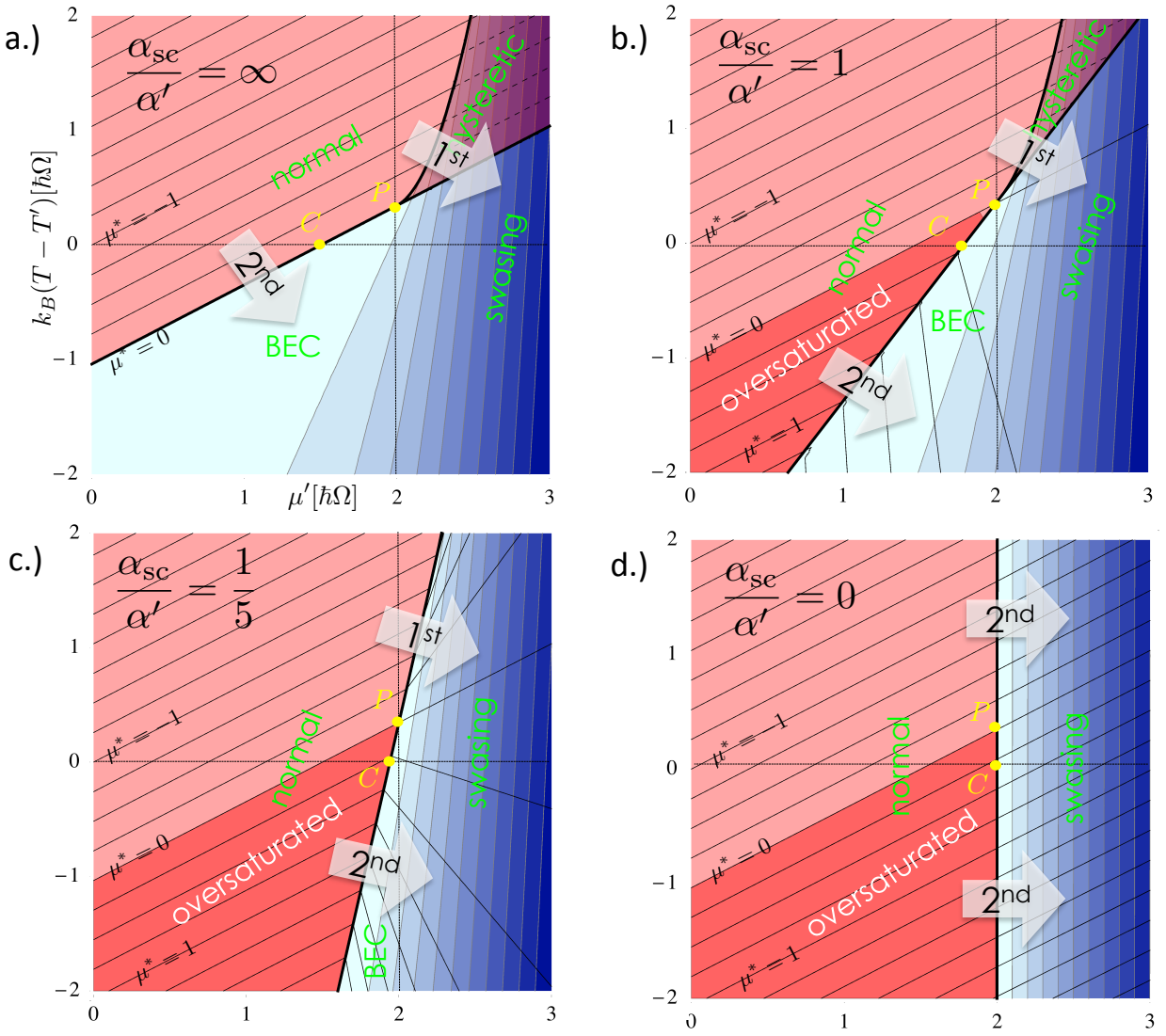

Figure 3.9: Fixed temperature plots with finite cloud-condensate interactions for a.) $\alpha_{sc}/\alpha' = \infty$, b.) $\alpha_{sc}/\alpha' = 1$, c.) $\alpha_{sc}/\alpha' = 1/5$, and d.) $\alpha_{sc} = 0$, with $k_B T = k_B T' = 10^2\hbar\Omega$, $s(A/\hbar\Omega)^{3/2}$, $K = \hbar\Omega$ and $\alpha = \alpha'$. At finite α_{sc}, oversaturated regions of the thermal cloud begin to appear, wherein $\mu^* > 0$ but the rate of transfer of excess angular momentum to the condensate is smaller than the relaxation rate of the condensation, precluding the formation of a steady-state condensate. In the extreme limit $\alpha_{sc} = 0$, the cloud and condensate are uncoupled, Bose-Einstein condensate does not occur (as thermal magnons cannot relax into the ground-state), and coherent magnetic dynamics can only be induced by the swasing instability.

coherent microwave radiation) can provide clear evidence of the presence of quasiequilibrated Bose-Einstein condensation of magnons. Consider a test-particle electron at a fixed distance $\mathbf{r}$ from the magnetic insulator. Provided that the electron experiences the insulator as a single quantum magnetic moment $\hat{\mathbf{m}}$, one may neglect details involving spatial fluctuations of the magnetization and allow the two systems to interact via dipole-dipole coupling; the Hamiltonian describing the interaction is therefore of the form:

$$\hat{H}_{\mathrm{d-d}} = \sum_{i,j=x,y,z} \hat{m}_i T_{ij} \hat{\sigma}_j \,,$$

where T_{ij} is a tensor that depends on $\mathbf{r}$ and $\hat{\sigma}$ is the electron spin operator. Supposing the electron, subjected to a strong applied magnetic field in the z direction, begins in the state $|\uparrow\rangle$, the probability that quantum fluctuations in the magnetization $\hat{\mathbf{m}}$ spin flip the electron is, to lowest order in T_{ij},

$$P_{\uparrow\to\downarrow}(t) = \int_0^t dt' \int_0^t dt'' \sum_{iji'j'} T_{ij} T_{i'j'} \left\langle \hat{m}_i\left(t'\right) \hat{m}_{i'}\left(t''\right)\right\rangle \left\langle\uparrow\right| \hat{\sigma}_j \left|\downarrow\right\rangle \left\langle\downarrow\right| \hat{\sigma}_{j'} \left|\uparrow\right\rangle e^{i\omega_z(t'-t'')} \,,$$

where ω_z is the electronic Larmor frequency in the applied magnetic field. Choosing our coordinate system to coincide with the eigenbasis of T_{ij} and for simplicity asserting cylindrical symmetry around the z axis (so that $T_{xx} = T_{yy} = T_\perp$), the transition probability becomes

$$P_{\uparrow\to\downarrow}\left(t\right) = \int_0^t dt' \int_0^t dt'' T_\perp^2 \left\langle \hat{m}^-\left(t'\right) \hat{m}^+\left(t''\right)\right\rangle e^{i\omega_z(t'-t'')} = t T_\perp^2 S_{-+}(\omega_z) \,,$$

where $S_{-+}(\omega) = \int dt e^{i\omega t} \langle \hat{m}^-(t) \hat{m}^+(0)\rangle \propto N_{\mathrm{gs}}$ is the spectral density of magnetic oscillations in a steady state. The transition rate is thus proportional to N_0, which scales linearly with the lateral dimensions of our junction in BEC phase and is size independent in normal phase. This simple treatment is pertinent to the case when the magnons condense at $\mathbf{q} = 0$. Otherwise (as is the case in YIG, for example) one needs to come up with means to couple coherently to magnetic fluctuations at a finite $\mathbf{q}$ (perhaps using some form of grating).

3.7 Conclusion

We studied the steady-state behavior of an insulating magnet driven by the combination of a thermal gradient and spin-transfer torque across its interface with an adjacent normal metal.

Agitated by the interfacial magnon-electron and bulk magnon-lattice interactions, our theory describes the emergent nonlinear coherent motion of the condensate (in a quasiequilibrium with the thermal cloud of magnons), demonstrating a surprisingly rich dynamic phase diagram.

The stability analysis of the driven coherent motion depends crucially on the form of the magnetic anisotropy. Our detailed analysis was specific to an easy-plane magnetic film subjected to a large out-of-plane magnetic field (such that the magnetic ground state is non-degenerate). In the case of other geometries and magnetic anisotropies, the phase diagram can be altered. Furthermore, in other configurations, where spin-rotational symmetry is broken in all directions, three-magnon scattering processes would violate magnon conservation, which is built into our model. We nevertheless expect that the essential nature of the first- and second-order instabilities predicted in our model to be generic, although the details would depend on the specific experimental realization. We emphasize that one of the key features predicted by our theory is a possibility of a continuous formation of the condensate in the presence of a temperature gradient alone, which may be less sensitive to the particular magnetic orientation than the more familiar instabilities invoked by a spin-transfer torque.

The presence of coherently-precessing magnetic phases may manifest experimentally in a variety of ways. Collective magnetic modes driven by dc currents may be detected either by their microwave signatures or differential dc response (both in the charge and thermal sectors) in the steady state, similarly to the conventional spin-transfer torque instabilities.[KSK03] The thermal properties of the magnon condensates, in particular, may differ dramatically from the normal phase, if, for example, the lateral propagation of heat in the plane of our heterostructure can be carried collectively by magnetic dynamics. In addition, unlike thermal magnons that generally travel diffusively with a microscopic spin-diffusion length, low-frequency condensates can carry spin signals over macroscopic distances.[Son10, **?**] Such collective and nonlocal transport signatures of condensation warrant further studies, both theoretically and experimentally.

CHAPTER 4

Thermal Spin Torques on an Insulating Ferromagnet

The growing field of spin caloritronics [BSV12b] complements the electrical degree of control of the spin current with a new experimental parameter: temperature. In contrast to electrical biasing, which couples to the electron's charge, transport under the application of a thermal flux is possible for neutral carriers. If, for example, a temperature gradient is applied to a magnetic insulator, a net flow of angular momentum, carried by thermally activated spin wave excitations, results. When integrated into larger structures, magnonically active elements open up the possibility of new effects and devices based on thermally driven transport.

One such effect is that of a thermally driven spin-transfer torque at a normal metal(N)/ insulating ferromagnetic (F) interface, which has been recently observed in [PAR11b, LSJ12b] via ferromagnetic resonance linewidth. Thermally driven magnetic dynamics was first predicted [HBZ07, HFC14] and observed [YGY10] for a *conducting* ferromagnetic layer, where the spin-transfer torque is provided by spin-polarized electric current driven into the magnetic layer by an interfacial spin-dependent Seebeck effect. In contrast, for an insulating ferromagnetic layer, spin-transfer torque is provided by a pure spin current mediated by ferromagnetic magnons. Here, exchange coupling at the interface makes possible the interconversion of magnons on the F side with electron spin in N, which serves as a reservoir of angular momentum.

In this Chapter, we provide a proper account of the physics of magnon-mediated spin-transfer torque at a normal metal (N)/ insulating ferromagnet (F) interface, building on the formalism developed in Chapter 2. In the first half of the paper, we propose a mechanism by which to realize a thermally driven spin-transfer torque at a single N/F interface, utilizing

the interactions between thermally activated magnons and the magnetic order parameter to effect a torque on the latter. In the second half, we investigate a spin valve, consisting of two electrically insulating magnetic layers separated by a normal metal spacer; metal leads attached to the ferromagnets provide angular momentum. Slonczewski[Slo10b] has proposed a similar scheme. There, a heat current is converted into a spin current via a ferrite, which is coupled to paramagnetic monolayer by superexchange; spin current is subsequently transferred to the conduction electrons of a spacer and ultimately to a free magnet. In contrast, our proposal relates the thermal spin-flux directly to the spin mixing conductance, a readily measurable quantity, circumventing the notion of a paramagnetic monolayer. The a thermo-magnon flux passing through the ferromagnetic components results in a spin accumulation in the normal metal spacer, which exerts a torque on the free layer similarly to a traditional electronic spin valve. In both structures, we consider analyze the damping and instabilities resulting.

4.1 Single Layer

The spin current density $\mathbf{j}$ entering F (assumed to be composed of a single domain) through an N/F interface, which is determined by the interfacial spin mixing conductance, is comprised of two orthogonal, physically distinct components. The first, $\mathbf{j}_{\parallel}$, is the spin current collinear with the spin density order parameter direction $\mathbf{n}$ (with $\mathbf{n}$ as a unit vector), carried by magnons each with angular momentum $-\hbar\mathbf{n}$. The second current, $\mathbf{j}_{\perp}$, which is orthogonal to $\mathbf{n}$ and linear in $\mathbf{n}\times\boldsymbol{\mu}$ (where $\boldsymbol{\mu}$ is the spin accumulation in N along the interface) and $\dot{\mathbf{n}}$, gives the *external* spin torque on $\mathbf{n}$ provided by N. A complete description of spin transport across the F/N interface requires that one solve the appropriate spin diffusion equation in N self-consistently with the F magnetic order parameter dynamics and magnon diffusion equations, using $\mathbf{j}$ as the boundary condition. In general, however, electron dynamics in N is much faster than the microwave frequency precession of $\mathbf{n}$; under the application of an interfacial temperature gradient, which gives rise to a magnon current $\mathbf{j}_{\parallel}$, the spin accumulation $\boldsymbol{\mu}$ is parallel to $\mathbf{n}$ (provided that the magnetic field is sufficiently small), and cannot exert a

torque $\propto \mathbf{j}_\perp$ on $\mathbf{n}$. Moreover, if N is a poor sink, the spin accumulation is carried away back into N altogether.

A thermal spin-torque on $\mathbf{n}$ in a single F film (Fig. 4.1) therefore requires SU(2) symmetry breaking by the film itself, which in the simplest case may be provided by the anisotropy. Consider a magnet with easy-plane anisotropy and spin density pinned along the hard axis by an applied magnetic field $H\mathbf{z}$ (in units of energy). The corresponding Hamiltonian is consists of the exchange, Zeeman and anisotropy terms:

$$\hat{\mathcal{H}} = \int d^3x \left(-\frac{A}{2s}\hat{\mathbf{s}} \cdot \nabla^2 \hat{\mathbf{s}} + H\hat{s}_z + \frac{K}{2s}\hat{s}_z^2 \right) , \tag{4.1}$$

where A is the exchange stiffness, s is the saturation spin density (in units of $\hbar$) and K, the anisotropy constant (in units of energy), which is easy plane (easy axis) when $K > 0$ ($K < 0$). The spin density operator $\hat{\mathbf{s}}$ consists of a coherent piece $\langle \hat{\mathbf{s}} \rangle = \tilde{s}\mathbf{n}$ around which the spin density fluctuates incoherently: $\delta\hat{\mathbf{s}} = \hat{\mathbf{s}} - \langle \hat{\mathbf{s}} \rangle$. These fluctuations are thermally activated magnons, which reduce the effective spin density to $\tilde{s} = s(1 - n/s)$, where n is the magnon density.

The exchange and anisotropy terms introduce magnon-magnon interactions. While thermal magnons interact via both terms, by rotational invariance it is clear that thermal magnons cannot induce a torque on the spatially uniform order parameter $\mathbf{n}$ by exchange coupling. Interactions arising from the anisotropy K do, however, open a three-(thermal)magnon scattering channel in which thermal magnons exchange angular momentum with the coherent order parameter. We begin by writing the spin density in terms of boson field operators $\hat{\Phi}(\mathbf{x})$ and $\hat{\Phi}^\dagger(\mathbf{x})$ via the Holstein-Primakoff transformation, Eqs. (1.24) and (1.25). Let us first consider the pole $\mathbf{n} = -\mathbf{z}$, which is a stable equilibrium in the absence of driving provided that the magnon gap $\hbar\Omega = H - K$ is positive. We will assume that the spin density (and fluctuations thereof) remains close to $-\mathbf{z}$, so that we may expand $\hat{s}_- \approx \sqrt{2s}\hat{\Phi}$. For incoherent (e.g. thermal) magnons, when the spin quantization axis (i.e. the order parameter $\mathbf{n}$) is collinear with the z axis, the transverse spin density vanishes, and $\langle\hat{\Phi}\rangle$=0. However, when $\mathbf{n}$ is tilted away from $-\mathbf{z}$, $\hat{\Phi}$ has a coherent component; for small tilting,

$$\hat{\Phi}(\mathbf{x}) = \hat{\varphi}(\mathbf{x}) + \sqrt{\frac{s}{2}}(\pi - \theta)e^{-i\phi} , \tag{4.2}$$

where θ is the angle between $\mathbf{n}$ and $\mathbf{z}$ (with $\pi - \theta \ll 1$), ϕ is the (U(1) symmetry breaking) azimuthal angle of the in-plane component of $\mathbf{n}$, and $\hat{\varphi}$ is the field operator for incoherent thermal magnons excited around $\mathbf{n}$ (with $\langle\hat{\varphi}\rangle = 0$). Eq. (4.2), when inserted into the anisotropy Hamiltonian (last term on the right-hand-side of Eq. (4.1)), generates a term:

$$\hat{\mathcal{H}}_{\rm sc}(\mathbf{n}) = \frac{K}{s}\sqrt{\frac{2}{s}}(\pi - \theta)e^{i\phi}\int d^3x\hat{\varphi}^\dagger(\mathbf{x})\hat{\varphi}(\mathbf{x})\hat{\varphi}(\mathbf{x}) + H.c. \tag{4.3}$$

describing three-magnon processes. When $\mathbf{n} = -\mathbf{z}$ (i.e. $\theta = \pi$), the magnon Hamiltonian $\hat{\mathcal{H}}$ is rotationally invariant, $\hat{\mathcal{H}}_{\rm sc} = 0$ and three-magnon processes are prohibited. When $\mathbf{n}$ is oriented away from equilibrium, however, the U(1) rotational symmetry of $\hat{\mathcal{H}}_{\rm sc}$ around $\mathbf{z}$ is broken, thus breaking the conservation of thermal magnons as well. The angular momentum lost (gained) by the annihilation (creation) of thermal magnons is transferred to the coherent order parameter $\mathbf{n}$, actuating a coherent spin-torque. (See Fig. 4.1).

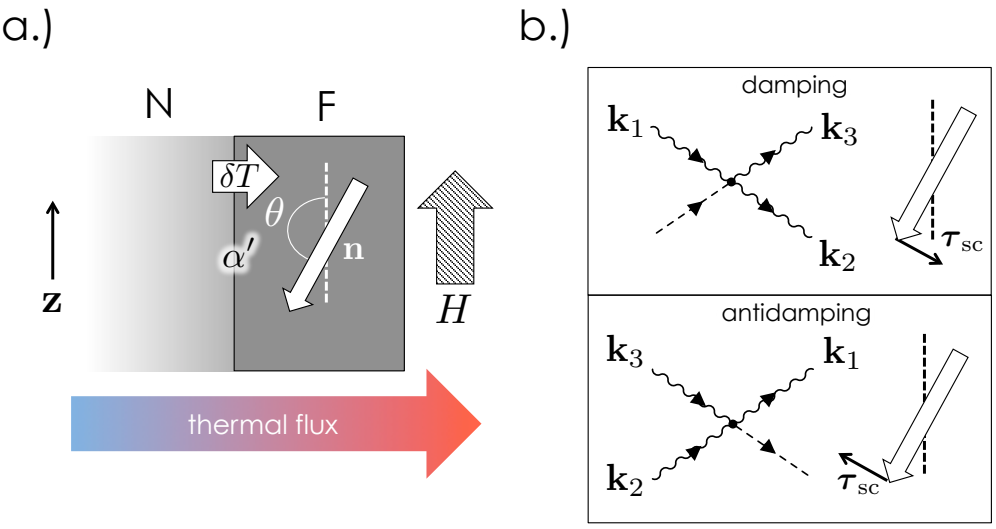

Figure 4.1: a.) Schematic for single magnetic film scenario. A temperature gradient, applied across the N/F interface, results in an effective interfacial temperature drop δT that drives angular momentum into F via the spin Seebeck effect, which is absorbed by the magnons. b.) Three-magnon processes, opened when the spin density order parameter $\mathbf{n}$ is misaligned with the F broken-symmetry axis. The annihilation of one finite $\mathbf{k}$ (thermal) magnon and the corresponding creation of two robs $\mathbf{n}$ of $\hbar$ of angular momentum in the $\mathbf{z}$ direction, resulting in a damping torque; the inverse process supplies generates an antidamping torque.

Four-magnon processes via the exchange interaction between thermal magnons do, however, occur. Provided $Ak^2 \sim T \gg K$, such four-magnon processes dominate over four- and three-magnon scattering stemming from anisotropy, and the cloud of thermal magnons therefore remains essentially internally thermalized to a Bose-Einstein distribution $f = 1/[e^{(\beta(\epsilon_{\mathbf{k}}-\mu^*)} - 1]$ with a well defined chemical potential μ and temperature $T = 1/\beta$ (in units of energy). Here, we have defined the chemical potential with respect to the magnon gap, so that $\epsilon_{\mathbf{k}} = A\mathbf{k}^2$ is the magnon exchange energy[1]. Strong coupling to a bath provides an additional mechanism by which thermal magnons are relaxed to a Bose-Einstein profile. For simplicity, let us suppose that the magnons are coupled to a such a bath (e.g. a poor spin-sink metal), capable of relaxing magnon energy but not spin, which establishes the equilibrium temperature of F. In addition, a diffusive bath (e.g. phonons), establishes the equilibrium chemical potential of the magnons, $\mu_e = -\hbar\Omega$, where $\hbar\Omega = H - K$ is the magnon gap when the magnetization is parallel to magnetic field (i.e. spin density is in the -**z** direction). Magnon-phonon coupling, however, is not so strong as to quench the magnon potential μ to μ_e; the injection of spin via the interfacial spin Seebeck effect causes the magnon chemical potential to deviate from its equilibrium value by an amount $\delta\mu = \mu - \mu_e$, which via three-magnon scattering, affects the transfer of angular momentum between the thermal cloud and the magnetic order parameter.

Provided that $\delta\mu \ll T$, the rate of change of the thermal magnon spin density due to three-magnon scattering is:

$$\hbar\dot{n}|_{\rm sc} = \frac{\hbar}{\tau}\left(\frac{\hbar\Omega - \delta\mu}{T}\right) n_c = -\,\hbar\dot{n}_c|_{\rm sc}\ , \tag{4.4}$$

where n is the magnon thermal cloud density. The quantity $n_c = s(1+\cos\theta) \approx s(\theta-\pi)^2/2$ is the "condensate" density. The timescale τ is given by:

$$\frac{1}{\tau} = \frac{2(K/s)^2}{(2\pi)^5\hbar^7}\int d^3k_1 \int d^3k_2 \int d^3k_3 \delta\left(\mathbf{k}_1 - \mathbf{k}_2 - \mathbf{k}_3\right)\delta\left(\epsilon_1 - \epsilon_2 - \epsilon_3\right)\left(1+f_1\right) f_2 f_3\,, \tag{4.5}$$

with the distributions f_i understood to be evaluated at equilibrium, $\mu = \mu_e$. Eq. (4.4) can be understood from the following entropic argument. Because the order parameter **n** carries

[1]In what follows, we consider temperatures much higher than the gap, where spin waves are dominated by the exchange over dipole interactions and are circularly polarized.

zero entropy, we need only consider the entropy of the thermal magnons. The change in entropy ΔS of the thermal magnons associated with the annihilation of one magnon and the corresponding creation of two magnons (increasing the internal energy of the thermal magnons by $\hbar\Omega$, the energy lost by the order parameter), is equal to $(\hbar\Omega - \delta\mu)/T$; the net creation of one magnon is favored over the inverse process when $\Delta S > 0$, resulting in the creation of thermal magnons, i.e. $\dot{n}|_{\rm sc} > 0$. Note that in the limit as $\tau \to 0$, according to Eq. (4.4) a nonzero value of n_c implies that $\hbar\Omega = \delta\mu$, or $\mu = 0$: in the strong coupling limit, then, we recover a noninteracting condensate wherein macroscopic occupation of the ground-state occurs when the chemical potential of the thermal cloud reaches the bottom of the magnon energy band.

The outflux (influx) of $+\hbar\mathbf{z}$ angular momentum from the thermal magnon cloud is absorbed by (emitted from) the order parameter when $\hbar\Omega > \delta\mu$ ($\hbar\Omega < \delta\mu$), contributing to the damping (antidamping) of the magnetization. The corresponding magnon scattering-induced rate of change of the order parameter polar angle $\dot{\theta}\Big|_{\rm sc} = -(\hbar\Omega - \delta\mu)(1/2\tau T)(\theta - \pi)$, Eq. (4.4), which is valid when $\theta \lesssim \pi$, can be written as a torque:

$$\hbar\dot{\mathbf{n}}|_{\rm sc} = \boldsymbol{\tau}_{\rm sc} = \alpha_{\rm sc}\mathbf{n} \times \tilde{\boldsymbol{\mu}} \times \mathbf{n}\,, \tag{4.6}$$

where

$$\alpha_{\rm sc} = \frac{\hbar}{2\tau T} \tag{4.7}$$

is the three-magnon scattering contribution to the damping, and $\tilde{\boldsymbol{\mu}} = \tilde{\mu}\mathbf{z} = (\delta\mu - \hbar\Omega)\mathbf{z}$ is the effective out-of-equilibrium internal "spin accumulation" of the thermal cloud (see Fig. 4.2). In equilibrium, ($\delta\mu = 0$) the creation of two magnons and annihilation of one increases the phase space of the system and therefore the entropy, resulting in the transfer of angular momentum from $\mathbf{n}$ and thus enhancing the damping.

Via the interfacial spin Seebeck effect, angular momentum in the $-\mathbf{n}$ direction is driven into or out of F by an interfacial temperature gradient and absorbed or emitted by the thermal cloud, a creating an out-of-equilibrium chemical potential $\delta\mu$. As a argued above, the spin accumulation $\boldsymbol{\mu} \propto \mathbf{n}$ does not affect magnetic dynamics, so for simplicity we assume that N is a poor spin sink ($\boldsymbol{\mu} = 0$), and the thermally driven spin current injected into F

from N is:

$$\mathbf{j}_{\parallel} = (-\mathbf{n})\left(g'\delta\mu - \mathcal{S}\delta T\right) , \tag{4.8}$$

where $\delta T = T' - T$ is the effective difference between the temperature T' in N and T in F. The quantities g' and $\mathcal{S}$ are the temperature-dependent interfacial magnon conductance and spin Seebeck coefficients, which are both proportional to $\alpha' = \Re[g_{\uparrow\downarrow}]/4\pi s d_F$, with $g_{\uparrow\downarrow}$ as the spin mixing conductance and d_F as the ferromagnet thickness. The resulting shift in the cloud chemical potential, then, is determined from the magnon density rate equation:

$$\hbar\dot{\sigma} = \partial_\mu \sigma \dot{\mu} = \mathbf{n}\cdot\mathbf{j}_{\parallel} - g_0\delta\mu + 2\alpha_{\rm sc}(\hbar\Omega - \delta\mu)\sigma_c \,, \tag{4.9}$$

where $g_0 \sim \alpha_0$ is the Gilbert damping conductance, describing the loss of magnons to intrinsic damping (parameterized by α_0), and $\sigma = n d_F$ is the magnon surface density. Coupled to, and which must be solved in conjunction with, Eq. (4.9) is the dynamics of the order parameter $\mathbf{n}$, which is dictated by the equation of motion:

$$(1 + \alpha_0 \mathbf{n}\times)\hbar\dot{\mathbf{n}} + \mathbf{n}\times\mathbf{H} = -\hbar(\alpha_i' + \alpha_r'\mathbf{n})\times\dot{\mathbf{n}} + \boldsymbol{\tau}_{\rm sc} \,, \tag{4.10}$$

where α_i and α_r are temperature-dependent quantities, respectively proportional to the imaginary and real parts of $g_{\uparrow\downarrow}/4\pi s d_F$. In most cases, $\alpha_i' \ll \alpha_r'$; we shall therefore neglect α_i' and abbreviate $\alpha' = \alpha_r'$. Eq. (4.10) (or more precisely, the last term on the right-hand side) is understood to be valid for near equilibrium ($\mathbf{n} = -\mathbf{z}$), where it may be transformed into a rate equation for n_c, which up to linear order in α_0, α' and $\alpha_{\rm sc}$ is:

$$\hbar\dot{\sigma}_c = -2(\alpha_0 + \alpha')\hbar\omega\sigma_c - 2\alpha_{\rm sc}(\hbar\Omega - \delta\mu)\sigma_c \,, \tag{4.11}$$

where $\sigma_c = n_c d_F$ is the condensate surface density and $\hbar\omega = \hbar\Omega_{\rm p} + K n_c/s$. Solving Eq. (4.9) in steady state for $\delta\mu$ and inserting into Eq. (3.17), one finds that for $\delta T \leq \delta T_{\rm crit} \equiv \hbar\Omega(\alpha_0 + \alpha' + \alpha_{\rm sc})(g + g')/\mathcal{S}\alpha_{\rm sc}$, $n_c = 0$ is a stable fixed point with $\delta\mu = \delta T\mathcal{S}/(g_0 + g')$, around which Eq. (4.11) may be linearized: $\hbar\dot{\sigma}_c = -2\alpha\hbar\Omega\sigma_c$, with

$$\alpha(\delta T) = \alpha_0 + \alpha' + \alpha_{\rm sc}\left(1 - \frac{\mathcal{S}\delta T/\hbar\Omega}{g_0 + g'}\right) \tag{4.12}$$

as the effective Gilbert damping, which may be measured directly via ferromagnetic resonance (FMR) linewidth. When $\alpha < 0$, the pole $\mathbf{n} = -\mathbf{z}$ is destabilized.

Let us now consider stability in $H-K$ space generally. Although above we considered the equilibrium position to be oriented in the $-\mathbf{z}$ direction, the pole $\mathbf{n} = +\mathbf{z}$ (with magnetization antiparallel to the magnetic field) may also correspond to an equilibrium in the absence of a thermal bias, provided that the gap $\hbar\tilde{\Omega} = -H - K$ is positive. The corresponding damping of $\mathbf{n}$ near $+\mathbf{z}$ is described by $\tilde{\alpha}$, which is given by Eq. (4.12) with $\hbar\Omega$ replaced by $\hbar\tilde{\Omega}$ (defining the critical temperature $\delta\tilde{T}_{\rm crit}$ for which $\tilde{\alpha}$ changes sign) and $\alpha_{\rm sc}$ replaced by $\tilde{\alpha}_{\rm sc}$, obtained by using $\mu_e = \hbar\tilde{\Omega}$ in Eq (6.12). Provided both $\hbar\Omega$ and $\hbar\tilde{\Omega}$ are both positive, the magnet is bistable when $\alpha_{\rm sc}$ and $\tilde{\alpha}_{\rm sc}$ are positive, and stable in the $-\mathbf{z}$ ($+\mathbf{z}$) direction when $\alpha_{\rm sc} > 0$, $\tilde{\alpha}_{\rm sc} < 0$ ($\alpha_{\rm sc} < 0$, $\tilde{\alpha}_{\rm sc} > 0$). When both poles are antidamped, the magnet is precessing in a dynamic mode (DM), the amplitude θ of which may be obtained near the pole $\mathbf{n} = -\mathbf{z}$ ($\theta \approx \pi$) by solving Eqs. (3.17) and (4.9) or near the pole $\mathbf{n} = \mathbf{z}$ ($\theta \approx 0$) by solving a corresponding set of coupled equations. (See Fig. 4.3).

The scattering time, Eq. (6.12), is obtained by expanding around a stable magnetic equilibrium near the broken symmetry axis z, defined by the magnetic field and anisotropy. When the gap $\hbar\Omega$ ($\hbar\tilde{\Omega}$) is negative, the pole $-\mathbf{z}$ ($+\mathbf{z}$) is unstable in the absence of a (e.g. thermal) torque. A negative gap, which enters Eq. (6.12) through the equilibrium distribution function f_e, results in a diverging τ ($\tilde{\tau}$), signifying that $-\mathbf{z}$ ($+\mathbf{z}$) is no longer an appropriate choice for an expansion. It is, however, possible that a torque resulting from a sufficiently large and negative δT may stabilize the order parameter dynamics. In this case low energy magnons, which would otherwise exponentially grow in the presence of a negative gap, are able to shed their angular momentum into other modes and ultimately the normal metal via spin Seebeck driven diffusion; three-magnon scattering then partially replenishes the loss of magnons, resulting in a damping-like torque that counteracts the Gilbert damping and spin-pumping. Such a scenario (corresponding to the grey regions in Fig. 4.3) would have to be approached by solving the full rate equation for the distribution function $f_{\mathbf{k}}$ for each mode, including magnon-magnon and/or magnon-bath interactions, and will not be considered here.

4.2 Spin Valve

Let us now consider a spin valve, composed of two ferromagnet layers (one free and one fixed) separated by a normal metal spacer, as depicted in Fig. 4.4. In contrast to the single layer, the symmetry breaking required to realize a thermal spin torque in the free layer is now provided by the fixed layer. In a conducting spin valve, angular momentum (and charge) inside the ferromagnets are primarily transported by electrons; provided that each ferromagnetic layer is thicker than the transverse spin coherence length but thinner than the exchange length so that the magnetization is monodomain, the spin current is carried by spin-majority and -minority electrons parallel and antiparallel, respectively, to the spin density. Electrical or thermal biasing then generates a spin current across the structure, which may exert a torque on the free layer. Because we are interested in pure spin transport in the presence of the temperature gradient, let us suppose now that the ferromagnet metallic layers are replaced by magnetic insulators. In this case, spin is transported in each magnetic layer by magnons, which carry angular momentum $\hbar$ opposite to the spin density. Under a thermal bias, a pure spin current flows across the structure, resulting in a torque on the free layer.

In contrast to conducting spin valves where, in steady state, every charge entering one end of the heterostructure is balanced by an equal charge exiting the opposite side, here angular momentum is not conserved. Inside the insulating ferromagnets, angular momentum is lost to Gilbert damping; in the normal metal, spin-orbit effects relax the spin accumulation. In order to maximize the efficiency of spin transport across the structure, let us assume that the thickness d_F of each the (monodomain) ferromagnet layers is much shorter than the thermal magnon diffusion length but longer than the transverse spin coherence length. Likewise, we take the normal metal spacer thickness d_s to be much shorter than the spin diffusion length, which may be accomplished, for example, by using a poor spin sink such as Cu. In contrast, let us for simplicity assume that normal metal leads are attached to the ferromagnets and are excellent spin-sinks, such as Pt, so that no spin accumulates inside them. We will suppose that the five layer structure (N lead/free F/N spacer/fixed F/N lead)

is structurally symmetric, with the two N leads and the two F layers composed of identical materials and dimensions. (See Fig. 4.4).

Now, consider a thermal gradient applied transversely across the structure. Spin is transported in each ferromagnetic layer by magnons, resulting in an instantaneous thermally driven spin accumulation $\boldsymbol{\mu}$ that builds in the normal metal spacer. By symmetry, when the magnetic moments of the two ferromagnetic layers are aligned, $\boldsymbol{\mu}$ vanishes; when they are antiparallel, $\boldsymbol{\mu}$ builds along the common axis. When the two magnetic layers are misaligned, the nonequilibrium driven spin accumulation exerts a torque on the free layer. In general, the magnetic dynamics of the free layer are governed by:

$$(1 + \alpha_0 \mathbf{n}\times)\hbar\dot{\mathbf{n}} + \mathbf{n} \times \mathbf{H} = -\hbar(\alpha_l' + \alpha_s')\mathbf{n} \times \dot{\mathbf{n}} + \alpha_s' \mathbf{n} \times \boldsymbol{\mu} \times \mathbf{n} \tag{4.13}$$

where $\mathbf{n}$ is the free layer spin density direction and α_0 is the intrinsic Gilbert damping. Here, α_l' and α_s' are respectively the real parts of $g_{\uparrow\downarrow}^{(l)}/4\pi s d_F$ and $g_{\uparrow\downarrow}^{(s)}/4\pi s d_F$, corresponding to the damping of the ferromagnetic layers provided by the leads (l) and spacer (s). The total magnetic field $\mathbf{H} = (H - n_z K)\mathbf{z}$ is comprised of the applied field H and the anisotropy field $-Kn_z$, which is easy plane when $K > 0$. In the absence of H and $\boldsymbol{\mu}$, easy-axis ($K < 0$) anisotropy defines the degenerate equilibria of the free layer: $\mathbf{n} = \pm\mathbf{z}$. By assumption, the spin density in the fixed layer is pinned (e.g. by exchange biasing) in the $-\mathbf{z}$ direction.

Before proceeding, some comments on length and timescales are in order. First, provided that the thermal correlation length provided by magnon-magnon interactions and/or magnon-thermal bath (e.g. a substrate on which the heterostructure sits) coupling is much shorter than the thickness of each layer, the local magnon temperature in each section is well defined. If the effective interfacial change δT (defined over this thermal coherence length on either side of the boundary) is larger than the change in temperature across each layer, we may treat the temperature as being uniform in each section. We will approximate the temperature in each layer as increasing in steps of δT from layer to layer, with the left lead at temperature T, the free layer at $T + \delta T$, etc, which requires an efficient coupling to a thermal bath. (A proper treatment of the effective temperature in each section requires a detailed treatment of how magnon energy is dissipated into other degrees of freedom, e.g.

the substrate, phonons, etc., and is unnecessary for a proof of principle calculation). Second, let us suppose that the thermalization timescale for magnons is much shorter than the magnon dwell time in the ferromagnets, so that, as above, magnons are described by a Bose-Einstein profile well-defined chemical potential μ. Third, as we shall suppose, if interfacial electron-magnon spin transport processes are much faster than the precessional dynamics of the monodomain free layer, a separation of timescales becomes possible. The "fast" magnon accumulation in each of the ferromagnetic layers and the corresponding spin accumulation $\boldsymbol{\mu}$ in the spacer may then be obtained for a fixed orientation of $\mathbf{n}$; in the steady state for magnon transport, the expression for spacer spin accumulation $\boldsymbol{\mu}(\mathbf{n})$, thus obtained, is inserted into Eq. (4.13) to obtain the "slow" precessional dynamics of $\mathbf{n}$.

Following this procedure, let us first turn to the fast dynamics of magnon transport at a fixed orientation of $\mathbf{n}$. The steady state magnon spin current density j_i into ferromagnetic layer F_i (with $i = 1$ as the free layer and $i = 2$ the fixed layer) is

$$j_i = j_{l\to i} + j_{s\to i} - j_0 = 0\,, \tag{4.14}$$

where $j_{l\to i} = -g_l\mu_i + \mathcal{S}_l\delta T$ is the current entering F_i from the lead, $j_{s\to i} = -g_s\mu_i - \mathcal{S}_s\delta T$ as the spin current entering F_i from the spacer, and $j_0 = g_0\mu_i$ the spin current lost to Gilbert damping of thermal magnons. In steady state the rate of change of the normal metal spin density $\boldsymbol{\rho} = D_F\boldsymbol{\mu}(\hbar/2)$ (with D_F as the Fermi surface density of states) vanishes:

$$\dot{\boldsymbol{\rho}} d_s = (-\mathbf{n})j_{1\to s} + \mathbf{z}j_{2\to s} = 0\,, \tag{4.15}$$

with $j_{i\to s} = -j_{s\to i}$. The coupled Eqs. (6.16) and (4.15) may then be solved to obtain the magnon accumulations μ_1 and μ_2 in the free and fixed layers, together with the two components of the spin accumulation $\boldsymbol{\mu} = \mu_z\mathbf{z} - \mu_\perp\mathbf{z}\times\mathbf{z}\times\mathbf{n}$, which lie in the plane of $\mathbf{n}-\mathbf{z}$ plane. Here, μ_z and $\mu_\perp$ are functions of both the orientation of $\mathbf{n}$ and the thermal bias δT.

Inserting the expression for $\boldsymbol{\mu}$ thus obtained into Eq. (4.13), we may characterize the steady state slow dynamics of $\mathbf{n}(t)$ by expanding the resulting equation of motion around the two poles $\mathbf{n} = \pm\mathbf{z}$. Near the parallel orientation ($\mathbf{n} = -\mathbf{z}$), the field-like torque $\boldsymbol{\tau} = -\alpha_s'\mathbf{n}\times\mathbf{n}\times\boldsymbol{\mu}$ in Eq. (4.13) is:

$$\boldsymbol{\tau} \approx \boldsymbol{\tau}_{\mathrm{p}} = -\alpha_{\mathrm{p}}\delta T\mathbf{n}\times\mathbf{n}\times\mathbf{z} \tag{4.16}$$

where

$$\alpha_{\rm p} = \alpha_s'(\mu_z(\pi) + \mu_\perp(\pi))/\delta T = \frac{\alpha_s'}{2}\left(\frac{(g_g+g_l)\mathcal{S}_s + g_s\mathcal{S}_l}{2g_s(g_s+g_g+g_l)}\right), \tag{4.17}$$

with $\mu_z(\pi) = 0$ by symmetry. Expanding Eq. (4.13) around $\theta = \pi$, one obtains an equation of motion $\hbar\dot{\theta} = -\epsilon_p(\theta - \pi)$, with $\epsilon_p = (\alpha' + \alpha_0)(H - K) - \alpha_p\delta T$ and $\alpha' = \alpha_l' + \alpha_s'$. When ϵ_p is positive, the parallel configuration is stable. Upon the application of an adequately large temperature gradient in one direction, the spin torque μ_p may become sufficiently positive that ϵ_p changes sign, the parallel configuration is destabilized. Meanwhile, near the antiparallel configuration ($\mathbf{n} = \mathbf{z}$), the thermally driven spin torque is:

$$\boldsymbol{\tau} \approx \boldsymbol{\tau}_{\rm ap} = -\alpha_{\rm ap}\delta T\mathbf{n}\times\mathbf{n}\times\mathbf{z} \tag{4.18}$$

where

$$\alpha_{\rm ap} = \alpha_s'\frac{\mu_z(0) - \mu_\perp(0)}{\delta T} = \frac{\alpha_s'}{2}\left(\frac{\mathcal{S}_s}{g_s} + \frac{\mathcal{S}_l}{g_g+g_l}\right) \tag{4.19}$$

The dynamics near the pole $\mathbf{n} = \mathbf{z}$ can be expanded $\hbar\dot{\theta} = -\epsilon_{\rm ap}\theta$, where $\epsilon_{\rm ap} = -(\alpha' + \alpha_0)(H + K) + \alpha_{\rm ap}\delta T$; similarly to the parallel configuration, beyond a sufficient temperature bias, $\epsilon_{\rm ap}$ changes sign, and the spin density is antidamped.

In $H - K - \delta T$ space, the planes $\epsilon_{\rm p} = 0$ and $\epsilon_{\rm ap} = 0$ define the phases of the spin valve. When both $\epsilon_{\rm p}$ and $\epsilon_{\rm ap}$ are positive, the free layer is bistable. When $\epsilon_{\rm p}$ is positive (negative) and $\epsilon_{\rm ap}$ is negative (positive), the free layer is stabilized in the $-\mathbf{z}$ ($+\mathbf{z}$ direction). Last, when both $\epsilon_{\rm p}$ and $\epsilon_{\rm ap}$ are negative, the dynamics stabilize to a limit cycle with $0 < \theta < \pi$, i.e. the magnet is a spin-torque oscillator (STO).

The interfacial conductances and spin Seebeck coefficients are generally dependent on the magnon gap $\hbar\Omega$, which depend on the orientation of $\mathbf{n}$. At high temperatures, $\hbar\Omega \ll T$, however, the gap dependence is weak, provided of course that the magnon gap is positive. For some regions of $H - K$ space and orientations of $\mathbf{n}$, however, the gap may become negative, and the quasi-equilibrium Bose-Einstein profiles from which the magnon conductances and spin Seebeck coefficients are obtained are, strictly speaking, no longer valid. However, in contrast to the scattering time τ in Eq. (6.12) for three-magnon-processes entering in our discussion of a single layer, which is nonanalytic as $\hbar\Omega \to 0$, the nonequilibrium distortion at the bottom of the thermal cloud distribution resulting from the antidamping of low energy

magnons ($\epsilon_{\mathbf{k}} < -\hbar\Omega$) gives only a small correction to the interfacial conductances and spin Seebeck coefficients, which may therefore be treated as constant at high temperatures. The resulting phase diagram is show in Fig. 4.5.

4.3 Conclusion

The thermally driven spin torques, Eqs. (4.6), (4.16) and (4.18), represent an interplay of several distinct physical effects: the spin Seebeck effect, magnon-magnon scattering, and spin-transfer torque. Below the critical thermal bias for each structure and configuration, the spin density is relaxed to an equilibrium orientation, with a damping enhanced or diminished depending on the sign of the applied thermal bias, δT, which manifests in the ferromagnetic resonance signature. The effect is maximized when the interfacial processes ($\propto \alpha'$) are stronger than the Gilbert damping ($\propto \alpha_0$). In the optimistic limit $\alpha' \gg \alpha_0$, thermal spin torques become comparable to the total damping $\sim \alpha_{\rm tot}$ (which can be obtained by a zero thermal bias FMR measurement) for a bias $\delta T \sim \hbar\Omega(\alpha_{\rm tot}/\alpha_{\rm sc})$ (for a single F layer) and $\delta T \sim \hbar\Omega(\alpha_{tot}/\alpha_s)$ (for a spin valve), and magnetization switching becomes a possibility. In the pessimistic scenario, $\alpha' \ll \alpha_0$, the efficiency of spin injection by a temperature gradient is reduced by a factor of α'/α_0 compared to the optimistic case, requiring a temperature gradient larger by a factor of α_0/α' to induce magnetic dynamics.

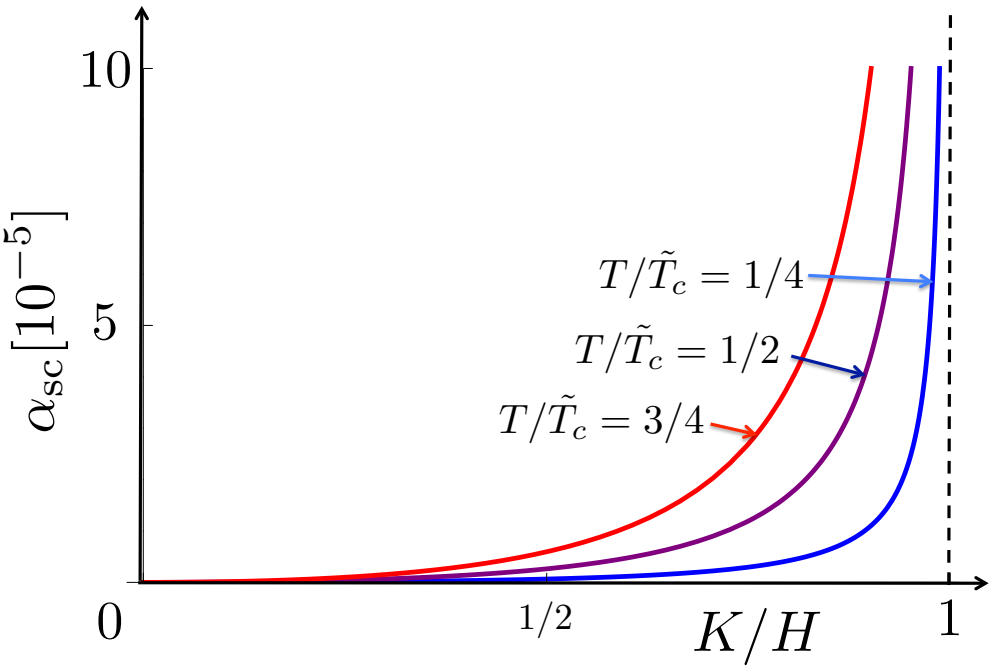

Figure 4.2: Effective three-magnon damping parameter $\alpha_{\rm sc}$, Eq. (4.7), obtained by numerically integrating Eq. (6.12) for a Curie temperature $\tilde{T}_c = s^{2/3}A = 200\hbar\Omega$.

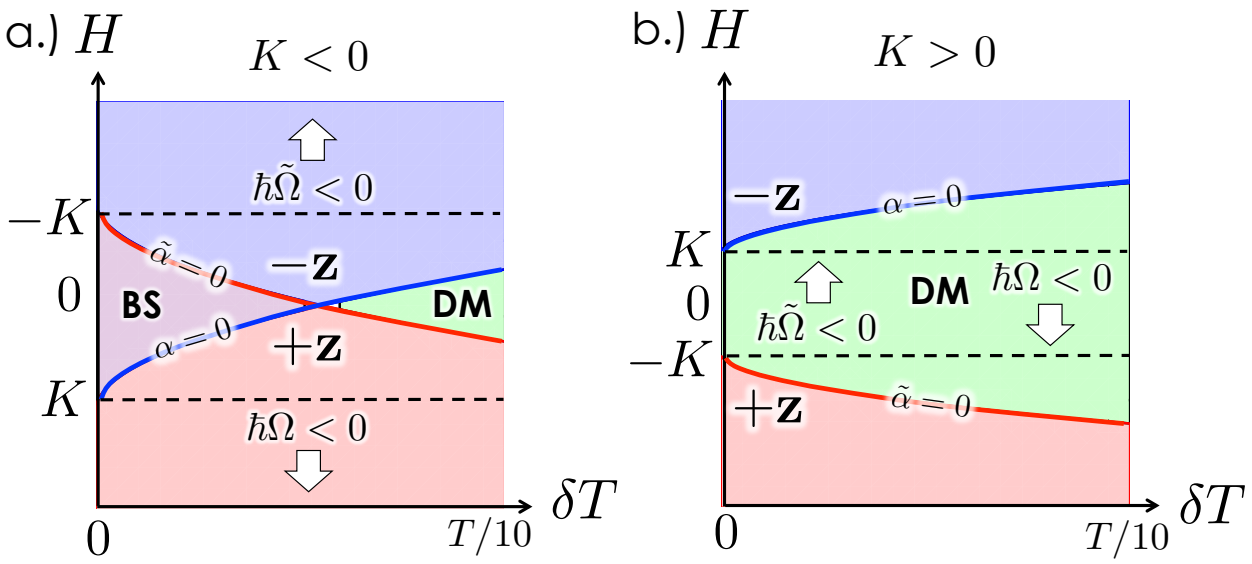

Figure 4.3: Phase diagram for F in the presence of a thermal spin-torque, obtained from Eq. (4.12) and the corresponding equation for $\tilde{\alpha}$ for a.) easy axis anisotropy ($K = -T/400$) and b.) easy plane anisotropy ($K = +T/400$), showing bistability (BS) and dynamical modes (DM). Here $T/T_c = 1/2$, and $\alpha_0 = \alpha' = 10^{-5}$. A negative gap for a given pole corresponds to a divergence in τ. When $\delta T > 0$, the thermal spin-torque for a pole with negative gap further destabilizes it. However, when δT is negative, thermal spin-torque may stabilize $\mathbf{n}$, requiring a nonequilibrium treatment; for this reason, the regions $\delta T < 0$ are omitted.

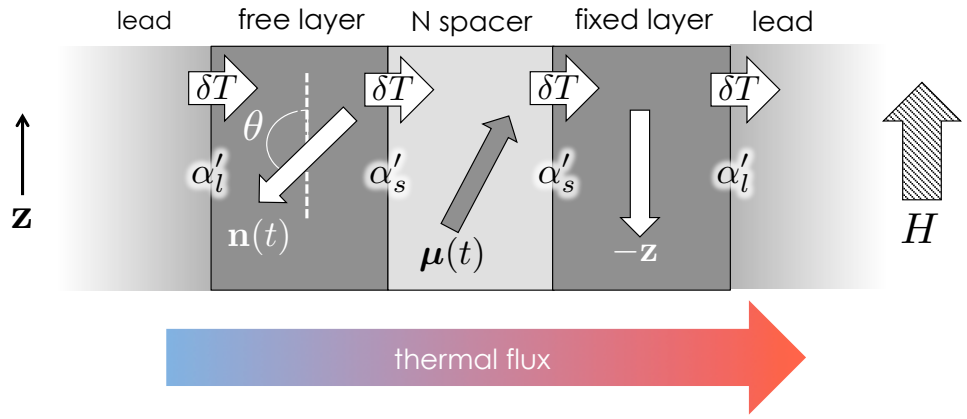

Figure 4.4: Thermally biased spin valve. A heat flux drives spin accumulation $\boldsymbol{\mu}$ (in the plane defined by $\mathbf{n}$ and $\mathbf{z}$) into the normal metal spacer. When free layer spin density $\tilde{s}\mathbf{n}$ is misaligned with the $\mathbf{z}$ axis, $\boldsymbol{\mu}$ is no longer collinear with $\mathbf{n}$, and the component of $\boldsymbol{\mu}$ perpendicular to $\mathbf{n}$ provides a torque.

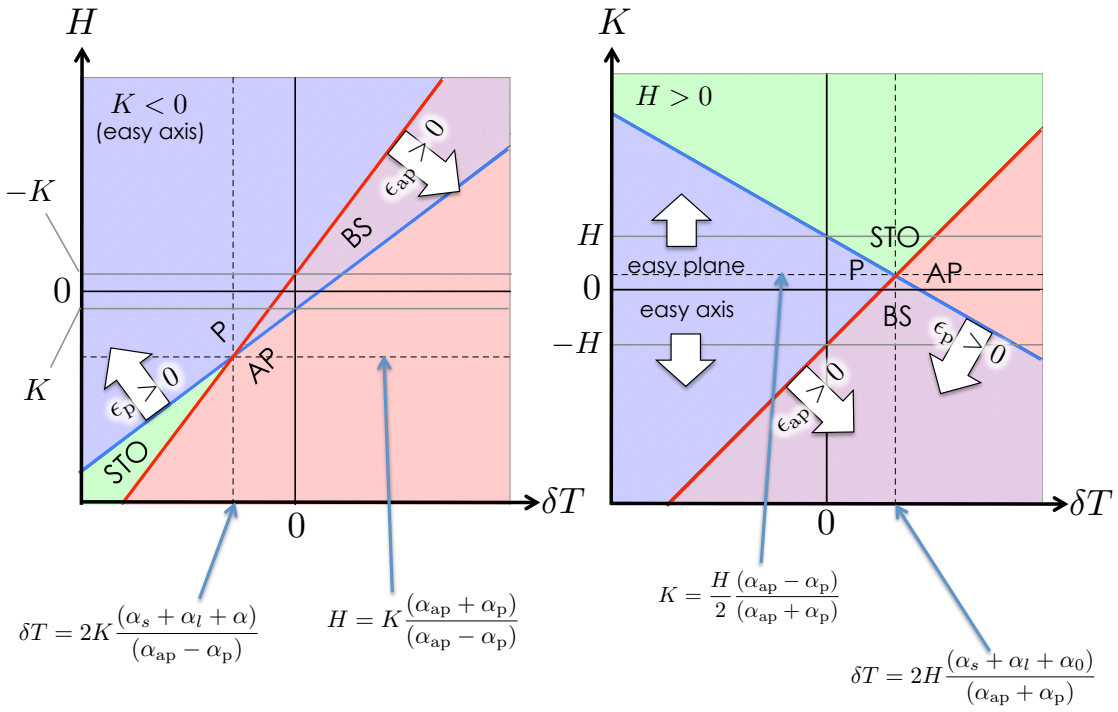

Figure 4.5: Phase diagrams for the free layer in the spin valve for constant $K(< 0)$ and constant $H(> 0)$, showing parallel (P), antiparallel (AP), bistable (BS) and spin-torque oscillator (STO) phases. When the anisotropy is easy plane and the magnetic field H is below the coercivity field K, at zero bias, the free layer is a zero-frequency spin-torque oscillator with $\mathbf{n}$ entirely in the xy plane (xy magnet).

CHAPTER 5

Microwave Response of a Magnetic Single-Electron Transistor

Recent work has demonstrated both theoretically [TMX08, XBB08] and experimentally [MCF08] that a dc electric current may be pumped through a ferromagnet|insulator|ferromagnet (F|I|F) tunnel junction by pinning one ferromagnet and precessing the other at frequency ω. This is analogous to spin pumping by a precessing ferromagnet into adjacent normal metals [TBB02a], which can subsequently induce a voltage across the ferromagnet by spin-flip processes. [WBW06] In these cases, the voltage generated by ferromagnetic dynamics is substantially smaller than $\hbar\omega$ (the quantum of energy supplied by the microwave source) in the absence of spin-spin or electron-electron correlation effects.

In this chapter, we study the interplay of ferromagnetic pumping and Coulomb blockade in single-electron transistors, which suggests for their use as sensitive detectors of microwave irradiation. Our proposal complements and extends into the magnetic realm the established techniques utilizing single-electron transistors, such as electrostatic sensing [ZFY00] and mechanical electron shuttling [SB04].

5.1 Microwave Pumping

We consider charge pumping by a microwave-driven ferromagnetic dot with a classically large spin resonantly precessing at frequency ω (see Fig. 5.1). The zero-dimensional nature of the quantum dot makes the electron-electron interactions relevant. Unlike static theoretical arrangements involving voltage-driven transport between an interacting quantum dot and magnetic leads, [WKM05] ours exhibits steady charge pumping by the magnetization preces-

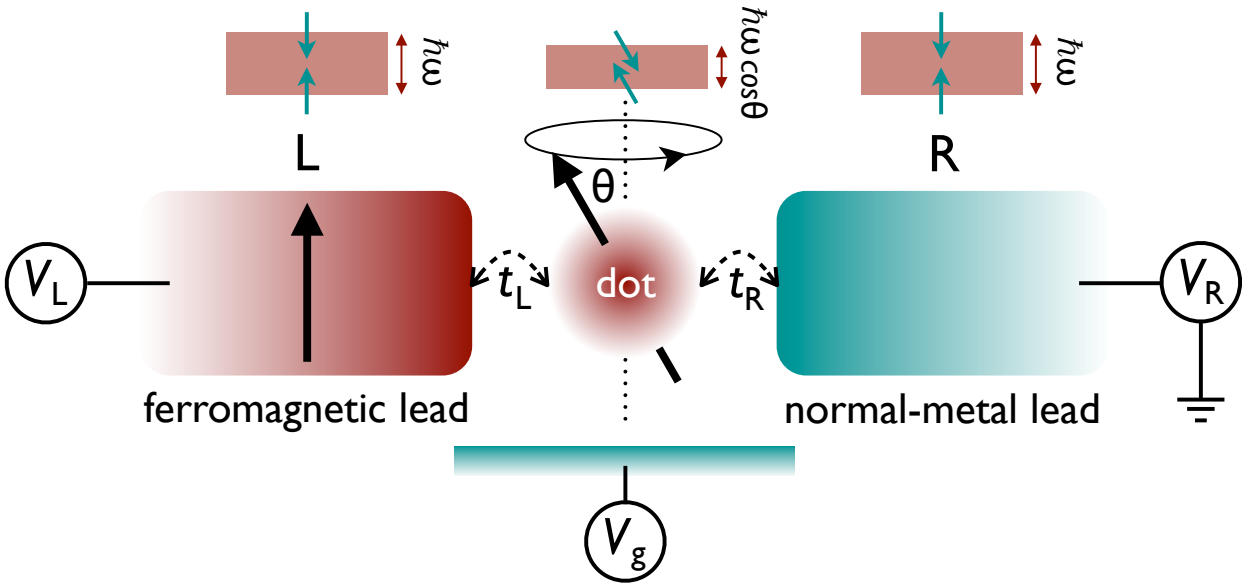

Figure 5.1: (Color online) Schematics of the precessing magnetic dot coupled to two large reservoirs and the effective spin splittings of the chemical potentials associated with the fictitious Zeeman field of $\hbar\omega$, according to Eqs. (5.2) and (5.3), in the rotating frame of reference. The long black arrows show magnetization directions.

sion. Quantum tunneling of the large magnetic moment is assumed to be strongly suppressed by the dissipative environment of the phonon continuum and/or electronic excitations associated with metallic regions; the dynamics of the dot are therefore dominated by classical precession, in contrast to the proposed macroscopic quantum tunneling of the dot's magnetic moment in Ref. [HOT09]. Traditional parametric spin and charge pumping by varying tunneling amplitudes and energy-level structure [Bro98b] in a strongly-interacting normal quantum dot contacted by magnetic reservoirs was considered recently in Refs. [SGK08].

In open circuits, the charge pumping induces an electrostatic buildup between the right and left leads, which we represent here as the bias $V_0 \equiv V_R - V_L$ that yields $I = 0$. (We will henceforth consider the right reservoir to be grounded, i.e., $V_R = 0$.) Without Coulomb blockade, this bias is linear in pumping frequency:[TMX08]

$$V_0 = \frac{\hbar\omega}{2e} \frac{P \sin^2\theta}{1 + P^2 \cos\theta} , \tag{5.1}$$

where $P = (D_\uparrow - D_\downarrow)/(D_\uparrow + D_\downarrow)$ is the polarization of the dot and ferromagnetic lead in terms

of the spin-dependent density of states D_s ($-e$ is the electron charge). The nominal *charge-pumping efficiency* $\mathcal{E} \equiv eV_0/\hbar\omega$ [as well as the differential efficiency $\mathcal{E}_{\rm diff} \equiv (e/\hbar)\partial V_0/\partial\omega$] is independent of the microwave frequency and small, vanishing as θ^2 when the precession angle goes to zero. To be specific, the dot is taken to be made of the same material as the ferromagnetic lead.

We demonstrate here that electron-electron interaction on the dot gives rise to a highly nonlinear response $V_0(\omega)$, which is also robust at small θ. The efficiency $\mathcal{E}$ of this response is greatly increased (although still less than one), while the differential efficiency $\mathcal{E}_{\rm diff}$ can become extremely large when $\hbar\omega$ is close to the Coulomb-blockade energy gap. This frequency (or, equivalently, Coulomb gap) sensitivity of $\mathcal{E}_{\rm diff}$ may pave way for microwave spectral analyzer and magnetoelectronic logic applications.

Central to our discussion is the observation that the precessing dot creates a fictitious spin-dependent voltage; this bias, in turn, drives electron transport via hopping onto and off of the dot from two metallic leads, one nonmagnetic ("right" lead) and one with spin-exchange splitting Δ in the z direction ("left" lead) (cf. Fig. 5.1). Supposing the dot is steadily precessing clockwise around the z axis at a constant angle θ, the total single-electron Hamiltonian (without including electron interactions on the dot) can be written as $\hat{H}(t) = \mathbf{p}^2/2m + V(\mathbf{r}) - \Delta\mathbf{m}(\mathbf{r},t)\cdot\hat{\boldsymbol{\sigma}}/2$, where $\hat{\boldsymbol{\sigma}}$ is a vector of Pauli matrices and $\mathbf{m}$ is the majority spin direction. The first two terms determine the tunneling Hamiltonian and energy spectra of the leads and dot, while $\mathbf{m}(\mathbf{r},t)$ is given by $(0,0,1)$ in the left lead, $(\sin\theta\cos(\omega t), \sin\theta\sin(\omega t), \cos\theta)$ in the dot, and is set to zero everywhere else. By going into the rotating frame of reference, the precession of the dot is formally eliminated, at the expense of transforming the Hamiltonian as follows:[TB05]

$$\hat{H}(t) \to \hat{R}^\dagger \hat{H} \hat{R} - i\hbar\hat{R}^\dagger\partial_t\hat{R} = \hat{H}(t=0) - (\hbar\omega/2)\hat{\sigma}_z, \tag{5.2}$$

where $\hat{R} = e^{-i\omega t\hat{\sigma}_z/2}$ is a rotation operator that transforms out dot precession while leaving the spin-independent energy terms (including Coulomb interaction) unaffected. Whereas, according to Eq. (5.2), the lead Hamiltonians pick up a fictitious spin-dependent potential

$-(\hbar\omega/2)\hat{\sigma}_z$, the dot Hamiltonian can be simplified in the rotating frame to

$$\hat{H}_{\rm dot}(t) \to \hat{H}_{\rm dot}(0) - (\hbar\omega/2)\hat{\sigma}_{\parallel}\cos\theta\,, \tag{5.3}$$

where $\hat{\sigma}_{\parallel} = \hat{\boldsymbol{\sigma}} \cdot \mathbf{m}_{\rm dot}(0)$ is the spin operator in the direction of the $t = 0$ dot magnetization $\mathbf{m}_{\rm dot}$, and we have disregarded the normal component of the fictitious field in the dot, which is valid in conventional ferromagnets with $\hbar\omega \ll \Delta$. The extra "inertia" terms in Eqs. (5.2) and (5.3) shift energies of the spin-up (down) electrons by $\mp\hbar\omega/2$ in the leads and $\mp(\hbar\omega/2)\cos\theta$ in the dot, thus creating an effective spin-dependent bias between leads and dot that can drive transport currents. Assuming strong spin relaxation in the dot, on the scale of the electron injection rate, no spin accumulation is built up there.

5.2 Sequential Tunneling Regime

In the sequential tunneling regime, the electric current flowing from, say, the left (ferromagnetic) lead to the metallic dot is given by a sum over the possible number of electrons N occupying the dot:[NB09] $I_L = -e\sum_N P(N)\left(\Gamma^L_{N\to N+1} - \Gamma^L_{N\to N-1}\right)$, where $\Gamma^L_{N\to N\pm1}$ is the tunneling rate for one electron to hop from (to) the ferromagnet to (from) the N-occupied dot and $P(N)$ is the probability that N excess electrons are contained on the dot at a given moment of time. Coulomb blockade effects are captured by introducing the electrostatic energy E_N associated with N electrons occupying the dot, where $E_N = E_c N(N-1)/2 - eV_g N$ and V_g is the gate voltage (renormalized by various mutual capacitances). The energy for adding a single electron to the N-electron dot is $\mu_N \equiv E_{N+1} - E_N = E_c N - eV_g$. Setting the equilibrium chemical potential of the leads to zero, the dot operates at the characteristic electron number $N \sim eV_g/E_c$. The energy scale E_c is realistically of the order of 10 meV, while the driving energy $\hbar\omega$ is typically not more than a fraction of an meV. This requires going to Kelvin-range temperatures if one is to completely disregard thermal effects. We suppose the gate voltage V_g on the dot can be tuned so that the gap for adding one excess electron is within the range of the driving frequency $\hbar\omega$, but higher occupancies are increasingly less likely due to a finite E_c.

Let us discuss a sufficiently large E_c, such that only the transitions $N \rightleftharpoons N+1$ between the dot and the leads are relevant. The dot electrons occupy parallel and antiparallel spin states that adiabatically evolve with the precessing magnetization. Both leads are also considered to be equilibrated in the lab frame of reference at the respective spin-independent voltages, so the tunneling rate for each is a sum over four channels for two spin projections of dot electrons hopping to (from) static up and down states in the leads:

$$\Gamma^{(l)}_{N\rightleftharpoons N+1} = k_B T \left|t_l\right|^2 \sum_{s,s'} D^{(l)}_s D_{s'} \left|\langle s|s'\rangle_\theta\right|^2 \times f\left(\pm\left[\mu_N + eV_l + (\hbar\omega/2)(s - s'\cos\theta)\right]\right). \tag{5.4}$$

Here, $l = L, R$ labels the left/right leads and $s = \uparrow, \downarrow$ (or $\pm$), spin projection along the magnetization direction (or z axis for the normal lead), while $D^{(L)}_s = D_s$, $D^{(R)}_s = D$ are the ferromagnetic and normal-metal densities of states, respectively. We consider the tunnel amplitudes t_L and t_R to be energy independent. The spin-space matrix elements squared are given by: $\left|\langle\uparrow \mid \uparrow\rangle_\theta\right|^2 = \left|\langle\downarrow \mid \downarrow\rangle_\theta\right|^2 = \cos^2(\theta/2)$ and $\left|\langle\uparrow \mid \downarrow\rangle_\theta\right|^2 = \sin^2(\theta/2)$. The temperature-dependent weighting function in Eq. (5.4) is $f(\epsilon) = (\epsilon/k_B T)(e^{\epsilon/k_B T} - 1)^{-1}$.

Let us count N with respect to a reference state, such that for $(k_B T, \hbar\omega) \ll E_c$ the dot switches between $N = 0$ and $N = 1$ occupancies, henceforth denoting $\mu \equiv E_1 - E_0$. The total steady-state electric current, $I = I_L = I_R$, is then:

$$I = -e\frac{\Gamma^L_{0\to1}\Gamma^R_{1\to0} - \Gamma^L_{1\to0}\Gamma^R_{0\to1}}{\Gamma^L_{0\to1} + \Gamma^R_{0\to1} + \Gamma^L_{1\to0} + \Gamma^R_{1\to0}}. \tag{5.5}$$

The current as a function of V_L (with $V_R = 0$) and ω is graphed in an inset of Fig. 5.2. Under the transformation $\mu_N \to -\mu_N$, $V_R \to -V_R$, $V_L \to -V_L$, and $\omega \to -\omega$, the electric current (5.5) changes sign, reflecting the electron-hole symmetry in our model. We can therefore choose to consider only positive ω. According to Eq. (5.5), the condition for zero current is

$$\Gamma^L_{0\to1}\Gamma^R_{1\to0} = \Gamma^L_{1\to0}\Gamma^R_{0\to1}. \tag{5.6}$$

The microwave-induced potential V_0 is thus independent of D, t_L, or t_R and depends only on ω, P, μ, and T.

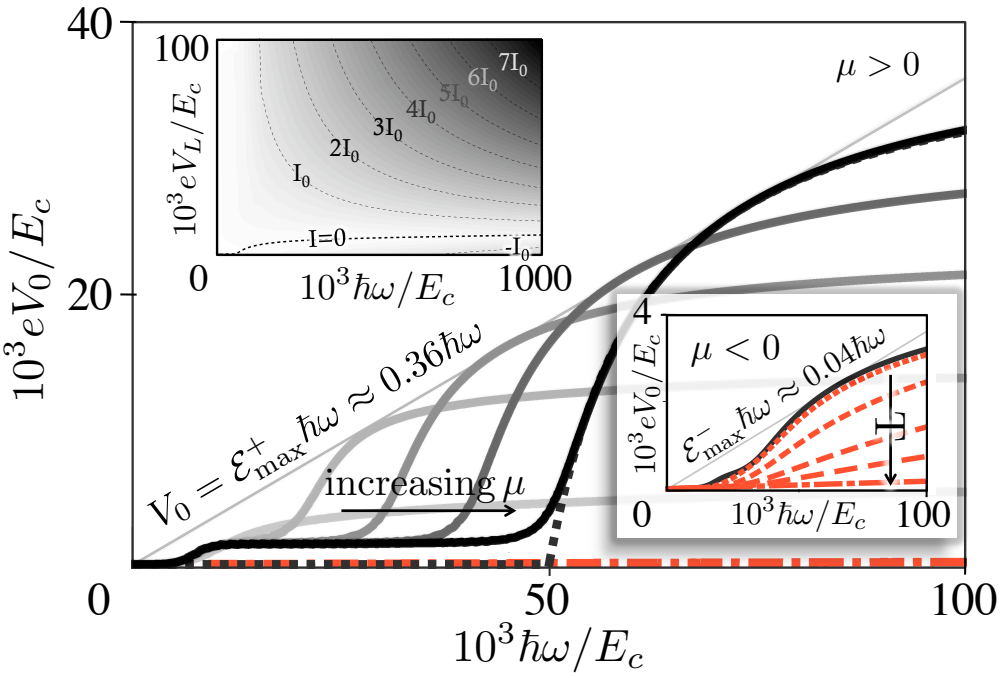

Figure 5.2: Low-frequency $I = 0$ ($\hbar\omega \ll E_c$) numerical curves for $\mu > 0$, $\theta = 5°$, $P = 2/3$, and $k_BT/E_c = 10^{-3}$. Here, the increasingly darker gray lines represent $\mu/E_c = (1, 2, 3, 4, 5) \times 10^{-2}$, respectively, while the dotted-dashed red line corresponds to zero Coulomb blockade, Eq. (5.1). The $T = 0$ small-angle analytic solution, Eq. (5.8), is shown as a dotted black line superimposed on the corresponding finite-temperature curve in black. Upper inset: High-frequency relief plot of current density for the same parameters as the solid black curve in the main panel, with $t_L = t_R = t$ and $I_0 = 0.02\, ek_BTD^2|t|^2$. Lower inset: thermal effects for $\mu/E_c = -3 \times 10^{-2}$. The black curve corresponds to $k_BT/E_c = 10^{-3}$ and the increasingly long red dashed lines to $k_BT/E_c = (5, 6, 7, 8) \times 10^{-3}/2$, respectively. The dotted-dashed red line illustrates the zero Coulomb-blockade case, as in the main panel.

Let us now turn to the zero-temperature properties, which can be found analytically. First, at arbitrary μ in the limit $\theta \to \pi/2$,

$$eV_0 = P\frac{\mu^2 - (\hbar\omega/2)^2}{P\mu - \hbar\omega/2}\Theta\left(\hbar\omega/2 - |\mu|\right), \tag{5.7}$$

where the Heaviside step function $\Theta(x)$ reflects the fact that the Coulomb-blockaded transport is blocked at low frequencies. At zero gap ($\mu = 0$), we have $V_0 = P\hbar\omega/2e$, in accord with Eq. (5.1). At nonzero gap, the system exhibits marginally increased or decreased charge pumping efficiency $\mathcal{E}$ over the noninteracting value (5.1), depending on μ and P. Second, we consider the limit $\theta \to 0$, keeping μ finite. Eq. (5.1) mandates that the charge pumping vanishes with $\theta \to 0$ when the electron-electron interactions are neglected. At a nonzero Coulomb-blockade gap μ, however, the induced voltage remains finite as $\theta \to 0$ and, in fact, is dramatically enhanced compared to the $\theta = \pi/2$ result, Eq. (5.7). At exactly $\theta = 0$, the total current vanishes, as it should, and $V_0 = 0$. However, as $\theta \to 0$, we obtain angle-independent zero-temperature solutions for $\mu \gtrless 0$ given by

$$eV_0 = \frac{P\mu(\mu \mp \hbar\omega)}{P\mu - [(1+P^2)/(1 \pm P)]\hbar\omega}\Theta\left(\hbar\omega \mp \mu\right). \tag{5.8}$$

Again, the step function $\Theta(x)$ shows the current to be blocked for small frequencies up to $\hbar\omega = |\mu|$, where the response V_0 abruptly switches on. It should be clear, however, that the limit $(\theta, T) \to 0$ is nonanalytic: a finite T makes V_0 vanish in the limit of $\theta \to 0$, progressively more abruptly so at small temperatures. The physical explanation for a finite V_0 at small angles and low temperatures in the presence of Coulomb blockade is as follows. First, we need to appreciate the importance of hopping involving a spin flip, although the rates of these processes with respect to the equilibrium state vanish as θ^2 (i.e., the spin-flip matrix elements squared) according to Eq. (5.4). The insets of Fig. 5.4 show as long red arrows the slower, bottlenecking step of the two-part sequential process for transport of a charge from lead to dot to opposite lead, in the presence of Coulomb blockade. The voltage V_0 would then develop in response to this weak out-of-equilibrium tunneling. The backaction of the voltage on tunneling will not be appreciable, however, until it approaches a finite value on the scale set by energies $\hbar\omega - |\mu|$ and μ, leading to Eq. (5.8). Note that, based on this

reasoning, we should anticipate that the time necessary for the build-up of a finite voltage (5.8) diverges as $\theta \to 0$, since the spin-flipped pumping rates vanish as θ^2.

At finite temperatures and arbitrary μ and θ, Eq. (5.6) is transcendental in V_0 and must be solved numerically or approximately. When the induced voltage is low, expanding Eq. (5.6) in V_0 gives

$$V_0(\omega) \approx \left. \frac{\Gamma^R_{0\to1}\Gamma^L_{1\to0} - \Gamma^R_{1\to0}\Gamma^L_{0\to1}}{\Gamma^R_{1\to0}\partial_{V_L}\Gamma^L_{0\to1} - \Gamma^R_{0\to1}\partial_{V_L}\Gamma^L_{1\to0}} \right|_{V_L,V_R=0}, \tag{5.9}$$

which can be used to find the pumping efficiencies $\mathcal{E}$ and $\mathcal{E}_{\text{diff}}$ (see Fig. 5.3). We have numerically graphed V_0 versus ω for various positive μ at $k_BT/E_c = 10^{-3}$ and $\theta = 5^\circ$ in Fig. 5.2, and confirmed that the analytical curves obtained from Eq. (5.9) (not shown) reproduce the numerical ones very closely. At low frequencies, the response V_0 is linear in ω, due to thermal excitations. At higher frequencies, the response increases gradually before plateauing at some V_0, the value of which depends on the sign of the gap μ. For both signs of μ, the plateau sets in at about $\hbar\omega/E_c \sim 10^{-2}$. However, once $\hbar\omega$ reaches $|\mu|$, the microwave driving starts to take over the Coulomb blockade, and V_0 increases rapidly (see, e.g., the dotted line in Fig. 5.2 for zero temperature). At some ω, this increase begins to fall off and, at high enough frequencies, the response becomes linear and of essentially the same slope as $\mu = 0$, albeit with an offset.

It can be noticed from Fig. 5.2 (see also the inset in Fig. 5.3) that $\mathcal{E}(\omega)$ attains some maximum value $\mathcal{E}_{\max}$ that depends only on the sign of μ (and the ferromagnetic polarization P) at low temperatures. We can straightforwardly obtain these $\mathcal{E}^{\pm}_{\max}(P)$ ($\pm$ here labeling positive/negative μ, respectively) from the zero-temperature expression, Eq. (5.8), valid at small θ. See Fig. 5.4 for the corresponding plots. For the parameters in Fig. 5.2, $\mathcal{E}^+_{\max} \approx 0.36$ and $\mathcal{E}^-_{\max}/\mathcal{E}^+_{\max} \approx 0.1$, while the noninteracting efficiency (5.1) is only $\mathcal{E} \approx 0.0018$.

The reason for different maximum efficiencies for opposite μ can be understood as follows. For a dot attractive to one electron (i.e., $\mu < 0$), the bottleneck process in sequential tunneling is releasing the electron off the dot, i.e., $\Gamma^{L,R}_{1\to0}$. Just above the threshold frequency $\hbar\omega = |\mu|$, the only contributing process to these rates is from electrons that spin-flip from a down-state in the dot to an up-state in the reservoirs (see the upper inset of Fig. 5.4). *Both*

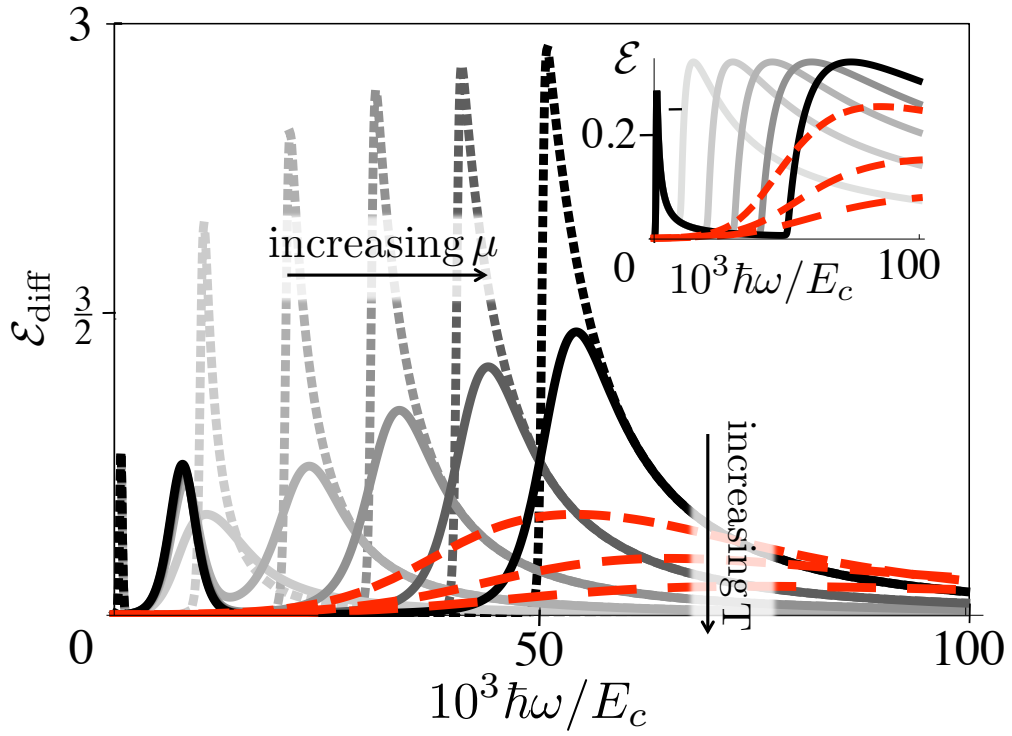

Figure 5.3: The solid grayscale curves in the main panel show the differential charge-pumping efficiency $\mathcal{E}_{\rm diff} = (e/\hbar)\,\partial V_0/\partial\omega$ for $\mu/E_c = (1,2,3,4,5)\times 10^{-2}$ at $\theta = 5°$, $P = 2/3$, and $k_BT/E_c = 10^{-3}$, according to Eq. (5.9). The dotted lines show sharper efficiency peaks as the temperature is lowered to $k_BT/E_c = 10^{-4}$. The dashed red lines show smearing of the peaks as the temperature is increased to $k_BT/E_c = (5,6,7)\times 10^{-3}$ for $\mu/E_c = 5\times 10^{-2}$. Note that $\mu = 0$ efficiency is too small to be seen. Inset: The nominal charge-pumping efficiency $\mathcal{E} = eV_0/\hbar\omega$ for the same parameters (omitting the $k_BT/E_c = 10^{-4}$ data).

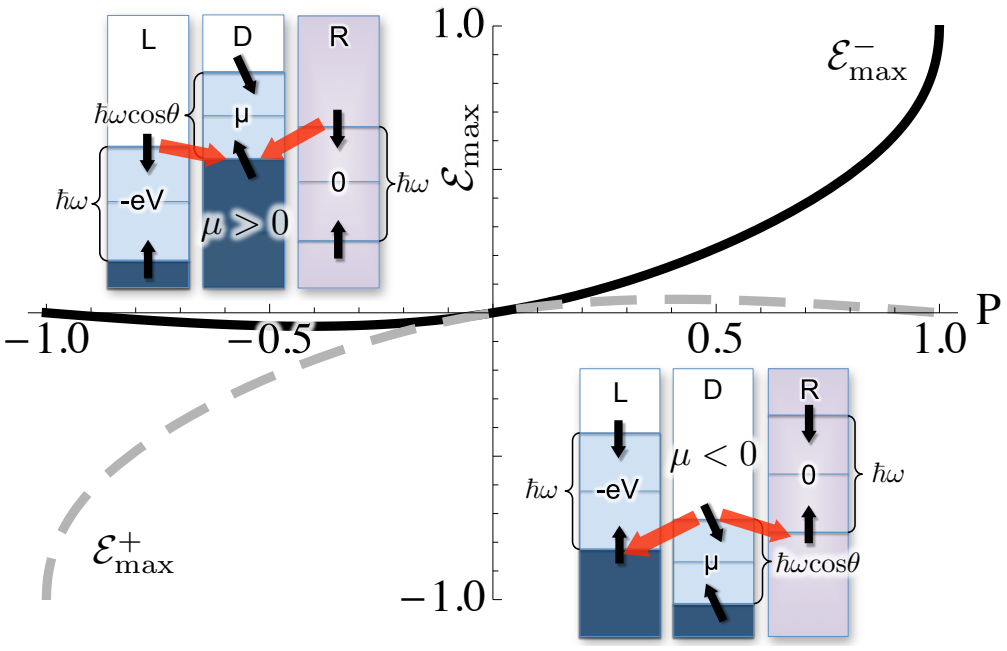

Figure 5.4: Maximum efficiencies $\mathcal{E}^{+}_{\max}$ and $\mathcal{E}^{-}_{\max}$ for positive and negative gating μ, respectively, at zero temperature and small angles θ, obtained from Eq. (5.8). $\mathcal{E}^{+}_{\max}(P) = -\mathcal{E}^{-}_{\max}(-P)$. The inset schematics illustrate the difference between the two cases. The short black arrows show the effective spin-up/down chemical potentials in the dot and the leads. $\mu \gtrless 0$ corresponds to the empty/occupied dot ($N = 0/1$) in equilibrium, which becomes populated/emptied by spin-flipped tunneling (shown by the long red arrows towards/from the dot) when $\hbar\omega > |\mu|$.

of these processes are proportional to the number of available spin-down states in the dot, $D_\downarrow$. In contrast, for a dot repulsive to an extra electron (i.e., $\mu > 0$), at the same threshold pumping, the bottleneck processes $\Gamma^{L,R}_{0\to 1}$ represent electrons tunneling from a down-state in the leads to an up-state in the dot (see the lower inset of Fig. 5.4), both being proportional to the number of available up-states in the dot, $D_\uparrow$. One should notice, furthermore, that in the $\mu > 0$ case, these bottleneck channels for tunneling into the two leads (which are here supplying the majority-spin electrons for the dot) become progressively more asymmetric between the two leads as $P \to 1$. We can, therefore, expect greater absolute maximum efficiency $|\mathcal{E}^+_{\max}|$ for a $\mu > 0$ dot when $P > 0$ and a greater absolute maximum efficiency $|\mathcal{E}^-_{\max}|$ for a $\mu < 0$ dot when $P < 0$, which is exactly what we find for the $\theta \to 0$ case in Fig. 5.4. In fact, $\mathcal{E}^\pm_{\max} \to 1$ and 0, respectively, as $P \to 1$. By the aforementioned electron-hole symmetry, $\mathcal{E}^\pm_{\max}$ switch roles when $\omega \to -\omega$, which corresponds to a different circular polarization of the ferromagnetic precession.

5.3 Conclusion

Finally, supposing one has a coherent source of microwaves of unknown wavelength, the microwave frequency can be measured by ensuring that the dot is in resonance with the source and slowly ramping the electrostatic gate voltage from $\mu = E_c/2$ down to zero, until the onset of strong charge pumping at $\mu = \hbar\omega\cos^2(\theta/2)$ (supposing $\theta < \pi/2$, to be specific). While this would require a frequency less than $E_c/2\hbar\cos^2(\theta/2)$ (or else other transitions become relevant) and low temperatures, it should be simple to detect the dramatic onset of pumping, either by the reverse bias V_0 directly or the differential efficiency $\mathcal{E}_{\text{diff}}$. Further, we note that by gating the dot so that it is occupied by one electron, we have a single-electron transistor, as evidenced by the zero-frequency I-V characteristics. By instead gating with the pumping frequency $\hbar\omega$, we can achieve an extremely high differential voltage gain $\mathcal{E}_{\text{diff}} = (e/\hbar)\partial V_0/\partial\omega$ at the onset of nonzero response V_0 (see Fig. 5.3). This offers a potential for the on-chip integration of such devices with highly-tunable and coherent microwave sources provided by the nanomagnet spin-torque oscillators [KSK03].

CHAPTER 6

Spin Hall phenomenology of magnetic dynamics

Several new directions of spintronic research have opened and progressed rapidly in recent years. Much enthusiasm is bolstered by the opportunities to initiate and detect spin-transfer torques in magnetic metals [ATH08, MGA10, MGG11, LMR11b, LPL12b] and insulator [KHT10b, SKC11b, BHK12a, HdK13], which could be accomplished by variants of the spin Hall effect [HLL13, BH14], along with the reciprocal electromotive forces induced by magnetic dynamics. The spin Hall effect stands for a spin current generated by a transverse applied charge current, in the presence of spin-orbit interaction. From the perspective of angular momentum conservation, the spin Hall effect allows angular momentum to be leveraged from the stationary crystal lattice to the magnetic dynamics. A range of nonmagnetic materials from metals to topological insulators have been demonstrated to exhibit strong spin-orbit coupling, thus allowing for efficient current-induced torques.

Focusing on quasi-two-dimensional (2D) geometries, we can generally think of the underlying spin Hall phenomena as an out-of-equilibrium magnetoelectric effect that couples planar charge currents with collective magnetization dynamics. In typical practical cases, the relevant system is a bilayer heterostructure, which consists of a conducting layer with strong spin-orbit coupling and ferromagnetic layer with well-formed magnetic order. In this case, the current-induced spin torque reflects a spin angular momentum flux normal to the plane, which explains the spin Hall terminology.

The microscopic interplay of spin-orbit interaction and magnetism at the interface translates into a macroscopic coupling between charge currents and magnetic dynamics. A general phenomenology applicable to a variety of disparate heterostructures can be inferred by considering a course-grained 2D system, which both conducts and has magnetic order as well

as lacks inversion symmetry (or else the pseudovectorial magnetization would not couple linearly to the vectorial current density). In a bilayer heterostructure, the latter is naturally provided by the broken reflection symmetry with respect to its plane.

6.1 General Phenomenology

Let us specifically consider a bilayer heterostructure with one layer magnetic and one conducting, as sketched in Fig. 6.1. The nonmagnetic layer can be tailored to enhance spin-orbit coupling effects in and out of equilibrium. Phenomenologically, we have a quasi-2D system along the xy plane, which will for simplicity be taken to be isotropic and mirror-symmetric in plane while breaking reflection symmetry along the z axis. In other words, the structural symmetry is assumed to be that of a Rashba 2D electron gas (although microscopic details could be more complex), subject to a spontaneous time-reversal symmetry breaking due to the magnetic order. Common examples of such heterostructures include a thin transition-metal [ATH08, MGA10, MGG11, LMR11b, LPL12b] or magnetic-insulator [KHT10b, SKC11b, BHK12a] film capped by a heavy metal, or a layer of 3D topological insulator doped on one side with magnetic impurities [CCA10, WXX10, CYO12, FUK14b].

The course-grained hydrodynamic variables used to describe our system are the three-component collective spin density (per unit area) $\mathbf{s}(\mathbf{r},t) = s\mathbf{n}(\mathbf{r},t) \equiv (sn_x, sn_y, sn_z)$ and the two-component 2D current density (per unit length) $\mathbf{j}(\mathbf{r},t) \equiv (j_x, j_y)$ in the xy plane. Considering fully saturated magnetic state well below the Curie temperature, we treat the spin density as a directional variable, such that its magnitude s is constant and orientational unit vector $\mathbf{n}$ parametrizes a smooth and slowly-varying magnetic texture. We will be interested in slow and long-wavelength agitations of the ferromagnet coupled to the electron liquid along with reciprocal motive forces. Perturbed out of equilibrium, the temporal evolution of the heterostructure is governed by the forces that couple to the charge flow and magnetic dynamics: the (planar) electric field and magnetic field, respectively.

6.1.1 Decoupled Dynamics

A uniform electric-current carrying state in the isolated conducting film, subject to a constant *external* vector potential $\mathbf{A}$, has the free-energy density

$$\mathcal{F}(\mathbf{p}, \mathbf{A}) = \mathcal{F}_0(\mathbf{p}) - \frac{\mathbf{p} \cdot \mathbf{A}}{c} + \mathcal{O}(A^2)\,, \tag{6.1}$$

where $\mathcal{F}_0 = L\mathbf{p}^2/2$ is the free-energy density in terms of the *paramagnetic* current $\mathbf{p}$ (i.e., the current defined in the absence of the vector potential $\mathbf{A}$), and L is the local self-inductance of the film (including inertial and electromagnetic contributions). According to time-reversal symmetry, in equilibrium $\mathbf{p} = 0$ when $\mathbf{A} = 0$. The gauge invariance (which requires that the minimum of $\mathcal{F}$, as a function of $\mathbf{p}$, is independent of $\mathbf{A}$), furthermore, dictates the following form of the free energy:

$$\mathcal{F} = \frac{L}{2}\left(\mathbf{p} - \frac{\mathbf{A}}{cL}\right)^2 . \tag{6.2}$$

Therefore, the phenomenological expression for the full current density is

$$\mathbf{j} \equiv -c\delta_{\mathbf{A}} F = \mathbf{p} - \frac{\mathbf{A}}{cL}\,, \tag{6.3}$$

with δ standing for the 2D functional derivative of the total electronic free energy $F[\mathbf{p}] = \int d^2\mathbf{r}\mathcal{F}(\mathbf{p})$. We conclude, based on Eqs. (6.2) and (6.3), that $\mathbf{j} = L^{-1}\delta_{\mathbf{p}} F$, which is thus the *force* thermodynamically conjugate to $L\mathbf{p}$. General quasistatic equilibration[LL80a] of a perturbed electron system can now be written as

$$L\dot{\mathbf{p}} = -\hat{\varrho}\mathbf{j}\,, \tag{6.4}$$

or, in terms of the physical current:

$$L\dot{\mathbf{j}} + \hat{\varrho}\mathbf{j} = \mathbf{E}\,, \tag{6.5}$$

where $\mathbf{E} \equiv -\partial_t \mathbf{A}/c$ is the electric field, and $\hat{\varrho}$ is identified as the resistivity tensor. This is the familiar Ohm's law, which, in steady state, reduces to

$$\mathbf{j} = \hat{g}\mathbf{E}\,, \tag{6.6}$$

in terms of the conductivity tensor $\hat{g} \equiv \hat{\varrho}^{-1}$. Based on the axial symmetry around z, we can generally write $\hat{g} = g + g_H \mathbf{z}\times$, where g is the longitudinal (i.e., dissipative) and g_H Hall conductivities.

The isolated magnetic-film dynamics, on the other hand, are described by the Landau-Lifshitz-Gilbert equation:[LP80, Gil04b]

$$s(1 + \alpha\mathbf{n}\times)\dot{\mathbf{n}} = \mathbf{H}^* \times \mathbf{n}\,, \tag{6.7}$$

where $\mathbf{H}^* \equiv \delta_{\mathbf{n}} F[\mathbf{n}]$ is the effective magnetic field governed by the magnetic free-energy functional $F[\mathbf{n}] = \int d^2\mathbf{r}\mathcal{F}(\mathbf{n})$. The (dimensionless) Gilbert damping α captures the (time-reversal breaking) dissipative processes in the spin sector.

The total dissipation power in our combined, but still decoupled, system is given by

$$-\dot{F} = -\int d^2\mathbf{r}\,(L\dot{\mathbf{p}}\cdot\mathbf{j} + \dot{\mathbf{n}}\cdot\mathbf{H}^*) = \int d^2\mathbf{r}\left(\varrho j^2 + \alpha s\dot{\mathbf{n}}^2\right)\,, \tag{6.8}$$

where $\varrho = g/(g^2 + g_H^2)$ is the longitudinal resistivity. According to the fluctuation-dissipation theorem [LL80a], finite-temperature fluctuations are thus determined by $\langle j_i(\mathbf{r},t)j_{i'}(\mathbf{r}',t')\rangle = 2gk_BT\delta_{ii'}\delta(\mathbf{r}-\mathbf{r}')\delta(t-t')$ and $\langle h_i(\mathbf{r},t)h_{i'}(\mathbf{r}',t')\rangle = 2\alpha s k_B T\delta_{ii'}\delta(\mathbf{r}-\mathbf{r}')\delta(t-t')$. Having mentioned this for completeness, we will not pursue thermal properties any further.

6.1.2 Coupled Dynamics

Having recognized $(L\mathbf{p}, \mathbf{j})$ and $(\mathbf{n}, \mathbf{H}^*)$ as two pairs of thermodynamically conjugate variables, their coupled dynamics must obey Onsager reciprocity.[LL80a] Charge current flowing through our heterostructure in general induces a torque $\boldsymbol{\tau}$ on the magnetic moment and, vice versa, magnetic dynamics produce a motive force $\boldsymbol{\epsilon}$ acting on the current, defined as follows:

$$s(\dot{\mathbf{n}} + \mathbf{n}\times\hat{\alpha}\dot{\mathbf{n}}) = \mathbf{H}^*\times\mathbf{n} + \boldsymbol{\tau}\,, \tag{6.9}$$

$$L\dot{\mathbf{j}} + \hat{\varrho}\mathbf{j} = \mathbf{E} + \boldsymbol{\epsilon}\,, \tag{6.10}$$

where $L\dot{\mathbf{j}} = L\dot{\mathbf{p}} + \mathbf{E}$, according to Eq. (6.3). In general, due to the spin-orbit interaction at the interface, Gilbert damping $\hat{\alpha}$ and resistivity tensor [NAC13, CTN13] $\hat{\varrho}$ can acquire

anisotropic **n**-dependent contributions. Let us start by expanding the motive force, according to the assumed structural symmetries, in the Cartesian components of **n**:

$$\boldsymbol{\epsilon} = [(\eta + \vartheta \mathbf{n}\times)\dot{\mathbf{n}}] \times \mathbf{z}\,, \tag{6.11}$$

where η is the *reactive* and ϑ the *dissipative* coefficients characterizing spin-orbit interactions in our coupled system. While η and ϑ can generally depend on n_z^2, we will for simplicity be focusing our attention on the limit when they are mere constants. The dimensionless parameter $\beta \equiv \vartheta/\eta$ describes their relative strengths. The Onsager reciprocity then immediately dictates the following form of the torque:

$$\boldsymbol{\tau} = (\eta + \vartheta \mathbf{n}\times)(\mathbf{z} \times \mathbf{j}) \times \mathbf{n}\,. \tag{6.12}$$

In line with the existing nomenclature [ATH08, KHT10b], we can write the dissipative coefficient as

$$\vartheta \equiv \frac{\hbar}{2ea_N} \tan\theta\,, \tag{6.13}$$

in terms of a length scale a_N, which we take to correspond to the normal-metal thickness, and dimensionless parameter θ identified as the effective *spin Hall angle* at the interface. The coefficient η in Eq. (6.12) parametrizes the so-called *field-like torque,* which could arise, for example, as a manifestation of the interfacial *Edelstein effect* [Ede95].

Another important effect of the nonmagnetic layer on the ferromagnet is the enhanced damping of the magnetization dynamics by spin pumping [TBB02a, TBB05], such that

$$\alpha = \alpha_0 + \frac{a^{\uparrow\downarrow}}{a_F}\,. \tag{6.14}$$

α_0 is the bulk damping, which is thickness a_F independent, and $a^{\uparrow\downarrow}$ parametrizes the strength of angular momentum [as well as energy, according to Eq. (6.8)] loss at the interface. Spin pumping into a perfect spin reservoir corresponds to [TBB02a, TBB05] $a^{\uparrow\downarrow} = \hbar g_r^{\uparrow\downarrow}/4\pi S$, where $g_r^{\uparrow\downarrow}$ is the (real part of the dimensionless) interfacial spin-mixing conductance per unit area and $S \equiv s/a_F$ is the 3D spin density in the ferromagnet. In reality, $a^{\uparrow\downarrow}$ depends on the spin-relaxation efficiency in the normal metal as well as the spin-orbit interaction at the interface, and may depend on a_N in a nontrivial manner (see Ref. [TBB02b] for a diffusive

model), so long as $a_N \lesssim \lambda_N$, where λ_N is the spin-relaxation length in the normal metal. With these conventions in mind and focusing on the limit of $a_N \gg \lambda_N$ and, in the case of a metallic ferromagnet, $a_F \gg \lambda_F$, we will suppose that the coefficients θ, β, and $a^{\uparrow\downarrow}$ defined above are thickness independent.

Unless otherwise stated, we will disregard anisotropies in α, which may in general depend on the directions of $\mathbf{n}$ and $\dot{\mathbf{n}}$, subject to the reduced crystalline symmetries and the lack of reflection asymmetry at the interface. In the same spirit, with the exception of Sec. **??**, we will not concern ourselves much with the $\mathbf{n}$-dependent interfacial magnetoresistance/proximity effects,[NAC13] which would enter through the resistivity tensor $\hat{\varrho}(\mathbf{n})$ in Eq. (6.10).

We remark that while we considered a nonequilibrium magnetoelectric coupling in terms of torque $\boldsymbol{\tau}$ and force $\boldsymbol{\epsilon}$ in Eqs. (6.9) and (6.10), we had retained the decoupled form of the free-energy density, $\mathcal{F}(\mathbf{p}) + \mathcal{F}(\mathbf{n})$. We exclude the possibility of a linear coupling of $\mathbf{p}$ to the magnetic order, since it would suggest a nonzero electric current in equilibrium.

6.2 Spin Hall Bilayer

The previous two models naturally produced the reactive coupling η between planar charge current and magnetic dynamics. Here, we recap a diffusive spin Hall model[MPF10, NAC13] that results in both η and ϑ, which is based on a film of a featureless isotropic normal-metal conductor in contact with ferromagnetic insulator. If electrons diffuse through the conductor with weak spin relaxation, we can develop a hydrodynamic description based on continuity relations both for spin and charge densities. We first construct bulk diffusion equations and then impose spin-charge boundary conditions, which allows us to solve for spin-charge fluxes in the normal metal and torque on the ferromagnetic insulator.

The relevant hydrodynamic quantities in the normal-metal bulk are 3D charge and spin densities, $\rho(\mathbf{r}, t)$ and $\boldsymbol{\rho}(\mathbf{r}, t)$, respectively. The associated thermodynamic conjugates are the electrochemical potential, $\mu \equiv -e\delta_\rho F$, and spin accumulation, $\boldsymbol{\mu} \equiv \hbar\delta_{\boldsymbol{\rho}} F$, where $F[\rho, \boldsymbol{\rho}]$ is the free-energy functional of the normal metal. Supposing only a weak violation of spin conservation (due to magnetic or spin-orbit impurities), we phenomenologically write spin-

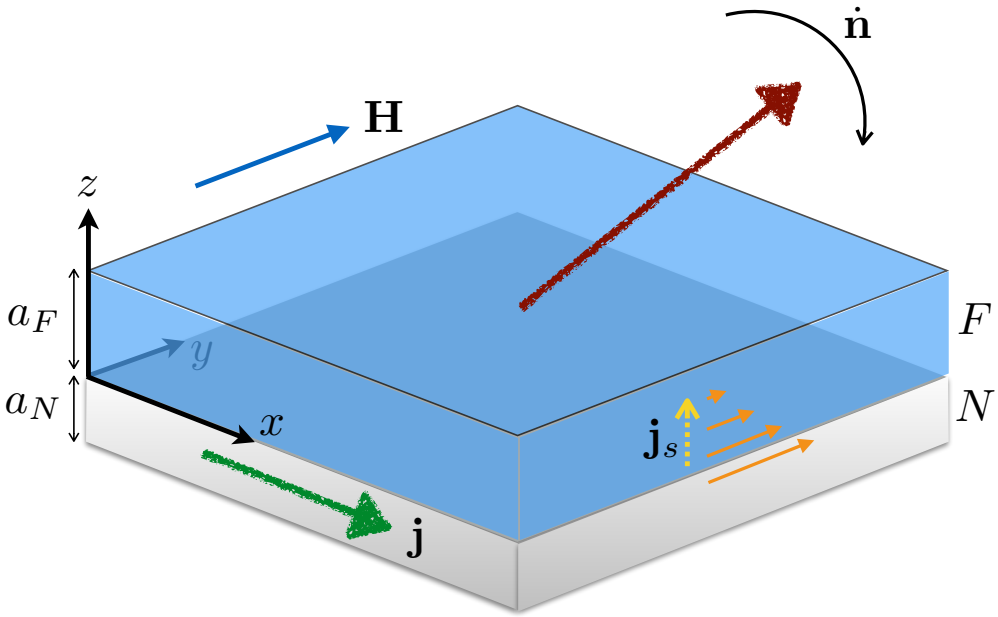

Figure 6.1: Heterostructure consisting of a magnetic top layer and conducting underlayer. The charge current $\mathbf{j}$ induces a torque $\boldsymbol{\tau}$ acting on the magnetic dynamics, which quantifies the spin angular-momentum transfer in the z direction. This can be thought of as a spin current $\mathbf{j}_s$ entering the ferromagnet at the interface. Reciprocally, magnetic dynamics $\dot{\mathbf{n}}$ induces a motive force $\boldsymbol{\epsilon}$ acting on the itinerant electrons in the conductor.

charge continuity relations as

$$\partial_t \rho = -\partial_\imath J_\imath \,, \;\; \partial_t \rho_\jmath = -\partial_\imath J_{\imath\jmath} - \Gamma \mu_\jmath \,, \tag{6.15}$$

where $\imath$ and $\jmath$ label Cartesian components of real and spin spaces, respectively, and the summation over the repeated index $\imath$ is implied. $\Gamma = \hbar \mathcal{N}/2\tau_s$, in terms of the (per spin) Fermi-level density of states $\mathcal{N}$ and spin-relaxation time τ_s. $J_\imath$ are the components of the 3D vectorial charge-current density and $J_{\imath\jmath}$ of the tensorial spin-current density, which can be expanded in terms of the thermodynamic forces governed by μ and $\boldsymbol{\mu}$:

$$J_\imath = \frac{\sigma}{e}\partial_\imath \mu - \frac{\sigma'}{2e}\epsilon_{\imath\jmath k}\partial_\jmath \mu_k \,, \tag{6.16}$$

$$\frac{2e}{\hbar} J_{\imath\jmath} = -\frac{\sigma_+}{2e}\partial_\imath \mu_\jmath - \frac{\sigma_-}{2e}\partial_\jmath \mu_\imath - \frac{\sigma'}{e}\epsilon_{\imath\jmath k}\partial_k \mu \,, \tag{6.17}$$

where σ is the (isotropic) electrical conductivity and σ' the spin Hall conductivity of the normal-metal bulk. The last terms of Eqs. (6.16) and (6.17) are governed by the same coefficient σ' due to the Onsager reciprocity. The bulk spin Hall angle θ' is conventionally defined by

$$\tan\theta' \equiv \frac{\sigma'}{\sigma} \,. \tag{6.18}$$

Bulk diffusion equations (6.16), (6.17) are complemented by the boundary conditions

$$J_z = 0 \;\; \text{at} \;\; z = -a_N, 0 \tag{6.19}$$

for the charge current, where $z = -a_N$ corresponds to the normal-metal interface with vacuum and $z = 0$ to the interface with the ferromagnet, and [TBB02a]

$$\mathbf{J}_z = \frac{1}{4\pi} \begin{cases} 0 & \text{at } z = -a_N \\ \left(g_i^{\uparrow\downarrow} + g_r^{\uparrow\downarrow} \mathbf{n}\times \right) \tilde{\boldsymbol{\mu}} \times \mathbf{n} & \text{at } z = 0 \end{cases} \,, \tag{6.20}$$

for the spin current, with $\mathbf{J}_z$ standing for $J_{z\jmath}$. Here, $\tilde{\boldsymbol{\mu}} \equiv \boldsymbol{\mu} - \hbar \mathbf{n} \times \dot{\mathbf{n}}$ captures contributions from the spin-transfer torque and spin pumping, respectively.

Having established the general structure of the coupled spin and charge diffusion, let us calculate the steady-state charge-current density $\mathbf{j}$ driven by a simultaneous application of a uniform electric field in the xy plane, $\boldsymbol{\nabla}\mu \to e\mathbf{E}$, and magnetic dynamics, $\dot{\mathbf{n}}$:

$$\mathbf{J} = \sigma \mathbf{E} - \frac{\sigma'}{2e} \boldsymbol{\nabla} \times \boldsymbol{\mu} \,. \tag{6.21}$$

The spin accumulation $\boldsymbol{\mu}$ is found by solving

$$\left(\frac{\sigma_+}{\sigma}+\frac{\sigma_-}{\sigma}\delta_{zj}\right)\partial_z^2\mu_j=\frac{\mu_j}{l_s^2}\,, \tag{6.22}$$

where $l_s\equiv\sqrt{\hbar\sigma/4e^2\Gamma}$ is the spin-diffusion length. Using Drude formula for the conductivity σ, we get the familiar $l_s=l/\sqrt{3\epsilon}$, where l is the scattering mean free path and $\epsilon\equiv\tau/\tau_s\ll 1$ is the spin-flip probability per scattering (τ is the transport mean free time). The boundary conditions are

$$\begin{aligned}&\sigma'\mathbf{z}\times\mathbf{E}-\frac{\sigma_+}{2e}\partial_z\boldsymbol{\mu}-\frac{\sigma_-}{2e}\boldsymbol{\nabla}\mu_z\\&\qquad=\frac{e}{h}\begin{cases}0 & \text{at } z=-a_N\\ \left(g_i^{\uparrow\downarrow}+g_r^{\uparrow\downarrow}\mathbf{n}\times\right)\tilde{\boldsymbol{\mu}}\times\mathbf{n} & \text{at } z=0\end{cases},\end{aligned} \tag{6.23}$$

where $h=2\pi\hbar$ is the Planck's constant.

In the limit of vanishing spin-orbit coupling, $\sigma_+\to\sigma$, $\sigma_-\to 0$, and $\theta'\to 0$. For small but finite spin-orbit interaction, we may expect $(\sigma_+-\sigma)\sim\sigma_-\sim\mathcal{O}(\theta'^2)$. In the following, we will neglect these quadratic terms and approximate $\tan\theta'\approx\theta'\ll 1$, in the spirit of the present construction.

In the limit of $l_s\ll a_N$, the spin accumulation decays exponentially away from the interface as $\boldsymbol{\mu}(z)=\boldsymbol{\mu}_0 e^{z/l_s}$, where

$$\boldsymbol{\mu}_0=(\xi_i+\xi\mathbf{n}\times)\left[\hbar\dot{\mathbf{n}}-2el_s\theta'(\mathbf{z}\times\mathbf{E})\times\mathbf{n}\right]+2el_s\theta'\mathbf{z}\times\mathbf{E}\,. \tag{6.24}$$

Here, $\xi\equiv\chi(1+\zeta+\zeta_i^2)$ and $\xi_i\equiv\chi\zeta\zeta_i$, in terms of $\zeta\equiv\sigma/g_Q g_r^{\uparrow\downarrow}l_s$, $\zeta_i\equiv g_i^{\uparrow\downarrow}/g_r^{\uparrow\downarrow}$, $\chi^{-1}\equiv(1+\zeta)^2+\zeta_i^2$, and the quantum of conductance $g_Q\equiv 2e^2/h$. The spin accumulation $\boldsymbol{\mu}_0$ consists of the decoupled spin-pumping and spin Hall contributions. Integrating the resultant charge-current density (6.21) over the normal-layer thickness a_N, we finally get for the 2D current density in the film:

$$\mathbf{j}=\sigma\left(a_N\mathbf{E}-\frac{\theta'}{2e}\mathbf{z}\times\boldsymbol{\mu}_0\right)=\hat{g}\left\{\mathbf{E}+[(\eta+\vartheta\mathbf{n}\times)\dot{\mathbf{n}}]\times\mathbf{z}\right\}\,, \tag{6.25}$$

where

$$\frac{\hat{g}}{\sigma}=\tilde{a}_N+l_s\theta'^2\left\{\xi_i n_z(\mathbf{z}\times)-\xi[n_z^2+(\mathbf{z}\times\mathbf{n}\times\mathbf{z})\mathbf{n}\cdot]\right\} \tag{6.26}$$

is the anisotropic 2D conductivity tensor ($\tilde{a}_N \equiv a_N + l_s\theta'^2 \approx a_N$), which is referred in the literature to as the spin Hall magnetoconductance,[NAC13] and

$$\eta \approx \frac{\hbar}{2ea_N}\theta'\xi_i\,, \quad \vartheta \approx \frac{\hbar}{2ea_N}\theta'\xi\,, \tag{6.27}$$

neglecting corrections that are cubic in θ'. If $\zeta_i \ll 1$, which is typically the case [BBK06], we have $\vartheta \gg \eta$. It could be noted that restoring $\sigma_- \sim \mathcal{O}(\theta'^2)$ in Eqs. (6.22) and (6.23) would affect $\hat{g}$ only at order $\mathcal{O}(\theta'^3)$.

The above spin accumulation can also be used to calculate the spin-current density injected into the ferromagnet at $z = 0$:

$$\begin{aligned}\mathbf{J}_z &= \frac{\hbar\sigma}{2e}\left(\theta'\mathbf{z}\times\mathbf{E} - \frac{\boldsymbol{\mu}_0}{2el_s}\right)\\ &\approx -s\mathbf{n}\times\hat{\alpha}\dot{\mathbf{n}} + (\eta + \vartheta\mathbf{n}\times)(\mathbf{z}\times\mathbf{j})\times\mathbf{n}\,,\end{aligned} \tag{6.28}$$

where

$$\hat{\alpha} = \frac{\hbar^2\sigma}{4e^2l_s s}(\xi - \xi_i\mathbf{n}\times)\,, \tag{6.29}$$

and we dropped terms that are cubic in θ', as before. The corresponding magnetic equation of motion $s\dot{\mathbf{n}} = \mathbf{H}^*\times\mathbf{n} + \mathbf{J}_z$ reproduces Eq. (6.10), with the current-driven torque of the form (6.12) that is Onsager reciprocal to the motive force in Eq. (6.25). Writing the Gilbert damping $\propto \xi$ in Eq. (6.29) as $a^{\uparrow\downarrow}/a_F$ identifies the interfacial damping enhancement in Eq. (6.14). In the formal limit $\sigma \to \infty$ (while keeping all other parameters, including l_s, fixed), which reproduces the perfect spin sink, this gives $a^{\uparrow\downarrow} = \hbar g_r^{\uparrow\downarrow}/4\pi S$. In the general case, ξ also captures the spin backflow from the normal layer [TBB02b]. An anisotropic contribution to the Gilbert damping would be produced at the cubic order in θ', had we not made any approximations in Eq. (6.28).

6.3 Conclusion

In summary, we have developed a phenomenology for slow long-wavelength dynamics of conducting quasi-2D magnetic films and heterostructures, subject to structural symmetries and Onsager reciprocity. The formalism could address both small- and large-amplitude magnetic

precession (assuming it is slow on the characteristic electronic time scales), including, for example, magnetic switching and domain-wall or skyrmion motion. Owing to the versatility of available heterostructures, including those based on magnetic and topological insulators, we have focused our discussion on the case of a ferromagnetic/nonmagnetic bilayer, which serves two purposes: It naturally has a broken inversion symmetry, and the spin-orbit and magnetic properties could be separately optimized and tuned in one of the two layers.

In the case when the spin-relaxation length in the normal layer is short compared to its thickness, we can associate the interplay between spin-orbit and exchange interactions to a narrow region in the vicinity of the interface, for which we define the kinetic coefficients such as the interfacially enhanced Gilbert damping parametrized by $a^{\uparrow\downarrow}$ and the spin Hall angle parametrized by ϑ. Such (separately measurable) phenomenological coefficients, which enter in our theory, must thus be viewed as joint properties of both of the bilayer materials as well as structure and quality of the interface.

We demonstrate the emergence of our phenomenology out of a spin Hall metal in contact with a magnetic insulator. In addition to Onsager-reciprocal spin-transfer torques and electromotive forces, our phenomenology also accommodates arbitrary Gilbert-damping and (magneto)resistance anisotropies, which are dictated by the same structural symmetries and may microscopically depend on the same exchange and spin-orbit ingredients as the reciprocal magnetoelectric coupling effects.

CHAPTER 7

Appendix

7.1 Adiabatic, Nondissipative Coupled Dynamics of Magnon Cloud and Condensate

The state of the ferromagnet is described by the spin density field $\hat{\mathbf{s}}(\mathbf{x})$ (expressed in units of $\hbar$), which is subject to the standard spin commutation relations: $[\hat{s}_i(\mathbf{r}), \hat{s}_j(\mathbf{r}')] = i\epsilon_{ijk}\delta(\mathbf{r} - \mathbf{r}')\hat{s}_k(\mathbf{r})$. The coherent local spin density is defined as: $\mathbf{s}(\mathbf{r}) = \langle\hat{\mathbf{s}}(\mathbf{r})\rangle = \tilde{s}(\mathbf{r})\mathbf{n}(\mathbf{r})$, where $\mathbf{n}$ is a local unit vector. We will suppose that the spin-space SU(2) symmetry of F is broken along a common axis (defined by the unit vector $\mathbf{z}$) by an applied magnetic field and the crystalline anisotropy of the underlying F lattice. If fluctuations of $\hat{\mathbf{s}}$ around $\mathbf{n}$ are small compared to the saturation spin density s (expressed in units of $\hbar$) and $|\mathbf{n}\cdot\mathbf{z}| \ll 1$, it is useful to map $\hat{\mathbf{s}}$ to a boson field operator $\hat{\Phi}(\mathbf{r})$, via the Holstein-Primakoff transformation, Eqs. (1.24) and (1.25). The quanta of $\hat{\Phi}$ are magnons with angular momentum $+\hbar\mathbf{z}$. When $\mathbf{z}$ is collinear with $\mathbf{n}$, $\langle\hat{s}_\pm\rangle = 0$, which implies $\langle\hat{\Phi}\rangle = 0$; when, however, $\mathbf{z}$ is misaligned with $\mathbf{n}$, one has a nonzero expectation value for $\langle\hat{\Phi}\rangle$, breaking U(1) symmetry around the z axis. The choice to define the Holstein-Primakoff transformation with respect to the broken symmetry axis z of F is, of course, made purely out of convenience. Alternatively, one may define a Holstein-Primakoff transformation with respect to direction $-\mathbf{n}$; the corresponding field operators $\hat{\varphi}^\dagger$ and $\hat{\varphi}$, the quanta of which are magnons carrying $\hbar$ in the $-\mathbf{n}$ direction, describe incoherent fluctuations around $\mathbf{n}$, with $\langle\hat{\varphi}\rangle = 0$. The two transformations may be related by a rotation $\hat{R}$ on spin-space: $\hat{\Phi} = \hat{R}\hat{\phi}\hat{R}^\dagger$ where

$$\hat{R} = e^{i\hbar^{-1}\int d^3r'(\pi-\theta(\mathbf{r},t))\mathcal{R}(\mathbf{r},t)\cdot\hat{\mathbf{S}}(\mathbf{r},t)}\,, \tag{7.1}$$

where $\mathcal{R}(\mathbf{r},t) = -\sin[\phi(\mathbf{r},t)]\mathbf{x} + \cos[\phi(\mathbf{r},t)]\mathbf{y}$, $\theta(\mathbf{r},t)$ is the local polar angle of $\mathbf{n}$ with respect to the z axis, and $\phi(\mathbf{r},t)$ is the local azimuthal angle of the order parameter $\mathbf{n}(\mathbf{r},t)$ in the xy plane; one may regard the condition $\langle\hat{\varphi}\rangle = 0$ as the defining condition for $\mathcal{R}$, which defines the spherical coordinates θ and ϕ and hence $\mathbf{n}$. The gauge transformation $\hat{R}$ "unwinds" the spin texture $\mathbf{n}$ to $\mathbf{n}' = -\mathbf{z}$, introducing a non-abelian gauge field, which is given by (for small angles $\theta \lesssim \pi$):

$$\hat{\Phi} = \hat{\varphi} + \Phi\left(1 - \frac{\hat{\varphi}^\dagger\hat{\varphi}}{2s} - \frac{\hat{\varphi}^2}{4s}\right) + \mathcal{O}(\Phi^2)\,, \tag{7.2}$$

where $\Phi = e^{-i\phi}(\pi - \theta)\sqrt{s/2}$. In writing Eq. (7.2), we expanded the radical in the Holstein-Primakoff to lowest nontrivial order in $\phi^\dagger\phi/s$, anticipating the role of interactions, which enter at the same order.

The bulk dynamics of the ferromagnetic spin density $\hat{\mathbf{s}}(\mathbf{x})$ is governed by the magnetic Hamiltonian:

$$\hat{\mathcal{H}} = \hat{\mathcal{H}}_{\text{ex}} + \hat{\mathcal{H}}_H + \hat{\mathcal{H}}_K\,. \tag{7.3}$$

Here,

$$\hat{\mathcal{H}}_{\text{ex}} = -\frac{A}{2s^2}\int d^3r\hat{\mathbf{s}}\cdot\nabla^2\hat{\mathbf{s}} \tag{7.4}$$

is the exchange Hamiltonian, with stiffness A,

$$\hat{\mathcal{H}}_{\text{H}} = \int d^3r\mathbf{H}_0\cdot\mathbf{s} = H_0\int d^3r\hat{\Phi}^\dagger\hat{\Phi} + const \tag{7.5}$$

is the Zeeman energy stemming from an applied field $\mathbf{H}_0 = H_0\mathbf{z}$ (measured in units of energy), and

$$\hat{\mathcal{H}}_K = \frac{K}{2s}\int d^3r\hat{s}_z^2 = -K\int d^3r\hat{\Phi}^\dagger\hat{\Phi} + \frac{K}{2s}\int d^3r\hat{\Phi}^\dagger\hat{\Phi}^\dagger\hat{\Phi}\hat{\Phi} + const \tag{7.6}$$

is the anisotropy term, with K measured in units of energy. Time evolution of the operator $\hat{\Psi}$ is governed by the Heisenberg equation of motion,

$$i\hbar\partial_t\hat{\Phi}(\mathbf{r}) = [\hat{\Phi}(\mathbf{r}), \hat{H}]\,, \tag{7.7}$$

into which we substitute Eq. (7.2). Keeping only terms up to order $\hat{\Phi}^2/s$[1], taking the

[1]for example, in the term $\sim \dot{\Phi}\hat{\varphi}^\dagger\varphi/2s$ on the left-hand side of Eq. (7.7) we may substitute $i\hbar\dot{\Phi} = (\hbar\Omega - A\nabla^2)\Phi + \mathcal{O}(\hat{\Phi}^2/s)$, where $\hbar\Omega = H_0 - K$ is the magnon gap

expectation value of the resulting expression and using $\langle\varphi\rangle = 0$, we obtain, after some work:

$$i\hbar\partial_t\Phi = (\hbar\Omega - A\nabla^2)\Phi + \langle[\hat{\varphi}, \hat{\mathcal{H}}_K^{(4)}]\rangle + \langle[\hat{\varphi}, \hat{\mathcal{H}}_{\rm ex}^{(4)}]\rangle\,, \tag{7.8}$$

where $\hat{\mathcal{H}}_K^{(4)}$ (given by the second term on the far right-hand side of Eq. (7.6)) and $\hat{\mathcal{H}}_{\rm ex}^{(4)}$ are the contributions to $\hat{\mathcal{H}}_K$ and $\hat{\mathcal{H}}_{\rm ex}$ which are quartic in $\hat{\Phi}$. The exchange Hamiltonian is invariant under global spin rotations; consequently $\hat{\mathcal{H}}_{\rm ex} = \hat{\Phi}$ must depend on $\nabla\Phi$. To lowest order in both $\hat{\Phi}/s$ and $\nabla\Phi$ and neglecting anomalous correlations $\langle\hat{\varphi}^2\rangle$, one has, using Eqs. (7.2) and (7.6):

$$\langle[\hat{\varphi}, \hat{\mathcal{H}}_{\rm ex}^{(4)}]\rangle = 2\frac{A}{is}\nabla\Phi\langle\hat{\varphi}^\dagger\nabla\hat{\varphi}\rangle\,, \tag{7.9}$$

which correspond to Berry phase effects of magnons moving through a texture Φ. The quartic anisotropy term has three nonvanishing contributions:

$$\langle[\hat{\varphi}, \hat{\mathcal{H}}_K^{(4)}]\rangle = \frac{K}{s}\langle\hat{\varphi}^\dagger\hat{\varphi}\hat{\varphi}\rangle + 2K\frac{n}{s}\Phi + K\frac{|\Phi|^2}{s}\Phi\,. \tag{7.10}$$

The first term gives a scattering rate for $\hat{\varphi}$ magnons into Φ; the correlator $\langle\hat{\varphi}^\dagger\hat{\varphi}\hat{\varphi}\rangle$ arises from the interactions $\sim K$. The second two terms in Eq. (7.10) are mean-field terms. Eq. (7.8) is therefore of the form of a Gross-Pitaevski equation:

$$i\hbar\partial_t\Phi = \left(\mathcal{H}_{\rm eff} + K\frac{|\Phi|^2}{s}\right)\Phi \tag{7.11}$$

where

$$\mathcal{H}_{\rm eff} = (\hbar\Omega - A\nabla^2) + 2Kn\Phi + K\,|\Phi|^2 + iR + 2\frac{A}{is}\langle\hat{\varphi}^\dagger\nabla\hat{\varphi}\rangle\nabla \tag{7.12}$$

and $iR = \Phi^{-1}(K/s)\langle\hat{\varphi}^\dagger\hat{\varphi}\hat{\varphi}\rangle$. It is instructive to transform Eq. (7.11) into an effective Landau-Lifshitz equation for $\mathbf{n} = (\sin\theta\cos\phi, \sin\theta, \sin\phi, \cos\theta)$:

$$\hbar\dot{\mathbf{n}} = -\mathbf{n}\times(\mathbf{H}_{\rm eff} - A\nabla^2\mathbf{n} + K\mathbf{n}_z) + \Re[R]\mathbf{n}\times\mathbf{n}\times\mathbf{z} + \frac{1}{s}\mathbf{j}\cdot\nabla\mathbf{n} \tag{7.13}$$

where $\mathbf{H}_{\rm eff} = (\hbar + 2Kn)$ is the effective magnetic field. The second term on the right-hand side of Eq. (7.13) is the coherent torque on $\mathbf{n}$ effected by thermal magnon scattering. The last term is the adiabatic Berry phase torque, with

$$\mathbf{j}_T = \frac{A}{i}\langle\hat{\varphi}^\dagger\nabla\hat{\varphi} - (\nabla\hat{\varphi}^\dagger)\hat{\varphi}\rangle \tag{7.14}$$

as the incoherent magnon spin flux. Incoherent magnons carry $\hbar$ along the local direction $-\mathbf{n}(\mathbf{x})$; as a magnon traverses the magnetic texture, the magnon quantization axis changes, and the change in angular momentum $-\hbar\Delta\mathbf{n}$ carried by the magnon is absorbed by the magnetic order parameter, $\mathbf{n}$.

Eq. (7.11), together with the equation of motion for φ (obtained by subtracting Eq. (7.11) from Eq. (7.7)), are formally identical to those of a superfluid of, e.g. atoms, of mass $m = \hbar^2/2A$ in a potential $V = \hbar\Omega$ with infinitely short-ranged repulsive interactions, aside from $\langle[\hat{\varphi}, \hat{\mathcal{H}}^{(4)}_{\rm ex}]\rangle$ in Eq. (7.8) and the corresponding Berry phase term in the equation of motion for φ, as well as the contributions from $\mathcal{H}_{\rm ex}$. In the semiclassical limit, then, we may borrow from the formalism of ZNG.

Following the ZNG theory, the equation of motion for φ may be transformed into a kinetic equation:

$$\partial_t f_{\mathbf{k}} + \frac{\mathbf{p}}{m} \cdot \nabla f_{\mathbf{k}} - \nabla U \cdot \nabla f_{\mathbf{k}} = C_{22} + C_{12} + C_{\rm sp} \tag{7.15}$$

for the distribution function $f = \langle \hat{f} \rangle$, where $\hat{f}$ is the Wigner operator

$$\hat{f}_{\mathbf{k}}(\mathbf{r}) = \int d^3r' e^{i\mathbf{k}\cdot\mathbf{r}'} \hat{\varphi}^\dagger(\mathbf{r} + \frac{1}{2}\mathbf{r}')\hat{\varphi}(\mathbf{r} - \frac{1}{2}\mathbf{r}')\,, \tag{7.16}$$

and $U = \hbar\Omega + K(n_c + 2n)/s$ is the effective potential, including mean-field effects. The collision integral C_{22} describes scattering between cloud magnons originating from $\hat{\mathcal{H}}^{(4)}_{\rm K}[\hat{\varphi}^\dagger, \hat{\varphi}]$ and $\hat{\mathcal{H}}^{(4)}_{\rm ex}[\hat{\varphi}^\dagger, \hat{\varphi}]$. Let us restrict ourselves to high temperatures $T \gg \hbar\Omega, K$; in this case, cloud magnon-magnon interactions are dominated by the latter contribution, yielding a scattering rate with a timescale τ_{22} that dominates over all others. For a hydrodynamics ansatz $f^{(e)}_{\mathbf{k}}(\mathbf{v}) = n_B[\beta(\epsilon_{\mathbf{k}-\mathbf{v}} - \mu^*)]$ (with μ^* as the local effective chemical potential), viewed from a reference frame moving at a velocity $-\mathbf{v}$, $C_{22}[f^{(e)}_{\mathbf{k}}(\mathbf{v})] = 0$; expanding $f_{\mathbf{k}}(\mathbf{v}) = f^{(e)}_{\mathbf{k}}(\mathbf{v}) + \delta f_{\mathbf{k}}(\mathbf{v})$ around this equilibrium (with $\delta f_{\mathbf{k}}(\mathbf{v})$ having a total momentum $\mathbf{p}/m$, so that it moves with the same velocity as the equilibrium distribution),

$$C_{22}[\delta f_{\mathbf{k}}(\mathbf{v})] \approx \frac{\delta f_{\mathbf{k}}(\mathbf{v})}{\tau_{22}} \tag{7.17}$$

where $\hbar\tau_{22}^{-1} \approx e^{-\beta\mu^*} T (T/T_c)^{3/2}$. Because we will focus on the regime in which driving of F is small in comparison, we are justified in assuming a hydrodynamic ansatz $f_{\mathbf{k}}(\mathbf{v}) = f^{(e)}_{\mathbf{k}}(\mathbf{v})$, so that C_{22} vanishes.

The collision integral C_{12} is given by

$$C_{12}\left[f_{\mathbf{k}},\Phi_{\mathbf{k}_c}\right]=\frac{8(K/s)^2 n_c}{(2\pi)^2 h^4}\int d^3k_1\int d^3k_2\int d^3k_3\times\delta\left(\mathbf{k}_c+\mathbf{k}_1-\mathbf{k}_2-\mathbf{k}_3\right)\delta\left(\epsilon_{\mathbf{k}_c}+\epsilon_{\mathbf{k_1}}-\epsilon_{\mathbf{k}_2}-\epsilon_{\mathbf{k}_3}\right)$$
$$\left[\delta\left(\mathbf{k}-\mathbf{k}_1\right)-\delta\left(\mathbf{k}-\mathbf{k}_2\right)-\delta\left(\mathbf{k}-\mathbf{k}_3\right)\right]\left[\left(1+f_1\right)f_2 f_3-f_1\left(1+f_2\right)\left(1+f_3\right)\right] \tag{7.18}$$

(where $\epsilon_{\mathrm{k}_c}=A\mathbf{k}_c^2+\hbar\Omega+2Kn_x+Kn_c$ is the condensate energy in the Thomas-Fermi approximation, neglecting contributions to higher order in $(K/\hbar\Omega)(n/s)$) describes three-(cloud)magnon processes which transfer $\hbar$ of angular momentum with the superfluid component Φ. These processes arise from the quartic anisotropy terms and is related to the three magnon-correlator $R=-i\Phi^{-1}(K/s)\langle\hat{\varphi}^\dagger\hat{\varphi}\hat{\varphi}\rangle$ by:

$$\frac{2}{\hbar}(n_c/s)\Re[R]=\int\frac{d^3k}{(2\pi)^3}C_{12}\equiv\Gamma\,, \tag{7.19}$$

where $\Gamma_{12}=\dot{n}_x|_{12}$ is rate of change of the magnon cloud density n_x due magnon scattering. For a hydrodynamic ansatz $f_{\mathbf{k}}^{(e)}(\mathbf{v})$, the collision integral vanishes when the cloud and condensate are in mutual equilibrium ($\mu_{\mathbf{k}_c}=m\mathbf{v}/\hbar$, $\mu_{\mathbf{k}_c}=\epsilon_{\mathbf{k}_c}-A\mathbf{k}_c^2=\mu^*+U$ or $\mu^*=0$), or when $n_c=0$, C_{12} vanishes. Near equilibrium, we can expand:

$$\Gamma=-\frac{n_c}{T\tau}\mu^* \tag{7.20}$$

where $\hbar\tau^{-1}$ is given by Eq. (6.12), which at high temperatures $T\gg\hbar\Omega$ goes $\hbar\tau^{-1}\approx(K^2/T)(T/T_c)^3/2$.

The last term, C_{sp} in Eq. (7.15), is the Berry phase term stemming from fictitious electric and magnetic fields due to the magnetic texture, with a contribution reciprocal to Eq. (7.14). A thermal magnon flux $\mathbf{j}_T$ can induce coherent dynamics at a finite wave vector $\mathbf{k}_c\sim 1/\lambda_x$, where λ_x is the exchange length; reciprocally, a dynamical magnetic texture can induce an incoherent magnon current. However in thin films (of thickness smaller than the magnetic exchange length), such as those considered in this thesis, spatial inhomogeneity of the coherent state, in contrast to the thermally activated excited magnons, is gapped out, and three-magnon scattering becomes the principle route by which coherent magnetic dynamics may be induced by the thermal cloud.

References

[AEM95] M H Anderson, J R Ensher, M R Matthews, C E Wieman, and E A Cornell. "Observation of Bose-Einstein Condensation in a Dilute Atomic Vapor." *science*, **269**(5221):198–201, July 1995.

[AIS09] K Ando, J Ieda, K Sasage, S Takahashi, S Maekawa, and E Saitoh. "Electric detection of spin wave resonance using inverse spin-Hall effect." *Applied Physics Letters*, **94**(26):262505, July 2009.

[AS12] K Ando and E Saitoh. "Spin Pumping Driven by Bistable Exchange Spin Waves." *Physical review letters*, **109**(2):026602, July 2012.

[Asi66] Joseph Richard Asik. "Spin-flip Scattering of Conduction Electrons from Impurities.", 1966.

[ATH08] K. Ando, S. Takahashi, K. Harii, K. Sasage, J. Ieda, S. Maekawa, and E. Saitoh. "Electric Manipulation of Spin Relaxation Using the Spin Hall Effect." *Phys. Rev. Lett.*, **101**:036601, Jul 2008.

[ATI11] K Ando, S Takahashi, J Ieda, Y Kajiwara, H Nakayama, T Yoshino, K Harii, Y Fujikawa, M Matsuo, S Maekawa, and E Saitoh. "Inverse spin-Hall effect induced by spin pumping in metallic system." *Journal of Applied Physics*, **109**(10):103913, May 2011.

[AUS13] H Adachi, K Uchida, and E Saitoh. "Theory of the spin Seebeck effect." *Reports on Progress in ...*, 2013.

[Bau] Gerrit E. W. Bauer. "Spin Caloritronics." arXiv:1107.4395.

[BBF88] M N Baibich, J M Broto, A Fert, F Nguyen Van Dau, and F Petroff. "Giant Magnetoresistance of (001)Fe/(001)Cr Magnetic Superlattices." *Phys. Rev. Lett.*, **61**(21):2472–2475, November 1988.

[BBK06] Arne Brataas, Gerrit E. W. Bauer, and Paul J. Kelly. "Non-collinear magnetoelectronics." *Phys. Rep.*, **427**:157–255, 2006.

[BDB14] Scott A. Bender, Rembert A. Duine, Arne Brataas, and Yaroslav Tserkovnyak. "Dynamic phase diagram of dc-pumped magnon condensates." *Phys. Rev. B*, **90**:094409, Sep 2014.

[BDT12] Scott A. Bender, Rembert A. Duine, and Yaroslav Tserkovnyak. "Electronic Pumping of Quasiequilibrium Bose-Einstein-Condensed Magnons." *Phys. Rev. Lett.*, **108**:246601, Jun 2012.

[Ber70] L Berger. "Side-jump mechanism for the Hall effect of ferromagnets." *Physical Review B*, 1970.

[Ber84] Michael V Berry. "Quantal phase factors accompanying adiabatic changes." *Proc.Roy.Soc.Lond.*, **A392**:45–57, 1984.

[Ber96a] L. Berger. "Emission of spin waves by a magnetic multilayer traversed by a current." *Phys. Rev. B*, **54**(13):9353–9358, 1996.

[Ber96b] L Berger. "Emission of spin waves by a magnetic multilayer traversed by a current." *Physical Review B*, **54**(13):9353–9358, October 1996.

[BF04] Henrik Bruus and Karsten Flensberg. *Many-Body Quantum Theory in Condensed Matter Physics: An Introduction*. Oxford University Press, September 2004.

[BFG05] J Barnaś, A Fert, M Gmitra, I Weymann, and V Dugaev. "From giant magnetoresistance to current-induced switching by spin transfer." *Physical Review B*, **72**(2):024426, July 2005.

[BGS89] G Binasch, P Grünberg, F Saurenbach, and W Zinn. "Enhanced magnetoresistance in layered magnetic structures with antiferromagnetic interlayer exchange." *Phys. Rev. Lett.*, **39**(7):4828–4830, March 1989.

[BH94] J Anthony C Bland and Bretislav Heinrich, editors. *Ultrathin Magnetic Structures I*. Springer Berlin Heidelberg, Berlin, Heidelberg, 1994.

[BH14] Arne Brataas and Kjetil M. D. Hals. "Spin–orbit torques in action." *Nat. Nanotechnol.*, **9**:86–88, 2014.

[BHK12a] C. Burrowes, B. Heinrich, B. Kardasz, E. A. Montoya, E. Girt, Yiyan Sun, Young-Yeal Song, and Mingzhong Wu. "Enhanced spin pumping at yttrium iron garnet/Au interfaces." *Appl. Phys. Lett.*, **100**(9):092403, 2012.

[BHK12b] C Burrowes, B Heinrich, B Kardasz, E A Montoya, E Girt, Yiyan Sun, Young-Yeal Song, and Mingzhong Wu. "Enhanced spin pumping at yttrium iron garnet/Au interfaces." *Applied Physics Letters*, **100**(9):092403, March 2012.

[BJZ98] Ya B Bazaliy, B A Jones, and S C Zhang. "Modification of the Landau-Lifshitz Equation in the Presence of a Spin-Polarized Current in CMR and GMR Materials." *Phys. Rev. B*, **57**(cond-mat/9706132. 6):3213–3216, 1998.

[BLV73] S. Bhagat, H. Lessoff, C. Vittoria, and C. Guenzer. "Spin-Wave Resonance Studies on Chemical Vapor Deposited YIG Films." *Phys. Status Solidi*, **20**:731–738, 1973.

[BMB05] S Bayrakci, I Mirebeau, P Bourges, Y Sidis, M Enderle, J Mesot, D Chen, C Lin, and B Keimer. "Magnetic Ordering and Spin Waves in Na0.82CoO2." *Physical review letters*, **94**(15):157205, April 2005.

[BNB00] Arne Brataas, Yu. V. Nazarov, and Gerrit E. W. Bauer. "Finite-Element Theory of Transport in Ferromagnet–Normal Metal Systems." *Phys. Rev. Lett.*, **84**(11):2481–2484, 2000.

[BNB01] A Brataas, Y V Nazarov, and GEW Bauer. "Spin-transport in multi-terminal normal metal-ferromagnet systems with non-collinear magnetizations." *The European Physical Journal B- ...*, 2001.

[BPT93] M Buttiker, A Prêtre, and H Thomas. "Dynamic conductance and the scattering matrix of small conductors." *Physical review letters*, 1993.

[Bro98a] P W Brouwer. "Scattering approach to parametric pumping." *Physical Review B*, 1998.

[Bro98b] P. W. Brouwer. "Scattering approach to parametric pumping." *Phys. Rev. B*, **58**(16):R10135–R10138, 1998.

[BSv12a] Gerrit E. W. Bauer, Eiji Saitoh, and Bart J. van Wees. "Spin caloritronics." *Nat. Mater.*, **11**:391–399, 2012.

[BSV12b] GEW Bauer, E Saitoh, and B J Van Wees. "Spin caloritronics." *Nature Materials*, 2012.

[BT] Scott A. Bender and Yaroslav Tserkovnyak. "Interfacial Spin and Heat Transfer between Metals and Magnetic Insulators." arXiv:1409.7128.

[BT12] A Brataas and Y Tserkovnyak. "Spin Pumping and Spin Transfer." pp. 1–30, March 2012.

[BT14] Scott A Bender and Yaroslav Tserkovnyak. "Interfacial Spin and Heat Transfer between Metals and Magnetic Insulators." *arXiv.org*, September 2014.

[BTB06] A Brataas, Y Tserkovnyak, and GEW Bauer. "Current-induced macrospin versus spin-wave excitations in spin valves." *Physical Review B*, 2006.

[BTB10] Scott A Bender, Yaroslav Tserkovnyak, and Arne Brataas. "Microwave response of a magnetic single-electron transistor." *Physical Review B*, **82**(18):180403, November 2010.

[But92] M Buttiker. "Scattering theory of current and intensity noise correlations in conductors and wave guides." *Physical Review B*, 1992.

[BV10a] Yuriy M Bunkov and Grigory E Volovik. "Magnon Bose–Einstein condensation and spin superfluidity." *Journal of Physics: Condensed Matter*, **22**(16):164210, March 2010.

[BV10b] Yuriy M. Bunkov and Grigory E. Volovik. "Magnon Bose–Einstein condensation and spin superfluidity." *J. Phys.: Condens. Matter*, **22**:164210, 2010.

[CCA10] Y. L. Chen, J.-H. Chu, J. G. Analytis, Z. K. Liu, K. Igarashi, H.-H. Kuo, X. L. Qi, S. K. Mo, R. G. Moore, D. H. Lu, M. Hashimoto, T. Sasagawa, S. C. Zhang, I. R. Fisher, Z. Hussain, and Z. X. Shen. "Massive Dirac Fermion on the Surface of a Magnetically Doped Topological Insulator." *Science*, **329**:659–662, 2010.

[CJ65] J B Comly and R V Jones. "Parallel-Pumped Instabilities in Magnetic Metal Films." *Journal of Applied Physics*, **36**(3):1201, 1965.

[CMD09] A Chumak, G Melkov, V Demidov, O Dzyapko, V Safonov, and S Demokritov. "Bose-Einstein Condensation of Magnons under Incoherent Pumping." *Physical review letters*, **102**(18):187205, May 2009.

[CMM06] A T Costa, R B Muniz, and D L Mills. "Ferromagnetic resonance linewidths in ultrathin structures: A theoretical study of spin pumping." *Physical Review B*, 2006.

[Com64] R L Comstock. "Parallel Pumping of Magnetoelastic Waves in Ferromagnets." *Journal of Applied Physics*, **35**(8):2427, 1964.

[CSW06] M V Costache, M Sladkov, S M Watts, C H Van der Wal, and B J Van Wees. "Electrical detection of spin pumping due to the precessing magnetization of a single ferromagnet." Technical report, September 2006.

[CTN13] Yan-Ting Chen, Saburo Takahashi, Hiroyasu Nakayama, Matthias Althammer, Sebastian T. B. Goennenwein, Eiji Saitoh, and Gerrit E. W. Bauer. "Theory of spin Hall magnetoresistance." *Phys. Rev. B*, **87**:144411, Apr 2013.

[CYO12] Joseph G. Checkelsky, Jianting Ye, Yoshinori Onose, Yoshihiro Iwasa, and Yoshinori Tokura. "Dirac-fermion-mediated ferromagnetism in a topological insulator." *Nature Phys.*, **8**:729–733, 2012.

[DDD06a] S O Demokritov, V E Demidov, O Dzyapko, G A Melkov, A A Serga, B Hillebrands, and A N Slavin. "Bose-Einstein condensation of quasi-equilibrium magnons at room temperature under pumping." *Nature*, **443**(7110):430–433, September 2006.

[DDD06b] S. O. Demokritov, V. E. Demidov, O. Dzyapko, G. A. Melkov, A. A. Serga, B. Hillebrands, and A. N. Slavin. "Bose-Einstein condensation of quasi-equilibrium magnons at room temperature under pumping." *Nature*, **443**:430–433, 2006.

[DDD08] V. E. Demidov, O. Dzyapko, S. O. Demokritov, G. A. Melkov, and A. N. Slavin. "Observation of Spontaneous Coherence in Bose-Einstein Condensate of Magnons." *Phys. Rev. Lett.*, **100**:047205, Jan 2008.

[DE61] R W Damon and J R Eshbach. "Magnetostatic modes of a ferromagnet slab." *Journal of Physics and Chemistry of Solids*, **19**(3-4):308–320, May 1961.

[Dem01] S Demokritov. "Brillouin light scattering studies of confined spin waves: linear and nonlinear confinement." *Physics Reports*, **348**(6):441–489, July 2001.

[Dol12] Voicu O Dolocan. "Spin-torque effect on spin wave modes in magnetic nanowires." *Applied Physics Letters*, **101**(7):072409, August 2012.

[DP71a] M I D'yakonov and V I Perel. "Current-induced spin orientation of electrons in semiconductors." *Physics Letters A*, 1971.

[DP71b] M I D'yakonov and V I Perel. "Possibility of orienting electron spins with current." *Soviet Journal of Experimental and ...*, 1971.

[DS12] Sergej O Demokritov and Andrei N Slavin. *Magnonics*. From Fundamentals to Applications. Springer Science & Business Media, August 2012.

[ECS12] Mikhail Erekhinsky, Fèlix Casanova, Ivan K Schuller, and Amos Sharoni. "Spin-dependent Seebeck effect in non-local spin valve devices." *Applied Physics Letters*, **100**(21):212401, May 2012.

[Ede95] Victor M. Edelstein. "Band-spin-orbit-energy effects in conductivity of two-dimensional weakly disordered semiconductor systems." *J. Phys.: Condens. Matter*, **7**:1–18, 1995.

[FBS12] J Flipse, F L Bakker, A Slachter, and F K Dejene. "Direct observation of the spin-dependent Peltier effect." *Nature*, 2012.

[FD87] T A Fulton and G J Dolan. "Observation of single-electron charging effects in small tunnel junctions." *Phys. Rev. Lett.*, **59**:109–112, 1987.

[FDW14] J. Flipse, F. K. Dejene, D. Wagenaar, G. E. W. Bauer, J. Ben Youssef, and B. J. van Wees. "Observation of the Spin Peltier Effect for Magnetic Insulators." *Phys. Rev. Lett.*, **113**:027601, Jul 2014.

[FSS06] M Fähnle, R Singer, D Steiauf, and V Antropov. "Role of nonequilibrium conduction electrons on the magnetization dynamics of ferromagnets in the s-d model." *Physical Review B*, **73**(17):172408, May 2006.

[FUK14a] Yabin Fan, Pramey Upadhyaya, Xufeng Kou, Murong Lang, So Takei, Zhenxing Wang, Jianshi Tang, Liang He, Li-Te Chang, Mohammad Montazeri, Guoqiang Yu, Wanjun Jiang, Tianxiao Nie, Robert N Schwartz, Yaroslav Tserkovnyak, and Kang L Wang. "Magnetization switching through giant spin–orbit torque in a magnetically doped topological insulator heterostructure." *Nature Materials*, **13**(7):699–704, April 2014.

[FUK14b] Yabin Fan, Pramey Upadhyaya, Xufeng Kou, Murong Lang, So Takei, Zhenxing Wang, Jianshi Tang, Liang He, Li-Te Chang, Mohammad Montazeri, Guoqiang Yu, Wanjun Jiang, Tianxiao Nie, Robert N. Schwartz, Yaroslav Tserkovnyak, and Kang L. Wang. "Magnetization switching through giant spin-orbit torque in a magnetically doped topological insulator heterostructure." *Nat. Mater.*, **13**:699–704, 2014.

[GCH01] J Grollier, V Cros, A Hamzic, J M George, H Jaffrès, A Fert, G Faini, J Ben Youssef, and H Legall. "Spin-polarized current induced switching in Co/Cu/Co pillars." *Applied Physics Letters*, **78**(23):3663, 2001.

[Gil04a] T L Gilbert. "Classics in Magnetics A Phenomenological Theory of Damping in Ferromagnetic Materials." *Magnetics, IEEE Transactions on*, **40**(6):3443–3449, November 2004.

[Gil04b] Thomas L. Gilbert. "A Phenomenological Theory of Damping in Ferromagnetic Materials." *IEEE Trans. Magn.*, **40**(6):3443–3449, 2004.

[GM96] A G Gurevich and G A Melkov. "Magnetization oscillations and waves." 1996.

[GMC08] G Y Guo, S Murakami, T W Chen, and N Nagaosa. "Intrinsic Spin Hall Effect in Platinum: First-Principles Calculations." *Phys. Rev. Lett.*, **100**:096401, 2008.

[GSR06] L Gravier, S Serrano-Guisan, F Reuse, and J P Ansermet. "Spin-dependent Peltier effect of perpendicular currents in multilayered nanowires." *Physical Review B*, 2006.

[Gui06] Santiago Serrano Guisán. "Spin Dependent Thermoelectric Effects in Magnetic Nanostructures.", 2006.

[HBM11] B. Heinrich, C. Burrowes, E. Montoya, B. Kardasz, E. Girt, Young-Yeal Song, Yiyan Sun, and Mingzhong Wu. "Spin Pumping at the Magnetic Insulator (YIG)/Normal Metal (Au) Interfaces." *Phys. Rev. Lett.*, **107**:066604, Aug 2011.

[HBT10] K. M. D. Hals, A. Brataas, and Y. Tserkovnyak. "Scattering theory of charge-current–induced magnetization dynamics." *Europhys. Lett.*, **90**:47002, 2010.

[HBZ07] Moosa Hatami, Gerrit Bauer, Qinfang Zhang, and Paul Kelly. "Thermal Spin-Transfer Torque in Magnetoelectronic Devices." *Physical review letters*, **99**(6):066603, August 2007.

[HdH] A. Hamadeh, O. d'Allivy Kelly, C. Hahn, H. Meley, R. Bernard, A. H. Molpeceres, V. V. Naletov, M. Viret, A. Anane, V. Cros, S. O. Demokritov, J. L. Prieto, M. Munöz, G. de Loubens, and O. Klein. "Electronic control of the spin-wave damping in a magnetic insulator." arXiv:1405.7415.

[HdK13] C. Hahn, G. de Loubens, O. Klein, M. Viret, V. V. Naletov, and J. Ben Youssef. "Comparative measurements of inverse spin Hall effects and magnetoresistance in YIG/Pt and YIG/Ta." *Phys. Rev. B*, **87**:174417, May 2013.

[HFC14] Christian Heiliger, C Franz, and Michael Czerner. "Thermal spin-transfer torque in magnetic tunnel junctions (invited)." *Journal of Applied Physics*, **115**(17):172614, April 2014.

[HI99] TOSHIRO HIRAMOTO and HIROKI ISHIKURO. "Coulomb blockade in VLSI-compatible multiple-dot and single-dot MOSFETs." *International Journal of Electronics*, **86**(5):591–603, May 1999.

[Hir99] J Hirsch. "Spin Hall Effect." *Physical review letters*, **83**(9):1834–1837, August 1999.

[HK13] S Hu and T Kimura. "Anomalous Nernst-Ettingshausen effect in nonlocal spin valve measurement under high-bias current injection." *Physical Review B*, 2013.

[HLL13] Paul M. Haney, Hyun-Woo Lee, Kyung-Jin Lee, Aurélien Manchon, and M. D. Stiles. "Current induced torques and interfacial spin-orbit coupling: Semiclassical modeling." *Phys. Rev. B*, **87**:174411, May 2013.

[HOT09] Pham Nam Hai, Shinobu Ohya, Masaaki Tanaka, Stewart E. Barnes, and Sadamichi Maekawa. "Electromotive force and huge magnetoresistance in magnetic tunnel junctions." *Nature*, **458**:489–492, 2009.

[HP40a] T Holstein and H Primakoff. "Field dependence of the intrinsic domain magnetization of a ferromagnet." *Physical Review*, 1940.

[HP40b] T. Holstein and H. Primakoff. "Field Dependence of the Intrinsic Domain Magnetization of a Ferromagnet." *Phys. Rev.*, **58**(12):1098–1113, Dec 1940.

[HST13] Silas Hoffman, Koji Sato, and Yaroslav Tserkovnyak. "Landau-Lifshitz theory of the longitudinal spin Seebeck effect." *Phys. Rev. B*, **88**:064408, Aug 2013.

[HUW02] B Heinrich, R Urban, and G Woltersdorf. "Magnetic relaxation in metallic films: Single and multilayer structures." *Journal of Applied Physics*, **91**(10):7523–7525, 2002.

[IRL02] S Ingvarsson, L Ritchie, X Liu, Gang Xiao, J Slonczewski, P Trouilloud, and R Koch. "Role of electron scattering in the magnetization relaxation of thin Ni81Fe19 films." *Physical Review B*, **66**(21):214416, December 2002.

[JAA13] M. B. Jungfleisch, T. An, K. Ando, Y. Kajiwara, K. Uchida, V. I. Vasyuchka, A. V. Chumak, A. A. Serga, E. Saitoh, and B. Hillebrands. "Heat-induced damping modification in yttrium iron garnet/platinum hetero-structures." *Appl. Phys. Lett.*, **102**(6):062417, 2013.

[JDM99] J Jorzick, S O Demokritov, C Mathieu, and B Hillebrands. "Brillouin light scattering from quantized spin waves in micron-size magnetic wires." *Physical Review B*, 1999.

[Jul75] M Julliere. "Tunneling between ferromagnetic films." *Physics Letters A*, **54**(3):225–226, September 1975.

[JXB11] Xingtao Jia, Ke Xia, and Gerrit E W Bauer. "Thermal Spin Transfer in Fe-MgO-Fe Tunnel Junctions." *Physical review letters*, **107**(17):176603, October 2011.

[KB13] André Kapelrud and Arne Brataas. "Spin Pumping and Enhanced Gilbert Damping in Thin Magnetic Insulator Films." *Phys. Rev. Lett.*, **111**:097602, Aug 2013.

[KDD11] H Kurebayashi, O Dzyapko, and V E Demidov. "Spin pumping by parametrically excited short-wavelength spin waves." *Applied Physics ...*, 2011.

[KHT10a] Y Kajiwara, K Harii, S Takahashi, J Ohe, and K Uchida. "Transmission of electrical signals by spin-wave interconversion in a magnetic insulator." *Nature*, 2010.

[KHT10b] Y. Kajiwara, K. Harii, S. Takahashi, J. Ohe, K. Uchida, M. Mizuguchi, H. Umezawa, H. Kawai, K. Ando, K. Takanashi, S. Maekawa, and E. Saitoh. "Transmission of electrical signals by spin-wave interconversion in a magnetic insulator." *Nature*, **464**:262–266, 2010.

[Kit58] C Kittel. "Interaction of Spin Waves and Ultrasonic Waves in Ferromagnetic Crystals." *Physical Review*, **110**(4):836–841, May 1958.

[KKD95] M P Kostylev, B A Kalinikos, and H Dötsch. "Parallel pump spin wave instability threshold in thin ferromagnetic films." *Journal of Magnetism and Magnetic Materials*, **145**(1-2):93–110, March 1995.

[KL54] R Karplus and J M Luttinger. "Hall effect in ferromagnetics." *Physical Review*, 1954.

[KOS07] T Kimura, Y Otani, T Sato, S Takahashi, and S Maekawa. "Room-Temperature Reversible Spin Hall Effect." *Physical review letters*, **98**(15):156601, April 2007.

[KPR04] S Kaka, M Pufall, W Rippard, T Silva, S E Russek, J Katine, and M Carey. "Spin transfer switching of spin valve nanopillars using nanosecond pulsed currents." Technical report, November 2004.

[KRK06] J Kasprzak, M Richard, S Kundermann, A Baas, P Jeambrun, J M J Keeling, F M Marchetti, M H Szymańska, R André, J L Staehli, V Savona, P B Littlewood, B Deveaud, and Le Si Dang. "Bose–Einstein condensation of exciton polaritons." *Nature*, **443**(7110):409–414, September 2006.

[KRL97] D L Klein, R S Roth, A K L Lim, A P Alivisatos, and P L McEuen. "A single-electron transistor made from a cadmium selenide nanocrystal." *Nature*, **389**(cond-mat/9710326):699, 1997.

[KS89a] Yu. D. Kalafati and V. L. Safonov. "Possibility of Bose condensation of magnons excited by incoherent pump." *JETP Lett.*, **50**:149–151, 1989.

[KS89b] B A Kalinkos and A N Slavin. "Theory of dipole-exchange spin wave excitation for ferromagnetic films with mixed exchange boundary conditions." In *International Magnetics Conference*, pp. BP13–BP13. IEEE, 1989.

[KS91] Yu. D. Kalafati and V. L. Safonov. "Theory of quasiequilibrium effects in a system of magnons excited by incoherent pumping." *Sov. Phys. JETP*, **73**(5):836–841, 1991.

[KSA08] J Kasprzak, D Solnyshkov, R André, Le Dang, and G Malpuech. "Formation of an Exciton Polariton Condensate: Thermodynamic versus Kinetic Regimes." *Physical review letters*, **101**(14):146404, October 2008.

[KSD11] J Klaers, J Schmitt, T Damm, F Vewinger, and M Weitz. "Bose–Einstein condensation of paraxial light." *Applied Physics B*, **105**(1):17–33, September 2011.

[KSK03] S. I. Kiselev, J. C. Sankey, I. N. Krivorotov, N. C. Emley, R. J. Schoelkopf, R. A. Buhrman, and D. C. Ralph. "Microwave oscillations of a nanomagnet driven by a spin-polarized current." *Nature*, **425**:380–383, 2003.

[KSV10] Jan Klaers, Julian Schmitt, Frank Vewinger, and Martin Weitz. "Bose-Einstein condensation of photons in an optical microcavity." *Nature*, **468**(7323):545–548, July 2010.

[KT12] Alexey A Kovalev and Yaroslav Tserkovnyak. "Thermomagnonic spin transfer and Peltier effects in insulating magnets." *EPL (Europhysics Letters)*, **97**(6):67002, March 2012.

[Lan68] J S Langer. "Coherent States in the Theory of Superfluidity." *Phys.Rev.*, **167**:183–190, 1968.

[LF11] R Lassalle-Balier and C Fermon. "Spin wave propagation in ferromagnetic wires with an arbitrary field direction." *Journal of Physics: Conference ...*, 2011.

[LH72] S K Lyo and T Holstein. "Side-jump mechanism for ferromagnetic Hall effect." *Physical review letters*, 1972.

[LHZ05] Z Li, J He, and S Zhang. "Magnetization instability driven by spin torques." *Journal of Applied Physics*, 2005.

[LL80a] L. D. Landau and E. M. Lifshitz. *Statistical Physics, Part 1*, volume 5 of *Course of Theoretical Physics*. Pergamon, Oxford, 3rd edition, 1980.

[LL80b] Lev Davidovich Landau and Evgenii Mikhailovich Lifshitz. *Statistical physics; 3rd ed.* Course of theoretical physics. Butterworth, Oxford, 1980.

[LMR11a] Luqiao Liu, Takahiro Moriyama, D C Ralph, and R A Buhrman. "Spin-Torque Ferromagnetic Resonance Induced by the Spin Hall Effect." *Physical review letters*, **106**(3):036601, January 2011.

[LMR11b] Luqiao Liu, Takahiro Moriyama, D. C. Ralph, and R. A. Buhrman. "Spin-Torque Ferromagnetic Resonance Induced by the Spin Hall Effect." *Phys. Rev. Lett.*, **106**:036601, Jan 2011.

[LP80] E. M. Lifshitz and L. P. Pitaevskii. *Statistical Physics, Part 2*, volume 9 of *Course of Theoretical Physics*. Pergamon, Oxford, 3rd edition, 1980.

[LPL12a] L Liu, C F Pai, Y Li, H W Tseng, D C Ralph, and R A Buhrman. "Spin-Torque Switching with the Giant Spin Hall Effect of Tantalum." *science*, **336**(6081):555–558, May 2012.

[LPL12b] Luqiao Liu, Chi-Feng Pai, Y. Li, H. W. Tseng, D. C. Ralph, and R. A. Buhrman. "Spin-Torque Switching with the Giant Spin Hall Effect of Tantalum." *Science*, **336**:555–558, 2012.

[LSJ12a] Lei Lu, Yiyan Sun, Michael Jantz, and Mingzhong Wu. "Control of Ferromagnetic Relaxation in Magnetic Thin Films through Thermally Induced Interfacial Spin Transfer." *Phys. Rev. Lett.*, **108**:257202, Jun 2012.

[LSJ12b] Lei Lu, Yiyan Sun, Michael Jantz, and Mingzhong Wu. "Control of Ferromagnetic Relaxation in Magnetic Thin Films through Thermally Induced Interfacial Spin Transfer." *Physical review letters*, **108**(25):257202, June 2012.

[LYB07] Leonid Lutsev, Sergey Yakovlev, and Christian Brosseau. "Spin wave spectroscopy and microwave losses in granular two-phase magnetic nanocomposites." *Journal of Applied Physics*, **101**(3):034320, February 2007.

[MAM02] S Mizukami, Y Ando, and T Miyazaki. "Effect of spin diffusion on Gilbert damping for a very thin permalloy layer in Cu/permalloy/Cu/Pt films." *Physical Review B*, **66**(10):104413, September 2002.

[MB02] M Moskalets and M Buttiker. "Floquet scattering theory of quantum pumps." *Physical Review B*, 2002.

[MB04] M Moskalets and M Buttiker. "Floquet scattering theory for current and heat noise in large amplitude adiabatic pumps." *Phys. Rev. B*, **70**(cond-mat/0407292):245305, 2004.

[MBC11] M Madami, S Bonetti, G Consolo, S Tacchi, G Carlotti, G Gubbiotti, F B Mancoff, M A Yar, and J Åkerman. "Direct observation of a propagating spin wave induced by spin-transfer torque." *Nature nanotechnology*, **6**(10):635–638, August 2011.

[MCF08] T. Moriyama, R. Cao, X. Fan, G. Xuan, B. K. Nikolić, Y. Tserkovnyak, J. Kolodzey, and John Q. Xiao. "Tunnel Barrier Enhanced Voltage Signal Generated by Magnetization Precession of a Single Ferromagnetic Layer." *Phys. Rev. Lett.*, **100**(6):067602, 2008.

[MGA10] Ioan Mihai Miron, Gilles Gaudin, Stéphane Auffret, Bernard Rodmacq, Alain Schuhl, Stefania Pizzini, Jan Vogel, and Pietro Gambardella. "Current-driven spin torque induced by the Rashba effect in a ferromagnetic metal layer." *Nat. Mater.*, **9**:230–234, 2010.

[MGG11] Ioan Mihai Miron, Kevin Garello, Gilles Gaudin, Pierre-Jean Zermatten, Marius V. Costache, Stéphane Auffret, Sébastien Bandiera, Bernard Rodmacq, Alain Schuhl, and Pietro Gambardella. "Perpendicular switching of a single ferromagnetic layer induced by in-plane current injection." *Nature*, **476**:189–193, 2011.

[MPF10] O. Mosendz, J. E. Pearson, F. Y. Fradin, G. E. W. Bauer, S. D. Bader, and A. Hoffmann. "Quantifying Spin Hall Angles from Spin Pumping: Experiments and Theory." *Phys. Rev. Lett.*, **104**(4):046601, Jan 2010.

[MRK99] E. B. Myers, D. C. Ralph, J. A. Katine, R. N. Louie, and R. A. Buhrman. "Current-Induced Switching of Domains in Magnetic Multilayer Devices." *Science*, **285**:867–870, 1999.

[MRK06] S Mangin, D Ravelosona, J A Katine, M J Carey, B D Terris, and Eric E Fullerton. "Current-induced magnetization reversal in nanopillars with perpendicular anisotropy." *Nature Materials*, **5**(3):210–215, February 2006.

[MVS12] Sadamichi Maekawa, Sergio O Valenzuela, Eiji Saitoh, and Takashi Kimura. *Spin Current*. Oxford University Press, July 2012.

[NAC13] H. Nakayama, M. Althammer, Y.-T. Chen, K. Uchida, Y. Kajiwara, D. Kikuchi, T. Ohtani, S. Geprägs, M. Opel, S. Takahashi, R. Gross, G. E. W. Bauer, S. T. B. Goennenwein, and E. Saitoh. "Spin Hall Magnetoresistance Induced by a Nonequilibrium Proximity Effect." *Phys. Rev. Lett.*, **110**:206601, May 2013.

[Nag06] N Nagaosa. "Anomalous Hall Effect–A New Perspective–." *Journal of the Physical Society of Japan*, 2006.

[NB00] Y Nazarov and G Bauer. "Finite-element theory of transport in ferromagnet–normal metal systems." *Physical review letters*, 2000.

[NB09] Yuli V. Nazarov and Yaroslav M. Blanter. *Quantum Transport*. Cambridge University Press, Cambridge, 2009.

[NKT96] Y Nakamura, D L Klein, and J S Tsai. "Al/Al2O3/Al single electron transistors operable up to 30 K utilizing anodization controlled miniaturization enhancement." *Applied Physics Letters*, **68**(2):275, 1996.

[NKW12] Y Niimi, Y Kawanishi, D H Wei, C Deranlot, H X Yang, M Chshiev, T Valet, A Fert, and Y Otani. "Giant Spin Hall Effect Induced by Skew Scattering from Bismuth Impurities inside Thin Film CuBi Alloys." *Physical review letters*, **109**(15):156602, October 2012.

[NSO10] N Nagaosa, J Sinova, S Onoda, and A H MacDonald. "Anomalous hall effect." *Reviews of Modern . . .*, 2010.

[OHB14] M Obstbaum, M Härtinger, H G Bauer, and T Meier. "Inverse spin Hall effect in Ni 81 Fe 19/normal-metal bilayers." *Physical Review B*, 2014.

[PAR11a] E. Padrón-Hernández, A. Azevedo, and S. M. Rezende. "Amplification of Spin Waves by Thermal Spin-Transfer Torque." *Phys. Rev. Lett.*, **107**:197203, Nov 2011.

[PAR11b] E Padrón-Hernández, A Azevedo, and S M Rezende. "Amplification of Spin Waves by Thermal Spin-Transfer Torque." *Physical review letters*, **107**(19):197203, November 2011.

[PAR11c] E Padrón-Hernández, A Azevedo, and S M Rezende. "Amplification of spin waves in yttrium iron garnet films through the spin Hall effect." *Applied Physics Letters*, **99**(19):192511, November 2011.

[Pec88] Louis Pecora. "Derivation and generalization of the Suhl spin-wave instability relations." *Physical Review B*, **37**(10):5473–5477, April 1988.

[PO56] O Penrose and L Onsager. "Bose-Einstein condensation and liquid helium." *Physical Review*, 1956.

[RBT97] D C Ralph, C T Black, and M Tinkham. "Phys. Rev. Lett. 78, 4087 (1997) - Gate-Voltage Studies of Discrete Electronic States in Aluminum Nanoparticles." *Physical review letters*, 1997.

[RCF03] C Rüegg, N Cavadini, A Furrer, H U Güdel, and K Krämer. "Bose–Einstein condensation of the triplet states in the magnetic insulator TlCuCl3." *Nature*, 2003.

[RRS13] S M Rezende, R L Rodríguez-Suárez, M M Soares, L H Vilela-Leão, D Ley Domínguez, and A Azevedo. "Enhanced spin pumping damping in yttrium iron garnet/Pt bilayers." *Applied Physics Letters*, **102**(1):012402, January 2013.

[RS08] D. C. Ralph and M. D. Stiles. "Spin Transfer Torques." *J. Magn. Magn. Mater.*, **320**:1190–1216, 2008.

[RSL00] P Recher, E V Sukhorukov, and D Loss. "Phys. Rev. Lett. 85, 1962 (2000) - Quantum Dot as Spin Filter and Spin Memory." *Physical review letters*, 2000.

[RZ69] S M Rezende and N Zagury. "Coherent magnon states." *Physics Letters A*, **29**(1):47–48, March 1969.

[SB60] R N Sinclair and B N Brockhouse. "Dispersion relation for spin waves in a fcc cobalt alloy." *Physical Review*, 1960.

[SB04] Dominik V. Scheible and Robert H. Blick. "Silicon nanopillars for mechanical single-electron transport." *Appl. Phys. Lett.*, **84**(23):4632–4634, 2004.

[SGK08] Janine Splettstoesser, Michele Governale, and Jürgen König. "Adiabatic charge and spin pumping through quantum dots with ferromagnetic leads." *Phys. Rev. B*, **77**(19):195320, May 2008.

[SKA10a] C W Sandweg, Y Kajiwara, K Ando, E Saitoh, and B Hillebrands. "Enhancement of the spin pumping efficiency by spin wave mode selection." *Applied Physics Letters*, **97**(25):252504, December 2010.

[SKA10b] C. W. Sandweg, Y. Kajiwara, K. Ando, E. Saitoh, and B. Hillebrands. "Enhancement of the spin pumping efficiency by spin wave mode selection." *Appl. Phys. Lett.*, **97**(25):252504, 2010.

[SKC11a] C W Sandweg, Y Kajiwara, A V Chumak, and A A Serga. "Phys. Rev. Lett. 106, 216601 (2011) - Spin Pumping by Parametrically Excited Exchange Magnons." *Physical Review*, 2011.

[SKC11b] C. W. Sandweg, Y. Kajiwara, A. V. Chumak, A. A. Serga, V. I. Vasyuchka, M. B. Jungfleisch, E. Saitoh, and B. Hillebrands. "Spin Pumping by Parametrically Excited Exchange Magnons." *Phys. Rev. Lett.*, **106**(21):216601, May 2011.

[Slo96] J. C. Slonczewski. "Current-driven excitation of magnetic multilayers." *J. Magn. Magn. Mater.*, **159**:L1–L7, 1996.

[Slo10a] John C. Slonczewski. "Initiation of spin-transfer torque by thermal transport from magnons." *Phys. Rev. B*, **82**(5):054403, Aug 2010.

[Slo10b] John C Slonczewski. "Initiation of spin-transfer torque by thermal transport from magnons." *Physical Review B*, **82**(5):054403, August 2010.

[Smi58] J Smit. "The spontaneous Hall effect in ferromagnetics II." *Physica*, 1958.

[SMM97] J Shirakashi, K Matsumoto, and N Miura. "Single-electron transistors (SETs) with Nb/Nb oxide system fabricated by atomic force microscope (AFM) nano-oxidation process." *Japanese journal of ...*, 1997.

[SN99] Ganesh Sundaram and Qian Niu. "Wave-packet dynamics in slowly perturbed crystals: Gradient corrections and Berry-phase effects." *Phys.Rev.*, **B59**(cond-mat/9908003. 23):14915–14925, 1999.

[Son10] E. B. Sonin. "Spin currents and spin superfluidity." *Adv. Phys.*, **59**(3):181–255, 2010.

[SSV12] A A Serga, C W Sandweg, V I Vasyuchka, M B Jungfleisch, B Hillebrands, A Kreisel, P Kopietz, and M P Kostylev. "Brillouin light scattering spectroscopy of parametrically excited dipole-exchange magnons." *arXiv.org*, **cond-mat.mes-hall**, May 2012.

[SSY80] V P Seminozhenko, V L Sobolev, and A Yatsenko. "Excitation of Spin Waves by Parallel Pumping in Ferromagnets with Magnetic Inhomogeneities." *SOV PHYS JETP*, 1980.

[Suh57] H. Suhl. "The theory of ferromagnetic resonance at high magnetic field." *J. Phys. Chem. Solids*, **1**:209–227, 1957.

[Suh58] H Suhl. "Origin and Use of Instabilities in Ferromagnetic Resonance." *Journal of Applied Physics*, **29**(3):416, 1958.

[TB02a] Y Tserkovnyak and A Brataas. "Enhanced Gilbert damping in thin ferromagnetic films." *Physical review letters*, 2002.

[TB02b] Y Tserkovnyak and A Brataas. "Spin pumping and magnetization dynamics in metallic multilayers." *Physical Review B*, **66**(cond-mat/0208091):224403, 2002.

[TB05] Yaroslav Tserkovnyak and Arne Brataas. "Spontaneous-symmetry-breaking mechanism of adiabatic pumping." *Phys. Rev. B*, **71**(5):052406, 2005.

[TB14a] Yaroslav Tserkovnyak and Scott A Bender. "Spin Hall phenomenology of magnetic dynamics." May 2014.

[TB14b] Yaroslav Tserkovnyak and Scott A Bender. "Spin Hall phenomenology of magnetic dynamics." *Physical Review B*, **90**(1):014428, July 2014.

[TBB01] Y Tserkovnyak, A Brataas, and G E W Bauer. "Enhanced Gilbert Damping in Thin Ferromagnetic Films." *Phys. Rev. Lett.*, **88**(cond-mat/0110247. 11):117601, October 2001.

[TBB02a] Yaroslav Tserkovnyak, Arne Brataas, and Gerrit E. W. Bauer. "Enhanced Gilbert Damping in Thin Ferromagnetic Films." *Phys. Rev. Lett.*, **88**(11):117601, 2002.

[TBB02b] Yaroslav Tserkovnyak, Arne Brataas, and Gerrit E. W. Bauer. "Spin pumping and magnetization dynamics in metallic multilayers." *Phys. Rev. B*, **66**(22):224403, 2002.

[TBB05] Yaroslav Tserkovnyak, Arne Brataas, Gerrit E. W. Bauer, and Bertrand I. Halperin. "Nonlocal magnetization dynamics in ferromagnetic heterostructures." *Rev. Mod. Phys.*, **77**(4):1375, 2005.

[TBB08] Yaroslav Tserkovnyak, Arne Brataas, and Gerrit E W Bauer. "Theory of current-driven magnetization dynamics in inhomogeneous ferromagnets." *Journal of Magnetism and Magnetic Materials*, **320**(7):1282–1292, April 2008.

[Tho67] E Thompson. "Inelastic Neutron Scattering in Ferromagnetic Metals." *Phys. Rev. Lett.*, **19**(11):635–636, September 1967.

[TJB98] M. Tsoi, A. G. M. Jansen, J. Bass, W.-C. Chiang, M. Seck, V. Tsoi, and P. Wyder. "Excitation of a Magnetic Multilayer by an Electric Current." *Phys. Rev. Lett.*, **80**(19):4281–4284, May 1998.

[TM08a] S Takahashi and S Maekawa. "Spin current, spin accumulation and spin Hall effect." *Science and Technology of ...*, 2008.

[TM08b] Yaroslav Tserkovnyak and Matthew Mecklenburg. "Electron transport driven by nonequilibrium magnetic textures." *Phys. Rev. B*, **77**(13):134407, 2008.

[TMX08] Yaroslav Tserkovnyak, T. Moriyama, and John Q. Xiao. "Tunnel-barrier-enhanced dc voltage signals induced by magnetization dynamics in magnetic tunnel junctions." *Phys. Rev. B*, **78**(2):020401(R), 2008.

[TS06] W K Tse and S D Sarma. "Spin Hall effect in doped semiconductor structures." *Physical review letters*, 2006.

[UAO10] Kenichi Uchida, Hiroto Adachi, Takeru Ota, Hiroyasu Nakayama, Sadamichi Maekawa, and Eiji Saitoh. "Observation of longitudinal spin-Seebeck effect in magnetic insulators." *Appl. Phys. Lett.*, **97**(17):172505, 2010.

[UTH08] K. Uchida, S. Takahashi, K. Harii, J. Ieda, W. Koshibae, K. Ando, S. Maekawa, and E. Saitoh. "Observation of the spin Seebeck effect." *Nature*, **455**:778–781, 2008.

[UXA10] K. Uchida, J. Xiao, H. Adachi, J. Ohe, S. Takahashi, J. Ieda, T. Ota, Y. Kajiwara, H. Umezawa, H. Kawai, G. E. W. Bauer, S. Maekawa, and E. Saitoh. "Spin Seebeck insulator." *Nat. Mater.*, **9**:894–897, 2010.

[VSC13] N Vlietstra, J Shan, V Castel, J Ben Youssef, G E W Bauer, and B J Van Wees. "Exchange magnetic field torques in YIG/Pt bilayers observed by the spin-Hall magnetoresistance." *Applied Physics Letters*, **103**(3):032401, July 2013.

[Wal58] L R Walker. "Resonant modes of ferromagnetic spheroids." *Journal of Applied Physics*, 1958.

[WBW06] Xuhui Wang, Gerrit E. W. Bauer, Bart J. van Wees, Arne Brataas, and Yaroslav Tserkovnyak. "Voltage Generation by Ferromagnetic Resonance at a Nonmagnet to Ferromagnet Contact." *Phys. Rev. Lett.*, **97**(21):216602, 2006.

[Win03] Roland Winkler. *Spin-orbit Coupling Effects in Two-Dimensional Electron and Hole Systems*. Springer Science & Business Media, October 2003.

[WKM05] Ireneusz Weymann, Jürgen König, Jan Martinek, Józef Barnaś, and Gerd Schön. "Tunnel magnetoresistance of quantum dots coupled to ferromagnetic leads in the sequential and cotunneling regimes." *Phys. Rev. B*, **72**(11):115334, Sep 2005.

[WLW13] Ziqian Wang, Wei Lu, and Bogen Wang. "Electrical Detection of Spin Wave Resonance in a Permalloy Thin Strip." *arXiv.org*, **cond-mat.mtrl-sci**, August 2013.

[WT09] C H Wong and Y Tserkovnyak. "Hydrodynamic theory of coupled current and magnetization dynamics in spin-textured ferromagnets." *Physical Review B*, 2009.

[WXX10] L. Andrew Wray, Su-Yang Xu, Yuqi Xia, David Hsieh, Alexei V. Fedorov, Yew San Hor, Robert J. Cava, Arun Bansil, Hsin Lin, and M. Zahid Hasan. "A topological insulator surface under strong Coulomb, magnetic and disorder perturbations." *Nature Phys.*, **7**:32–37, 2010.

[XBB08] Jiang Xiao, Gerrit E. W. Bauer, and Arne Brataas. "Charge pumping in magnetic tunnel junctions: Scattering theory." *Phys. Rev. B*, **77**(18):180407, 2008.

[YGY10] Haiming Yu, S Granville, D P Yu, and J Ph Ansermet. "Evidence for Thermal Spin-Transfer Torque." *Physical review letters*, **104**(14):146601, April 2010.

[YUF14] Guoqiang Yu, Pramey Upadhyaya, Yabin Fan, Juan G Alzate, Wanjun Jiang, Kin L Wong, So Takei, Scott A Bender, Li-Te Chang, Ying Jiang, Murong Lang, Jianshi Tang, Yong Wang, Yaroslav Tserkovnyak, Pedram Khalili Amiri, and Kang L Wang. "Switching of perpendicular magnetization by spin–orbit torques in the absence of external magnetic fields." *Nature nanotechnology*, **9**(7):548–554, May 2014.

[ZFY00] N. B. Zhitenev, T. A. Fulton, A. Yacoby, H. F. Hess, L. N. Pfeiffer, and K. W. West. "Imaging of localized electronic statesin the quantum Hall regime." *Nature*, **404**:473–476, 2000.

[Zha00] Shufeng Zhang. "Spin Hall Effect in the Presence of Spin Diffusion." *Physical review letters*, **85**(2):393–396, July 2000.

[ZHL09] Yiqiang Zhan, Erik Holmström, Raquel Lizárraga, Olle Eriksson, Xianjie Liu, Fenghong Li, Elin Carlegrim, Sven Stafström, and Mats Fahlman. "Efficient Spin Injection Through Exchange Coupling at Organic Semiconductor/Ferromagnet Heterojunctions." *Advanced Materials*, **22**(14):1626–1630, December 2009.

[ZL04] S Zhang and Z Li. "Roles of Nonequilibrium Conduction Electrons on the Magnetization Dynamics of Ferromagnets." *Physical review letters*, **93**(12):127204, September 2004.

[ZLS75] V E Zakharov, V S L'vov, and S S Starobinets. "Spin-wave turbulence beyond the parametric excitation threshold." *Soviet Physics Uspekhi*, 1975.

[ZNG99] E Zaremba, T Nikuni, and A Griffin. "Dynamics of trapped Bose gases at finite temperatures." *arXiv.org*, **cond-mat.stat-mech**, March 1999.

[54 pages, revtex, 6 postscript figures, final version accepted for publication in Journ. Low Temp. Physics.]